https://doi.org/10.15388/vu.thesis.504
https://orcid.org/0000-0002-2616-0577

VILNIUS UNIVERSITY
CENTER FOR PHYSICAL SCIENCE AND TECHNOLOGY

Agnė Butkutė

Fabrication of Functional Arbitrary Shape Microstructures from Transparent Materials Using Femtosecond Laser-Induced Selective Laser Etching

DOCTORAL DISSERTATION

Technological Sciences,
Material Engineering (T 008)

VILNIUS 2023

This dissertation was written between 2019 and 2023 at Vilnius University, Laser Research Center. The research was supported by the Research Council of Lithuania.

Academic supervisor - Prof. Habil. Dr. Valdas Sirutkaitis (Vilnius University, Technological Sciences, Material Engineering, T 008)

Dissertation Defence Panel:
Chairman – Prof. Dr. Mikas Vengris (Vilnius University, Technology Science, Material Engineering, T 008).
Members:
Dr. Martynas Beresna (University of Southampton, Natural Science, Physics, N 002),
Dr. Paulius Gečys (Center For Physical Sciences And Technology, Natural Science, Physics, N 002),
Assoc. Prof. Dr. Vytautas Jukna (Vilnius University, Technology Science, Material Engineering, T 008),
Prof. Dr. Tomas Tamulevičius (Kaunas University of Technology, Technology Science, Material Engineering, T 008).

The dissertation shall be defended at a public meeting of the Dissertation Defence Panel at 15 h on 15th of September 2023 in Room 306 of the Laser Research Center. Address: Saulėtekio al. 10, Vilnius, Lithuania. Tel. (8-5) 236 6050 ;

The text of this dissertation can be accessed at the libraries of Vilnius University, as well as on the website of Vilnius University: www.vu.lt/lt/naujienos/ivykiu-kalendorius

https://doi.org/10.15388/vu.thesis.504
https://orcid.org/0000-0002-2616-0577

VILNIAUS UNIVERSITETAS
FIZINIŲ IR TECHNOLOGIJOS MOKSLŲ CENTRAS

Agnė Butkutė

Funkcinių laisvai parenkamos architektūros mikrodarinių gamyba iš skaidrių medžiagų, panaudojant femtosekundiniu lazeriu indukuotą selektyvų ėsdinimą

DAKTARO DISERTACIJA

Technologijos mokslai,
medžiagų inžinerija (T 008)

VILNIUS 2023

Ši disertacija buvo parengta 2019–2023 Vilniaus universiteto Lazerių tyrimų centre. Mokslinius tyrimus rėmė Lietuvos mokslo taryba.

Mokslinis vadovas - prof. habil. dr. Valdas Sirutkaitis (Vilniaus universitetas, technologijos mokslai, medžiagų inžinerija, T 008)

Gynimo taryba:
Pirmininkas – prof. dr. Mikas Vengris (Vilniaus universitetas, technologijos mokslai, medžiagų inžinerija, T 008).
Nariai:
dr. Martynas Beresna (Southamptono universitetas, gamtos mokslai, fizika – N 002),
dr. Paulius Gečys (Fizinių ir technologijos mokslų centras, gamtos mokslai, fizika – N 002),
doc. dr. Vytautas Jukna (Vilniaus universitetas, technologijos mokslai, medžiagų inžinerija, T 008),
prof. dr. Tomas Tamulevičius (Kauno technologijos universitetas, technologijos mokslai, medžiagų inžinerija, T 008).

Disertacija ginama viešame Gynimo tarybos posėdyje 2023 m. rugsėjo mėn. 15 d. 15 val. Lazerinių tyrimų centro 306 auditorijoje. Adresas: Saulėtelio al. 10, Vilnius, Lietuva, tel. (8-5) 236 6050;

Disertacija galima peržiureti Vilniaus universiteto bibliotekose ir VU interneto svetaineje adresu: https://www.vu.lt/naujienos/ivykiu-kalendorius

Acknowledgement

One brand suggests ignoring gravity, and actually, this quite accurately describes what I was doing all these four years of Ph.D. study. Gravity contributes to almost everything in this universe. However, gravity also creates many difficulties in this life for all of us. I believe that everything in life can happen in all possible ways; however, due to the entropy, it will most likely will happen in a way you do not want. Thus, we need to work mostly against gravity. Every day I tried to do impossible things. Every day I improved by taking baby steps. Baby steps are much better than standing still. In this way, I learned to celebrate small achievements and eat an elephant one bite at a time. The end result of this path is in front of your eyes. It was not easy, but I learned a lot and not only physics.

I want to thank the people who were together with me on this journey. Thanks to my parents Audronė and Dangiras, who raised me and helped me all my life and for my sister Ieva who grew up together with me. Thanks to my friend Tautvydas who supported me, and my dog Marsas, who cheered me up daily. Special thanks to my supervisor, prof. Valdas Sirutkaitis, who believed that I could. I am grateful to the LTC team and V. Sirutkaitis group (D. Paipulas, R. Sirutkaitis, S. Butkus, D. Stonytė and others) for all their help in my research. Thanks to the Femtika present and past team (Tomas B., Tomas J., Jokūbas, Eglė, Rugilė, Giedrė, Greta M., Rokas, Gabrielius, Deividas A., Deividas Č., Henrikas, Titas T., Titas G., Vidmantas, and many more.) Special thanks to Linas, who always encourages me to do everything better and more and Darius, who always explains reality.

Contents

List of abbreviations **8**

Introduction **9**

1 Conceptual overview **16**

1.1 Nonlinear light and material interaction 16

1.1.1 The nature of nonlinear radiation and material interaction 16

1.1.2 Nonlinear effects 17

1.1.3 Thermal effects 19

1.2 Glass processing using fs radiation 20

1.3 Selective laser-induced etching (SLE) 23

1.3.1 Laser modification inscription importance for SLE . . . 25

1.3.2 Etchant influence on SLE 26

1.3.3 SLE of other transparent materials 27

1.3.4 SLE applications 28

2 Optimization of UVFS SLE **30**

2.1 Motivation 30

2.2 Experimental methods 32

2.2.1 Experimental methods of scanning optimization 33

2.2.2 Experimental methods of etchant optimization 34

2.3 Summary of results 34

2.3.1 Summary of scanning parameters optimization results . 34

2.3.2 Summary of etchant optimization results 41

3 SLE of crystalline sapphire **47**

3.1 Motivation 47

3.2 Experimental methods 47

3.3 Summary of results 49

4 Applications **55**

4.1 Micromechanics 55

4.1.1 Motivation 55

4.1.2 Experimental methods 55
4.1.3 Summary of results 56
4.2 Microfluidics 60
4.2.1 Motivation 60
4.2.2 Experimental methods 60
4.2.3 Summary of results 62

Conclusions **66**

SANTRAUKA **68**

Curriculum vitae **97**

Bibliography **99**

List of abbreviations

1D	one-dimensional
2D	two-dimensional
3D	three-dimensional
AFM	atomic force microscope
CW	continuous-wave (laser operation regime)
DLW	direct laser writing
fs	femtosecond
HF	hydrofluoric acid
H_3PO_4	phosphoric acid
H_2SO_4	sulfuric acid
IR	infrared (range or wavelength)
KOH	potassium hydroxide
LAZ	laser affected zone
LOC	lab-on-chip
NA	numerical aperture
NaOH	sodium hydroxide
ns	nanosecond
OOC	organ-on-chip
ps	picosecond
RMS	root mean square
SEM	scanning electron microscope
SLE	selective laser-induced etching
UV	ultraviolet (range or wavelength)
UVFS	ultraviolet grade fused silica
YAG	yttrium aluminum garnet; $Nd{:}Y_3Al_5O_{12}$

Introduction

Transparent and high-hardness materials have become an object of wide interest due to their optical and mechanical properties, most notably concerning technical glasses and crystals such as sapphire. However, the processing of such brittle materials is rather complicated. They tend to crack when affected by high mechanical pressure or high-intensity radiation due to the high strain induced during processing. Femtosecond laser-based microprocessing techniques are a desirable alternative for glass and crystal microprocessing due to minimized thermal effects [1]. Various laser machining techniques have already been adapted for glasses and crystals micromachining: to make 2D surface structures, dicing [2] or direct laser ablation could be used [3, 4]. Direct ablation is a relatively efficient and straightforward process enabling surface functionalization. Ablation could be combined with additional processes such as laser-induced plasma-assisted ablation [5, 6] or laser-induced backside wet etching [7, 8, 9] to improve the quality of laser-processed surfaces. By using ablation in combination with additional thermal processing [10] or direct laser writing in combination with chemical post-processing, optical components such as lenses [11, 12] or diffractive optical elements [13, 14, 15] could be made. However, these technologies are limited to the microprocessing and achievement of 2D geometries, and most cannot produce arbitrary-shaped 3D structures. Of course, ablation could be combined with other femtosecond laser-based microprocessing techniques, such as welding. In this way, surface structures could be additionally sealed and closed cavities could be created, which is helpful in microfluidic chip fabrication. On the other hand, multi-layer channels would require a lot of effort to make in this way.

Meanwhile, the selective laser-induced etching (SLE) technique could be a good option even for high-complexity 3D structure formation from glasses and crystals. SLE is a multiple-step microprocessing technique. First, porous modifications called nanogratings [16] are inscribed inside the glass volume. Subsequently, laser-modified samples are etched in aggressive etchants such as HF or KOH, which are used to etch out modified material [17]. In this way, arbitrary shaped structures in glass or crystals can be created [18]. A critical parameter in SLE is selectivity, which is the ratio between the etching rate of

laser-modified and unmodified material. In SLE, the process' selectivity describes the maximum possible aspect ratio of produced structures. Thus, high aspect ratio structures require high selectivity values, which means that the etching rate of modified material needs to be maximized while the unmodified material etching rate needs to be minimized. The widely investigated material in SLE is UVFS, which is one of the most popular and widely used glasses. Many works in literature concentrate on techniques with which selectivity optimization in UVFS can be done [19, 20]. Typical selectivity for SLE is a few hundred and could be increased to over 1000. However, the process still faces many limitations in UVFS SLE, which could be solved.

On the other hand, other materials also could be used in SLE, starting from other glass types such as borosilicate [21, 22], to other transparent materials as crystals starting from crystalline quartz [23] to sapphire [24], YAG [25] or others. One of the most popular crystals due to its hardness and mechanical resistance is sapphire. It has already been shown that SLE could be used in sapphire microprocessing [25]. The selectivity demonstrated for sapphire exceeds many times the selectivity shown in UVFS [26]. However, there are only a few examples of SLE-made structures in sapphire. This is due to the high selectivity results from almost zero etching rate of unmodified material, while the modified material etching rate is significantly lower than in the UVFS case. This shows that, even chemically, sapphire is a very resistant material. Hence, new and different approaches need to be used for this material. A comparison between different processing protocols will be presented in this thesis.

Such a high selectivity value allows for the formation of complex high aspect ratio structures such as micromechanical parts or components [27, 18], microfluidics [28, 29] and even complex microfluidics with an already integrated micromechanical component [30, 31]. Application areas for such structures are sensing [32, 33], lab-on-chip devices [30, 18, 31], nozzles [18, 34] and possibly others. In this study we will present even more sophisticated microstructures which could be used in microrobotics or lab-on-chip applications using optimized protocols.

The technology mentioned sounds perspective in many areas. Thus, this dissertation is dedicated to improving the fused silica selective laser-induced etching technique and developing the crystalline sapphire selective laser-induced etching process. Finally, selective laser-induced etching will be applied to functional structure formation, and some perspective applications of formed structures will be presented.

Goal of the dissertation

The goal of this dissertation is to develop and improve existing SLE techniques for complex functional 3D structure formation out of UVFS and sapphire.

Tasks of the work

In order to achieve the research goal the following tasks were set:

1. Optimise fused silica SLE parameters such as laser and scanning and etching parameters to maximize process selectivity. Measure the consequent process properties such as etched surface roughness.

2. Test various sapphire SLE protocols, such as different laser parameters and etchants, to find suitable parameter combinations for sapphire structure fabrication.

3. Fabricate functional 3D structures out of glass and test the structures produced.

Novelty and importance of the work

The novelty of this work lies in the optimized glass and sapphire SLE processes which create the possibility of forming high aspect ratio 3D structures using SLE:

1. Selectivity and etched surfaces' dependence on the spacing between scanning lines in different laser-inscribed planes were tested, as well as etchant wetting properties and concentration. Furthermore, due to the performed optimization of the scanning and etching procedures, we demonstrate high selectivity, which leads to a high aspect ratio and complexity of formed structures.

2. Consequently, movable assembly-free micromechanical structures are presented, and various complicated microfluidic systems with integrated functional elements are shown.

3. Moreover, an SLE protocol for sapphire processing was developed. Multiple parameters sets (laser radiation wavelength, pulse duration, and others) for nanograting formation, and various etchants for the nanograting etching were tested and compared. The most suitable process protocol was chosen, and microstructures out of crystalline sapphire were demonstrated.

Key statements for defence

1. In the case of SLE 3D structure formation, structures are combined out of a single array of single lines stacked in horizontal or vertical planes. Smaller spacing between the lines in the plane (approximately 90% of inscribed modifications overlapping) for both directions gives the highest etching rates (up to 1000 μm/h) and the lowest surface roughness values (below 200 nm RMS).

2. SLE process selectivity is dependent on the wetting properties of the etchant. Selectivity was increased by decreasing the etchant contact angle with the substrate when part of the water in the etchant is replaced with a suitable organic solvent (isopropanol). A selectivity value up to approximately 3000 was reached using 2 mol/L KOH solution where 10% of water is replaced with isopropanol.

3. Crystalline sapphire can be used as material for SLE 3D structure. However, standard etchants, such as HF or KOH, need to be changed to a sulphuric and phosphoric acid mixture. Out of all the tested etchants, only sulphuric and phosphoric acid mixture at 270°C temperature could remove laser-induced nanogratings. The highest observed selectivity using the mentioned etchant was 66.

4. UVFS SLE could be used for high-complexity micromechanical components or microfluidic chip fabrication. A compliant type micromechanical spring, movable gear type mechanism, and lab-on-chip type microfluidic system were fabricated with low surface roughness (< 250 nm RMS) and μm scale features and precision.

Layout of the dissertation

This dissertation is divided into four sections. The first chapter introduces the topic and presents the theoretical background of the whole work. The second chapter is dedicated to giving an optimization of UVFS SLE. In the third chapter, the SLE of crystalline material is presented. And finally, the fourth chapter presents possible applications for SLE.

Contribution of the author and co-authors

The main co-authors of the research results presented in the thesis are Prof. V. Sirutkaitis, Dr. D. Paipulas, Dr. L. Jonušauskas, Dr. D. Gailevičius, Dr. T. Tičkūnas, T. Baravykas, G. Merkininkaitė, R. Vargalis,

dr. R. Sirutkaitis, T. Jurkšas, J. Stančikas. V. Sirutkaitis supervised and consulted on most of the research. D. Paipulas and D. Gailevičius consulted on sapphire SLE research and helped with publication preparation. L. Jonušauskas and T. Tičkūnas consulted on UVFS SLE research and helped with preparation of publications. T. Baravykas prepared models and fabrication codes for complex 3D structure fabrication. G. Merkininkaitė and R. Vargalis helped with the chemical part and did some measurements, such as SEM and contact angle measurement. R. Sirutkaitis helped with sapphire etching. T. Jurkšas and J. Stančikas did part of the experiments in etchant optimization and fabricated part of the glass structures.

The role of the thesis author is to plan experiments and perform experimental activities. The author did most of the measurements, fabricated a significant part of the glass structures shown, analyzed results, and prepared all publications related to the dissertation.

Approbation of the research results

This section presents the lists of papers and conferences related to the dissertation. In this doctoral thesis, Roman numbers in square brackets refer to the following articles.

List of papers related to the dissertation

I A. Butkutė and L. Jonušauskas, 3D manufacturing of glass microstructures using femtosecond laser, Micromachines **12**(5), 499 – 526 (2021).

II A. Butkutė, T. Baravykas, J. Stančikas, T. Tičkūnas, R. Vargalis, D. Paipulas, V. Sirutkaitis and L. Jonušauskas, Optimization of selective laser etching (SLE) for glass micromechanical structure fabrication, Opt. Express **29**(15), 23487 – 23499 (2021).

III A. Butkutė, G. Merkininkaitė, T. Jurkšas, J. Stančikas, T. Baravykas, R. Vargalis, T. Tičkūnas, J. Bachmann, S. Šakirzanovas, V. Sirutkaitis, and L. Jonušauskas, Femtosecond Laser Assisted 3D Etching Using Inorganic-Organic Etchant, Materials **15**(8), 2817 – 2826 (2022).

IV A. Butkutė, R. Sirutkaitis, D. Gailevičius, D. Paipulas, and V. Sirutkaitis, Sapphire Selective Laser Etching Dependence on Radiation Wavelength and Etchant, Micromachines **14**(1), 7 – 16 (2023).

V A. Butkutė, T. Jurkšas, T. Baravykas , B. Leber, G. Merkininkaitė, R. Žilėnaitė, D. Čereška, A. Gulla, M. Kvietkauskas, K. Marcinkevičiūtė,

P. Schemmer, K. Strupas, Combined Femtosecond Laser Glass Microprocessing for Liver-on-Chip Device Fabrication, Materials **16**(6), 2174 – 2183 (2023).

List of conference contributions related to the dissertation

1. A. Butkutė, T. Baravykas, T. Tičkūnas, L. Jonušauskas and V. Sirutkaitis, Optimization of selective laser etching process for arbitrary shape 3D micro-structure fabrication, Laser Precision Microfabrication Symposium 2020 – LPM2020, virtual conference, 2020. Oral presentation.
2. A. Butkutė, T. Baravykas, T. Tičkūnas, L. Jonušauskas and V. Sirutkaitis, 3D selective laser glass etching for medical applications, Additive Manufacturing Meets Medicine – AMMM2020, virtual conference, 2020. Oral presentation.
3. A. Butkutė, T. Baravykas, J. Stančikas, T. Tičkūnas, L. Jonušauskas and V. Sirutkaitis, Optimization of selective laser etching for assembly-free 3D micromechanic fabrication, SPIE Photonics West, virtual conference, 2021. Oral presentation, invited.
4. A. Butkutė, T. Baravykas, J. Stančikas, L. Jonušauskas and V. Sirutkaitis, Aukšto matmenų santykio 3D stiklinių darinių gamyba selektyvaus lazerinio ėsdinimo technologija, 44th Lithuanian National Physics Conference, Vilnius, Lithuania, 2021. Oral presentation.
5. A. Butkutė, B. Siaurytė, D. Paipulas, R. Sirutkaitis and V. Sirutkaitis, Selective laser etching of Crystalline Sapphire for 3D Structure Fabrication, SPIE Photonics West, San Francisco, USA, 2022. Poster presentation.
6. A. Butkutė, T. Baravykas, J. Stančikas, L. Jonušauskas and V. Sirutkaitis, Selective laser etching of high aspect ratio 3D glass microstructures, SPIE Photonics West, San Francisco, USA, 2022. Oral presentation.
7. A. Butkutė, R. Sirutkaitis, D. Gailevičius, D. Paipulas, K. Staliūnas and V. Sirutkaitis, Formation of high aspect ratio glass and crystalline structures, Laser Precision Microfabrication Symposium 2020 – LPM2022, hybrid conferenece, Dresden, Germany, 2022. Oral presentation.

List of papers unrelated to the dissertation

1. A. Butkutė L. Čekanavičius, G. Rimšelis, D. Gailevičius, V. Mizeikis, A. Melninkaitis, T. Baldacchini, L. Jonušauskas and M. Malinauskas,

Optical damage thresholds of microstructures made by laser three-dimensional nanolithography, Opt. Lett. **45**, 13 – 16 (2020).

2. D. Andrijec, D. Andriukaitis, R. Vargalis, T. Baravykas, T. Drevinskas, O. Kornyšova, A. Butkutė, V. Kaškonienė, M. Stankevičius, H. Gricius, A. Jagelavičius, A. Maruška and L. Jonušauskas, Hybrid additive-subtractive femtosecond 3D manufacturing of nanofilter-based microfluidic separator, Appl. Phys. A **127**(10), 781 – 787 (2021).

1. Conceptual overview

This chapter presents the physics fundamentals behind SLE technology and a literature review of SLE. Information provided in this chapter is published in paper **I**.

1.1. Nonlinear light and material interaction

1.1.1. The nature of nonlinear radiation and material interaction

First, the basic mechanisms of laser and material interaction should be presented before discussing laser material processing. When the material is affected by high-intensity radiation, its response becomes nonlinear. High intensities in the beam focal spot are achieved due to temporal and spatial energy compression. Spatial light compression is achieved by sharp focusing using high numerical aperture (NA > 0.2) objectives or lenses. Temporal light compression is done using ps – fs pulse radiation where the energy reaches the material in short periods. As a result, the material is affected by very high peak intensity I (more than GW/cm^2, which corresponds to more than mJ/cm^2 energy density). Material response to high I is nonlinear and conceptually differs from the material response to low-intensity radiation. When radiation travels through the dielectric material, it polarizes the material. When radiation intensity is not high enough, material polarization linearly depends on the radiation electric field E (Equation 1.1). In general, light intensity is proportional to squared electric field $I \sim |E^2|$, when radiation creates an electric field that is stronger than 10^7 V/m, material polarization dependency on the electric field becomes nonlinear (Equation 1.2).

$$P(t) = \epsilon_0 \chi^{(1)} E(t), \tag{1.1}$$

$$P(t) = \varepsilon_0 \chi^{(1)} E(t) + \varepsilon_0 \chi^{(2)} E^{(2)}(t) + \varepsilon_0 \chi^{(3)} E^{(3)}(t) + ..., \tag{1.2}$$

here ε_0 is vacuum dielectric permeability, $\chi^{(1)}$ is linear optical susceptibility, $\chi^{(2)}$ – second order nonlinear optical susceptibility, o $\chi^{(3)}$ – third order nonlinear optical susceptibility.

Different member in the nonlinear polarization equation decides various phenomena observed in the material. For instance, effects determined by square nonlinear susceptibility, like sum and difference frequency generation, are observed only in non-central symmetrical crystals. Meanwhile, cubic nonlinear susceptibility-affected phenomena, like radiation self-interaction such as the Kerr effect or light filament formation, are observed in all dielectric materials. Other possible nonlinear effects are multi-photon absorption, tunneling ionization, etc. It is important to note that various nonlinear light-interaction regimes can be induced simultaneously, leading to a complex process picture. [35].

1.1.2. Nonlinear effects

As mentioned before, when the material is affected by high-intensity radiation, various nonlinear light and material interaction effects are governed by different-order nonlinear susceptibility. When a material is exposed to high-intensity radiation, the radiation electric field changes the material's refractive index for the upcoming light. This means that the light changes the conditions in the material itself. The mentioned effect is called the Kerr effect. The Kerr effect is caused by cubic nonlinear susceptibility. Transparent material exposed to a Gaussian beam creates a non-uniform index change due to beam intensity distribution. This phenomenon creates a lens effect and induces light self-focussing, which could lead to light filamentation. Due to the Kerr effect, focused light changes its ideal shape when focused on transparent media such as glass [36].

Another nonlinear effect is multiphoton absorption. Multiphoton absorption is the simultaneous absorption of two or more photons through virtual levels from the ground to an excited state. Two-photon absorption is decided by third-order nonlinear optical susceptibility. Meanwhile, three-photon absorption is determined by fifth-order nonlinear optical susceptibility. Hence, higher-order multiphoton absorption is decided by higher-order nonlinear optical susceptibility. Multiphoton ionization is usually a negative effect that distorts radiation in nonlinear optics. However, multiphoton absorption can be used for positive practical applications such as multiphoton spectroscopy, microscopy, and transparent material laser processing.

In general, the electrons have to be excited from the valance band to the conductive band to induce a modification in the dielectric material. Numerous processes might cause permanent modification. The most important and prevailing nonlinear effects when a material is illuminated with high-intensity I fs radiation are multiphoton ionization, tunneling ionization, and avalanche

ionization. Multiphoton ionization is a process by which an electron absorbs several photons simultaneously and is excited to a conductive band *via* virtual levels. The principal scheme of this process is shown in Figure 1.1 (b). Another nonlinear effect is tunneling ionization. An electric field created by intense laser radiation can distort the potential barrier which holds electrons to material atoms. An intense electric field could decrease the potential barrier; as a consequence, the possibility of electron tunneling increases. Thus, more and more electrons are excited to the conduction band. This process is depicted in Figure 1.1 (c).

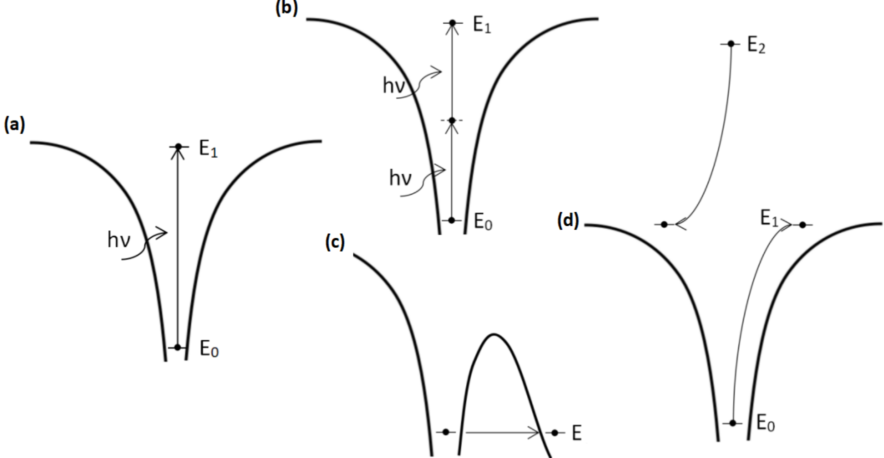

Figure 1.1: Principle schemes of main nonlinear processes: (a) linear ionization, (b) nonlinear (multi-photon) ionization, (c) tunneling ionization, and (c) avalanche ionization.

Which process (multi-photon ionization or tunneling ionization) will dominate depends on laser ω and I. This dependency is described by the Keldysh parameter [37] which can be expressed as Equation 1.3:

$$\gamma = \frac{\omega}{e}\sqrt{\frac{m_e \Delta E \varepsilon_0}{I}}, \tag{1.3}$$

here e – electron charge, m_e – electron mass, I – laser intensity, ϵ_0 – vacuum dielectric permeability, ΔE – band gap.

When γ is more than 1.5, multi-photon ionization will dominate. When γ is less than 1.5, tunneling ionization will dominate. Meanwhile, a transitional regime of ionization occurs when the Keldysh parameter is close to 1.5. In this case, multi-photon and tunneling ionization have approximately the same influence on material ionization. To sum up, tunneling ionization prevails in a high laser intensity and low-frequency regime. In contrast, multi-photon ionization dominates in high-intensity and high-frequency cases. In laser material pro-

cessing, controlling which effect will dominate is necessary to reach the desired effect.

Avalanche ionization is another critical process that appears due to nonlinear radiation and material interaction. The principal scheme of this process is shown in Figure 1.1 (d). Electrons are released from material atoms to the lattice when radiation interacts with the material. The radiation-induced intense electric field accelerates free electrons. Electrons can reach energies higher than a potential barrier for neighboring atom electrons and release other electrons from atoms. In this way, more and more electrons are released, and the material can be damaged [35].

1.1.3. Thermal effects

When a material is processed with relatively long laser pulses (> 10 ps), thermal effects can be observed in the material. This results from heat dissipation from the laser-affected area, which occurs while a long laser pulse still interacts with the material in the focal point. This process occurs around 1 ns after radiation absorption [1] and usually reduces material processing quality. When quantifying a thermal effect, the term Laser Affected Zone (LAZ) is introduced. It encompasses all the volume affected by the heat generated by a laser, even if it is outside the focal point [38].

An ultrafast laser can allow control and, if needed, significantly reduce thermal effects caused by the light-matter interaction. Looking from the temporal perspective, interactions needed for processing occur relatively fast. For instance, material ionization occurs after $\sim$1 ps, followed by ablation and removal after $\sim$100 ps [1]. Therefore, the LAZ can be significantly reduced if no additional energy is introduced while subsequent thermal effects occur. As a result, the material does not suffer from substantial thermal effects in the fs pulses. That is why femtosecond material laser processing sometimes is called cold material processing. However, it is essential to note that alongside pulse duration, pulse repetition rate also plays a vital role in the thermal aspect of processing. If several pulses reach the affected zone before initial heat dissipation, even fs pulses can induce material melting and a noticeable LAZ. Another important factor for the thermal accumulation process is the deposited energy. By maintaining the same pulse duration and repetition rate and, at the same time, by increasing the energy of each pulse, the sample is affected by a higher radiation dose. We obtain higher thermal effects if the energy does not have enough time to be relaxed out of the substrate by increasing pulse energy. Higher pulse energy shows greater affected volume around the laser focus [38], which means more substantial thermal effects. While this might be detrimental in some cases, it can also be helpful in applications like laser welding. This distinction will be made throughout the article where it applies.

These thermal effects are significant for glass processing. Glass is a pretty fragile material that can be easily broken by treating it with stresses [39] or temperature-caused volume tensions [40]. By processing glass with longer pulses or even a CW laser, it is tough to avoid cracks in the glass [41]. However, short pulse laser development allows for minimizing thermal effects by using a shorter pulse duration [42] and processing material locally without affecting the surrounding volume.

1.2. Glass processing using fs radiation

Light-based glass processing is a complex process. Most glasses (with some exceptions like chalcogenide glasses) are transparent materials for near-UV, visible and near-IR radiation, meaning that linear interaction with such photons is negligible. As a result, one way to induce a modification in glasses is by choosing a wavelength that a specific glass absorbs. Some works use such an interaction for glass surface structuring based on linear glass absorption [43, 44]. This direct material removal by the laser beam is called laser ablation. Nevertheless, 3D processing in such cases is greatly limited due to direct absorption being a surface-bound process limiting its use for 3D structuring.

Alternatively, intense and focused radiation can be used. The reaction between light and material becomes nonlinear, making it possible to modify the volume of transparent material. For this reason, most laser-based glass 3D processing techniques are based on such processes. As we have already discussed, when radiation I is high enough (GW/cm^2 – PW/cm^2), multiple photons (in most cases two) can be absorbed simultaneously during multi-photon ionisation [35]. Intensity I high enough for the process can be reached only by focused laser light. This creates inherent localization of the process. The scheme of this idea is shown in Figure 1.2. Keeping in mind that in most cases, NA in the range from 0.01 to 1.4 is used, the volume in which the modification is induced can range from a hundred nm to hundreds of μm in a transverse direction and from a few μm to several mm in a longitudinal direction. The elongated modification is an inherent feature of a Gaussian beam generally used for such processing [45] while other types of voxel shapes are possible with beam structuring. Due to the nonlinear nature of these interactions, sub-diffraction limited features are also possible, both directly and indirectly. Regardless, localization and selectivity of the process in the glass volume are critical components of why a fs laser is the primary tool for high-precision 3D fabrication. Keep in mind that lasers can be used in many ways, not only for glass processing; any laser-based fabrication process can be called direct laser writing DLW [46].

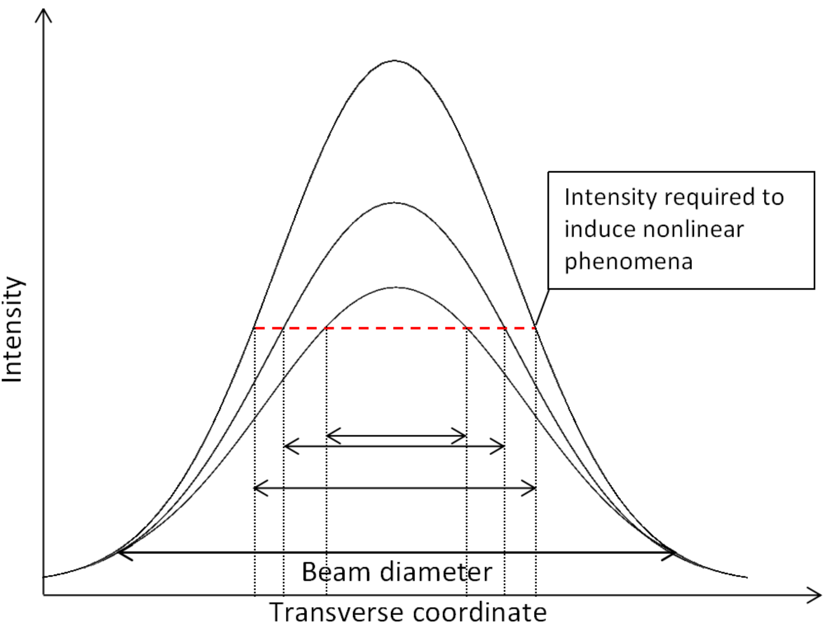

Figure 1.2: Focused laser beam spot diameter required to induce nonlinear effects dependency on radiation intensity.

Light-glass interactions used in DLW can induce different types of modifications. These depend on laser parameters such as radiation intensity, repetition rate, pulse duration, or wavelength, to name a few [47]. Of course, induced modifications depend on the material itself [47, 21]. In the literature, it is possible to find three primary stable modification types that can be induced in glass. Nevertheless, some exceptions apply in specific cases. For instance, silver clusters can be formed in silver-containing glasses, resulting in a type Argentum (or type A) modification [48]. However, in this review, we will concentrate on the three primary modification types referring to any exceptions when applicable.

Type I modification is material refraction index change. The change depends on various laser parameters and on the material itself. In a standard case, it is considered that this variation is mainly decided by pulse energy. An example photo of this modification can be seen in Figure 1.3 (b) and (c) [47]. In standard glass, the amplitude of refractive index change is in the order of 10^{-3}.

The type II material modification consists of periodical porous modifications in the glass called nanogratings. From an optical standpoint, this modification creates birefringence alongside changing just the material's refractive index. An example of nanograting is shown in Figure 1.4. Many different explanations about nanaograting formation exist in the literature [49, 50]. That implies that it is not completely clear how nanogartings are formed. However, most expla-

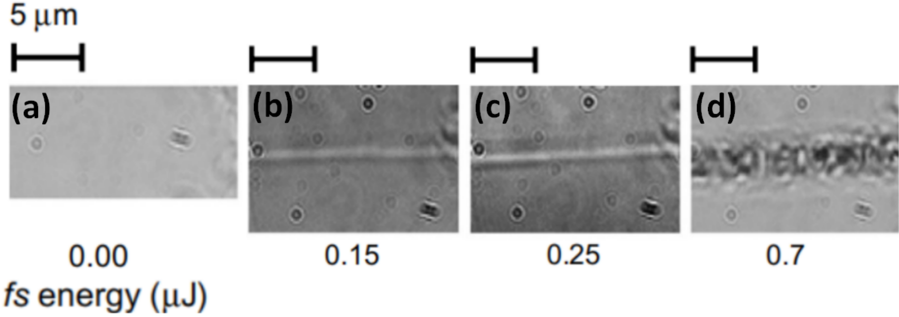

Figure 1.3: Glass modification examples. (a) Unmodified material, (b, c) I type of glass modification or refractive index changes, (d) II type modification or nanogratings [47].

nations rely on excited plasma interaction with light [50]. Some explanations state that nanogratings result from the interference of the bulk electron plasma longitudinal wave with the incident light [26, 51]. Pulse interaction with the material creates plasma waves that interfere with consecutive pulses in the pulse train. Other works suggest an explanation of nanogratings formation through nanoplasma formation [52]. According to this theory, a focused ultrashort light pulse ionizes defects and color centers, leading to the formation of inhomogeneous plasma. The mentioned plasma zones evolve into nanoplasma after several laser pulses. The local field enhancement at the nanoplasma boundary creates critical electron density, where nanoplanes forms. On the other hand, alternative theories based on attractive interaction and self-trapping of exciton–polaritons exist. In this theory, nanogratings result from the interference of exciton–polariton modes [53].

The nanograting ripple size is a sub-diffraction, i.e., in the range of tens of nm. Usually, nanograting period can be described by this equation: $\Lambda = \lambda/2n$ [54]. However, exact nanograting periodicity depends on other laser parameters such as pulse energy and pulse duration [55]. The pulse repetition rate plays quite an important role, as it denotes the thermal aspect of the interaction [56]. In general, by increasing the pulse repetition rate, the pulse energy window in which nanograting could be formed becomes narrower [55, 57, 52]. One of the critical properties of this interaction is the tendency of nanogratings to be strongly influenced by the polarization of the incident beam. Nanograting ripple direction is perpendicular to polarization [16, 21]. This property is illustrated in Figure 1.4.

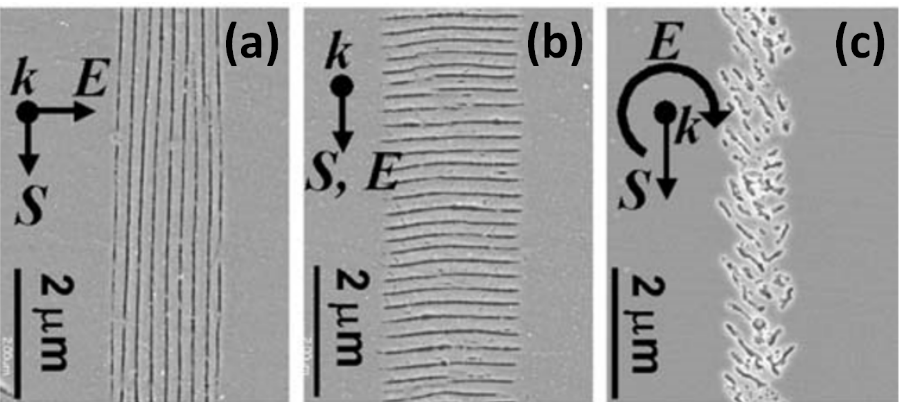

Figure 1.4: Examples of type II glass modifications. (a) Nanogratings induced when the scanning direction is perpendicular to light linear polarization direction, (b) nanogratings induced when the scanning direction is parallel to light linear polarization direction, (c) nanogratings induced with circular light polarization. Here S denotes scanning direction, and E is radiation polarization vector [21].

Type III modification denotes the formation of nano/micro-voids. When radiation intensity exceeds a particular value higher than needed for type II modification, micro-explosion in the volume of glass occurs and forms microcavities. This phenomenon is demonstrated in various studies [58, 59]. It is the most violent form of processing with the fs laser, leading to a relatively large modification area with several phase-changes along the modified region. Particular radiation intensities to induce these modifications depend on the materials themselves.

All previously mentioned laser glass modification types can be used for different microprocessing techniques. Type I modification can be used for smooth laser refractive index modification [47] and waveguide formation in glass [60, 32]. Type II can be used for diffractive optical component formation such as Q-plates [61] or photonic crystals [62]. Type II modification combined with a subsequent etching step is used for SLE [63]. Meanwhile, type III modification is used for laser ablation [64, 42] when material is removed directly or laser welding [65, 66, 67] when two transparent materials can be connected by melting the contact between two glass substrates. These techniques have different natures and provide various possibilities for glass microprocessing. However, the SLE process will be discussed in more detail in this work.

1.3. Selective laser-induced etching (SLE)

SLE is a unique process because it is a suitable technique for making 3D structures from various transparent materials. Implementation of this technique

consists of two steps. First, nanogratings or type II modifications are inscribed inside the glass volume. Subsequently, the sample with inscribed modifications is etched in aggressive etchants such as KOH or HF [68]. The scheme of the SLE process is shown in Figure 1.5. Currently, the most investigated material in this technology is UVFS which is pure SiO_2. However, other glasses such as borosilicate glass (BK7, Pyrex, Borofloat) [69, 21, 22], Foturan [70] can be used in SLE, as well. Different materials have various implementation processes. Therefore we will start here from the UVFS case.

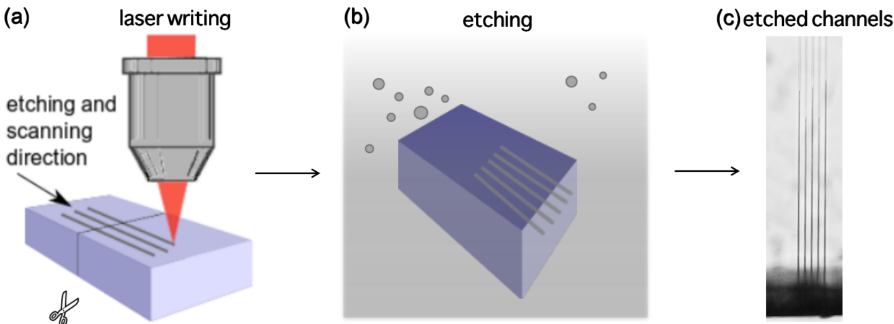

Figure 1.5: Visualization of SLE steps. (a) Laser modifications are inscribed inside the volume of glass. (b) Etching is performed in a specific etchant. (c) The final structure with etched channels.

Since SLE consists of two different processes, the parameters of both technological steps can influence the efficiency of the SLE. This section will discuss how laser parameters for laser inscription and the etching can affect SLE. However, the idea of SLE efficiency measurement needs to be presented first. In general, it is known that laser-inscribed nanogratings can be etched many times faster than unmodified material due to a few reasons, such as the higher surface area of nanogratings. Moreover, laser radiation induces material structural variations when the binding angles of the lattice change. Oxygen atoms become more reactive and, as a result, more effectively interact with the etchant [68]. In general, the unmodified glass and the modified material are etched at the same time. Typically, the etch rate of fused silica is a few μm/h. Of course, it depends on the etchant due to a different reaction with the material [17]. Meanwhile, the etching rate of modified material can be up to a few hundred of μm/h [19]. On the one hand, quantitative evaluation of the SLE etching rate is essential. Usually, the modified material etching rate is measured as a single scanning channel, etch for a single hour, length [16, 19]. Meanwhile, the unmodified material etching rate can be evaluated as substrate thickness decrement over the time. However, it is intuitive that the ratio between the etching rates of modified and unmodified materials gives us qualitative information. The ratio between the laser-modified and unmodified materials' etching

rate is called selectivity. Selectivity describes the highest aspect ratio of the etched features in an SLE-made structure. Combined with the capability to inscribe laser modifications in 3D, it leads to the SLE ability of arbitrary shape structure fabrication [68].

1.3.1. Laser modification inscription importance for SLE

Various laser and scanning parameters strongly affect the SLE process. Selectivity itself strongly depends on pulse energy. While sufficient pulse energy is needed to induce type II modification, the formation of LAZ can also be induced if too powerful pulses are used. LAZ affects etching properties [38]. Higher laser pulse energy with wider LAZ zones results in a wider etched zone. This effect could be used for scanning up large volumes, while, on the contrary, this phenomenon could be disadvantageous in high aspect ratio structure fabrication. Moreover, pulse duration and laser repetition rate affect LAZ and change etching properties as well [19, 56, 71]. Longer pulse duration leads to more substantial thermal effects. Higher pulse repetition rates prevent energy from being relaxed from the lattice. On the other hand, pulse energy not only changes LAZ but also changes the size of the modification and the nanograting configuration itself, which leads to different selectivity induced by various pulse energies [16, 21, 19]. However, almost all the research mentioned refers to the optimal particular parameter value, which varies by changing other parameters. We can see that it is not individual parameters but rather the whole parameter set that is important for the SLE process. By changing pulse energy, the pulse repetition rate changes the deposited dose. Hence, a particular radiation dose is hiding under these parameter sets. Overall, it can be seen that the SLE process needs to be ensured by specific conditions – a specific radiation dose [19] and these conditions can be altered by different thermal regimes [38].

Alongside radiation parameters, scanning strategies also play an immense role in SLE effectiveness. Overall, translation velocity and pulse overlap while hatching/slicing denote the pulse overlap, which, in turn, governs the accumulated radiation dose [19]. Moreover, scanning velocity similarly affects the accumulated radiation dose as pulse repetition rate. As a result, selectivity dependency on scanning velocity has been investigated in many studies [72, 19, 73]. The acquired results vary, painting a more complicated picture of interaction as different sets of laser and scanning parameters were shown to work quite effectively [19, 73]. Interestingly, in some works, almost no significant selectivity dependency on scanning speed was noticed [72]. The translation velocity question, in general, is crucial, as it is one of the main parameters determining structuring rate, i.e., what volume will be processed in a given amount of time. Thus a better understanding of these contradicting results is a topic for further research in the field.

The specific separation between scanning lines should be chosen during the inscribing process. Unsurprisingly, this also influences etching rate and selectivity [17, 73]. One non-trivial observation was that the optimal Z separation value varies when a different etchant is chosen [17]. Separation along a horizontal axis (i.e., the slicing step) should also not exceed the voxel height [73]. Overall, due to the complex nature of the process and a vast amount of independent parameters, the exact interplay is still an object of active investigation, with the goals of different groups distributed between trying to achieve the best selectivity, highest etching rate, lowest surface roughness or some combination of all.

It is essential to pay attention to the importance of polarization during the SLE process. Polarization is responsible for the direction of the nanogratings as depicted in Figure 1.4. Several studies investigated selectivity dependency on laser beam polarization. When radiation polarization is perpendicular to the scanning direction, we get the highest etching rate [16, 21]. The same applies to selectivity because the unmodified material etching rate in all the cases remains the same [17]. Meanwhile, polarization parallel to the scanning direction gives the lowest etching rate [16, 21]. Circular polarization gives a reasonable etching rate as in the perpendicular polarization case [21]. This is extremely important because polarization might be considered invariable for any scanning strategy, heavily simplifying an already complicated process and becoming favorable for application-oriented fabrication. Nevertheless, care should be taken when considering the interplay between pulse duration and polarization. This trend always appears when femtosecond laser pulses are used to write modification. However, when ps pulses are used for SLE, selectivity does not depend on radiation polarization [71]. This property comes from the nature of this process. By using femtosecond pulses, it is possible to induce nanograting modification. Meanwhile, ps pulses yield modifications more reminiscent of nanocracks. These can be considered as different modification types that are still suitable for SLE.

1.3.2. Etchant influence on SLE

From the etchant side, HF and KOH are the most popular. These etchants react with materials differently. The reaction equation of KOH and HF with one of the most popular glasses, fused silica, is shown in Equation 1.4 and Equation 1.5. When SiO_2 reacts with etchant in both reaction equations, the reaction product is salt and water. HF, after reaction with SiO_2, dilutes more than KOH. These reaction equations show that concentrated KOH solution benefits HF etchant due to the minor saturation behavior in elongating channel structures [74]. More and more articles have been published where NaOH is used as an etchant instead of HF or KOH [75, 76]. The reaction of this etchant

is similar to KOH and is shown in 1.6.

$$SiO_2 + 4HF \rightarrow SiF_4 + 2H_2O. \tag{1.4}$$

$$SiO_2 + 2KOH \rightarrow K_2SiO_3 + H_2O, \tag{1.5}$$

$$SiO_2 + 2NaOH \rightarrow Na_2SiO_3 + H_2O. \tag{1.6}$$

KOH etching properties are strongly affected by KOH concentration and temperature [73]. Usually, in literature, we can find that 8 – 10 mol/L concentration KOH solution is used at 85 – 90°C temperature [30, 17, 73]. In general, a higher KOH concentration yields a higher etching rate. Nevertheless, a higher etchant concentration does not guarantee better selectivity, potentially leading to a contradictory result [73]. This can be tied to the higher etching rate of both laser-processed and unaffected areas. When discussing the etching rate, a similar trend can be observed with KOH temperature. Butkus et al. have demonstrated that the best selectivity is achieved at 80°C [73]. Regarding HF, if fast etching is desired, high (tens of %) HF concentrations should be used [77]. However, as one of the primary goals of SLE is achieving intricate 3D structures, lower concentrations (5% or even lower) at ambient conditions are used to avoid overetching laser unexposed parts [17]. Curiously, experimentation on various conditions which might be utilized for SLE using HF (like temperature manipulation) is limited. One of the main reasons why more experiments are not performed with HF acid is the hazardous nature of this chemical, which explains why more research groups prefer KOH over HF. Nevertheless, both etchants can find their applications. To get higher etching rates (up to a few hundred of μm/h), HF can be used [78]. Meanwhile, KOH should be used when high selectivity (up to 1000) is required [17], for instance, producing high aspect ratio features. Some publications state that NaOH can even exceed KOH performance regarding selectivity [75]. Of course, combining various etchants one after another in single structure production and using different etchants' advantages is possible. This technique is called hybrid chemical etching [30, 79].

1.3.3. SLE of other transparent materials

One exciting prospect of SLE is the possibility of processing crystals like sapphire (Al_2O_3), Yttrium Aluminum Garnet ($Y_3Al_5O_{12}$ or YAG), lithium niobate ($LiNbO_3$) or crystalline quartz [80, 25, 81, 23]. Some publications affirm that nanogratings induced in a sapphire crystal are similar to those inscribed in fused silica [82, 26, 83]. However, the etching mechanism of the crystals is slightly different from amorphous materials. Laser-modified regions of crystalline material become amorphous [84]. Then, amorphous and porous regions

are etched out in aggressive etchants like concentrated (40% − 50%) HF at room temperature [82, 26, 83, 85, 86, 87] or around 35% KOH solution heated to 85 − 100°C [88]. Even more exotic etchant choices were demonstrated − sapphire was etched in a phosphoric and sulfuric acid mixture at 300°C temperature [13, 14, 89]. This showed that sapphire etched in 40% HF solution has selectivity which is in the order of a few thousand (up to 10000) [82, 26], and this value exceeds all the results showed on fused silica. YAG crystal shows even better selectivity, estimated at around 10^5 in HF acid. However, the SLE of crystals faces other problems: it is tough to avoid cracks. Cracks are caused by modified crystalline material becoming amorphous and creating significant volume tensions, which results in cracking the material [24]. Moreover, high selectivity comes from very low etching rates of unmodified material. Even the modified material etching rate is meager, as little as up to 100 μm/h [82, 25], for practical usage when a quite large structure is required, such a low etching rate can be unacceptable.

1.3.4. SLE applications

SLE stands in a relatively exciting place when considering practical implementation. The process itself needs a lot of considerations in terms of laser parameters and writing strategies. On the other hand, it is one of the most straightforward ways to produce 3D glass microstructures. As a result, possible applications have been shown in microfluidics, micromechanics, optics, and photonics. In photonics, some works demonstrated that SLE could be used for precise photonic component fabrication. By using tightly focused laser beams, it is possible to form tiny (down to ∼100 nm) repeatable structures which, after etching, can be used as photonic components [13, 14, 25]. Micro optic element fabrication was also shown using SLE [90]. However, direct fabrication of optical components is impossible due to relatively high surface roughness after the SLE process (∼hundred nm RMS). Thus, after etching, some annealing or other smoothing procedure is needed.

SLE excels in microfluidics for lab-on-chip (LOC) device fabrication. Glass is the preferred material for many set applications, as it is chemically inert in organic solvents, transparent, and mechanically robust. SLE provides a relatively easy and highly controllable method for producing surface and embedded channels. Here, SLE allows the formation of even complicated, curved, embedded 3D structures in glass [30, 18, 91, 29]. Paie et al. demonstrated that such channels could focus particles in the loops of the channels [91]. Other mentioned systems have the potential to be used in liquids filtering, such as on-chip flow cytometry [91]. Also, LOC microfluidic channels and some sort of integrated device inside it can be formed [72, 92]. Moreover, complicated microfluidic chains, including a filter and free movable integrated micro-switcher,

can be fabricated [30, 31]. This device can perform fluid filtering. In the larger channels, narrower channels volume is inserted, and only the smallest particles can go through the most narrow channels. Moreover, fabricated channels with a free movable valve can control the fluid flow direction. Other 3D microfluidic devices, which would be highly challenging for any different technique, can be fabricated [18].

SLE also demonstrates enormous promise in the field of micromechanics. For instance, a glass mechanical gripper can be produced and coated with metal to thermally induce movement [93, 27]. A similar optical sensor can also be made [32]. The SLE-made mechanical device is coated with a metallic coat layer, which moves when the potential changes. Information is read through the already integrated waveguide, and the signal strength depends on the displacement of the structure. The beauty of this device is that it can be fabricated out of one piece of fused silica. It is possible to integrate the waveguide and fabricate the structure at the same time, combining type I and type II modifications in one fabrication step by changing the laser parameters. Also, the device can be of arbitrary size, downscaled, and used as a component in more complex systems. Free movable micromechanical structures are also doable with SLE, such as gear systems [94]. The devices mentioned previously conceptually differ from this micro-mechanical structure. In the first case, we get movement by fabricating a structure with very high aspect ratio detail, making very thin glass details flexible. In the second case, a movable glass structure is fabricated because a slight gap is etched between rotating parts. Thus, using the SLE technique, various movable structures can be obtained.

2. Optimization of UVFS SLE

UVFS is a commonly used and widely investigated material in SLE. However, there still is some space for improvement to be done. This chapter will present two options for optimizing the SLE process. The first approach is laser and scanning parameters optimization. Another alternative is etching process optimization. The results provided in this chapter are based on papers **II** and **III**.

2.1. Motivation

SLE is a unique technology due to the opportunity to form 3D structures, which is complicated with other ultrafast laser glass microprocessing techniques e.g., laser ablation. In SLE, many process parameters play a significant role. On the one hand, laser parameters such as pulse energy highly affect induced nanograting properties and etching rate. On the other hand, the etching rate is influenced by pulse overlapping, which is a consequence of scanning velocity. However, regarding 3D structure fabrication, not only is pulse overlapping in a single line caused by scanning velocity critical, but modifications overlapping in XY planes and Z directions also play an important role.

Here we need to remember that SLE is subtractive technology where we need to modify material that needs to be removed. That means that we need to inscribe a negative of the original structure. From first sight, we can modify all the required volume by stacking scanning lines in an XY plane and repeating these planes in the Z direction. In this case, we have scanning spacing in the XY plane which we call hatching. Meanwhile, spacing in the Z direction will be called slicing. However, in many cases, glass tends to crack due to laser modification-induced volume tensions. The larger the volume modified, the higher the induced stress will be. Another side effect of dense scanning is the long fabrication time. Thus, complex structures cannot be formed blindly by scanning all the volumes. Instead, 3D structures must be constructed of specific components to reduce scanning volume and maintain only essential modifications. In general, even the most complex system can be built out of 3 different elements: planes, contours, and volume division into smaller parts. Thus the scanning strategy, in general, is chosen depending on the structure which needs

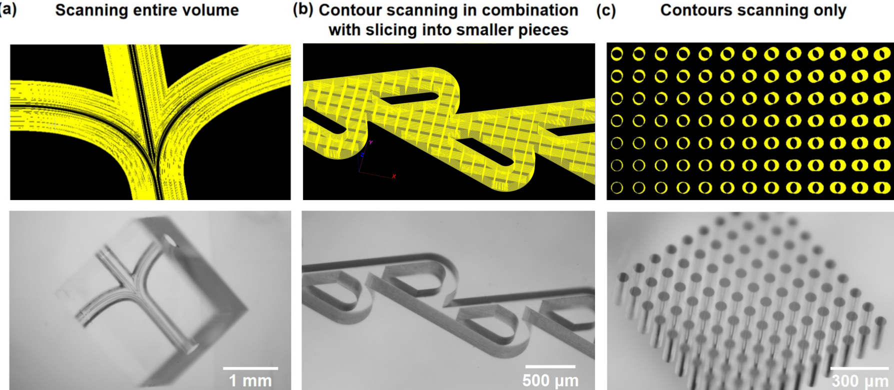

Figure 2.1: Demonstration of how different scanning strategies can be applied in various structures formation. (a) Scanning entire volume used for closed channel fabrication, (b) contour scanning in combination with slicing into smaller pieces applied in open channel chip fabrication, (c) contours scanning only applied in the production of holes matrix manufacturing.

to be formed. The idea of this is shown in Figure 2.1. For 3D channel structures in the volume, the entire channel volume needs to be modified to etch it efficiently, as seen in Figure 2.1 (a). For other 3D structures, possibly all three mentioned components are necessary, as demonstrated in Figure 2.1 (b). 2D-type forms can be done only by inscribing contours into the glass. Optimal hatching and slicing values must be chosen to maintain efficient etching for all these components. Thus the first experiment which needs to be done is the test of how etching depends on modification overlapping in different directions, which later constitutes mentioned 3D structures' construction components.

We have already discussed the importance of laser and scanning parameters in the SLE process. However, another significant part is etching. Not only do laser parameters affect etching rates, but also etchant reaction with the modified material. Many parameters, such as etchant concentration or etching temperature, can be varied in the etching process. Therefore, we must consider several factors when choosing the optimal parameters set. Usually, the goal is to have as high etching rates as possible. On the other hand, to form high aspect ratio structures, not only the laser-modified material etching rate matters but also the ratio between modified and unmodified material etching rates. In this way, micrometer precision and resolution structures can be produced.

This chapter will present how the laser radiation and scanning parameters affect the etching rate. Etchant optimization will also be presented. Etchant optimization relies on a simple assumption that the etching rate could be increased by increasing the wetting properties of the used etchant. Replacing part of the water with organic solvent reduces the contact angle of the prepared etchant and glass substrate. This phenomenon should stimulate the etchant

to penetrate inside inscribed channels. Later on, complex micromechanical structures will be demonstrated using the results obtained.

2.2. Experimental methods

Experiments described in this section are done with the "Laser Nanofactory" setup (Femtika Ltd.) whose optical scheme is shown in Figure 2.2. "Pharos" laser (Light Conversion Ltd.) is used as a radiation source. 1030 nm wavelength, 610 kHz repetition rate, and ~700 fs pulse duration laser radiation were used in this experiment. SLE dependency on the pulse duration has already been presented in previous works [19]. It was shown that the optimal pulse duration value is between 600 − 800 fs within the used experimental conditions. The previously mentioned parameters will remain constant during these experiments. The laser beam is focused on the sample with a 20x 0.45 NA objective with aberration correction. That means aberration can be compensated depending on the writing depth in the glass. Aberrations are compensated by rotating a ring on the objective, which changes the position of a specific lens group. Thus, aberrations are compensated for all modifications written in the described experiments. For all modifications written in the XY plane, the focusing depth was 500 μm. Laser radiation was focused to 1.5 μm diameter focused beam spot (at $1/e^2$ radiation intensity level) in the XY direction and ~15 μm in the Z direction. Aerotech ANT130XY positioning stages were used for sample positioning. The workstation used has a 5-axis positioning system (stages and scanner). However, only positioning stages were used in the described experiment to guide the laser beam over the sample. In these tests, almost pure amorphous SiO_2, normally referred to as fused silica glass (UVFS), was used.

This section will present a test of different etching rates by varying the process parameters. The standard way to evaluate the etching rate and selectivity is to measure volume modification or channel length after a single hour of etching. Single scan channels are written inside the bulk of glass with varying parameters. A test where only single-line channels are inscribed will be called a 1D test. The test where multiple intersected lines in a plane are written will be called the 2D test. If the inscribed channels are entirely in the bulk of the glass and do not have any opening to the surface, the glass substrate is cut in the middle of the channel at a right angle using a diamond-tip glass cutter. A scratch on the surface is formed, and the samples are broken through the created scratch. The cut side of the glass is polished. After that, the substrate with inscribed modifications is etched. Here all etching rate results were measured using an optical microscope Olympus IX73. By dividing channel length by etching time, the etching rate is calculated. In these experiments, the results are depicted not as etching rate dependency but as selectivity dependency.

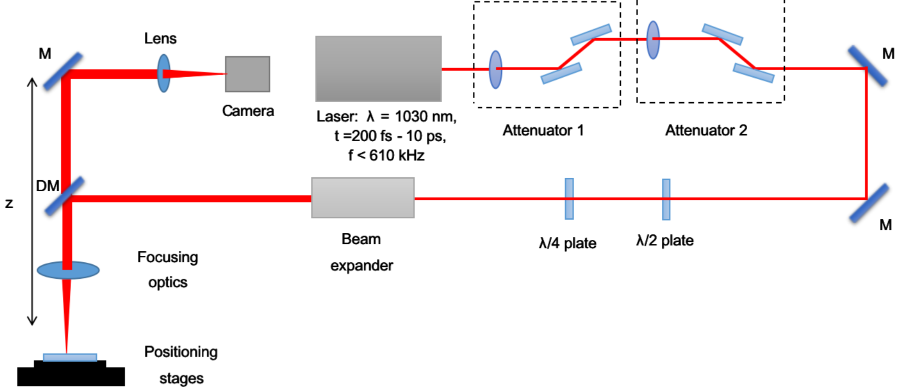

Figure 2.2: Scheme of the optical system used for SLE experiments. The optical setup consists of a femtosecond laser, two attenuators for power control, several mirrors (M), $\lambda/2$ and $\lambda/4$ waveplates for polarization control, a beam expander, dichroic mirror (DM), focusing optics, positioning stages, a camera for process monitoring and lens to focus the view to the camera.

We needed to measure the unmodified material etching rate for each case to calculate selectivity. This was done by measuring the thickness of the bulk of glass and etching the glass bulk for 24 h. After the etching process, glass thickness was measured again, and the unmodified material etching rate was calculated by dividing the etched glass thickness by the etching time. Finally, the selectivity is calculated by dividing the modified material etching rate by the unmodified material etching rate.

2.2.1. Experimental methods of scanning optimization

1D tests were performed to test the etching rate dependency on pulse energy, scanning speed, and light polarization. Single scanning lines varying mentioned parameters were inscribed inside the volume of glass. 40 μm width planes were inscribed to test the etching rate dependency on pulse overlapping in the XY and XZ planes. In this test, scanning speed was maintained constant at 50 mm/s, and only two different pulse energies were tested (246 and 369 nJ pulse energies which corresponds to 13.9 and 20.9 J/cm^2 energy density, accordingly. Acceleration and deceleration zones were prescribed in the fabrication algorithm to maintain constant exposure in all the modification zones. In all the cases, after the sample is exposed to the fs laser, the modified volume is etched out in 10 mol/L concentration KOH solution at 90°C.

2.2.2. Experimental methods of etchant optimization

Subsequently, etchant optimization experiments were done. Again the methodology of the experiment is similar to previous tests. Several identical single scanning lines were inscribed in the XY plane volume of the glass. In this test, all laser and scanning parameters remained the same – scanning speed was 10 mm/s, and average laser power was 300 mW, corresponding to 369 nJ pulse energy or 20.9 J/cm^2 energy density. To obtain the highest possible selectivity, linear polarization perpendicular to the scanning direction was used for selectivity testing experiments. The laser processing procedure was repeated on a few separate glass substrates, and each glass substrate was etched in a different etchant. Etching was performed in an aqueous KOH solution with varying isopropanol and KOH concentrations at 85°C. Exact concentrations will be listed where applicable. After a specified time, etched channel lengths are measured using an optical microscope.

2.3. Summary of results

2.3.1. Summary of scanning parameters optimization results

First, a 1D experiment was performed. The general schematics of this test are given in Figure 2.3 (a). By translating the sample in the XY direction, single lines were written inside the volume of the glass with particular sets of parameters such as different pulse energies, scanning velocities, and polarization. Afterward, the selectivity tests of the planes (i.e., 2D case) were performed. A set of lines with particular spacing in XY or Z direction were written inside the glass according to the schemes shown in Figure 2.5. Despite the varying spacing between lines, the width of the line blocks for hatching tests and the depth of the line blocks for the slicing test were kept the same (40 μm). Next, the glass substrates were cut in the middle according to the markings on the scheme. Sample cutting was needed only when modifications were entirely inside the glass volume and had no exit to any surface. Subsequently, samples were immersed in the etchant for 1 hour, rinsed in distilled water, and dried in ambient air. Finally, the etched channels' length was measured using an optical microscope. In this way, the 1D experiment showed selectivity dependence on the pulse energy, writing velocity, and light polarization. Meanwhile, 2D experiments showed plane selectivity dependence on the overlapping of scanned lines, pulse energy, light polarization, and etching direction.

The results of the 1D experiments are shown in Figure 2.3. After writing single lines in the XY plane, the highest obtained selectivity value is around ∼650. It was achieved with the polarization perpendicular to the scanning di-

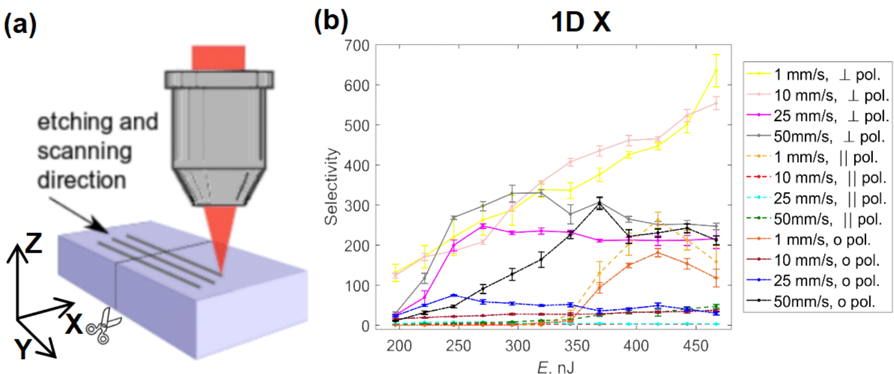

Figure 2.3: (a) Schematics of 1D selectivity experiment. (b) Single line selectivity test results. Single lines are written in the XY plane with various parameters such as different pulse energies, scanning velocities, and light polarization.

rection, the lowest tested scanning velocity (1 mm/s), and the highest tested pulse energy (492 nJ). The particular scanning velocity and pulse repetition rate combination control overlapping between the pulses which define thermal relaxation of the energy. However, if pulse spatial and temporal overlapping is high, the volume heats. On the other hand, overlapping of the pulses changes the total dose absorbed by the volume unit. Thus, with lower scanning velocity, we transfer more energy to the material and observe stronger thermal effects, which leads to greater volume modification, changes modification morphology [21], and gives higher selectivity. Also, it can be seen that polarization perpendicular to the scanning direction gives the highest selectivity value. Meanwhile, polarization parallel to the scanning direction shows the lowest selectivity. This etching process dependency on polarization has already been reported in previous studies [16], and in this work, the results obtained correlate with previously reported results. Furthermore, the selectivity tends to saturate for the most tested parameters. Interestingly, the selectivity even drops when the pulse energy increases.This was also demonstrated in previous works [21, 19, 56]. SLE has a specific parameter window where formed nanogratings react with an etchant effectively. If the pulse energy is lower, the most likely inscribed modification is a type I modification; if the pulse energy is higher, possibly a type III modification is formed. None of these is suitable for effective etching. However, the absolute value of the pulse energy depends on the whole parameter set. Thus, optimal pulse energy values need to be chosen for the most effective SLE process.

On the one hand, the specific parameters set change the material structural properties, influencing the modified material reactivity with the etchant. However, specific parameter sets influence the size of the modification itself. This can be seen in Figure 2.4, where SEM images of nanogratings inscribed with

different tested pulse energies (246 and 369 nJ) and different polarizations are shown. Before SEM measurements, samples with formed nanogratings were washed in a 5% HF solution and rinsed in water. This was done to clean nanogratings from the debris after laser modification. According to SEM images, modifications inscribed with higher pulse energies are larger than those inscribed with lower pulse energies. Moreover, modifications inscribed with circular polarization appear to have a round shape. Meanwhile, a modification written with linear polarization tends to be elliptical and elongated in the direction of nanogratings. These modification size properties could also impact etching rates because larger channels can be etched faster due to easier etchant penetration into the sample and better etchant diffusion in the channel. On the other hand, different pulse energies do not change the nanogratings periodicity significantly. Despite that, we can see that the upper layer of modification written with higher pulse energy reacts with the etchant faster, which implies that higher pulse energies create greater material structure changes. However, additional research on material structural changes needs to be done to confirm that.

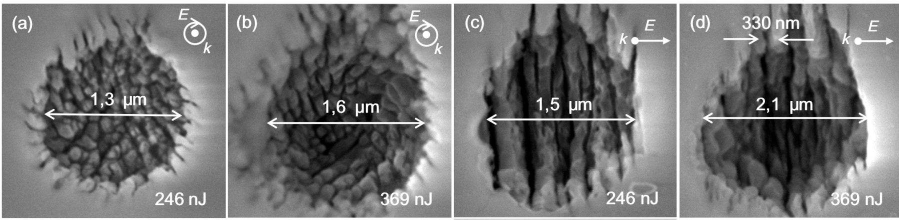

Figure 2.4: SEM images of laser-induced nanogratings in UVFS. (a) Nanogratings created with circular polarization, and 246 nJ pulses, (b) with circular polarization, and 369 nJ pulses (c) with linear polarization, and 246 nJ pulses, and (d) with linear polarization, and 369 nJ pulses.

This test aimed to optimize processing for high-throughput 3D glass manufacturing. In SLE, laser inscription is a process that cannot be to parallelized with a standard laser workstation. On the other hand, etching may be a time-consuming process, but it is easy to etch many structures simultaneously and have a parallel process. In this work, throughput will be mentioned as the efficiency of the laser inscription process. Several important conclusions were drawn from the results already obtained. The highest tested translation velocity (50 mm/s) was chosen for further experiments to get the highest throughput. Also, we chose 2 pulse energies – the lowest possible pulse energy, which gives a selectivity value close to the maximum in case of polarization perpendicular to the scanning direction (246 nJ), and the pulse energy value that gives the highest value with circular polarization (369 nJ). Higher pulse energy is not a practical choice for complex 3D structure fabrication due to high volume ten-

sions leading to structure cracks. Usually, the lowest possible pulse energy is beneficial because lower pulse energy leads to lower tensile stress in the volume, minimizing the possibility of crack formation.

While 1D experiments give interesting insights into the process, they do not paint the complete picture. 2D experiments are much closer to the actual experimental conditions of 3D fabrication and, thus, are investigated next. The motivation underlying such experiments lies in a relatively limited understanding of the etching process outside single-line fabrication (i.e., 1D case). It is known that light polarization affects nanograting orientation direction [16]. Pores parallel to the scanned lines are obtained in the case of polarization perpendicular to the scanning direction. When considering this in the context of SLE, this nanograting configuration allows the etchant to penetrate deep inside the modification. In this way, light polarized parallel to the scanning direction induces pores perpendicular to the scanning direction. With this nanograting configuration, the etchant quickly penetrates only to the first pore, resulting in a thin wall between pores that must be etched. These thin walls between the pores slow down the etching. However, these insights are viable when considering single lines. The process becomes more complex when we form the planes of multiple lines. Different polarization-induced modifications might be induced in the same volume of the material, potentially overlapping each other [95]. Additionally, in the case of planes, the initial opening formed during etching is bigger, allowing easier diffusion of the etched glass, further expediting the process. Some planes, such as XZ plane etching properties, have already been reported. However, due to the voxel shape, this only represents part of the picture of the process for 3D structure formation. Thus, here we present a broader view of 2D plane SLE research, leading to a better understanding of arbitrary shape structure formation.

The primary goal of the 2D experiments was to test etching rate peculiarities depending on the direction of the inscribed plane and etching direction. The most common way to fabricate 3D structures is layer-by-layer fabrication. Thus, in this experiment, we will only consider orthogonal planes tied to axes of the positioning system: XY, XZ, and YZ. From a laser structuring perspective, XZ and YZ planes can be considered equivalent, as in the Gaussian focusing case voxel is symmetrical in the XY plane, leaving only two types of planes: horizontal and vertical. One additional variable from the etching experiment side is the etching direction, i.e., from which side inscribed modifications will be exposed to the etchant. Therefore, 4 different cases can be distinguished to get the complete picture of the process (Figure 2.5).

2D horizontal (XY) plane test results when etching directions are parallel and perpendicular to the scanning directions are shown in Figure 2.5 (a) and (b), respectively. When the etching direction is parallel to the line writing direction, the highest selectivity of around 1200 is obtained by inscribing lines with

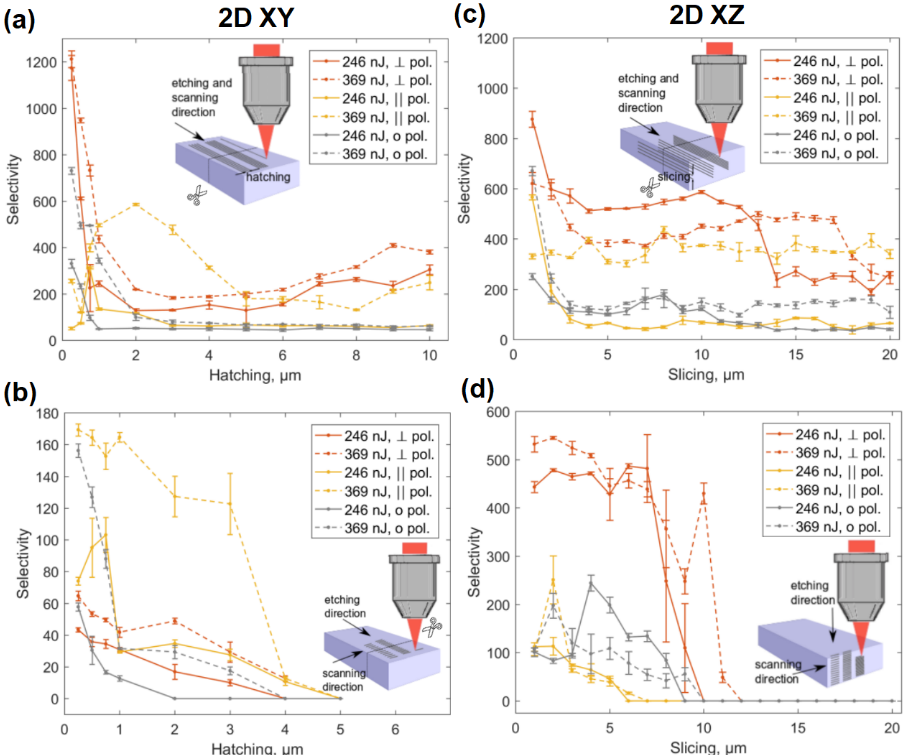

Figure 2.5: 2D (plane) selectivity test results. (a) XY plane etched parallel to the scanning direction selectivity dependency to hatching, (b) XY planes etched perpendicularly to the scanning direction selectivity dependency to hatching, (c) XZ planes etched parallel to the scanning direction selectivity dependency to slicing, (d) XZ planes etched perpendicular to the scanning direction selectivity dependency to slicing.

the lowest tested hatching step (0.25 μm which corresponds to appoximately 90% inscribed modifications overlapping) and by adopting polarization perpendicular to the scanning direction. In our experiment, by increasing hatching values to more than 2 μm the overlapping between adjacent lines is lost (spot diameter of used 0.45 NA objective – $2\omega_0 = 1.5$ μm), and selectivity drops to the values below 500. It is remarkably similar to the single-line selectivity achieved in 1D experiments. As expected, when the etching direction is perpendicular to the scanning direction, the obtained selectivity is around 6 times lower than in the previous case test (up to ∼17). However, this test determines the maximum possible hatching step, which in this case is 4 μm when modifications no longer overlap. From the practical perspective, during structuring, both instances are combined (if XZ and YZ planes are fabricated without tuning polarization), leading to undesired results, as if selectivity is close to 0 for at least one direction, it will be impossible to etch the entire 3D structure. As an outcome, fast polarization control is needed if light polarization is to be tied to the translation direction. As such an approach is hard to achieve, a much simpler solution is to use circular polarization. Then, translation direction is no longer a variable during structuring. Additionally, this work shows that the etching rate does not drop dramatically when circular polarization is used. Thus, due to practical considerations, circular polarization was used to fabricate all the 3D structures in this work.

Later, vertical 2D (XZ/YZ) plane tests were performed. The results of these tests are shown in Figure 2.5 (c, d). The highest selectivity is achieved with the lowest tested slicing between scanning lines (1 μm). When slicing is increased, selectivity drops drastically. However, when polarization is parallel to the scanning direction, a further increment in slicing slightly increases the etching rate. This indicates that interference between modifications creates suitable volume nanopatterns, which affect the etching properties. The test with the etching direction perpendicular to the scanning direction determines the maximum possible slicing parameter, around 10 μm which corresponds to approximately 30% of the inscribed modifications overlapping. Higher slicing values will be an obstacle to surface etching. Overall, the higher maximal slicing step can be explained by the inherent elongation of the voxel in the Z direction due to Gaussian focusing properties. Here we determine that with our tested setup, maximum hatching could be 4 μm and slicing 10 μm with linear polarization. However, for the practical 3D structure formation, lower values are desired in order to have higher selectivity. Usually, circular polarization is required for 3D structure formation to maintain a similar etching rate in all directions. Hence, the maximum hatching value with circular polarization should not exceed 1 μm hatching and 9 μm slicing, which corresponds to approximately 40% of the inscribed modifications overlapping.

In Figure 2.3 (b) and Figure 2.5 (a – d), error bars appear, which was

calculated as RMS from separate lines measurement. On the one hand, it represents the accuracy of the obtained result. On the other hand, it can be interpreted as an anisotropy of the etching. Several lines inscribed with identical parameters usually are not identical in length due to anisotropy of the etching caused by uncertainties of etchant diffusion during the etching. Inscribed planes after the etching typically do not have sharp and regular ends to the same anisotropy. However, the scale of error bars in most cases does not exceed 10% of the total result, implying that anisotropy of the etching is not a critical factor in the tested cases, and it should not substantially impact 3D structure formation.

Finally, it was decided to measure the surface roughness of the etched surfaces. Here we measured both XY and XZ/YZ surface roughness. These results are depicted in Figure 2.6 (a, b). In both plane cases, the lowest surface roughness of around 200 nm RMS is obtained with the lowest tested slicing/hatching (0.5 μm). Increasing the spacing between lines raises the roughness value which reaches around 800 nm RMS. Looking back to the same surface selectivity, it can be concluded that higher surface selectivity gives lower surface roughness. Selectivity correlation with surface roughness has already been reported in other works [73]. However, polarization influence on fabricated structure surface roughness has not been studied before. As shown earlier, polarization strongly affects selectivity. Nonetheless, surface roughness dependency on polarization is insignificant, and the lowest value in both cases is obtained independently of polarization. In conclusion, spacing between scanning lines affects formed surfaces more significantly than pulse energy or light polarization. Also, in addition to minimal surface roughness, SLE allows for achieving minimal taper on vertical surfaces (Figure 2.6 (c)). This is very attractive for usage in precise microfluidics or as a highly rigid molding master for soft lithography [96].

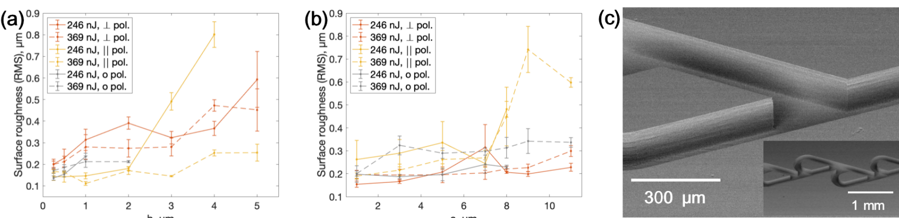

Figure 2.6: Surface roughness (calculated as RMS) acquired using SLE of horizontal (a) and vertical (b) surfaces. All values are below 1 μm. (c) Zoomed in SEM image of surfaces of an example structure (with the whole element being in the inset), showing good surface quality and minimal taper achievable in practice.

2.3.2. Summary of etchant optimization results

This experiment begins with testing isopropanol's influence on the etching rates of unmodified fused silica by changing KOH and isopropanol concentrations. The chosen range was 1 – 10 mol/L for KOH and 0% – 50% for isopropanol. The unmodified material etching rate measurement was performed by measuring the thickness of the fused silica sample before etching and then etching it for 24 h. After etching, the thickness was measured again, and the etching rate of the unmodified material was calculated. Since the etchant does not need to penetrate inside the glass volume and the etchant's diffusion is not confined, the etching rate of unmodified material should remain practically the same over the experiment time scale. Results are shown in Figure 2.7 (a). The KOH concentration influenced the etching rate of unmodified material more than the amount of isopropanol in the mixture. The peak value of ~1.5 μm/h was achieved at the highest KOH concentration and a low 5% concentration of isopropanol.

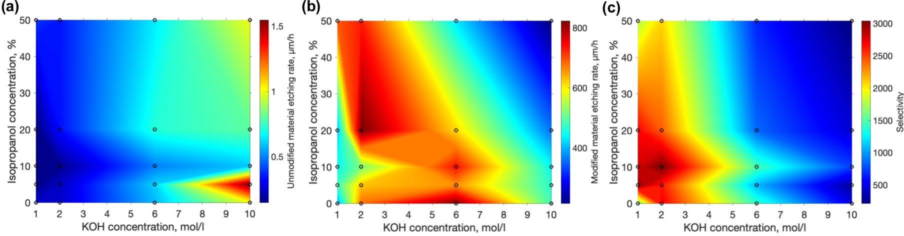

Figure 2.7: Etching rates of unmodified (a) and laser modified (b) fused silica acquired with different KOH and isopropanol concentrations. The highest achieved values are ~1.50 μm/h for unmodified and ~820 μm/h for modified materials, respectively. (c) Selectivity is derived by dividing results of part (b) by part (a). The highest value is ~3000 at 2 mol/L KOH and 10% isopropanol, showing a clear tendency that lower KOH concentrations and a moderate amount of isopropanol positively impact the selectivity.

Next, the etching rate of the modified material was measured. The experiment protocol followed the idea of inscribing horizontal lines into the material one after another. The etching rate was determined by measuring the length of a 1 h etched channel formed during the described process. Measured values are plotted in Figure 2.7. In contrast to the unmodified material etching results, the highest etching rate (~820 μm/h) was achieved at 6 mol/L KOH concentration and with no isopropanol. However, another peak of the higher etching rate of ~820 μm/h was observed at the 2 mol/L KOH concentration and with 20% of isopropanol, showing that organic solvent, under special conditions, can have a positive impact on the etching rate of laser modified material.

The selectivity always limits the complexity and feature size of SLE-produced structures since it describes the limit of the maximum aspect ratio of

etched features. Thus, here we provide results in terms of selectivity. The selectivity calculated in this work is given in Figure 2.7 (c). The highest achieved value is ∼3000, which is more than two times higher than the highest value reported in the literature to the best of our knowledge [18, 20]. In addition, it was achieved in a mixture containing small amounts of both KOH (2 mol/L) and isopropanol (10%). This is also far from both peak etching rates of unmodified and modified materials. If no isopropanol were used, 2 mol/L of KOH would yield a selectivity of ∼2700, which is ∼13% lower than the maximum value. Therefore, the positive impact on selectivity of using small amounts of isopropanol is evident. Interestingly, it is a far higher value than the selectivity of ∼500 at 10 mol/L KOH – a standard value used by multiple groups. Thus, another conclusion that can be drawn from this work is that even a reduction in KOH can help increase selectivity. However, care should be taken when applying this methodology since a decrease in KOH concentration would result in longer etching times.

The primary idea behind introducing isopropanol into the aqueous KOH mixture is to improve the wetting properties of the liquid and, hence, allow easier diffusion of dissolved silicate ions from the fused silica-etchant interface. Thus, to obtain further insights into the acquired etching results, contact angles of different ratios of KOH and isopropanol on fused silica were measured. Results are given in Figure 2.8. Generally, with the increase of isopropanol concentration, the contact angle becomes smaller, proving that this organic solvent should increase wetting properties. However, the area with the lowest contact angle, which is below 2 mol/L KOH and above 20% of isopropanol, coincides neither with the highest etching rates nor with the highest selectivity. On the contrary, the highest etching rates are achieved under experimental conditions with relatively high contact angles – 34.5° for the highest etching rate for unmodified material and 32.1° for laser-affected volume. Nevertheless, the highest selectivity value coincides pretty well with the area where the contact angle starts to drop significantly (17°) at the highest selectivity conditions. At the same time, it is not at the lowest achieved contact angle – 5.2°. Therefore, some other interactions should be considered.

The chemical aspect has to be considered to understand the complete picture of the process. Indeed, when etching is performed, the resulting chemical reaction is the same in both cases with and without isopropanol. When fused quartz is exposed to a solution of KOH, potassium silicate, and water are formed (see Equation 2.1). However, in addition to the increased wetting effect of fused quartz described above, the introduction of isopropanol into the system also negatively influences selectivity. The requirement for the reaction is the formation and dissolution of K_4SiO_4 in the reaction mixture. Potassium silicate is soluble in water (it is possible to dissolve salt in boiling water) and slightly or completely insoluble in alcohols. Potassium silicate dissolves

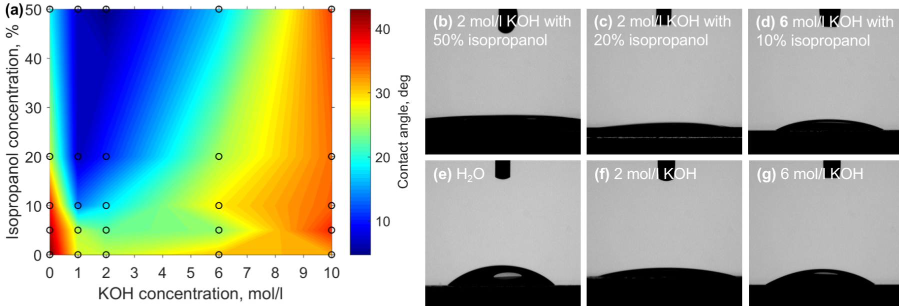

Figure 2.8: (a) Contact angle at different mixtures of KOH and isopropanol. While at the point of highest selectivity contact angle is relatively reduced, it is not the lowest measured value. (b – g) different etching solutions contact angle measurement pictures.

more readily under pressure at a temperature of 80°C [97, 98]. Even though the etching was carried out at a temperature of 85°C, in a closed system, the temperature of the etchants had to be lower because of the boiling point of isopropanol, which is 82.5°C. Consequently, the higher isopropanol concentration determines the lower temperature of the mixture and the lower amount of a more suitable solvent, resulting in a slower etching process at extremely high isopropanol concentrations.

$$SiO_{2(s)} + 4K^{+}OH^{-}_{(aq)} \rightarrow K_4^{+}[SiO_4]^{4-}_{(aq)} + 2H_2O_{(I)}. \tag{2.1}$$

The solubility of potassium hydroxide is ∼11 g/10 mL (28°C) and 121 g/100 mL (25°C) in isopropanol and water, respectively. It can be suggested that isopropanol acts as a surfactant, accumulates at the solid/liquid interface, and thereby prevents KOH access to the silica sample's surface. We considered a model of the behavior of isopropanol molecules at the surface during etching. The described model considers that, for a saturated concentration, a layer of isopropanol molecules is formed at the solution's surface rather than being diluted. The abundance of isopropanol affects the formation of a monolayer of alcohol molecules at the surface of the sample [99, 100, 101]. The highest selectivity value was obtained for 2 mol/L (10.89 g/100 mL, here KOH molar mass 56.1056 g/mol, isopropanol density at 28°C is 0.7783 g/mL) KOH concentration, which corresponds to the maximum alkali solubility in isopropanol. Further increasing the alkali concentration in the mixture results in a decrease in selectivity. This evidence confirms the described model of isopropyl-alcohol monolayer formation on the surface because the etching reaction takes place only at the surface and the etchant contact. However, to prove this hypothesis, further studies need to be performed.

Thus, overall, while a lower contact angle helps with easier etchant and

product diffusion between the solution and the fused silica interface, behaviors of isopropanol, such as lower boiling point and limited dissolution of KOH, result in a slowed-down reaction, forming an ideal balance at experimental conditions of 2 mol/L KOH and 10% isopropanol.

Despite the impressive etching rate and selectivities demonstrated, etching rates tend to diminish over time. It was measured how the etching rate changed over time. The results of the etching rate after 2, 4, 8, and 12 h are depicted in Figure 2.9 (a – d). Comparing etching rates after 1 hour of etching and after 2 hours of etching, the rates drop approximately twice (a). After 4 h, etching rates decrease twice again. Finally, after 8 and 12 h, the etching rate is between 100 and 200 μm/h. The explanation for such a decrease in etching rate is simple – the deeper the etchant needs to penetrate into the channels, the more it dilutes and struggles to etch the channel at the deepest point. Nonetheless, a unique property of the etchant can be observed with isopropanol. Isopropanol allows the maintenance of a higher etching rate. Possibly, isopropanol induces more effective penetration into the channel. Thus, another positive side of isopropanol is the possibility of achieving and maintaining a higher etching rate for longer. In general, according to these graphs, we can conclude that if high selectivity and a high etching rate are desired, the etching time should be short enough (shorter than 2 – 3 h). Otherwise, it is impossible to maintain selectivity and an aspect ratio higher than 1000 because of the reduction in the etching rate during longer etching times. This might be problematic if relatively large or long structures are needed.

After we performed some experiments, we noticed one more exciting property, which is affected by the etchant. We have observed that structures etched with lower KOH concentration etchants tend to have worse surface quality than structures etched with high concentration etchants. To check this phenomenon, we inscribed the surface in the XY plane and etched it away with different concentrations of etchant. Surfaces were then inspected with an SEM. SEM pictures of the surfaces formed are shown in Figure 2.10 (a – g). Although the surfaces look different, surface roughness was measured for these surfaces by using an optical profilometer (Sensofar PLμ2300). Figure 2.10 (h) shows the correlation between surface roughness and etchant concentrations. The higher the etchant concentration is, the lower the surface roughness that could be obtained. On the other hand, looking back to previous results, lower etchant concentrations give higher selectivities. For comparison in Figure 2.10 (h), we added a surface etched with 5% HF solution with a surface roughness of around 200 nm RMS. Usually, HF shows substantially lower selectivities than KOH [17]. Thus, contrary to the previous part, we conclude that the higher the selectivity, the higher the surface roughness achieved after the etching. High selectivity usually means a low unmodified material etching rate. The result of a low unmodified material etching rate is that the etchant struggles to etch the

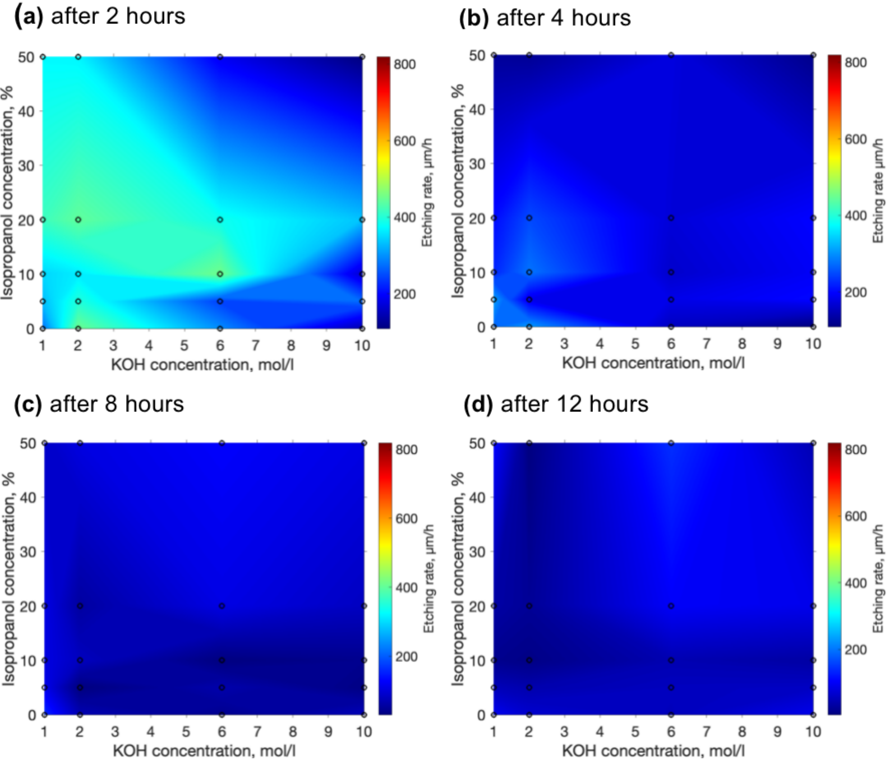

Figure 2.9: Etching rate evolution over time. (a) Etching rate after 2 h of etching, (b) after 4 h, (c) after 8 h, and (d) after 12 h.

walls between nanogratings. These not completely etched nanograting walls make the surfaces rougher. However, in most applications, the preferable option is to maintain both. Combined etching techniques need to be used to get that result. For example, etch the structure with low-concentration KOH etchant and smooth the surface with low-concentration HF solution. This is called the hybrid etching technique, which has already been demonstrated elsewhere [30]. A combination of a few different types of etchant, such as HF and KOH, allows us to obtain the highest throughput because HF shows a higher etching rate for effective large-volume removal. Meanwhile, KOH enables us to achieve high selectivity for precise feature etching.

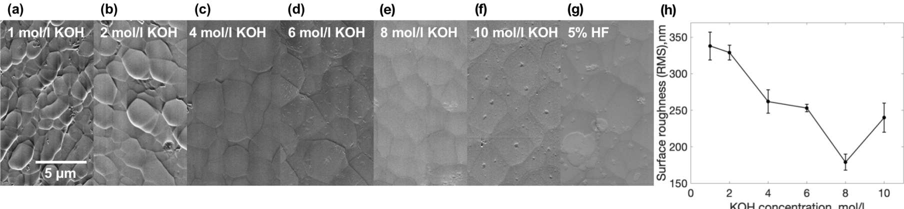

Figure 2.10: (a – g) SEM micrographs of surfaces etched in various concentrations etchants. (h) Surface roughness dependency on etchant concentration.

3. SLE of crystalline sapphire

This chapter is dedicated to presenting the SLE of crystalline sapphire. The results provided in this chapter are based on paper **IV**.

3.1. Motivation

Due to high mechanical resistance and good optical properties, sapphire is attractive in many applications. However, the usage of this material is limited due to the complicated processing of sapphire. Sapphire could be processed in many ways, from mechanical CNC machining to direct laser processing, such as ablation [3, 4, 10]. On the other hand, SLE also can be applied for sapphire processing. Sapphire SLE is less investigated than SLE for UVFS. Sapphire SLE still needs to be fully developed to fabricate functional 3D devices. Therefore, research on a sapphire SLE and testing different process parameters, such as various laser wavelength and etching protocols, will be presented here. We have chosen widely adopted potassium hydroxide, sodium hydroxide [75], hydrofluoric acid [85], and a mixture of sulphuric and phosphoric acids [89] etching protocols and compared them. Moreover, different radiation wavelengths for modification inscription were tested because the induced nanogratings periodicity is determined by wavelength [26], which later affects the etching properties. Finally, we identified the best protocol for sapphire SLE and made some test structures using this approach.

3.2. Experimental methods

SLE experiments were performed with C-cut crystalline sapphire. In these tests, 0.5 mm thickness sapphire substrates were used. Many different laser parameters, as well as various etching protocols, were tested. In these experiments, different wavelengths – 1st (1030 nm), 2nd (515 nm), and 3rd (343 nm) harmonics of Yb: KGV femtosecond laser (Pharos, Light Conversion Ltd., Lithuania) – were applied for nanogratings inscription. Focusing optics differed for all tested wavelengths to maintain the same focused beam diameter. A 0.4 NA aspherical lens was used to focus 1030 nm radiation. A

0.2 NA aspherical lens was used to focus 515 nm radiation, and a 0.1 NA objective focused 343 nm radiation. All tested wavelengths were focused to an approximately 1.5 μm beam spot (at $1/e^2$ radiation intensity level) in the XY direction. In these experiments, circular and linear polarized light was used. In single-line tests, linear polarization perpendicular to the scanning direction was used to maintain the etching rate as high as possible. Meanwhile, circularly polarized radiation was used in the experiment where scanning in all XY directions was done, for example, in 3D structure experiments. Sample positioning was performed by using XYZ linear positioning stages (Aerotech, USA). In this part, inscribed nanogratings were etched with various chemicals such as a 35% potassium hydroxide (KOH) mixture with water, a 25% sodium hydroxide (NaOH) mixture with water, and a 48% hydrofluoric acid (HF) and 78% sulphuric, and 22% phosphoric acid mixture (H_2SO_4 and H_3PO_4). Utilization of all of these etchants differs: KOH and NaOH were used at 90°C, HF was used at the ambient temperature (20°C), and H_2SO_4 and H_3PO_4 were used at 270°C.

First of all, principal experiments of single lines in the XY plane were performed to test how pulse energy (100, 200, 300, 400, and 500 nJ), radiation wavelength (1030 nm, 515 nm, 343 nm), and the used etchants (NaOH, KOH, HF, H_2SO_4 and H_3PO_4) affect the etching rate. In this experiment, pulse duration (200 fs) and pulse repetition rate (610 kHz) remain constant. The light was linearly polarized perpendicularly to the scanning direction to obtain etching rates that were as high as possible. The main idea of the experiment is to write single lines inside the bulk of the sapphire. Then, the substrate is divided in the middle perpendicularly to the written lines. Finally, the side of the divided plate was polished (using a fine diamond powder on the lapping machine), and modifications were etched. The etching rate was evaluated by measuring the length of the etched channel and dividing it by the etching time. This experiment gives us data about the etching rate of the modified material. The idea of this test is shown in Figure 3.1 (a). Additionally, during the same experiment, etching rates of unmodified material were evaluated by measuring substrate thickness before and after etching. The etching rate of unaffected material allows us to estimate selectivity in each case.

Subsequently, etching experiments of 3D structures were executed. During this experiment, cylindrical 1 mm diameter 3D structures were written into a plate of sapphire. The scheme of this experiment is depicted in Figure 3.1 (b). During this experiment, we tested etching dependency on radiation wavelengths, pulse duration (200 fs – 1 ps), and different etchants to find a protocol for 3D structure fabrication. Finally, when optimal parameters for the etching were found, the morphology of the modified areas was investigated after and before the etching process. For that, 10 μm wide surface modifications were written and etched in the previously mentioned etchants. The scheme of

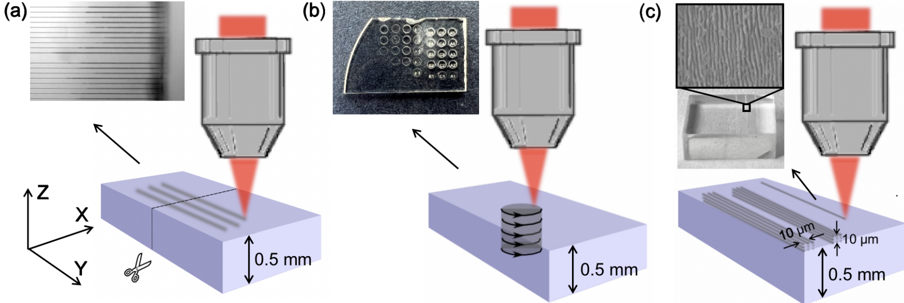

Figure 3.1: The schemes and the resulting pictures after the etching of performed experiments. (a) Single lines experiment when lines from a single scanning are written in the volume of material to test the etching rate of modified material. (b) Scheme of 3D experiments when cylindrical structures are written through the whole plate thickness. (c) Laser-induced surface changes for modification morphology observation after the etching procedure.

this experiment is shown in Figure 3.1 (c). These morphologies provide some insights into why some etchants are not suitable for sapphire 3D structures' fabrication. Finally, a few 3D structures were fabricated from sapphire using the same setup and employing the determined fabrication protocol.

3.3. Summary of results

We will start the discussion with the single-line test results, shown in Figure 3.2 (a). During the experiment, it was found that the highest etching rate (200 μm/h) is obtained with an H_2SO_4 and H_3PO_4 mixture when the material is irradiated with 1st harmonic radiation and the highest tested pulse energy of 500 nJ, which corresponds to 28.2 J/cm^2 energy density. Meanwhile, lower etching rates up to 100 μm/h were obtained with NaOH and KOH etchant. The lowest etching rates of up to 50 μm/h were demonstrated by modifications etched with HF. In all the cases, the modification written with 1st harmonic radiation showed the highest etching rates, which was at least a few percent higher than those of the results achieved with the 2nd harmonic, and at least a few times higher than the etching rates obtained with the 3rd harmonic. This result could be explained by the higher periodicity of the nanogratings. The nanograting period is equal to $\lambda/2n$, where λ is the wavelength of the radiation used and n – is the refractive index of the material [54, 26]. The same tendency was observed in these experiments. SEM images of nanogratings inscribed with 1030 nm, 515 nm, and 343 nm are demonstrated in Figure 3.3. Nanograting periods induced with 1030, 515, and 343 nm are correspondingly 340, 150, and 100 nm. These values are close to theoretical values. Subsequently, longer periods that result from higher wavelengths enable easier liquid penetration into the

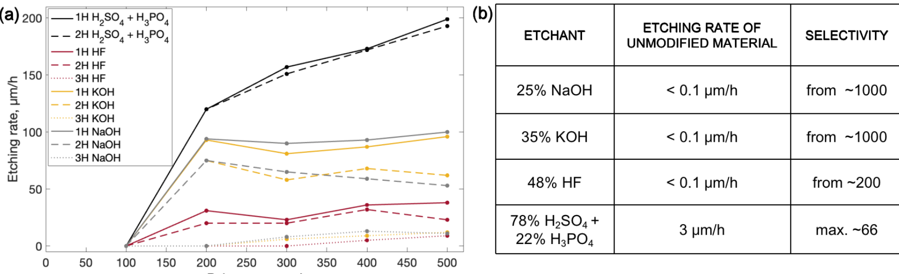

ETCHANT	ETCHING RATE OF UNMODIFIED MATERIAL	SELECTIVITY
25% NaOH	< 0.1 µm/h	from ~1000
35% KOH	< 0.1 µm/h	from ~1000
48% HF	< 0.1 µm/h	from ~200
78% H_2SO_4 + 22% H_3PO_4	3 µm/h	max. ~66

Figure 3.2: (a) Graphs of etchings rates of single lines written and etched by different processing protocols. 1H, 2H and 3H stand for 1st, 2nd, and 3rd harmonics of 1030 nm wavelength laser, which is 1030 nm, 515 nm and 343 nm, respectively. (b) Table of the etching rate of unmodified material etched by different etchants and selectivity evaluation according to modified and unmodified material etching rate results.

nanogratings due to the capillary forces and surface-wetting properties [102]. Etching rates that were only slightly lower than the maximum results were achieved by using 2nd harmonic 500 nJ pulse energy or 28.2 J/cm^2 energy density radiation. Meanwhile, modifications created by the 3rd harmonic radiation show only a few μm/h etching rates. To fabricate 3D structures, the etching rate of modified versus unmodified regions also matters. A high ratio between modified and unmodified material etching rates is required to obtain a high aspect ratio of fabricated structure features. The unmodified material etching rate was evaluated, and, subsequently, the selectivity value could be calculated. For some tested etchants, the unmodified material etching rate value was in the range of the accuracy of the used device. Therefore, only approximate selectivity values are provided. The results of the unmodified material etching rate and the evaluation of selectivity are shown in Figure 3.2 (b). Only the H_2SO_4 and H_3PO_4 mixture showed a significant unmodified material etching rate of around 3 μm/h. Meanwhile, unmodified material could be barely etched by using NaOH, KOH, or HF. When we try to evaluate selectivity with such a low unmodified material etching rate for NaOH, KOH, and HF, it leads to high selectivity values starting from 1000. The high etching rate of unmodified material with sulphuric and phosphoric acid leads to a low selectivity value of 66; despite that, this etchant shows the highest etching rate of modified material.

In this experimental part, the main goal is to demonstrate 3D structures that come out of sapphire. Thus, after single lines tests, 3D tests were performed to find the protocol that could allow us to obtain 3D structures. Identical parameters set for the single lines test were investigated. Additionally, various pulse durations were tested. Cylindrical structures through the whole sample depth were written into a 500 μm thickness sapphire plate by changing parameters for each cylinder. The results of this experiment can be seen

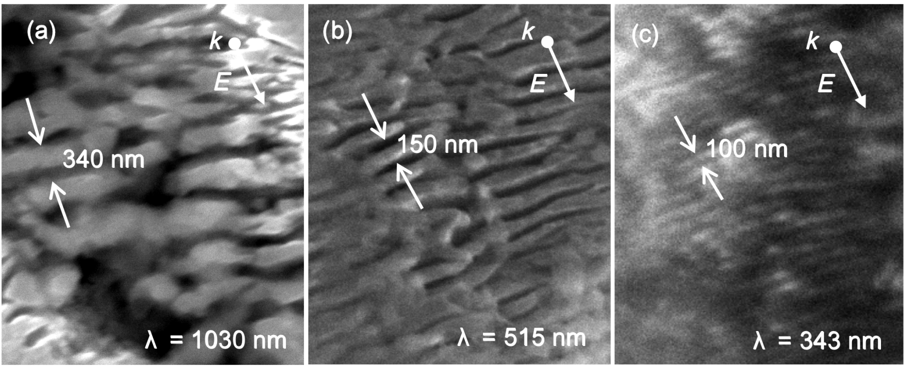

Figure 3.3: SEM images of nanogratings induced with (a) 1030 nm, (b) 515 nm, and (c) 343 nm radiation.

in Figure 3.4. The 3D experiment showed that the best parameters, which allow the most efficient etching of the structures, are 1st harmonic radiation with 200 fs duration pulses and 300 – 500 nJ pulse energies that correspond to 16.9 – 28.2 J/cm^2 energy densities of one pulse. The only etchant which etched the structures out of the plate was an H_2SO_4 and H_3PO_4 mixture. By using other tested etchants KOH, NaOH and HF, cylindrical structures could not be etched out of the plate even after 48 h of etching. This result raised the question of what is the reason the other tested etchants cannot etch out 3D structures.

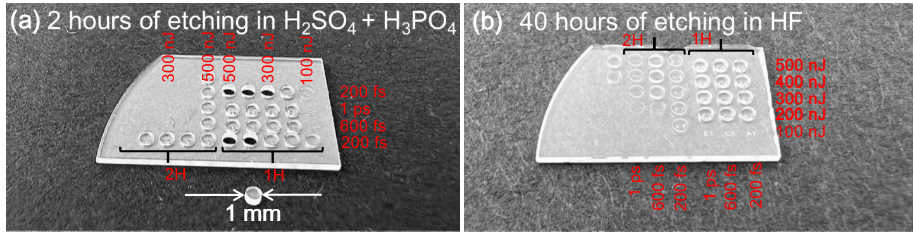

Figure 3.4: Cylindrical structures written with different wavelengths and pulse duration radiation. (a) Structure etched in H_2SO_4 and H_3PO_4 mixture, (b) structure etched in HF acid.

To test this phenomenon, it was decided to investigate etched and unetched surface modifications and indicate their behavior before and after the etching. Surface modifications were written within the parameter set determined as the most efficient in the previous experiment (1030 nm wavelength radiation, 600 kHz pulse repetition rate, 200 fs pulse duration, and 500 nJ pulse energy). Written 10 μm deep and 10 μm wide modifications on the surface of the sample was etched in different etchants. Scanning electron microscope (SEM) pictures of variously etched and unetched modifications are presented

in Figure 3.5. Moreover, the depth of the etched modifications was measured in each case. In Figure 3.5 (a), an unetched modification can be seen right after the laser processing. Before the etching, material modifications are covered by residue remaining after the processing. The unetched modification already has a depth of approximately 0.5 μm. After 1 h of etching in 35% of KOH and 25% of NaOH at 90 °C and at 48% of HF, all the residue is etched and nanogratings are uncovered. Pictures of nanogratings after the etching are depicted in Figure 3.5 (b – d). Depths of modifications etched in KOH, NaOH, and HF are 3 μm, 3 μm, and 7 μm, respectively. In contrast, after the etching modification only for 20 min in the H_2SO_4 and H_3PO_4 mixture, not only is there residue of lasering, but the nanogratings themselves are etched, which can be seen in Figure 3.5 (e). The depth of the etched groove is 9 μm. All these etchants react to material differently. Visually, HF etches out impurities from the surface the most efficiently. Meanwhile, after etching in NaOH, the highest amount of residue remains. In comparison with single lines results, HF tends to etch everything from the surface, NaOH and KOH tend to penetrate inside nanogratings. However, none of these etchants etch nanogratings, or in other words, the walls between laser-created pores. Thus, KOH, NaOH, and HF etchants cannot etch out 3D structures because part of the laser-affected material remains unetched. This insight suggests that not all material in nanogratings becomes amorphous or the amorphized material partly recrystallizes after laser-material interaction stops. Due to the crystalline phase dominant in the nanogratings, HF, KOH, and NaOH cannot be used effectively because they do not etch crystalline sapphire, as shown in Figure 3.2. On the other hand, H_2SO_4 and H_3PO_4 could etch both crystalline and amorphous materials.

After all the previous insights were acquired, the most efficient tested protocol was used for structure fabrication out of crystalline sapphire. A few basic 3D structures were fabricated for demonstration. These structures were fabricated out of a 0.5 mm C-cut sapphire plate using 1030 nm wavelength, 200 fs pulse duration, 610 kHz pulse repetition rate laser radiation, and H_2SO_4 and H_3PO_4 mixtures as an etchant. The first demonstrational structure was a hole array. In one case, holes of 100 μm diameter through the complete height of the plate with a pitch of 1 mm were produced, see Figure 3.6 (a, b). Additionally, a narrow single Z scanning line channels fabrication with a pitch of 10 μm is demonstrated in Figure 3.6 (c, d). In Figure 3.6, it can be seen that, after the etching, the etched walls are not perfectly vertical. The edges of the structure have non-written planes cut, and it forms after the etching due to the sapphire crystalline lattice. This is caused by the high etching rate of unmodified crystalline material. Subsequently, the honeycomb structure was produced out of sapphire. A structure with a 400 μm wall of a hexagon and a 200 μm wall thickness between hexagons is shown in Figure 3.6 (e – g). The surface roughness of the mentioned structure was measured using an optical profilome-

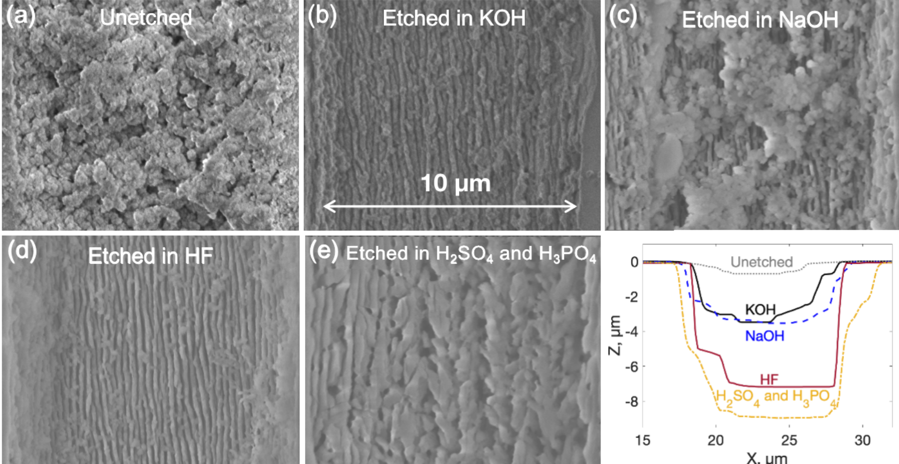

Figure 3.5: SEM pictures of laser-irradiated surface morphologies and measured profiles of the processed material. (a) Unetched surface modification, (b) surface modification etched in 35% KOH solution for 1 h, (c) surface modification etched in 25% NaOH solution for 1 h, (d) surface modification etched in 48% HF for 1 h, and (e) surface modification etched in H_2SO_4 and H_3PO_4 for 20 min. (f) Optical profilometer measured processed profiles of all presented modifications.

ter by placing the structure on its side, giving a value of 300 nm RMS. This value is comparable with those shown in fused silica SLE-made surfaces [73]. The lowest demonstrated etched fused silica surface roughness is approximately 100 nm RMS. Surface roughness is mostly determined by the morphology of induced nanogratings and how effectively material between nanogratings could be etched. Since fused silica is a less chemically inert material than sapphire, the expected etched sapphire structure roughness should be higher than for the same surfaces made in fused silica. To show the versatility of this technology, similar honeycomb designs with 100 μm and 50 μm wall thicknesses were also made (Figure 3.6 (h, i)). Walls thinner than 50 μm were fragile and did not survive the etching procedure. Since we were working with crystalline sapphire, it shows different etching rates of unmodified material in various crystalline orientations [89]. Thus, the tendency of a repeating sapphire crystalline structure can be seen in honeycomb structures. The edges of the etched structures appear to have a chamfer and are inclined according to a sapphire crystalline lattice. Nonetheless, these structures show the possibility of producing 3D structures out of crystalline sapphire. Due to the high mechanical and chemical resistance of sapphire, such structures show potential as micromechanical components in complex miniaturized systems.

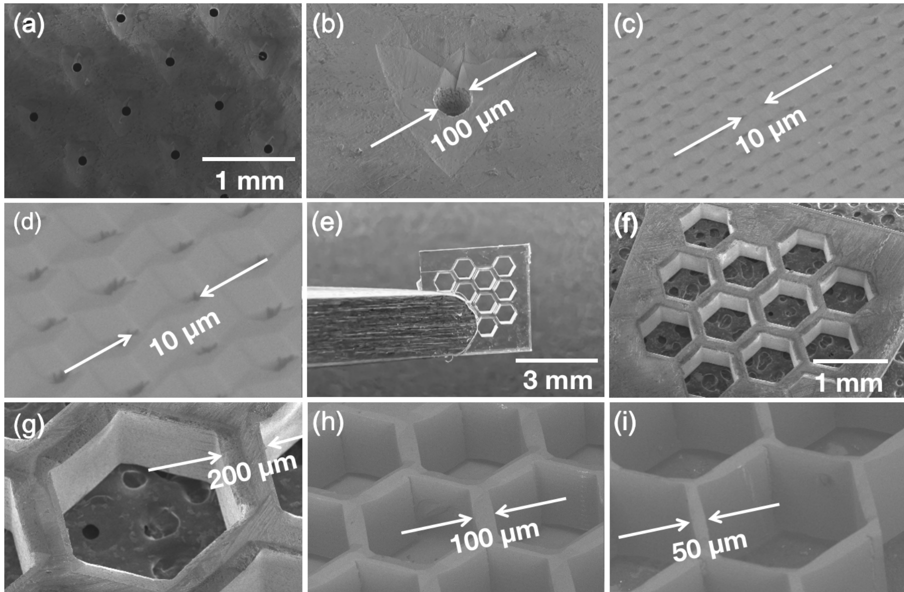

Figure 3.6: Structures fabricated out of crystalline C-cut sapphire. (a, b) 100 μm diameter hole matrix, (c, d) single line 10 μm pitch hole matrix, (e – g) honeycomb structure where the side of the hexagon is 400 μm, and the walls between hexagon are 200 μm, (h, i) similar hexagon structure with diminished walls between hexagon respectively 100 μm and 50 μm.

4. Applications

This chapter is dedicated to discussing applications for SLE-made structures. The chapter will be divided into two parts: SLE application in micromechanics and in microfluidics. In this part, structures fabricated out of UVFS will be presented. The parameter set found in section 2 will be used for structural fabrication. The information and results provided in this chapter are based on papers **II** and **V**.

4.1. Micromechanics

4.1.1. Motivation

The prominent uniqueness of SLE is the possibility to form arbitrary shaped 3D structures out of glass. This property brings the possibility of creating micromechanical systems out of glass. A notable advantage of glass micromechanics is that SLE allows the production of micromechanical structures that do not require additional assembly. Here I will suggest two movement mechanisms for glass micromechanics. The first is a compliant mechanism, and the other is a joint-like mechanism. This chapter will present a few examples of such mechanisms. The main applications for such devices could be miniaturized mechanical systems such as microrobotics or microfluidics with active components [31].

4.1.2. Experimental methods

"Laser Nanofactory" setup (Femtika Ltd.) was used in these experiments. "Pharos" laser (Light Conversion Ltd.) is used as a radiation source. Radiation parameters: 1030 nm wavelength, pulse duration $\sim$700 fs, pulse repetition rate – 610 kHz. Circularly polarised light is used in this experiment. The laser beam is focused on the sample with a 20x 0.45 NA objective equipped with automated aberration correction (add-on device by Femtika Ltd.). Aberrations are compensated by rotating a ring on the objective, which changes the position of a specific lens group in the objective. Aberration compensation or ring position depends on the writing depth in the glass. Correction ring position

automatically follows positioning Z-axis movements. For sample positioning, Aerotech positioning stages and galvoscanners are used IFOV regime. In this test, UVFS glass was used. The thickness of the sample depends on the structure. Minimal possible thickness glass is used in each experiment. After the sample is exposed to the fs laser, the modified volume is etched in 10 mol/L concentration KOH solution at 90°C. Samples were characterized using an optical microscope and scanning electron microscopes (SEM). The surface roughness was measured using an atomic force microscope (AFM).

4.1.3. Summary of results

One of the basic micromechanical structures is a spring. A single helix 4-turn spring was produced out of glass (Figure 4.1 (a)) to demonstrate a deformable glass structure. The structure's diameter is 1 mm, with the width of the helix itself being 50 μm. The combined length of the whole helix was around 12 mm. As a result, this allowed us to repeatedly compress the spring up to 50% (from 600 μm to 300 μm) without damaging it. Fabrication of this structure was performed using both strategies: segmenting (in the middle of the structure) and full-volume exposure (for fine springs). Due to this, the structure can be produced in ∼4 min. As such springs can be mass-produced on-demand in mass-customized series, they could be attractive in such fields as the watch industry or microrobotics. While not trivial at first sight, these structures can be made to be mechanically resistant to compressive forces and, at the same time, robust against shock due to the possibility of using some advanced architectures like gyroids in the support part of the spring (which in our case is a simple bulk plate). Due to their minimized weight, such structures could prove to be extremely mechanically resilient to shock and vibrations.

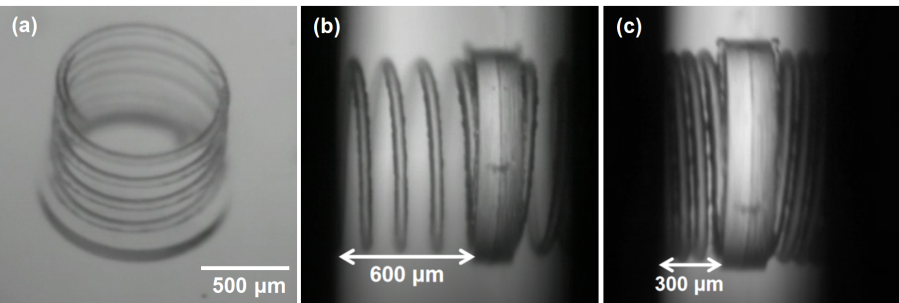

Figure 4.1: Images of fused silica single helix 4 turn spring. (a) Overall view. (b) and (c) shows compression of the spring. Due to the small thickness (diameter – 50 μm) and relatively long length of the helix (∼12 mm) it can be compressed repeatedly from 600 to 300 μm (50% of overall helix height) without any damage to the structure.

In contrast to deformable micromechanics, one might consider structures made of different independently moving components. Usually, such systems are made part by part and then assembled. However, SLE allows true 3D modification of glass volume. As a result, openings needed for structure motion can be embedded before etching and then revealed by it. Therefore, assembly-free movable multi-part 3D glass structures can be produced relatively easily, expanding the micro-mechanics field's current capabilities. We first produced a chain with free movable ball joints to demonstrate it. This structure employs the idea of etching out the narrow gaps between the separate parts of the structure. In this way, a joint-like structure that can move is created. The exact model and optical microscope photos of the manufactured structure are shown in Figure 4.2. The bending amplitude of the produced structure (which is 30°) coincides well with the value predicted from the mechanical CAD model. As the structure is very complex, and the opening of the outer ball is 450 μm in diameter, the whole inside of the outer ball was exposed to laser radiation. For this reason, the fabrication of such a structure heavily relies on the understanding of etching rates. If the chosen processing parameters are insufficient, the fine opening would either not etch out or etch out too much, resulting in the disassembly of the ball joint. Therefore, when manufacturing such delicate structures, substantial attention should be paid to both process and model optimization in order to achieve the best possible result.

Finally, a complex micromechanical structure called the Geneva mechanism was fabricated (Figure 4.3). This structure contains two intermeshing elements. By rotating one gear every 360° rotation, it moves another gear by fixed 90° increments. SLE technology allows fabricating such mechanisms out of a single piece of glass without requiring an assembly step. As this structure is assembly-free, it can be produced at a very small scale (down to hundreds of μm) without needing extremely complex micromanipulation. Moreover, by attaching a small magnet to this mechanism and placing it over a rotating magnet, we show the smooth movement of this structure. This is possible due to very fine gaps between different moving parts of the structure (less than 10 μm) and very good surface roughness ($\sim$200 nm RMS) possible due to optimization presented previously in this thesis, which allows minimizing excessive friction. Pictures of the Geneva mechanism movement are shown in Figure 4.3 (g). During the testing, the mechanisms showed an ability to rotate up to 2000 RPM, and it could run continuously for more than 100 hours without any damage or other adverse impacts on the functionality. It is important to note that the measurement of Geneva mechanism rotation was carried out using a simple rotating magnet underneath the structure itself. As it was a proof-of-concept experiment, our goal was to see if the mechanism would rotate without any trouble. Thus, the upper limit of the experiment was determined not by the structure but by the measurement equipment. We estimate that at particularly

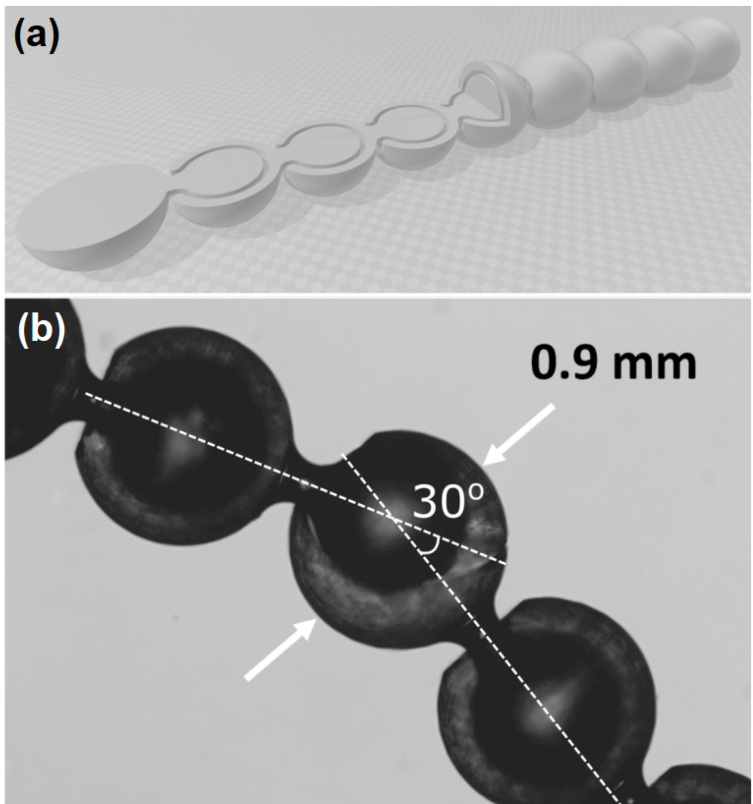

Figure 4.2: Flexible chain with ball joints. (a) 3D model of a structure, with 1/4 of the structure cut away to show hollow openings separating outer and inner balls in the joint. (b) Optical microscope image of part of the structure. Bending at modeled 30° is achieved. Also, inner and outer balls in the joint are clearly visible.

high rotation speeds the axis of the fragile mechanism would not be able to hold the rotation of the whole mechanism and break. However, we did not manage to reach such RPM in this work, leaving this investigation for future research.

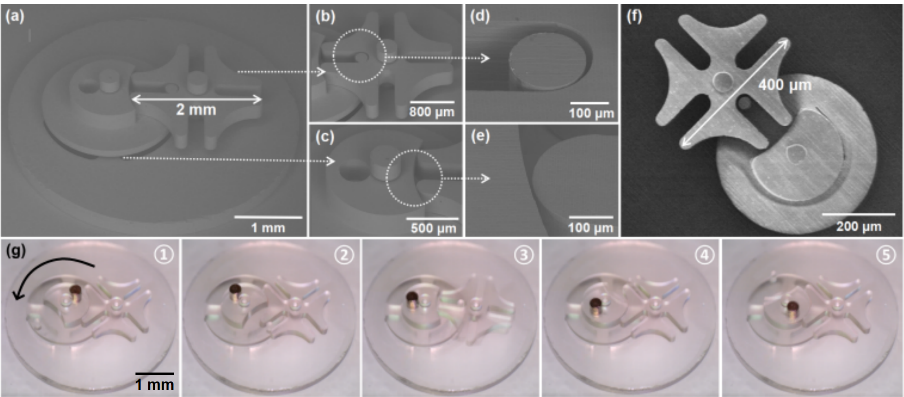

Figure 4.3: Pictures of a produced Geneva mechanism. (a) Scanning electron microscope (SEM) image of the whole mechanism, (b – e) SEM pictures of the most important features and surfaces of the mechanism, and (f) SEM image of 5 times smaller Geneva mechanism than in part (a). (g) Chronological pictures of Geneva mechanism movement, black arrow indicates the rotation direction. Magnet is attached to the structure and the whole mechanism is inserted into a changing magnetic field for the movement automation.

The scalability of SLE should also be commended. As such structures will most likely find their way to being used in high-precision complex devices, the possibility to easily tune the size and shape of structures towards mass customization is one of the top priorities. To demonstrate that SLE complies with such requirements, we made a Geneva mechanism that is 5 times smaller than the original one (Figure 4.3 (f)). Of course, some peculiarities exist on such a scale. The phenomena of selectivity play the most crucial role in this process. As a result, reducing the size of a structure is relatively easier than making it bigger. The etching rate should be sufficient if larger structures are needed to avoid over-etching of unexposed parts of the structure. An increase in selectivity has a fundamental limit, restricting complex SLE 3D fabrication to structures that are below several cm. Nevertheless, this is not a hard limit if some compromises can be made to the structure accuracy, as the main hindrance of long etching times is an excessive dissolving of laser-unaffected glass volume. If some taper can be tolerated, even cm-sized structures can be produced using SLE.

4.2. Microfluidics

4.2.1. Motivation

Another trending application is lab-on-chip devices (LOC). Lab-on-chip is a miniaturized device that can perform limited laboratory functions. To name a few examples, we could mention lab-on-chip for blood plasma separation [103], for various pathogens detection in food [104, 105], viruses [106, 107] or bacteria [108]. Moreover, lab-on-chip could be used to mimic particular organs or tissues. These devices are called organ-on-chip (OOC). One of many examples is a liver-on-chip device [109]. Compared with usual testing methods, OOC is becoming more popular because of its versatility and advantages. LOC is rapidly merging directions. However, it is still an open area for innovations, from new materials to innovative design research. Dominating technology in such device production is molding [110, 111]. On one side, molding is a very effective and cheap technique for mass production [112]. On the other hand, it becomes costly for prototyping when new master structures are needed for any changes in the chip design. This section proposes an alternative solution based on ultrafast laser material processing for OOC device fabrication. Femtosecond laser micromachining is an appealing option for LOC device prototyping. A combination of a few different femtosecond glass microprocessing techniques will be demonstrated for liver-on-chip device manufacturing. Two microprocessing techniques – SLE and welding – will be combined to produce a liver-on-chip device. Finally, manufactured device test results will be provided.

4.2.2. Experimental methods

For liver-on-chip fabrication, two different laser microprocessing methods are used. Plates with channel systems and integrated filters are fabricated by the SLE method. SLE is performed on amorphous UV-grade fused silica (UVFS). 1 mm thickness UVFS substrates are chosen for channel system fabrication. Laser microfabrication is done by a Laser NanoFactory workstation (Femtika Ltd., Lithuania). The utilized workstation is equipped with a Yb:KGV femtosecond laser (Pharos, Light Conversion Ltd., Lithuania). For the SLE experiments, fundamental wavelength – (1030 nm), ~700 fs pulse duration, and 610 kHz of the mentioned laser are exploited. Laser radiation is focused by 20x 0.45 NA Nikon focusing objective equipped with automated aberration correction (add-on device by Femtika Ltd.). Subsequently, after inscribing particular material modification, the sample is etched in a 6 mol/L concentration potassium hydroxide (KOH, Eurochemicals, Lithuania) solution with distilled water at 90°C temperature.

Since we need an encapsulated microfluidic channel system, channels formed on the plates must be sealed. Another femtosecond laser radiation-based tech-

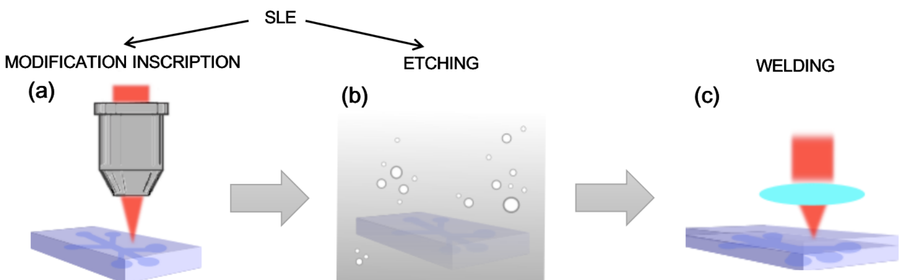

Figure 4.4: A basic scheme of lab-on-chip device laser processing. (a) nanogratings inscription to the glass plate by focusing light with a microscopic objective. (b) subsequent etching of laser-processed sample. (a, b) together present the SLE technique. (c) laser welding process used to seal the channel system with an additional glass plate.

nique - laser welding [65, 66] is used for that. Only the contact between two plates can be affected without damaging the surface by using high-intensity radiation due to nonlinear light-material interaction. With high power, material in the contact can be melted, and a firm connection is formed in the samples mentioned. The laser welding part is done with the same Laser NanoFactory workstation. Laser welding experiments are done with the same 1030 nm wavelength, approximately 200 fs pulse duration, and 610 kHz pulse repetition rate. Laser radiation is focused with a 0.5 NA aspherical lens. After the etching and before the welding, samples are washed in a piranha solution (4:1 v/v of sulfuric acid (95 – 98%, Sigma-Aldrich, Germany) and hydrogen peroxide (50%, Sigma-Aldrich, Germany), respectively). Afterward, samples are rinsed in distilled water and isopropanol. The basic scheme of chip fabrication is shown in Figure 4.4.

Manufactured liver-on-chip prototypes are rinsed with sterilized aqua dest, submerged in 70% ethanol solvent for initial disinfection, and UV irradiated for 20 min for further sterilization. Chips are coated with Poly-L-lysine polymers to promote cell adhesion. The coating is performed by filling the chamber with 10 μL Poly-L-lysine solution (Sigma Aldrich, Vienna, Austria) through a seeding channel followed by an incubation period at 37°C until they dry completely. These prepared liver-on-chip systems are stored in standard sterile conditions until use.

The human liver HCC cell line HepG2(GS) is used for biocompatibility testing. These cells are cultivated under standard conditions (37°C, 5% CO_2 in humidified atmosphere) in MEM media (Gibco, Thermo Fisher Scientific, Vienna, Austria) supplemented with 10% fetal bovine serum (GE Healthcare Life Sciences, UT, USA) and 1% Penicillin/Streptomycin (Sigma Aldrich, Vienna, Austria). The media is renewed every other day, and cells are passaged once they grow to 80 – 90% confluence. The chambers of liver-on-a-chip sys-

tems are filled with 10 μL of a cell suspension to reach 2×10^4 HepG2(GS) cells/cm^2 through the seeding channels. Chips are submerged in culture media in a Petri dish and placed in a cell incubator under standard conditions (37°C, 5% CO_2 in the humidified atmosphere) overnight to avoid evaporation. Then, cell adherence and growth are determined by daily microscopy examination. The media is renewed every other day in a standard manner. The experiment is continued for nine days and repeated three times. Finally, a Trypan Blue exclusion test is conducted to confirm cell viability further.

4.2.3. Summary of results

We begin the research by producing microfluidics chips with integrated filters on a glass substrate. The picture of the fabricated chip and SEM pictures of its particular parts are shown in Figure 4.5. In general, the filter is a row of elliptical glass pillars. Dimensions of every pillar are 36 μm wide and 55 μm long. The spacing between each pillar is 14 μm, corresponding to the filter's pore. The height of the fabricated pillars is 200 μm, which is identical to the depth of the microfluidic channel. Filters are integrated into a 5 mm length and 0.9 mm wide channel. In the mentioned area, two rows of pillars divide that zone into three distinguished channels: side channels are 200 μm wide, and the central one is 400 μm wide.

Visually, smooth features and a high channel aspect ratio are obtained. However, not only modified but also unmodified material is etched during the etching process. Thus, this leads to widened channels and features. The mentioned effect creates critical aspect ratio limitation, which is especially important in microfilter fabrication. Since the cells are micro-scale objects, the precision of the integrated filter is essential. Here in the model, the gap between pillars shown in Figure 4.5 (c) and (g) was a single line inscription, which is a minimal laser modification between pillars. However, after the etching, the gap between pillars tends to increase up to 14 μm, which limits the accuracy and minimal feature of the filter. In LOC applications surface quality of the channel is critical, as well. This feature affects liquid flow. The higher the roughness of the surface, the more friction it creates. Thus, channels become difficult to fill due to the higher surface roughness. The surface quality of processed channels are evaluated by an optical profilometer. The surface roughness of the etched channels is around 250 nm RMS.

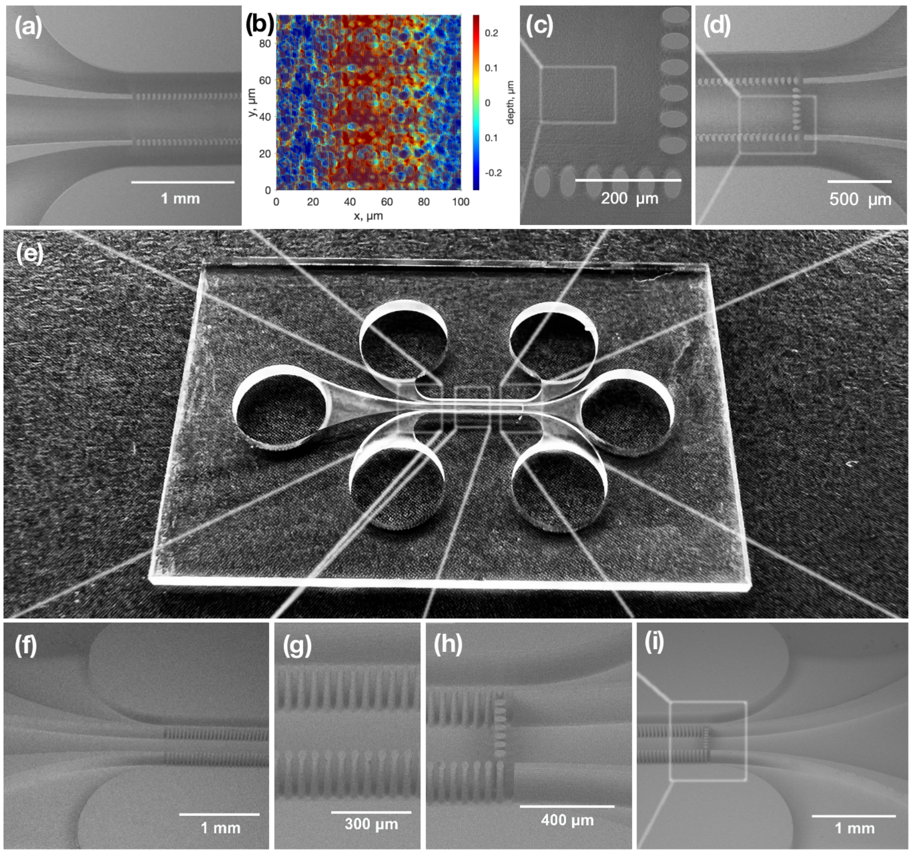

Figure 4.5: Pictures of produced liver-on-chip device. (e) Optical picture of a full device. (a) and (c – d) SEM top images of specified chip parts. (f – i) 45° SEM images of specified chip parts. (b) Surface topology of the channel surface.

The chips are sealed by laser welding. Optical contact is required to create firm contact between plates. That means the gap between two surfaces should be a few times smaller than the used wavelength, which is 1030 nm. To achieve this, high cleanness and surface quality of the samples are needed. Thus, the sample is washed in piranha solution to remove all organic remains from the chip. Before welding, the chip is rinsed in isopropanol and distilled water. Two glass plates are put on each other when it is still wet. Isopropanol is a liquid that forms a low contact angle with a glass [102], which means it wets the surfaces. Thus, due to wet contact with isopropanol, the two plates tend to have a smaller gap between each other, which enhances welding quality. The two plates are welded in contact everywhere around the channel system without damaging or affecting channels or the filters themselves. Welding seams are made within 100 μm spacing. The view of welding seams around microfluidic channels is demonstrated in Figure 4.6 (b). An optical picture of the produced chip is shown in Figure 4.6 (a).

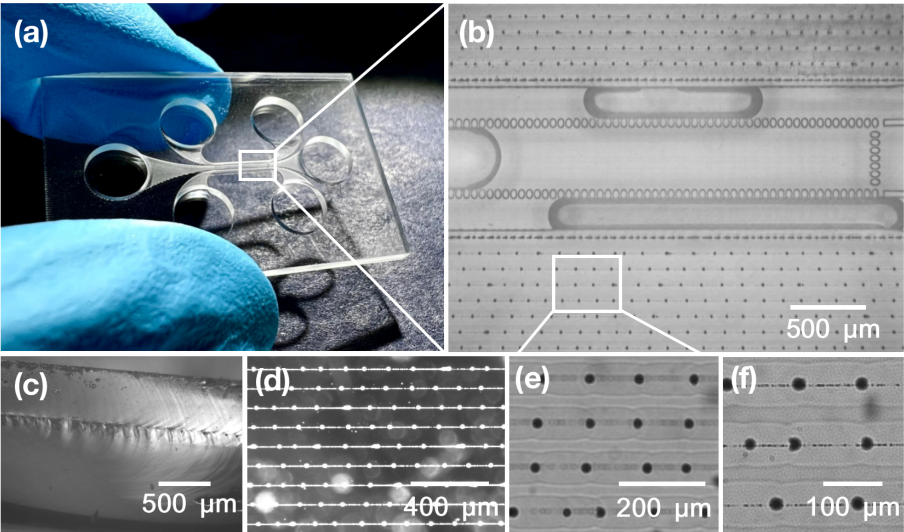

Figure 4.6: (a) Picture of a final liver-on-chip device. (b) Optical picture of produced microfluidic chip part where channel with filter and welding seams can be observed. (c) Cross section of the welded chip. (d) Welding seams optical microscope picture made with crossed polarizators. (e) and (f) Optical photos of welding seams with different magnifications.

The prototype device functionality is tested with liver cells. A homogeneous film of Poly-L-lysine is formed on the surface of liver-on-chip systems. The uncoated chips are also tested. However, HepG2(GS) does not adhere due to the smooth chip surface, while cells attach well on the coated surface. 24 h after seeding, HepG2(GS) cells start to grow in a monolayer. The number of spheroids and size are consistent with the starting cell density. During the media change, the cell monolayers remain adherent on the surface and grow continuously. After 96 h of culture, HepG2(GS) cells create large irregular spheroids. From 7 days of culture, the growth of spheroids leads to the formation of large clusters of spheroids in the whole liver-on-chip system. The picture of this test is shown in Figure 4.7. From day 7, cell viability decreases, as seen by the round shape of some cells. After 9 days most of the cells are dead, according to the Trypan Blue. In general, the Trypan Blue exclusion test shows that the adhesive cells have good viability during the 7 day experimental period.

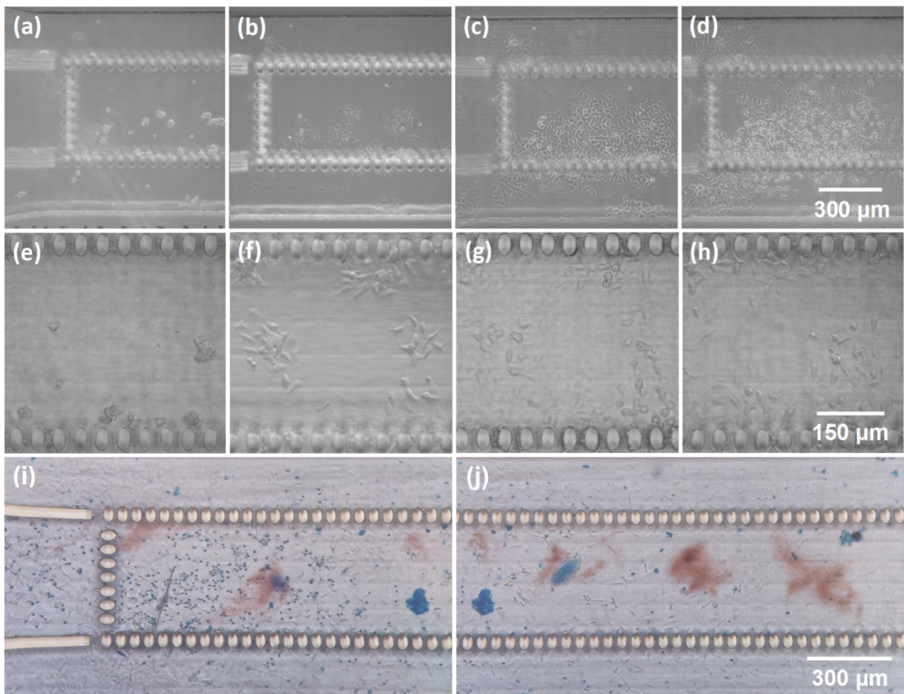

Figure 4.7: Optical pictures of the fabricated microfluidic channels seeded with HepG2(GS) liver cancer cells (a, e) right after the seeding, (b, f) after 24 hours, (c, g) after 96 hours, (d, h) after 7 days, (i, j) after 9 days with Trypan Blue.

Conclusions

1. 3D structures consist of 2 different types of planes in XY and XZ directions. After testing planes inscribed with various parameters, it was noticed that lower spacing between scanning lines (0.25 μm in horizontal and 1 μm in a vertical plane, which corresponds to approximately 90% of induced size modification overlapping) gives higher etching rates (up to approximately 1000 μm/h), which at the same time leads to the lower surface roughness of formed planes ($<$ 200 nm RMS).

2. Etchant concentration and its wetting properties change the etching rate and selectivity of the UVFS SLE process. Higher concentration etchant increases the etching rate of modified and unmodified material. Lower concentration etchant gives a lower modified and unmodified material etching rate. Adding an organic solvent to standard etchants could make the etchant wet the surface more due to a lower contact angle. The organic solvent in the etchant decreases the etching rate of unmodified material due to material and etchant chemical reactions. At the same time, it increases the etching rate of the modified material due to the high surface area of the modified material. This way, 2 mol/L KOH with 10% isopropanol etchant allows it to reach a selectivity of approximately 3000.

3. Etchant concentration influences formed UVFS surface roughness. In tested cases, a higher concentration of KOH gives lower surface roughness. The highest surface roughness of 340 nm RMS was obtained with 1 mol/L KOH solution. Meanwhile, the lowest surface roughness of 180 nm RMS was obtained with 8 mol/L KOH solution.

4. After comparing different sapphire SLE algorithms, the best process parameters for sapphire SLE were chosen. The parameters suitable for sapphire structure formation are 1030 nm wavelength radiation, 200 fs pulse duration, 610 kHz pulse repetition rate, and 300 – 500 nJ pulse energy. The only etchant which is suitable for structure formation was found to be a sulphuric and phosphoric acids mixture at 270°C. The selectivity of the chosen protocol is around 66. The mentioned acids mixture was the

only etchant out of those tested that showed the ability to etch inscribed nanogratings.

5. Using SLE technology, a few micromechanics and microfluidics structures such as a spring, Geneva mechanism, ball-joint structure, and a lab-on-chip device were formed, showing that the SLE technique is suitable for functional device manufacturing. Furthermore, fabricated micromechanical devices were tested in motion. Meanwhile, a lab-on-chip device was tested for biomedical testing of liver cells.

SANTRAUKA

Įvadas

Skaidrios ir tvirtos medžiagos, kaip antai techniniai stiklai bei kristalai, dėl savo mechaninių ir optinių savybių yra patrauklūs daugelyje sričių. Tačiau minėtosios medžiagos yra ganėtinai trapios, tad sunku jas apdirbti. Šios medžiagos yra linkusios skilti paveiktos stiprių mechaninių jėgų ar didelio intensyvumo spinduliuotės. Tačiau femtosekundiniu lazeriu paremtas medžiagų apdirbimas yra patraukli alternatyva apdirbti stiklus bei kristalus. Įvairios lazerinės mikroapdirbimo technologijos jau yra plačiai taikomos stiklų bei kristalų apdirbimui: dvimačių struktūrų gamyboje naudojami įvairūs abliacijos ir pjaustymo metodai [3, 4, 2]. Abliacija yra gana efektyvus ir palyginti paprastas procesas, kuris leidžia tiek apdirbti paviršius, tiek formuoti 2D darinius. Siekiant pagerinti abliuotų darinių kokybę abliacija gali būti kombinuojama su papildomais procesais, taip išgaunant tikslesnį ar greitesnį apdirbimą [5, 6, 7, 8, 9]. Kombinuojant abliaciją su papildomu terminiu apdirbimu [10] ar tiesioginį lazerinį rašymą su cheminiu apdirbimu gali būti formuojami net ir optiniai komponentai, kaip kad lęšiai [11, 12] ar difrakciniai optiniai elementai [13, 14, 15]. Tačiau minėtos technologijos yra ribotos, nes suteikia galimybę formuoti tik 2D geometrijos komponentus ir neleidžia formuoti laisvos formos 3D darinių.

Tačiau selektyvaus lazeriu indukuoto ėsdinimo (SLE) technologija gali būti gera alternatyva kompleksinių 3D komponentų formavimui iš stiklo. SLE yra metodas, sudarytas iš kelių technologinių procesų, kai pirmiausia stiklo tūryje yra įrašomos porėtos modifikacijos, vadinamosios nanogardelės [16]. Galiausiai šios modifikacijos yra ėsdinamos agresyviuose ėsdikliuose, kaip antai hidrofluoridinė rūgštis ar kalio šarmas [17]. Tokiu būdu gali būti formuojami laisvos architektūros dariniai iš stiklų ar kristalų [18].

Dėl didelio selektyvumo, naudojant SLE metodą, galima suformuoti itin aukšto matmenų santykio struktūras, kaip kad: mikromechaniniai prietaisai [27, 18], mikrofluidiniai prietaisai [28, 29] ar net itin sudėtingos mikrofluidinės sistemos su integruotais mikromechaniniais komponentais [30, 31]. Tokios struktūros gali būti taikomos sensorikoje [32, 33], laboratorijų ant lustų [30, 18, 31], purkštukų gamybai [18, 34] ar kitose srityse.

Minėta technologija atrodo perspektyvi daugelyje sričių. Todėl ši disertacija skirta lydyto kvarco SLE metodo tobulinimui ir kristalinio safyro SLE metodo vystymui. Galiausiai tyrimų metu įgytos žinios pritaikytos funkcinių darinių, kaip antai mikrofluidinių ir mikromechaninių prietaisų, gamybai SLE metodu.

Naudojami trumpiniai

1D	vieno matmens, vienmatis
2D	dviejų matmenų, dvimatis
3D	trijų matmenų, trimatis
fs	femtosekundinis
HF	hidrofluoridinė rūgštis
H_3PO_4	fosforo rūgštis
H_2SO_4	sieros rūgštis
YAG	itrio aliuminio granatas
KOH	kalio šarmas
NaOH	natrio šarmas
SEM	skenuojantis elektronų mikroskopas
SLE	selektyvus lazeriu indukuotas ėsdinimas
SiO_2	silicio dioksidas
UV	ultravioletinis, ultravioletinė spinduliuotė

Disertacijos tikslas

Vystyti ir optimizuoti femtosekundinio lazerio indukuotą selektyvaus ėsdinimo metodą funkcinių laisvos architektūros darinių formavimui iš skaidrių medžiagų, kaip kad lydytas kvarcas ar safyras.

Darbo naujumas ir svarba

Šio darbo naujumas slypi optimizuotame stiklo ir safyro SLE procese, kuris atveria galimybę formuoti aukšto matmenų santykio 3D darinius naudojant SLE:

1. Buvo ištirta skirtingų tarpų tarp skenavimo linijų įtaka bei ėsdiklio koncentracijos ir drėkinimo savybių įtaka proceso efektyvumui bei formuojamų paviršių kokybei. Dėl optimizuoto skenavimo ir ėsdinimo procedūrų pademonstruotas aukštas selektyvumas, kuris leidžia formuoti sudėtingas struktūras su didelio matmenų santykio detalėmis.

2. Optimizavus procesą, pademonstruotos judančios mikromechaninės struktūros, nereikalaujančios papildomo surinkimo, ir kompleksinė mikrofluidikos sistema su integruotais funkciniais elementais.

3. Taip pat buvo išvystytas SLE protokolas safyro apdirbimui. Ištestuoti skirtingi lazerio parametrų (skirtingos lazerio harmonikos, impulsų trukmė ir kt.) rinkiniai nanogardelių formavimui bei įvairūs ėsdikliai nanogardelių ėsdinimui. Palyginus skirtingų apdirbimo protokolų rezultatus, pasirinktas protokolas, kurį pritaikius buvo pagamintos mikrostruktūros iš kristalinio safyro.

Ginamieji teiginiai

1. Gaminant SLE metodu 3D darinius, šie sudaromi iš atskirų lazeriu skenuotų linijų masyvų, kurie sudaro vertikalias arba horizontalias plokštumas. Skenuodami minėtas linijas mažesniais tarpais (apie 90% įrašytų modifikacijų persiklojimu) abiem atvejais gauname didesnę ėsdinimo spartą (iki 1000 μm/h) bei mažesnį ėsdintų paviršių šiurkštumą (mažiau nei 200 nm RMS).

2. Ėsdiklio drėkinimo savybės keičia SLE proceso selektyvumą. Selektyvumas gali būti padidintas sumažinus ėsdiklio kontaktinį kampą su bandiniu, kai ėsdiklyje dalis vandens yra pakeičiama tinkamu organiniu tirpikliu (izopropanoliu). Apie 3000 selektyvumo vertė buvo pasiekta kaip ėsdiklį naudojant 2 mol/l KOH tirpalą, kuriame 10% vandens yra pakeista izopropanoliu.

3. Naudojant SLE technologiją, gali būti formuojami 3D dariniai iš kristalinio safyro. Tačiau standartiniai ėsdikliai, kaip kad HF, KOH, turi būti pakeisti sieros ir fosforo rūgščių mišiniu. Tarp testuotų ėsdiklių vienintelis sieros ir fosforo rūgščių mišinys 270°C temperatūroje galėjo praėsdinti lazeriu suformuotas nanogardeles. Naudojant minėtą ėsdiklį, gauta didžiausia selektyvumo vertė yra 66.

4. SLE metodu apdirbant lydytą kvarcą, gali būti formuojami aukšto kompleksiškumo mikromechaniniai komponentai ir mikrofluidiniai lustai. Mikromechaniniai komponentai, kaip antai: lanksti spyruoklė, besisukantis krumpliaračio tipo mechanizmas bei laboratorijos ant lusto tipo mikrofluidinė sistema, gali būti pagaminta išlaikant žemą ėsdintų paviršių šiurkštumą ($<$ 250 nm RMS) ir pasiekiant μm skalės tikslumą.

Trumpas teorijos aptarimas

Stiklo apdirbimas ultratrumpaisiais impulsais

Apdirbant skaidrias medžiagas ultratrumpųjų impulsų spinduliuote, sąveika tarp spinduliuotės ir medžiagos vyksta dėl netiesinių reiškinių [35]. Medžiaga

paveikiama itin aukšto intensyvumo spinduliuote (GW/cm^2 – PW/cm^2), kuri gaunama naudojant laikinį energijos impulsuose suspaudimą bei erdvinį energijos suspaudimą fokusuojant naudojamą spinduliuotę 0,01 – 1,4 skaitinės apertūros optika. Minėtas spinduliuotės intensyvumas gaunamas tik spinduliuotės židinyje, tad spinduliuotės ir medžiagos sąveika lokalizuojama. Ši situacija grafiškai pavaizduota 1 paveiksle. Atsiranda galimybė modifikuoti medžiagos tūrį bet kokia norima forma. Taip pat dėl netiesinės medžiagos ir spinduliuotės sąveikos galima įrašyti subdifrakcinio dydžio modifikacijas.

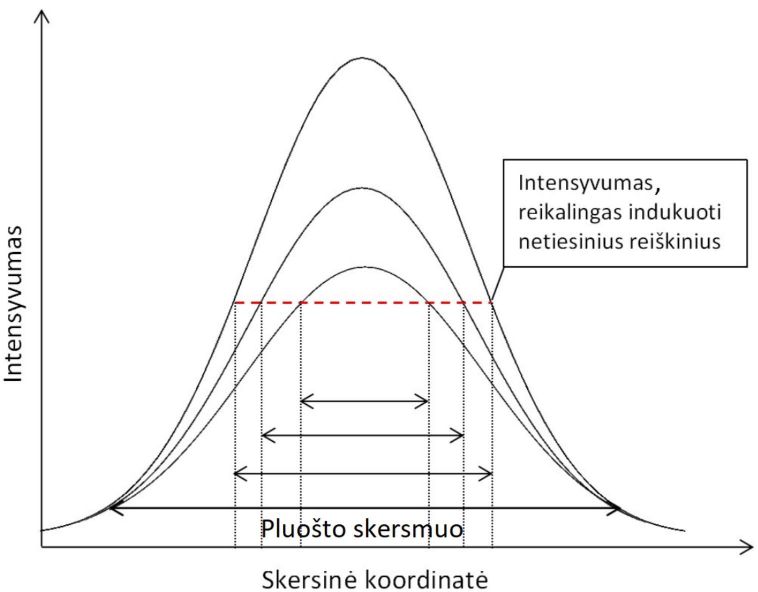

1 pav. Fokusuoto pluošto inicijuotos pažaidos raiškos priklausomybė nuo spinduliuotės intensyvumo.

Paveikus skaidrią medžiagą (stiklą) ultratrumpaisiais impulsais, galima suformuoti trijų skirtingų tipų modifikacijas, kurios dažniausiai vadinamos atitinkamai pirmojo, antrojo ir trečiojo tipo modifikacijomis. Specifinės sąlygos, kurioms esant galima suformuoti tam tikras modifikacijas, priklauso nuo pačios medžiagos [47, 21]. Pirmo tipo modifikacija yra medžiagos lūžio rodiklio pokytis. Tokia modifikacija susiformuoja, kai fokusuotos spinduliuotės židinyje medžiaga perlydoma. Standartiniuose stikluose absoliučiąja verte lūžio rodiklis pokytis yra 10^{-3} eilės. Antrojo tipo modifikacija yra periodinė porėta modifikacija stikle, kitaip dar vadinama nanogardelėmis. Optiniu požiūriu nanogardelės yra dvejopalaužės. Nanogradelių pavyzdys yra pateiktas 2 paveiksle. Nanogardelės susidaro dėl sąveikos tarp lazerio sugeneruotos plazmos ir lazerio spinduliuotės. Sugeneruotos elektronų plazmos bangos medžiagoje interferuoja su krentančia spinduliuote ir sukelia interferencines modifikacijas [50, 49]. Nanogardelės ir jų periodas priklauso nuo daugelio spinduliuotės

parametrų [55, 57, 52]. Svarbu paminėti, jog nanogardelių orientacija priklauso nuo spinduliuotės poliarizacijos skenavimo krypties atžvilgiu [16, 21]. Ši priklausomybė matyti 2 paveiksle. Trečiojo tipo modifikacija – tai nano/mikro ertmių formavimasis. Kai spinduliuotės intensyvumas viršija tam tikrą vertę, kuri yra didesnė nei reikalinga antrojo tipo modifikacijai, stiklo viduje įvyksta mikrosprogimas ir susidaro mikroertmės. Šis reiškinys parodytas įvairiuose darbuose [58, 59].

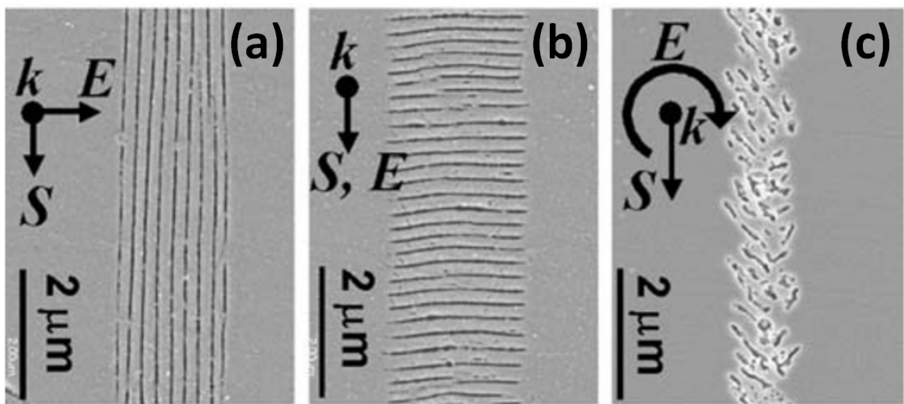

2 pav. Antrojo tipo stiklo modifikacijos pavyzdžiai, kai nanogardelės suformuotos: (a) skenuojant medžiagą statmenai spinduliuotės tiesinės poliarizacijos krypčiai; (b) medžiagos skenavimo kryptis yra lygiagreti su spinduliuotės tiesinės poliarizacijos kryptimi; (c) naudojama apskritiminė spinduliuotės poliarizacija. S – lazerio pluošto skenavimo kryptis medžiagos atžvilgiu, E – lazerio spinduliuotės poliarizacijos vektorius [21].

Visos prieš tai minėtos stiklo modifikacijos gali būti panaudotos skirtingoms stiklo apdirbimo technikoms. Pirmojo tipo modifikacija gali būti panaudota lūžio rodiklio modifikavimui [47] bei bangolaidžių formavimui stiklo tūryje [60, 32]. Antrojo tipo modifikacija gali būti panaudota difrakcinių optinių komponentų, kaip kad Q-plokštelės [61], formavimui. Kombinuojant antrojo tipo modifikaciją su papildomu ėsdinimu, realizuojama SLE technologija [63]. Trečiojo tipo modifikacija yra naudojama lazerinei abliacijai [64, 42], tiesiogiai jonizuojant ir pašalinant medžiagą, ar lazeriniam virinimui [65, 66, 67], kai dvi skaidrios medžiagos yra sujungiamos, paveikus jų kontaktą tarp dviejų skairių medžiagų aukšto intensyvumo spinduliuote. Įvardytos stiklo apdirbimo technologijos yra gana skirtingos ir suteikia daug galimybių. Tačiau šiame darbe plačiau aptariama SLE technologija bei jos pritaikymo galimybės.

SLE

SLE yra unikalus procesas, leidžiantis formuoti 3D struktūras iš skaidrių medžiagų. Ši technologija susideda iš dviejų procesų. Pirmiausia stiklo tūryje

įrašoma antrojo tipo modifikacija, tuomet lazeriu modifikuotas bandinys ėsdinamas agresyviuose ėsdikliuose, kaip kad KOH ar HF [68]. Šio proceso schema pavaizduota 3 paveiksle. SLE plačiausiai naudojama medžiaga yra amorfinis lydytas kvarcas, kuris yra grynas SiO_2. Žinoma, ši technologija yra išbandyta ir su kitomis stiklų rūšimis, kaip antai borosilikatas [69, 21, 22] ar *Foturan* [70]. Skirtingos medžiagos reikalauja individualios proceso adaptacijos, tad pradėsime nuo lydyto kvarco.

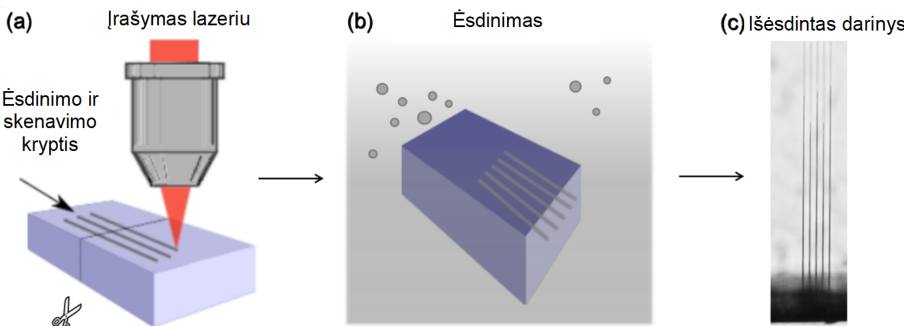

3 pav. SLE proceso žingsniai: (a) fokusuota lazerio spinduliuote įrašoma tūrinė modifikacija skaidrioje terpėje; (b) toliau lazeriu modifikuotas bandinys yra ėsdinamas; (c) galutinis darinys po ėsdinimo, šiuo atveju mikrokanalų masyvas tūryje.

SLE susideda iš dviejų skirtingų procesų – medžiagos modifikavimo lazeriu bei ėsdinimo, todėl abu procesai reikšmingai lemia galutinį rezultatą bei SLE efektyvumą. Lazeriu suformuotos nanogardelės agresyviuose tirpaluose yra ėsdinamos daug kartų greičiau nei nemodifikuota medžiaga dėl kelių priežasčių. Pirma, dėl savo porėtumo nanogardelių paviršiaus plotas yra gerokai didesnis nei nemodifikuotos medžiagos. Antra, lazerio spinduliuotė sukelia struktūrinius pokyčius medžiagoje, kai pakeičiami gardelės atomų sąryšio kampai. Deguonies atomai gali efektyviau reaguoti su ėsdikliu [68]. Žinoma, ėsdinant bandinį vienu metu yra ėsdinama tiek lazeriu modifikuota, tiek nemodifikuota medžiaga. Paprastai, nemodifikuoto lydyto kvarco ėsdinimosi sparta yra keli μm/h. Žinoma, šis dydis priklauso nuo ėsdiklio [17]. Tačiau lazeriu modifikuotos medžiagos ėsdinimosi sparta gali siekti kelis šimtus μm/h [19]. Įvairiuose darbuose SLE efektyvumui apibūdinti dažnai naudojamas minėtų ėsdinimo spartų santykis, kuris dar yra vadinamas selektyvumu. Bendru atveju selektyvumas apibūdina didžiausią galimą ėsdintų dalių matmenų santykį, t. y. maksimalų kanalo, įrašyto stiklo tūryje, gylio ir pločio santykį.

Selektyvumą lemia tiek lazeriu įrašyta modifikacija tiek ėsdinimas. Selektyvumas priklauso nuo bene visų spinduliuotės parametrų, t. y. impulsų energijos [16, 21, 19], impulsų pasikartojimo dažnio [19, 56, 71] ir impulsų trukmės [19]. Šių parametrų visuma apibūdina spinduliuotės dozę, kuria yra

suformuotos nanogardelės [19]. SLE proceso selektyvumas taip pat priklauso nuo spinduliuotės poliarizacijos skenavimo krypties atžvilgiu [16, 21, 17]. Skenavimo greitis bei skenavimo linijų tankis apibūdina impulsų bei modifikacijų persiklojimą, tai taip pat reikšmingai paveikia SLE procesą [19, 17, 73]. Selektyvumui daro įtaką ir ėsdinimo procesas. Ėsdiklio pasirinkimas bei ėsdiklio savybės lemia selektyvumo vertę bei ėsdinimosi spartą [17, 73].

SLE technologija gali būti taikoma ir kristalams, kaip antai safyras, YAG, ličio neobatas ar kristalinis kvarcas [80, 25, 81, 23]. Yra parodyta, kad safyre galima suformuoti nanogardeles, panašias į formuojamas lydytame kvarce [82, 26, 83]. Tačiau ėsdinimo mechanizmai apdirbant kristalines medžiagas skiriasi nuo amorfinių. Lazeriu paveikus kristalus, modifikuota medžiaga amorfizuojasi [84]. Ėsdinimui naudojami ėsdikliai yra panašūs į amorfinių medžiagų, tačiau dažnu atveju aukštesnės koncentracijos [82, 26, 83, 85, 86, 87, 88]. Kristalų ėsdinimui buvo pademonstruoti ir gerokai egzotiškesni ėsdiklių pasirinkamai – fosforo ir sieros rūgščių mišinys 300°C temperatūroje [13, 14, 89]. Selektyvumo vertės pademonstruotos safyre gerokai pranoksta vertes, gautas ėsdinant lydytą kvarcą, ir siekia 10000 [82, 26]. Deja, apdirbant kristalus SLE susiduriama su kitomis problemomis – itin sunku išvengti medžiagos skylimų, kuriuos sukelia lazerio spinduliuotės indukuoti įtempiai [24]. Taip pat pademonstruotos kristalinių medžiagų ėsdinimosi spartos yra itin mažos ir siekia vos 100 μm/h [82, 25], tai gali būti nepriimtina praktiniams taikymams.

Lydyto kvarco SLE optimizacija

SLE technologijoje daugelis proceso parametrų lemia galutinį rezultatą. Tad šioje dalyje pateikiama SLE proceso priklausomybė nuo įvairių procesų parametrų. Selektyvumo verčių priklausomybė lydytame kvarce yra nagrinėjama disertacijos straipsniuose **II** ir **III**.

Formuojant 3D darinius svarbu yra ne vien tik gaunamas selektyvumas. Gaminant sudėtingesnius elementus atsiranda poreikis įrašyti daugelį gretimų modifikacijų skirtingomis trajektorijomis. Tad ypač svarbios yra ir pasirinktos skenavimo strategijos. Čia išskiriamos kelios esminės skenavimo strategijos, kurios gali būti naudojamos darinių formavimui: visos medžiagos skenavimas, tik kontūrų skenavimas bei kontūrų skenavimas, dalijant medžiagą į mažesnes dalis. Minėtos strategijos yra pavaizduotos 4 paveiksle. Iš pirmo žvilgsnio gali pasirodyti, kad daugeliu atvejų paprasčiausia yra tiesiog daug nesukti galvos ir lazeriu modifikuoti visą medžiagos tūrį. Tačiau, siekiant sumažinti tiek įrašymo laiką, tiek minimizuojant indukuojamus įtempius ir sukeliamų skylimų tikimybes, galima pasirinkti alternatyvią strategiją, kai įrašomi tik detalių kontūrai ir pašalinama medžiaga dar papildomai sudalijama į mažesnes dalis. Ši strategija dažnu atveju ir yra pasirenkama formuojant kompleksinius 3D darinius.

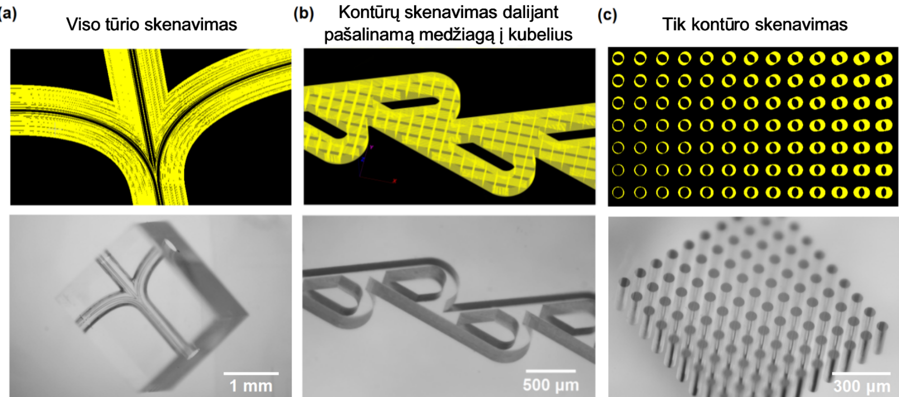

4 pav. Darinių formavimui SLE metodu naudojamos skenavimo strategijos: (a) viso tūrio išskenavimas, naudojamas tūrinių kanalų formavimui; (b) kontūro skenavimo kombinacija su likusios neišskenuotos medžiagos padalijimu į mažesnes dalis, naudojamas kanalų ant substrato paviršiaus gamybai; (c) tik kontūro skenavimas, naudojamas skylučių matricos gamybai.

Naudojant minėtąją skenavimo strategiją visi dariniai susideda iš trijų esminių komponentų: pagrindų, kontūrų bei pašalinamos medžiagos sudalijimų į mažesnius gabalėlius. Taigi visos sudėtingos 3D struktūros sudarytos iš 2D plokštumų, kurios yra įrašomos XY arba XZ/YZ plokštumose. Šioje dalyje aptariama, kokią įtaką poliarizacija, skenavimo sąlygos bei impulso energija daro skirtingų plokštumų ėsdinimui. Visi pristatomi eksperimentai atlikti įrašant modifikacijas specifiniu būdu skaidrios medžiagos tūryje. Vėliau įrašytos modifikacijos buvo atveriamos pjaunat stikliuką statmenai modifikacijoms. Ėsdinant įrašytas tūrines modifikacijas įvertinamos ėsdinimosi spartos.

Aprašomiems eksperimentams buvo naudojama optinė sistema, kurios principinė schema pavaizduota 5 paveiksle. Sistemoje naudojamas femtosekundinis lazeris *Pharos* (*Light Conversion Ltd.*). Modifikacijoms įrašyti naudojama fundamentinės harmonikos spinduliuotė (1030 nm), ~700 fs trukmės impulsai, 610 kHz impulsų pasikartojimo dažnis. Spinduliuotė fokusuojama 20x 0,45NA objektyvu *Nikon*. Fokusuotos spinduliuotės skersmuo židinyje XY kryptimi yra $2\omega_0$=1,5 μm, XZ kryptimi – 15 μm. Bandinio pozicionavimas atliekamas *Aerotech* pozicionavimo staliukais. Įrašytos modifikacijos ėsdinamos 10 mol/L koncentracijos KOH tirpale 90°C temperatūroje.

Pirmiausia buvo atliktas 1D eksperimentas, kurio schema ir rezultatai pavaizduoti 6 paveiksle. Skenuojant mėginius XY kryptimi, pavienės linijos buvo įrašytos stiklo tūryje su tam tikrais parametrais, kaip antai: skirtingos impulsų energijos, skenavimo greičiai ir poliarizacija. Po pavienių linijų įrašymo XY plokštumoje testo, aukščiausia pasiekta selektyvumo vertė yra apie ~650, kai skenuojama su poliarizacija statmena skenavimo krypčiai, mažiausiu išbandytu skenavimo greičiu (1 mm/s) ir didžiausia išbandyta impulsų energija (492 nJ).

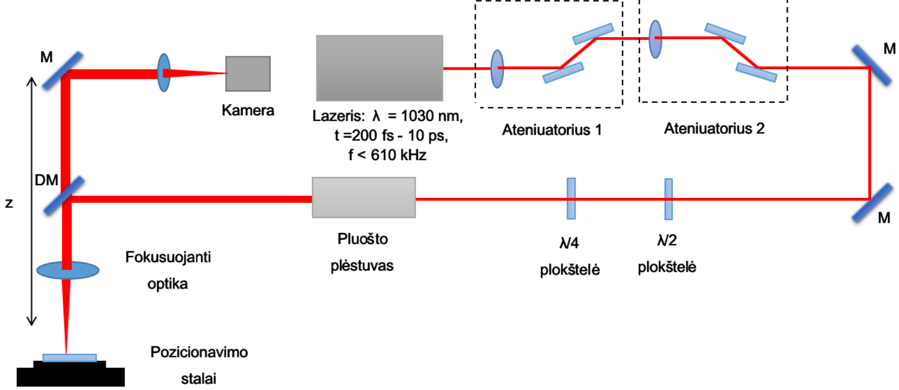

5 pav. Lazerinės sistemos, naudotos aprašytiems eksperimentams, principinė schema. Naudota optinė sistema susideda iš: femtosekundinio lazerio, dviejų ateniuatorių tiksliai galios kontrolei, keletos veidrodžių (M), $\lambda/2$ ir $\lambda/4$ banginių plokštelių poliarizacijos kontrolei, pluošto plėstuvo, dichroinio veidrodžio (DM), fokusuojančios optikos, pozicionavimo stalų, kameros proceso stebėjimui ir lęšio fokusuojančio vaizdą į kamerą.

Keičiant skenavimo greitį valdomas impulsų persiklojimas, tai keičia spinduliuotės dozę tūrio vienetui. Todėl mažesniu skenavimo greičiu perduodama daugiau energijos medžiagai ir šiuo atveju gaunama didesnė selektyvumo vertė. Taip pat matyti, kad poliarizacija statmena skenavimo krypčiai suteikia didžiausią selektyvumo vertę, o poliarizacija, lygiagreti su skenavimo kryptimi, rodo mažiausią selektyvumą. Ši SLE savybė jau buvo aprašyta ankstesniuose darbuose [16]. Lydytame kvarce suformuotų nanogardelių SEM atvaizdai pateikiami 7 paveiksle. Matyti, kad atsižvelgiant į impulso energiją keičiasi suformuotos modifikacijos dydis. Nuo pasirinktos poliarizacijos priklauso įrašomos modifikacijos forma. Nanogardelių periodas pateiktuose paveiksluose išlieka pastovus. Taigi galima manyti, jog selektyvumas priklauso tiek nuo medžiagos struktūrinių pokyčių, tiek nuo suformuotų modifikacijų morfologijos. Daugumai ištestuotų parametrų pastebima tendencija, kad selektyvumo vertė yra linkusi sotintis. Įdomu tai, kad selektyvumo vertė pradeda mažėti, kai didinama impulsų energija. Tai taip pat buvo demonstruota ankstesniuose darbuose [21, 19]. Tačiau absoliuti impulsų energijos vertė priklauso nuo viso parametrų rinkinio. Todėl reikia pasirinkti optimalias impulsų energijos vertes siekiant efektyviausio SLE proceso.

Toliau atlikti plokštumų ėsdinimo testai (t. y. 2D atvejis). Į stiklo tūrį buvo įrašomos plokštumos, kaip parodyta 8 paveiksle. Atliekant 2D testus, buvo įrašomi 40 μm pločio modifikacijų masyvai, išlaikant nurodytus tarpus tarp skenavimo linijų. Pagrindinis 2D eksperimentų tikslas – ištestuoti ėsdinimo greičio ypatybes, atsižvelgiant į modifikacijų įrašymo plokštumą ir ėsdinimo kryptį. Aprašytų testų tikslas buvo optimizuoti procesą 3D stiklo gamybai,

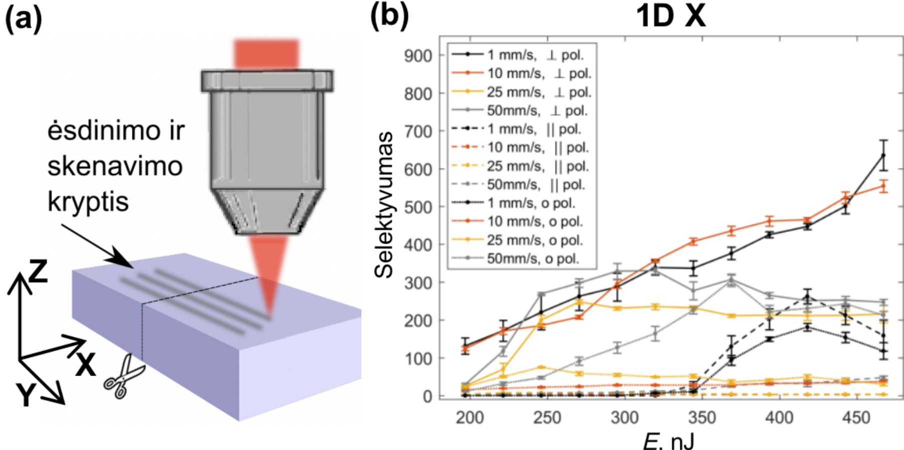

6 pav. Pavienių linijų selektyvumo tyrimo: (a) schema ir (b) rezultatai. Pavienės linijos įrašytos XY plokštumoje keičiant skirtingus parametrus, kaip antai: impulso energija, skenavimo greičiai ir spinduliuotės poliarizacija skenavimo atžvilgiu.

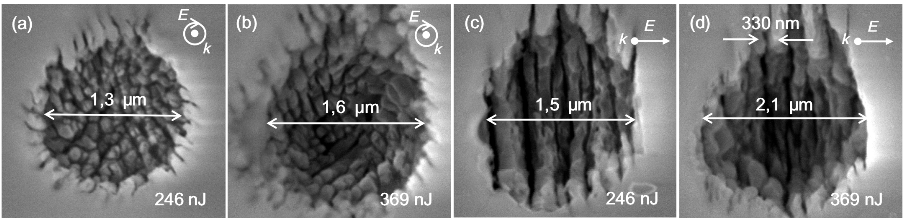

7 pav. Lazeriu suformuotų nanogardelių lydytame kvarce SEM atvaizdai, kai nanogardelės įrašytos: (a) apskritiminės poliarizacijos ir 246 nJ impulsais; (b) apskritiminės poliarizacijos ir 369 nJ impulsais; (c) tiesinės poliarizacijos ir 246 nJ impulsais; (d) tiesinės poliarizacijos ir 369 nJ impulsais.

todėl pagal gautus rezultatus tolimesniems testams pasirinktas didžiausias išbandytas skenavimo greitis (50 mm/s), siekiant išlaikyti aukštą proceso spartą. Taip pat buvo pasirinktos 2 impulsų energijos – mažiausia impulsų energija, kuri suteikia selektyvumo vertę arti maksimalios, kai poliarizacija statmena skenavimo krypčiai (246 nJ impulso energija arba 13,9 J/cm^2 energijos tankis), ir impulsų energijos vertė, kuri suteikia didžiausią reikšmę esant apskritiminei poliarizacijai (369 nJ impulso energija arba 20,9 J/cm^2 energijos tankis).

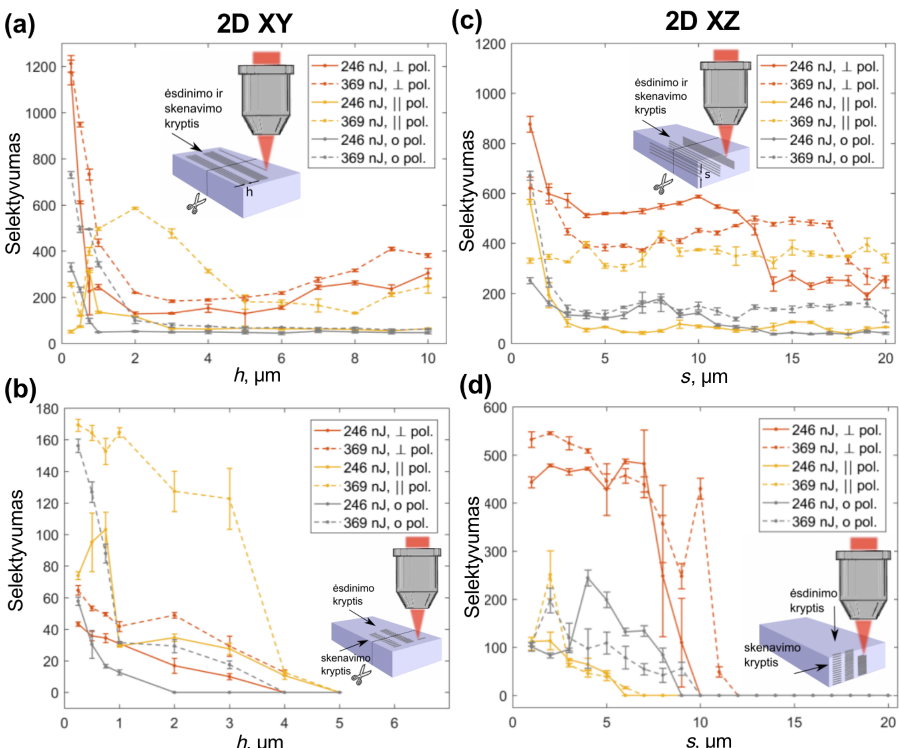

8 pav. 2D (plokštumų) selektyvumo testavimo rezultatai. Ėsdintų plokštumų selektyvumo priklausomybė nuo tarpo tarp skenavimo linijų: (a) XY plokštumos, ėsdintos lygiagrečiai su modifikacijų įrašymo kryptimi; (b) XY plokštumos, ėsdintos statmenai modifikacijų įrašymo krypčiai; (c) XZ plokštumos, ėsdintos lygiagrečiai su modifikacijų įrašymo kryptimi; (d) XZ plokštumos, ėsdintos statmenai modifikacijų įrašymo krypčiai.

2D horizontalios (XY) plokštumos testavimo rezultatai, kai ėsdinimo kryptys yra lygiagrečios su skenavimo kryptimi ir joms statmenos, pateikti 8 paveiksle, atitinkamai (a) ir (b) dalyse. Kai ėsdinimo kryptis yra lygiagreti su linijų rašymo kryptimi, didžiausias selektyvumas (apie 1200) gaunamas įrašant linijas su mažiausiu išbandytu tarpu tarp gretimų skenavimo linijų (0,25 μm, įrašytų modifikacijų persiklojimas apie 90%) ir pasirinkus poliarizaciją, statmeną skenavimo krypčiai. Šiame eksperimente didinant tarpus tarp skersavimo linijų

iki daugiau nei 2 μm, gretimos modifikacijos nebepersikloja, o selektyvumas nukrenta žemiau 500. Tai labai panašu į pavienių linijų selektyvumo reikšmes. Kaip ir tikėtasi, kai ėsdinimo kryptis yra statmena skenuojamai krypčiai, didžiausias gautas selektyvumas yra apie 6 kartus mažesnis nei ankstesniuoju atveju (iki ~170). Tačiau šis testas nustato maksimalų galimą tarpą tarp linijų horizontalia kryptimi, kuris šiuo atveju yra 4 μm, ir kuriuo dar įmanoma praėsdinti plokštumą, tačiau įrašytos modifikacijos jau nebepersikloja. Praktiškai abu aptarti atvejai vyksta vienu metu, tad jei selektyvumas bent vienai krypčiai yra arti 0, 3D struktūros ėsdinimas bus neįmanomas.

Toliau buvo atlikti 2D vertikaliųjų (XZ/YZ) plokštumų testai. Šių testų rezultatai pateikti 8 paveiksle, (c) ir (d) dalyse. Didžiausias selektyvumas pasiektas esant mažiausiam išbandytam tarpui tarp gretimų skenavimo linijų (1 μm, tai atitinka apie 90% įrašytų modifikacijų persiklojimą). Padidinus skenavimo žingsnį, selektyvumas drastiškai mažėja. Tačiau, kai poliarizacija yra lygiagreti su skenavimo kryptimi, tolesnis skenavimo žingsnio didinimas šiek tiek padidina ir ėsdinimo greitį. Tai rodo, kad modifikacijų interferencija sukuria tinkamas nanostruktūrų konfigūracijas, kurios daro poveikį ėsdinimo savybėms. Bandymas su ėsdinimo kryptimi, statmena skenavimo krypčiai, nurodo maksimalų galimą skenavimo tarpą tarp gretimų linijų Z kryptimi, kuris yra apie 10 μm, kai įrašytų modifikacijų persiplojimas yra vos 30%. Didesni tarpai tarp skenavimo linijų bus kliūtis paviršiaus ėsdinimui. Iš esmės didesnės maksimalios tarpų tarp linijų vertės gali būti paaiškintos jau minėtu vokselio ištempimu Z kryptimi dėl Gauso pluošto fokusavimo savybių. Čia mes sužinome, kad, naudojant mūsų išbandytą konfigūraciją, maksimalus skenavimo žingsnis X ar Y kryptimi galėtų būti 4 μm, o Z kryptimi – 10 μm esant tiesinei poliarizacijai. Praktiniam 3D struktūros formavimui pageidaujamos mažesnės vertės, kad būtų pasiektas didesnis selektyvumas. Vis dėlto formuojant 3D darinius reikia naudoti apskritinimę poliariaciją, kad išlaikytume panašią ėsdinimosi spartą visomis kryptimis. Tad pasirenkamas ne didesnis nei 1 μm persiklojimas X/Y kryptimi bei 9 μm persiklojimas Z kryptimi, tai atitinka apie 40% įrašytų modifikacijų persiklojimo.

Galiausiai buvo išmatuoti skirtingai skenuoti ėsdintų paviršių šiurkštumai. Buvo išmatuoti tiek XY, tiek XZ/YZ paviršiai. Šie rezultatai pavaizduoti 9 paveiksle, (a) ir (b) dalyse. Abiem atvejais mažiausias paviršiaus šiurkštumas, apie 200 nm RMS, gaunamas su mažiausiais testuotais tarpais tarp skenavimo linijų (0,5 μm). Padidinus atstumą tarp linijų, šiurkštumo vertė kyla ir pasiekia apie 800 nm RMS. Pažvelgus atgal į tą patį paviršiaus selektyvumą, galima padaryti išvadą, kad didesnis paviršiaus selektyvumas lemia mažesnį paviršiaus šiurkštumą. Selektyvumo koreliacija su paviršiaus šiurkštumu jau buvo minėta kituose darbuose [73]. Savo ruoštu poliarizacijos kryptis stipriai veikia selektyvumą. Vis dėlto gaunama priklausomybė nuo paviršiaus šiurkštumo poliarizacijos požiūriu nėra labai reikšminga ir mažiausia gaunama vertė

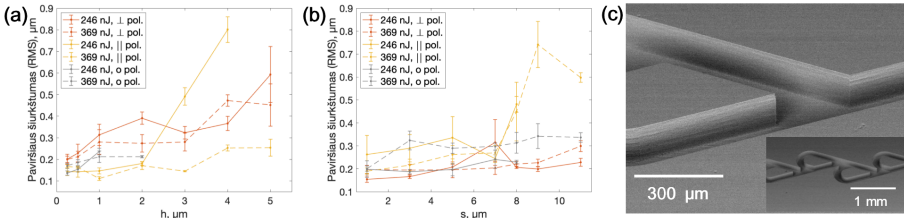

9 pav. Paviršiaus šiurkštumo priklausomybė nuo tarpo tarp skenavimo linijų (pateiktas RMS įvertis) (a) horizontaliems ir (b) vertikaliems paviršiams. (c) Padidinto mastelio SEM vaizdas, rodantis pavyzdinės struktūros paviršių kokybę vertikaliems ir horizontaliems paviršiams.

abiem atvejais nepriklauso nuo poliarizacijos. Išvada: linijų tarpusavio atstumas veikia susidarančius paviršius kur kas daugiau nei impulsų energija ar spinduliuotės poliarizacija. Be to, be minimalaus paviršiaus šiurkštumo, SLE leidžia išgauti vertikalias sienas, kaip pavaizduota 9 paveiksle, (c) dalyje.

Ne mažesnę įtaką SLE nei lazerio parametrai ar skenavimo pasirinkimas daro ir ėsdiklio bei jo savybių pasirinkimas. Šioje dalyje pristatoma idėja, kaip nesunkiai galima reikšmingai padidinti proceso seketyvumą šiek tiek adaptavus ėsdiklį. Buvo iškelta hipotezė, kad jei pavyktų pagerinti ėsdiklio drėkinimo savybes stiklui, ėsdiklis būtų labiau linkęs skverbtis gilyn į įrašytą modifikaciją ir dėl tokios priežasties ėsdinimosi sparta padidėtų. Pastebėta, kad organiniai tirpikliai drėkina stiklą labiau nei vanduo, tad atrodo intuityvu, jog pakeitus KOH tirpale vandenį organiniu tirpikliu (šiuo atveju pasirinktas izopropanolis) ėsdiklis stipriau drėkintų bandinį. Tačiau atsiranda kelios kliūtys realizuoti šią mintį. Įprastai ėsdiklis naudojamas 90°C tempeartūroje ir yra 8 – 10 mol/l koncentracijos. Tačiau žinoma, kad izopropanolis verda apie 78°C temperatūroje, o KOH tirpumas izopropanolyje yra daugiau nei 8 kartus mažesnis nei vandenyje, tad pagaminti minėtų koncentracijų tirpalų vien tik su izopropanoliu neįmanoma. Tad buvo testuojama galimybė dalį vandens ėsdiklyje pakeisti izopropanoliu ir taip pagerinti ėsdiklio drėkinimo savybes.

Eksperimento metu buvo įrašomos pavienių linijų modifikacijos 369 nJ energijos impulsais (20,9 J/cm^2 energijos tankis) ir 10 mm/s skenavimo greičiu. Kiekvienas bandinys atskirai buvo ėsdinamas skirtinguose ėsdikliuose, varijuojant KOH koncentraciją 1–10 mol/l ir keičiant izopropanolio koncentraciją 0%–50%. Išmatavus bandinio storį prieš ir po ėsdinimo buvo įvertinta nemodifikuotos medžiagos ėsdinimo sparta. Po ėsdinimo išmatavus susiformavusio kanalo ilgį įvertinta lazeriu modifikuotos medžiagos ėsdinimo sparta. Padalijus modifikuotos medžiagos ėsdinimo spartą iš nemodifikuotos medžiagos ėsdinimo spartos įvertintas selektyvumas. Šie rezultatai yra pavaizduoti 10 paveiksle. Matyti, kad nemodifikuota medžiaga greičiausiai ėsdinama ~1,5 μm/h su 10 mol/l KOH tirpalu, kuriame 5% vandens pakeista izopropanoliu. Lėčiau-

siai nemodifikuota medžiaga ėsdinama ~0,15 μm/h su 1 mol/l KOH tirpalu, kuriame yra 10% izopropanolio. Tačiau modifikuota medžiaga sparčiausiai ėsdinama ~820 μm/h su 2 mol/l KOH tirpalu, kuriame yra 20% izopropanolio. Lėčiausiai modifikuota medžiaga ėsdinama ~210 μm/h su 10 mol/l KOH tirpalu, kuriame 50% vandens pakeista izopropanoliu. Galiausiai yra įvertinamas selektyvumas kiekvieno ėsdiklio atveju. Didžiausia selektyvumo vertė ~3000 gaunama ėsdinant 2 mol/l KOH tirpale su 10% izopropanolio priemaiša. Gauta selektyvumo vertė turimomis žiniomis yra didžiausia iki šiol pademonstruota SLE procesui lydytame kvarce [18, 20]. Matome, jog pradžioje iškelta hipotezė nėra visiškai teisinga, tačiau tam tikra dalis izopropanolio tirpale leidžia padidinti tiek ėsdinimosi spartas modifikuotoje medžiagoje, tiek selektyvumą.

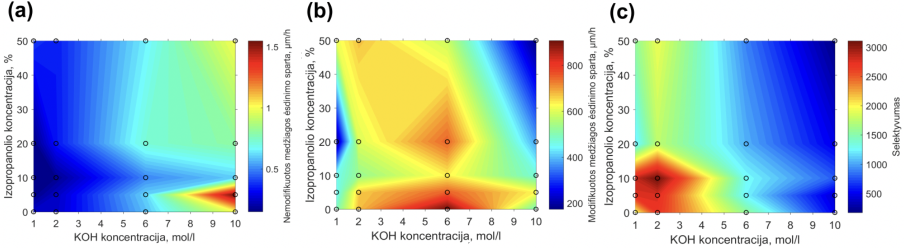

10 pav. Lazeriu nemodifikuotos (a) ir modifikuotos (b) medžiagos ėsdinimosi spartų priklausomybė nuo ėsdiklio koncentracijos ir izopropanolio priemaišos koncentracijos. Selektyvumo priklausomybė nuo ėsdiklio savybių (c) : grafikas gaunamas padalijus (b) dalies rezultatus iš (a) dalies rezultatų.

Prieš darant išvadas apie gautus rezultatus, buvo išmatuoti tirtų tirpalų drėkinimo kampai naudotam UVFS stiklui. Šie rezultatai pavaizduoti 11 paveiksle. Mažiausi kontaktiniai kampai gauti su nedidelės koncentracijos KOH tirpalais (1 – 2 mol/l) bei didesnėmis izopropanolio priemaišomis (10 – 50%). Kaip matyti gauti ėsdinimo rezultatai tiesiogiai nekoreliuoja su kontaktinio kampo matavimo rezultatais.

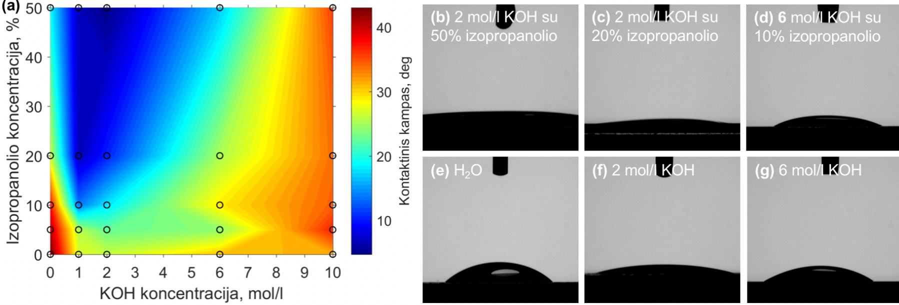

11 pav. (a) Skirtingų KOH koncentracijos tirpalų kontaktinių kampų matavimo rezultatai. (b) – (g) Skirtingų koncentracijų ėsdiklių kontaktinių kampų matavimo pavyzdžiai.

Norint suprasti visą procesą, reikia atsižvelgti ir į cheminį aspektą. Ėsdinimo metu cheminės reakcijos rezultatas yra toks pat tiek su izopropanoliu, tiek ir be jo. Ėsdinant UVFS KOH ėsdikliu, susidaro kalio silikatas ir vanduo. Nepaisant to, jog ėsdiklyje turint izopropanolio priemaišą gerėja ėsdiklio drėkinimo savybė, bet selektyvumas vis vien mažėja. Norint turėti efektyvų ėsdinimo procesą, reakcijos metu susidariusios druskos turi būti tirpios ėsdiklio tirpikliuose, tačiau susidariusios druskos gerokai prasčiau tirpsta izopropanolyje. Todėl turint didelį izopropanolio kiekį tirpale reakcijos metu susidariusios druskos visiškai sustabdo ėsdinimosi reakciją. Tačiau ant paviršiaus susidarančios izopropanolyje netirpios druskos mažina nemodifikuotos medžiagos ėsdinimo spartą, tai savaime didina selektyvumo vertę. Taigi, viena vertus, izopropanolis skatina ėsdiklio įsiskverbimą į medžiagą, bet, kita vertus, ėsdinimo metu susidariusios druskos prastai tirpta izopropanolyje. Tačiau šis efektas smarkiai mažina ir nemodifikuotos medžiagos ėsdinimosi spartą. Tad izopropanolio priemaiša ėsdiklyje turi tiek teigiamų, tiek neigiamų pasekmių, tačiau geriausi rezultatai gaunami su nedidelėmis izopropanolio koncentracijomis tirpale.

Nepaisant įspūdingų ėsdinimo spartų ir selektyvumų, ėdinimo greitis yra linkęs mažėti skverbiantis gilyn į struktūras. Todėl buvo įvertinta, kaip ėsdinimo greitis keičiasi laiko atžvilgiu. Rezultatai po 2, 4, 8 ir 12 valandų parodyti 12 paveiksle, (a) – (d) dalyse. Lyginant ėsdinimo greičius po 1 ir po 2 valandų ėsdinimo, modifikuotos medžiagos ėsdinimo greitis sumažėja apie du kartus. Po 4 valandų ėsdinimo greičiai vėl sumažėja dvigubai. Galiausiai po 8 ir 12 valandų, ėsdinimo greitis yra tarp 100 ir 200 μm/h. Toks ėsdinimo greičio mažėjimo paaiškinimas yra paprastas – kuo giliau ėsdikliui reikia įsiskverbti į ėsdintą kanalą, tuo labiau prasiskiedžia ėsdiklis ir vis sunkiau pasiekia giliausią kanalo vietą. Vis dėlto izopropanolis leidžia ne tik pasiekti, bet ir palaikyti didesnį ėsdinimo greitį ilgiau, nes padeda ėsdikliui efektyviau įsiskverbti į kanalą. Iš šių grafikų galime padaryti išvadą, kad jei norima pasiekti aukštą selektyvumą ir didelį ėsdinimo greitį, ėsdinimo laikas turi būti pakankamai trumpas (trumpesnis nei 2 – 3 valandos). Kitu atveju dėl ėsdinimo greičio praradimo ilgesniu laikotarpiu, neįmanoma palaikyti selektyvumo ir aukšto matmenų santykio, didesnio nei 1000.

Ėsdinant bandinius skirtingų koncentracijų tirpaluose buvo pastebėta, kad struktūrų, ėsdintų mažesnės KOH koncentracijos tirpaluose, paviršiaus kokybė yra prastesnė nei struktūrų, ėsdintų didesnių koncentracijų KOH tirpaluose. Siekiant patikrinti šį reiškinį, buvo įrašyti keli paviršiai XY plokštumoje ir ėsdinti skirtingų koncentracijų ėsdikliuose. Gauti paviršiai buvo vizualizuojami naudojant SEM. Suformuotų paviršių SEM atvaizdai pateikiami 13 paveiksle, (a) – (g) dalyse. Gautų paviršių šiurkštumas išmatuotas naudojant optinį profilometrą ($Sensofar\ PL\mu$2300). Koreliacija tarp paviršiaus šiurkštumo ir ėsdiklio koncentracijų pateikiama 13 paveiksle (h). Kuo didesnė ėsdiklio koncentracija, tuo mažesnis paviršiaus šiurkštumas gali būti pasiektas. Kita ver-

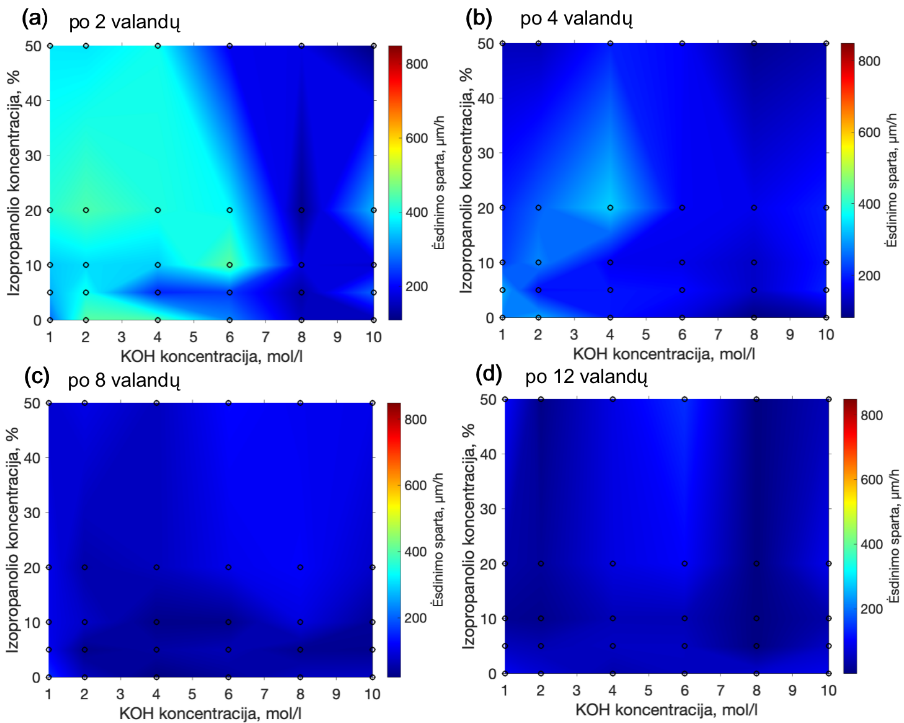

12 pav. Ėsdinimo spartos kitimas: (a) po 2 h; (b) po 4 h; (c) po 8 h ir (d) po 12 h ėsdinimo.

tus, žvelgiant į ankstesnius rezultatus, mažesnės ėsdiklio koncentracijos leidžia pasiekti didesnį selektyvumą. Palyginimui, 13 paveiksle (h) pavaizduotas paviršius, ėsdintas 5% HF tirpale, kurio paviršiaus šiurkštumas yra apie 200 nm (RMS). Paprastai, naudojant HF gaunamas žymiai mažesnis selektyvumas nei KOH [17]. Čia galime daryti visiškai priešingą išvadą prieš tai buvusiai – kuo didesnis selektyvumas, tuo didesnis paviršiaus šiurkštumas pasiekiamas. Tačiau dažniausiai norima išlaikyti tiek didelį selektyvumą, tiek mažą paviršiaus šiurkštumą. Tam reikia naudoti kombinuotas ėsdinimo technikas [30]. Pavyzdžiui, ėsdinti darinius mažos KOH koncentracijos tirpaluose ir sumažinti paviršiaus šiurkštumą papildomai ėsdinant mažos koncentracijos HF tirpale.

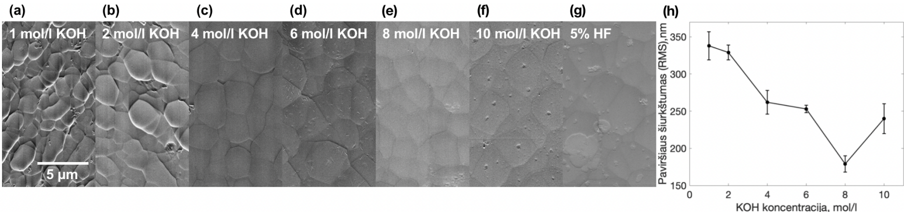

13 pav. (a) – (g) Įvairiose ėsdiklio koncentracijose ėsdintų paviršių SEM atvaizdai. (h) Ėsdintų paviršių šiurkštumo priklausomybė nuo ėsdiklio koncentracijos.

Kristalinio safyro SLE

Kai kuriuose taikymuose skamba itin patraukliai vietoj lydyto kvarco ar kitų stiklų naudoti kristalus, tokius kaip safyras. Safyras pasižymi dideliu mechaniniu atsparumu, tačiau yra ganėtinai sunkiai apdirbama medžiaga. Literatūroje galim rasti ne vieną publikaciją, kurioje nagrinėjamas SLE metodo pritaikymas darinių formavimui iš safyro. Tačiau iki šiol yra parodyta labai nedaug struktūrų, suformuotų iš safyro SLE metodu, pavyzdžių. Tai rodo, kad ne visi pademonstruoti protokolai yra visiškai tinkami darinių formavimui iš safyro. Safyro SLE yra nagrinėjama disertacijos straipsnyje **IV**.

Šioje dalyje pristatoma įvairių safyro apdirbimo SLE metodu protokolų palyginimas. Buvo ištirta kelių skirtingų parametrų įtaką safyro SLE. Modifikacijų įrašymui safyre testuoti trys skirtingi bangos ilgiai: pirmos trys Yb:KGW lazerio harmonikos (1030 nm, 515 nm, 343 nm), skirtingos impulsų trukmės (200, 600, 1000 fs) bei impulsų energijos (100, 200, 300, 400 ir 500 nJ). Taip pat buvo tirta, kokią įtaką SLE procesui daro skirtingų ėsdiklių pasirinkimas, todėl ištestuoti 4 skirtingi ėsdikliai: 35% KOH 90°C temperatūroje, 25% NaOH 90°C temperatūroje, 48% HF kambario temperatūroje ir H_2SO_4 bei H_3PO_4 rūgščių mišinys 270°C temperatūroje.

Tiriant minėtų faktorių įtaką SLE procesui atlikti 3 skirtingi testai pavaizduoti 14 paveiksle. Pirmiausia buvo įrašomos pavienės linijos medžiagos tūryje,

bandinys su modifikacijomis perpjaunamas statmenai modifikacijoms ir ėsdinamas skirtingomis sąlygomis. Po ėsdinimo įvertinama skirtingomis sąlygomis gaunama ėsdinimo sparta. Kitas eksperimentas – cilindrinių skylių per visą bandinio storį įrašymas. Taip įvertinama galimybė išėsdinti 3D darinį safyre. Galiausiai įrašomos paviršinės modifikacijos, kurios leidžia stebėti nanogardelių morfologijos pokyčius po ėsdinimo.

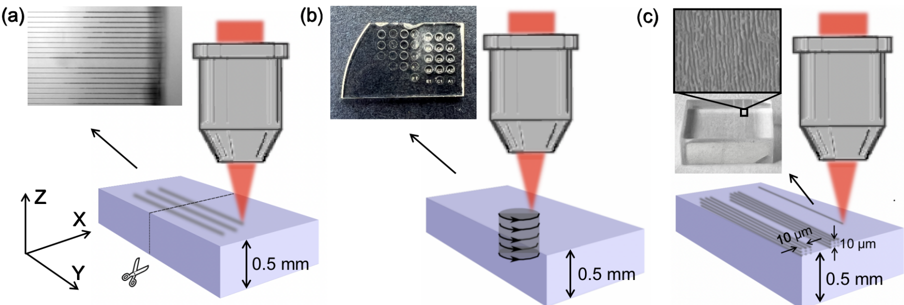

14 pav. Safyro SLE tyrimui atliktų eksperimentų schemos: (a) Pavienių linijų įrašytų medžiagos tūryje eksperimentas; (b) cilindrinių skylių per visą substrato aukštį įrašymo eksperimentas; (c) lazeriu indukuotų medžiagos pokyčių morfologijos įvertinimas po ėsdinimo.

Atskirų linijų eksperimento rezultatai pavaizduoti 15 paveiksle (a). Atlikus minėtą eksperimentą aukščiausia ėsdinimo sparta (iki 200 μm/h) gauta ėsdinant sieros ir fosforo rūgščių mišiniu. Kiek mažesnės ėsdinimo spartos gautos ėsdinant KOH ir NaOH, žemiausios – ėsdinant HF. Visais atvejais pirmąja harmonika įrašytos modifikacijos leido išgauti bent keliais procentais didesnes ėsdinimo spartas nei įrašytos antrąja lazerio harmonika. Tačiau trečiąja harmonika įrašytų modifikacijų ėsdinimo spartos buvo itin nedidelės (iki 20 μm/h). Tokios tendencijos gali būti paaiškintos skirtingais nanogardelių periodais. Nanogardelių, suformuotų skirtingomis lazerio harmonikomis, atvaizdai pateikiami 16 paveiksle. Pirmąja harmonika įrašytos nanogardelės turi didžiausias poras, tad ėsdikliui lengviau įsiskverbti į medžiagą. Taip pat pastebėta, kad bene visais atvejais didžiausia impulso energija leidžia išgauti didžiausias ėsdinimo spartas. Kaip jau minėta, svarbus parametras SLE yra selektyvumas, tačiau šiuo atveju šį parametrą įvertinti sudėtinga dėl itin nedidelės nemodifikuoto safyro ėsdinimo spartos. Tad įvertinamos bent apytikslės selektyvumo vertės naudojant skirtingus ėsdiklius. Jos pateiktos 15 paveiksle (b).Didžiausias selektyvumas ($\sim$1000) gali būti gautas naudojant NaOH ar KOH, o žemiausias selektyvumas (66) gaunamas naudojant sieros ir fosforo rūgščių mišinį.

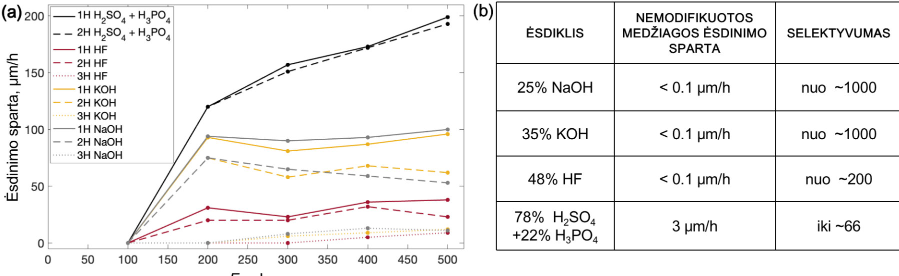

ĖSDIKLIS	NEMODIFIKUOTOS MEDŽIAGOS ĖSDINIMO SPARTA	SELEKTYVUMAS
25% NaOH	< 0.1 μm/h	nuo ~1000
35% KOH	< 0.1 μm/h	nuo ~1000
48% HF	< 0.1 μm/h	nuo ~200
78% H_2SO_4 +22% H_3PO_4	3 μm/h	iki ~66

15 pav. (a) Pavienių linijų, įrašytų ir ėsdintų naudojant skirtingus protokolus, ėsdinimo spartų grafikas. 1H, 2H ir 3H indikuoja 1030 nm bangos ilgio lazerio pirmąją, antrąją ir trečiąją harmonikas, atitinkamai 1030 nm, 515 nm ir 343 nm. (b) Lentelėje pateiktos nemodifikuotos medžiagos ėsdinimo spartos, naudojant skirtingus ėsdiklius ir selektyvumo įverčius, remiantis modifikuotų ir nemodifikuotų medžiagų ėsdinimo spartų rezultatais.

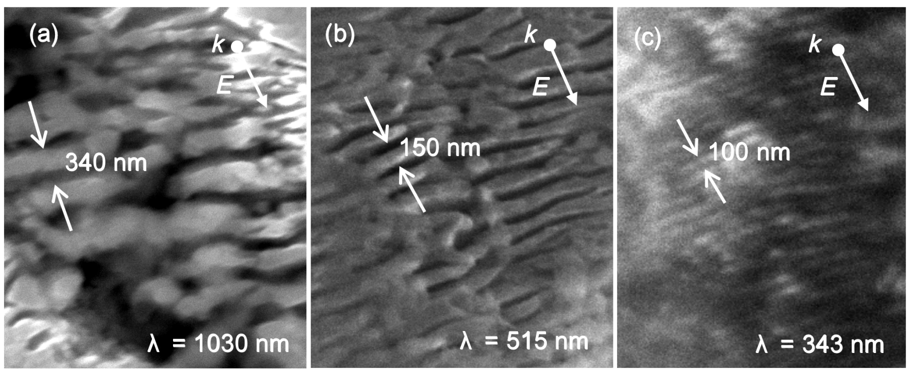

16 pav. SEM atvaizdai nanogardelių, suformuotų skirtingais lazerio bangos ilgiais: (a) 1030 nm; (b) 515 nm; (c) 343 nm.

Šios eksperimento dalies tikslas yra pademonstruoti 3D struktūras, pagamintas iš safyro. Tad po pavienių linijų testų, buvo atlikti 3D testai, po kurių galima atsirinkti SLE protokolus, leidžiančius išgauti 3D darinius. Ištirti identiški parametrai kaip ir prieš tai atliktame eksperimente. Taip pat papildomai išbandyti įvairūs impulsų trukmės variantai. Keičiant parametrus kiekvienam dariniui į 500 μm storio safyro plokštę įrašytos cilindrinės struktūros per visą plokštelės storį. Šio eksperimento rezultatai pavaizduoti 17 paveiksle. 3D eksperimentas parodė, kad geriausi parametrai, leidžiantys efektyviausiai modifikuoti struktūras, yra pirmosios harmonikos spinduliuotė, 200 fs trukmės impulsai ir 300 – 500 nJ impulsų energija, kuri atitinka 16,9 – 28,2 J/cm^2 energijos tankį vienam impulsui. Vienintelis cheminis ėsdiklis, kuris sėkmingai išėsdino suformuotas modifikacijas buvo H_2SO_4 ir H_3PO_4 mišinys. Naudojant kitus testuotus ėsdiklius (KOH, NaOH ir HF) cilindrinės struktūros nebuvo

išėsdintos iš plokštelės net po 48 valandų ėsdinimo. Kyla klausimas, kodėl kiti išbandyti ėsdikliai nėra tinkami 3D darinių formavimui.

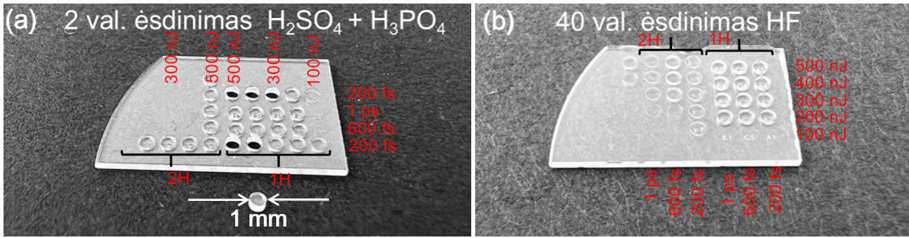

17 pav. Cilindrinės struktūros įrašytos skirtingais bangos ilgiais, impulso trukmėmis bei impulso energijomis: (a) bandinys ėsdintas H_2SO_4 ir H_3PO_4 rūgščių mišinyje; (b) bandinys ėsdintas HF rūgštyje.

Norint patikrinti minėtus pastebėjimus, buvo įrašytos 10 μm gylio ir pločio modifikacijos ant safyro paviršiaus. Modifikacijos įrašytos parametrų rinkiniu, kuris buvo nurodytas tinkamiausias 3D darinių formavimui (1030 nm bangos ilgio spinduliuotė, 600 kHz impulsų pasikartojimo dažnis, 200 fs impulsų trukmė ir 500 nJ impulsų energija). Įrašytos modifikacijos ėsdintos skirtinguose ėsdikliuose. Galiausiai gauti rezultatai buvo įvertinti naudojantis SEM. SEM atvaizdai su skirtingai ėsdintomis modifikacijomis pateikti 18 paveiksle. Kiekvienu atveju išmatuotas ėsdintų modifikacijų gylis. Po apdirbimo lazeriu nanogardelės padengtos įvairiomis nuosėdomis. Po 1 valandos ėsdinimo 35% KOH ir 25% NaOH 90°C temperatūroje ir 48% HF didelė dalis nuosėdų nusiėsdina ir tampa aiškiai matomos nanogardelės (18 paveikslas, (b) – (d) dalys). Tačiau paėsdinus modifikaciją tik 20 minučių H_2SO_4 ir H_3PO_4 mišinyje, ne tik nelieka lazerio apdorojimo likučių, bet yra ėsdinamos ir pačios nanogardelės (18 paveikslas (e)). Visi minėti ėsdikliai reaguoja su medžiaga skirtingai. Vizualiai HF efektyviausiai pašalina po apdirbimo likusius likučius nuo paviršiaus. Naudojant NaOH po ėsdinimo lieka daugiausia likučių ant paviršiaus. Lyginant su atskirų linijų testo rezultatais, HF linkęs šalinti medžiagą nuo paviršiaus, o NaOH ir KOH linkę patekti į nanogardelių vidų. Vis dėlto nė viena iš minėtų ėsdikliu neėsdina pačių nanogardelių, kitaip tariant, sienų tarp lazeriu indukuotų porų. Todėl KOH, NaOH ir HF ėsdikliai negali visiškai išėsdinti 3D struktūrų, nes vis dar lieka ne iki galo pašalintos nanogardelės. Šis pastebėjimas mums suteikia pagrindo manyti, kad ne visa medžiaga nanogardelėse tampa amorfinė arba amorfinė medžiaga iš dalies rekristalizuojasi po to, kai ji nebėra veikiama lazerio. Kita vertus, H_2SO_4 ir H_3PO_4 ėsdina tiek nemodifikuotą medžiagą, tiek ir pačias nanogardeles, tad ėsdiklis yra tinkamas dariniams iš safyro formuoti.

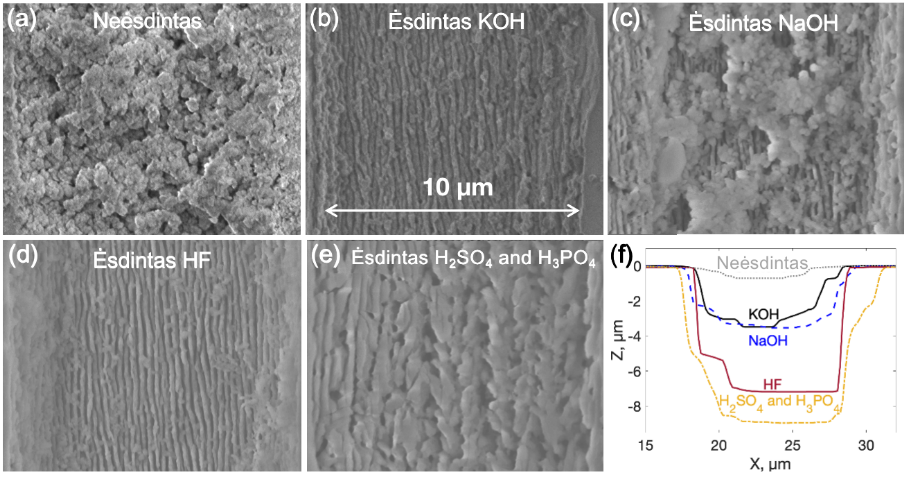

18 pav. Lazeriu indukuotų paviršinių modifikacijų SEM atvaizdai ir išmatuoti modifikacijų gyliai: (a) neėsdinta paviršinė modifikacija; (b) paviršinė modifikacija ėsdinta 35% KOH 1 h; (c) paviršinė modifikacija ėsdinta 25% NaOH 1 h; (d) paviršinė modifikacija ėsdinta 48% HF 1 h; (e) paviršinė modifikacija ėsdinta H_2SO_4 ir H_3PO_4 20 min. (f) Optiniu profilometru išmatuoti skirtingai ėsdintų modifikacijų gyliai.

Galiausiai buvo suformuotos kelios struktūros iš safyro (19 paveikslas): šešiakampių bei apvalių skylių matricos. Dariniai pagaminti iš 0,5 mm C kristalinės orientacijos safyro plokštelių kaip ėsdiklį naudojant sieros ir fosforo rūgščių mišinį. Pirmiausia pagaminti skirtingo skersmens skylių masyvai: 100 μm ir vos 2 μm skersmens skylės. Taip pat suformuotos 400 μm sienų ilgio šešiakampės išpjovos. Pagamintos kelios panašios struktūros su vis mažesniais (200, 100 ir 50 μm) sienų storiais tarp išpjovų. Struktūra su dar siauresnėmis 25 μm sienomis buvo itin trapi, tad neišliko. Svarbus pastebėjimas suformavus šias struktūras yra tai, kad ėsdinant safyrą ant bandinio paviršiaus formuojasi skirtingų pokrypių plokštumos, kurios atsiranda dėl skirtingo safyro ėsdinimosi spartų atskiroms kristalinėms orientacijoms. Tačiau bendru atveju šios struktūros demonstruoja galimybę formuoti įvairias struktūras iš kristalinio safyro.

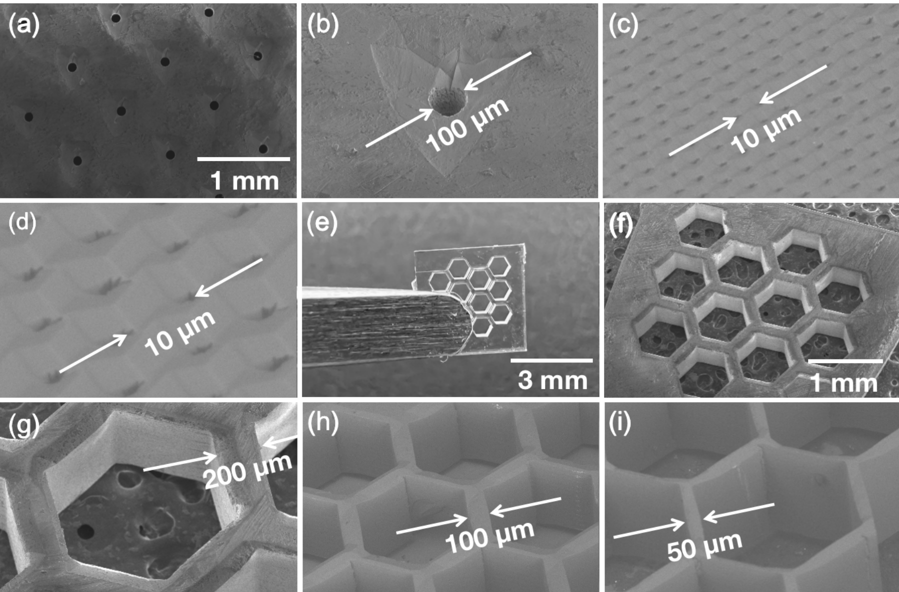

19 pav. Dariniai, pagaminti iš C kristaline orientacija supjaustyto kristalinio safyro: (a), (b) 100 μm skersmens skylių matrica; (c), (d) pavienio skenavimo linijomis suformuotų 10 μm periodo skylių matrica; (e) – (g) korio tipo darinys, kurio šešiakampės išpjovos sienos ilgis yra 400 μm, o sienos storis tarp išpjovų lygus 200 μm; (h), (i) panašūs korio tipo dariniai, kurių sienų storis tarp išpjovų yra atitinkamai 100 μm ir 50 μm.

SLE taikymai

SLE metodu pagaminti komponentai bei prietaisai gali būti panaudoti įvairiose taikymų srityse, kaip antai mikromechanika ar mikrofluidika. Šiame skyriuje aptariami funkciniai prietaisai, pagaminti iš lydyto kvarco. Darinių gamybai naudojami parametrų rinkiniai įvardyti kaip efektyviausi 2 skyriuje. Minėti taikymų pavyzdžiai aptarti straipsniuose **II** ir **V**.

Stiklinė mikromechanika

SLE būdu galima formuoti visiškai laisvos architektūros darinius, tad atsiranda ir galimybė gaminti judančius mikromechaninius mechanizmus, kurie nereikalauja jokio surinkimo proceso. Tokie dariniai gali būti itin maži bei tikslūs (iki keleto μm tikslusmo). Tokius mikromechaninius mechanizmus būtų galima suskirstyti į du tipus: mechanizmai, kurie juda dėl lanksčių detalių ir kurie juda aplink suformuotas ašeles. Taigi šiame darbe buvo pademonstruota keletas įvardytų tipų mechanizmų. Žinoma, kad plonos bei didelio matmenų santykio stiklinės detalės yra lanksčios, tad gebant formuoti tikslias ir didelio matmenų

santykio detales galima pagaminti tokiu judėjimo metodu paremtus mechanizmus. Vienas tokių yra stiklinė spyruoklė, kuri, kaip matyti iš 20 paveikslo, gali būti suspausta, o galiausiai grįžti į pradinę padėtį. Spyruoklės vijos plotis yra 50 μm, o bendras apvijos ilgis siekia apie 12 mm.

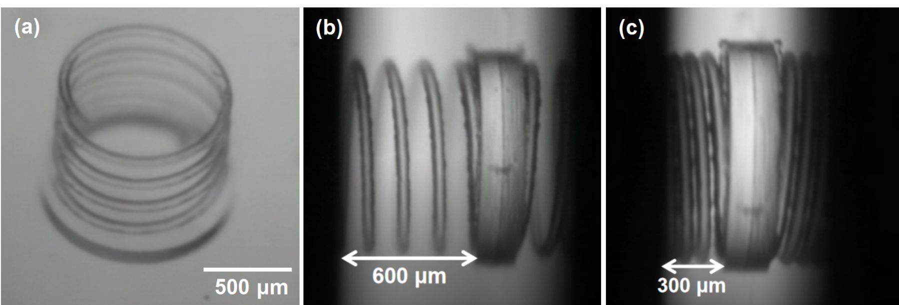

20 pav. Stiklinės spyruoklės optinės nuotraukos: (a) bendras darinio vaizdas, o (b) ir (c) rodo galimybę suspausti darinį. Dėl nedidelio apvijų storio (skersmuo – 50 μm) ir gana didelio bendro spyruoklės apvijos ilgio (12 mm), spyruoklė pakartotinai gali būti suspaudžiama nuo 600 iki 300 μm aukščio (t. y. 50% viso spyruoklės aukščio) nesugadinant darinio.

Taip pat buvo pagaminti ir keli kiek kitokie mikromechaniniai mechanizmai – tai lanksto tipo grandinėlė ir Ženevos mechanizmas. Šie dariniai pavaizduoti 21 ir 22 paveiksluose. Pagrindinė idėja gaminant tokį mechanizmą yra ta, jog lazeriu modifikuojama medžiaga tarp ašelės ir aplink ją besisukančio mechanizmo. Tokiu būdu iš karto po ėsdinimo gaunama struktūra, kuri gali judėti. SLE būdu pagamintų struktūrų paviršiaus šiurkštumas yra nedidelis (apie 200 – 300 nm RMS), tad mechanizmai gali sklandžiai judėti. Pagrindinis tokių mechanizmų privalumas yra didelis tikslumas ir tai, kad jie nereikalauja papildomo surinkimo. Kai kalbame apie precizinius mikromechanizmus, tai yra didelis privalumas.

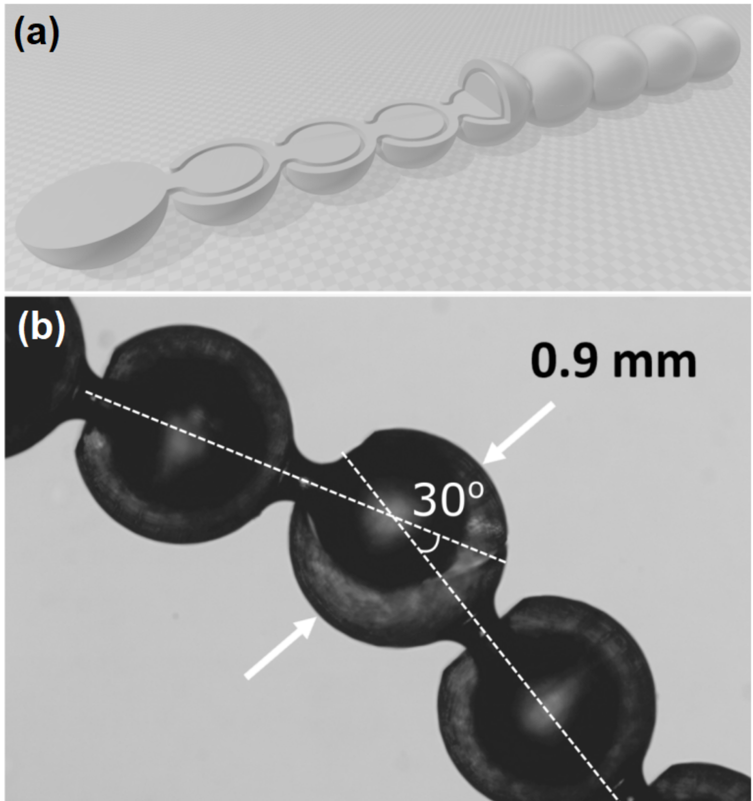

21 pav. Judanti grandinėlė sudaryta iš daugelio lanksto tipo mechanizmų: (a) struktūros 3D modelis su 1/4 struktūros nuopjova, siekiant parodyti vidinę sistemos architektūrą ir jos judėjimo mechanizmą; (b) pagaminto darinio optinio mikroskopo nuotrauka. Pasiektas kiekvieno lanksto lenkimo kampas yra apie 30°.

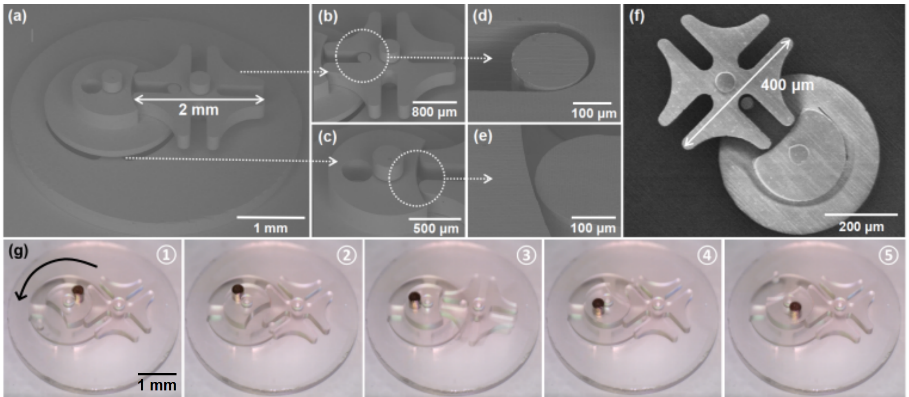

22 pav. SLE metodu pagaminto Ženevos mechanizmo nuotraukos ir atvaizdai: (a) viso mechanizmo SEM atvaizdai; (b) – (e) svarbiausių mechanizmo detalių SEM atvaizdai; (f) 5 kartus mažesnio nei dalyje (a) Ženevos mechanizmo SEM atvaizdas; (g) chronologinės judančio Ženevos mechanizmo nuotraukos. Juoda rodyklė nurodo sukimosi kryptį. Darinio judėjimas yra automatizuojamas pritvirtinant nedidelį magnetą ant mechanizmo ir patalpinant darinį išoriniame magnetiniame lauke.

Laboratorija ant lusto

Kita galima SLE taikymo sritis yra mikrofluidinės sistemos bei prietaisai. Didelė dalis įvairių testavimų gali būti perkelta iš masyvių laboratorijų į kompaktiškesnes mikrofluidines sistemas, taip taupant tiek medžiagų kiekius, tiek vengiant tam tikrų testavimų su žmonėmis, gyvūnais ar jų organais. Taigi šioje darbo dalyje pateikiamas laboratorijos ant lusto pavyzdys. Buvo testuota kepenų ant lusto sistema, kuri pagaminta, naudojant kelias skirtingas femtosekundinio apdirbimo technikas, iš jų ir SLE.

Pagrindinė kepenų ant lusto prietaiso idėja – trijų nepriklausomų kanalų sistema. Lusto vidurinėje dalyje šie trys kanalai atskirti stulpelių tipo filtrais, per kuriuos vėliau centriniame kanale patalpintos kepenų ląstelės gali sąveikauti su medžiaga, esančia gretimuose kanaluose. Pasirinktas mikrofluidinis prietaisas pagamintas sujungiant kelias femtosekundinio lazerio spinduliuote paremtas apdirbimo technikas. Lusto gamybos strategijos schema pavaizduota 23 paveiksle. Pirmiausia naudojantis SLE metodu suformuojami mikrofluidiniai kanalai ant lydyto kvarco bandinio paviršiaus. Kartu su mikrofluidine sistema yra pagaminami ir stulpelių tipo filtrai lusto centre. Pagaminus tokią mikrofluidinę sistemą, ši yra enkapsuliuojama užvirinant tokio paties dydžio lydyto kvarco plokštelę ant pokštelės su paviršiniais kanalais. Virinimo procesas įgyvendinamas – paveikus kontaktą tarp dviejų skaidrių medžiagų aukšto intensyvumo fokusuota spinduliuote ir taip atskiruose taškuose sulydant dvi plokšteles tarpusavyje.

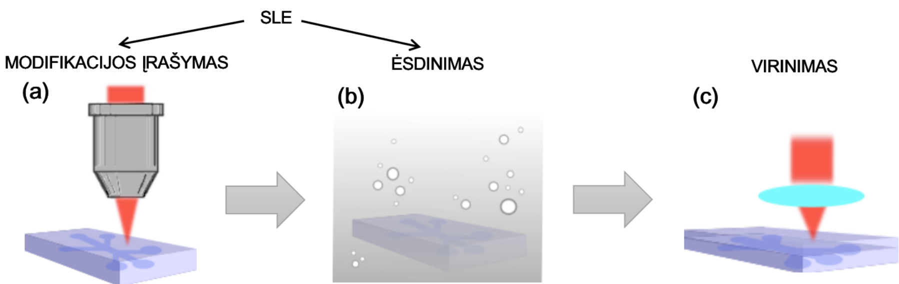

23 pav. Laboratorijos ant lusto gamybos schema: (a) nanogardelių įrašymas stiklo tūryje fokusuota femtosekundine spinduliuote; (b) lazeriu modifikuoto bandinio ėsdinimas; (a) ir (b) dalys kartu sudaro SLE metodą; (c) SLE metodu pagaminti paviršiniai kanalai uždaromi užvirinant stiklinę plokštelę ant bandinio su paviršiniais kanalais.

Apibūdintomis metodikomis pagamintas stiklinis lustas pavaizduotas 24 paveiksle. Matyti, kad naudojantis SLE suformuojama tiksli mikrokanalų sistema, kurioje kartu su kanalu pagaminamas ir filtras. Filtras sudarytas iš stulpelių, kurių ilgis ir plotis yra 36 μm ir 55 μm, o aukštis 200 μm. Tarpai tarp atskirų stulpelių yra 14 μm. Galutinis prietaisas po virinimo pavaizduotas 25 paveiksle. Paveikslo dalyje (b) matyti aplink kanalą susiformavusios virinimo siūlės, kanaliukai yra užpildyti nedideliu kiekiu vandens tikrinant, ar virinimas hermetiškai užsandarino mikrofluidinę sistemą.

Prototipinio prietaiso funkcionalumas yra testuojamas naudojant kepenų ląsteles. Mikrofluidinės sistemos kanalai padengiami homogeniška poli-L-lizino plėvele. Buvo testuoti ir papildomu sluoksniu nepadengti lustai, tačiau HepG2 (GS) neprisitvirtino ant lygaus lustų paviršiaus. Ląstelės gerai prisitvirtina ant plėvele padengto paviršiaus. Po 24 valandų apsėtos HepG2 (GS) ląstelės pradeda augti monosluoksnyje. Sferoidų skaičius ir dydis atitinka pradinį ląstelių tankį. Keičiant terpę, ląstelių monosluoksniai lieka pritvirtinti prie paviršiaus ir nuolat auga. Po 96 valandų HepG2 (GS) ląstelės sudaro didelius nereguliarius sferoidus. Po 7 dienų sferoidų augimas lemia didelių sferoidų klasterių formavimąsi visoje kepenų ant lusto sistemoje. Aprašyto bandymo nuotraukos pateiktos 26 paveiksle. Nuo 7 dienos ląstelių gyvybingumas mažėja, kaip matyti iš kai kurių ląstelių apvalios formos. Remiantis "Trypan Blue" testu, po 9 dienų dauguma ląstelių yra negyvos. Prisitvirtinusios ląstelės yra gyvybingos 7 dienas nuo eksperimento pradžios. Taigi iš atliktų eksperimentų matyti, kad tokios sistemos gali būti tinkamos įvairiems biologiniams tyrimams.

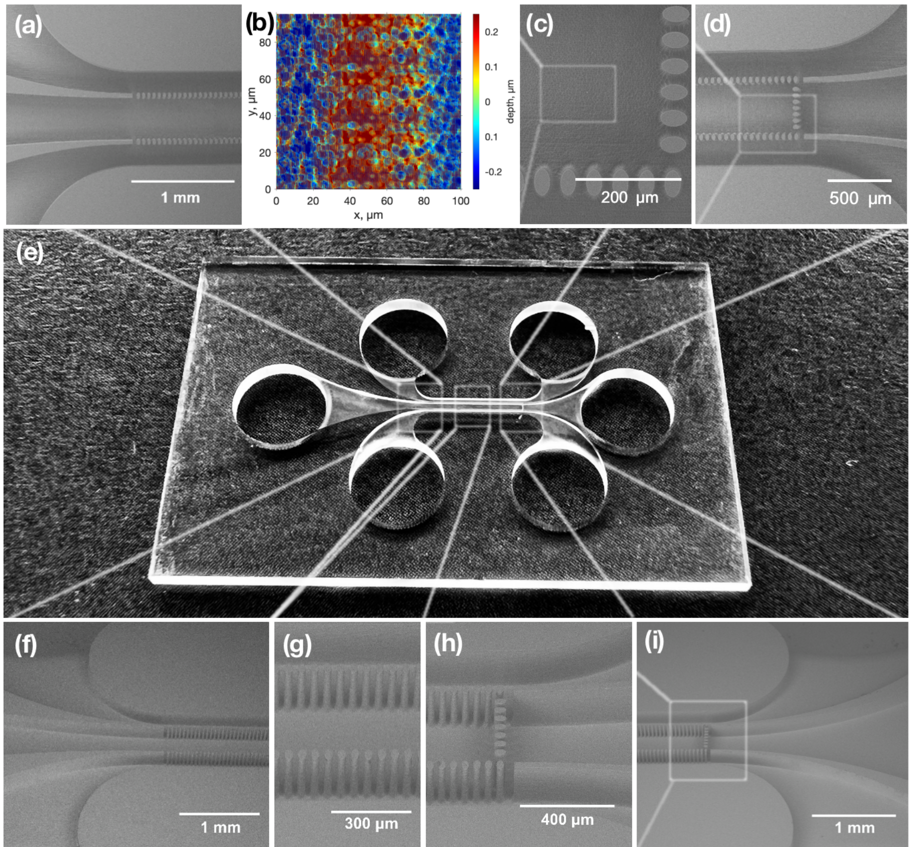

24 pav. Pagamintos laboratorijos ant lusto nuotraukos; (d) viso prietaiso optinė nuotrauka; (a), (c) ir (d) atskirų darinio dalių SEM atvaizdai žiūrint iš viršaus; (f) – (i) atskirų darinio dalių SEM atvaizdai žiūrint 45° kampu; (b) kanalo paviršiaus topologijos atvaizdavimas optiniu profilometru.

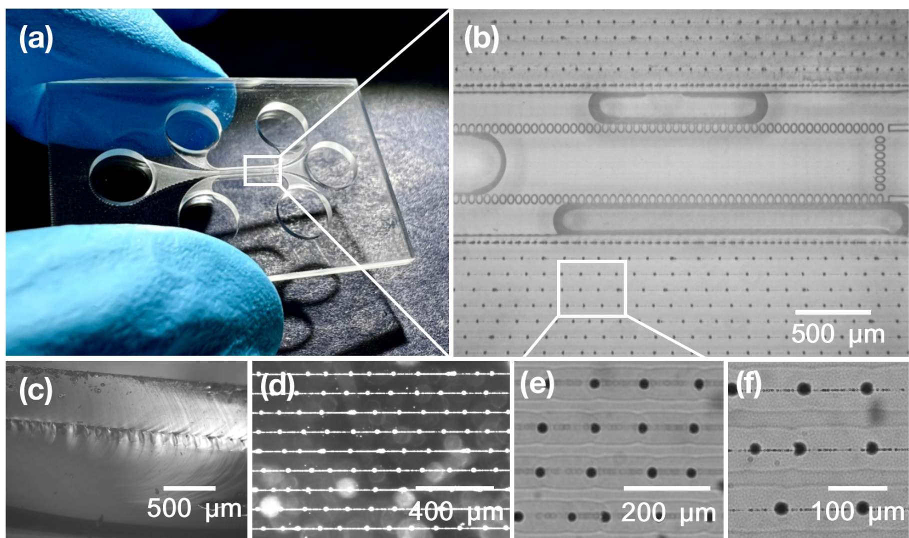

25 pav. (a) Laboratorijos ant lusto nuotrauka. (b) Pagaminto mikrofluidinio lusto optinė nuotrauka, kurioje matyti virinimo siūlės. (c) Suvirinto lusto pjūvio optinė nuotrauka. (d) Virinimo siūlių optinė nuotrauka su sukryžiuotais poliarizatoriais. (e) ir (f) Optinės virinimo siūlių nuotraukos, gautos skirtingo didinimo objektyvais.

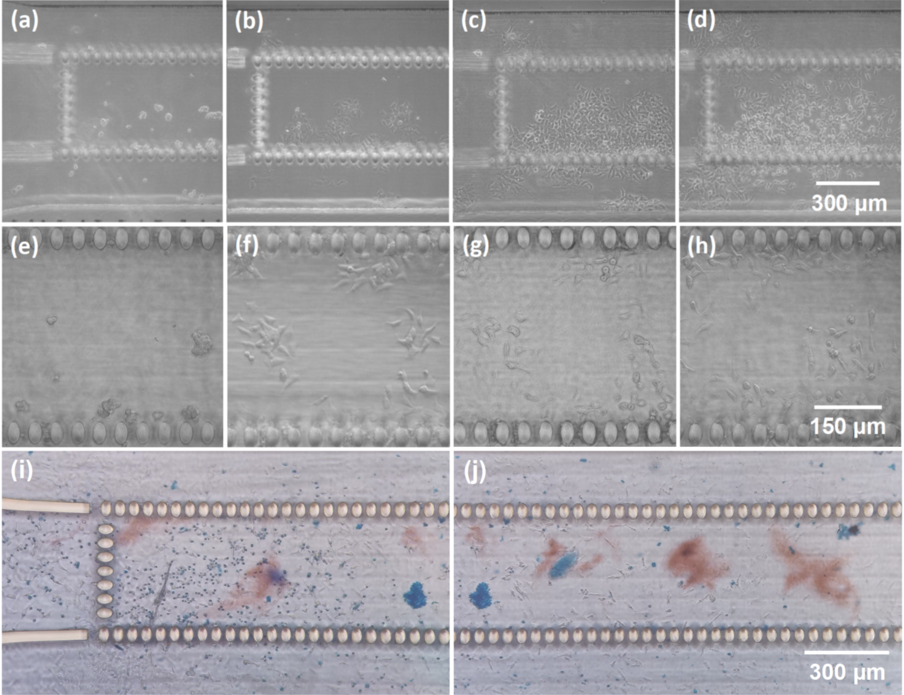

26 pav. Mikrofluidiniu kanalų, apsėtų HepG2(GS) kepenų ląstelėmis, optinės nuotraukos: (a), (e) iš karto po apsėjimo ląstelėmis; (b), (f) po 24 valandų; (c), (g) po 96 valandų; (d),(h) po 7 dienų; (i), (j) po 9 dienų atlikus *Trypan Blue* testą.

Išvados

1. 3D struktūros sudarytos iš dviejų skirtingų plokštumų. Įrašius minėtas plokštumas skirtingais parametrais, pastebėta, kad abiem atvejais mažiausias testuotas atstumas tarp skenavimo linijų (0,25 μm horizontalioje plokštumoje ir 1 μm vertikalioje plokštumoje, tai atitinka apie 90% įrašytų modifikacijų persiklojimą) suteikia didesnį ėsdinimo greitį (iki maždaug 1000 μm/h), o mažesnis tarpas tarp skenavimo linijų lemia mažesnį suformuotų plokštumų paviršiaus šiurkštumą (<200 nm RMS).

2. Ėsdiklio koncentracija ir drėkinimo savybės keičia UVFS ėsdinimo greitį ir selektyvumą. Didesnė ėsdiklio koncentracija padidina modifikuotos ir nemodifikuotos medžiagų ėsdinimo greitį. Priešingai, mažesnė ėsdiklio koncentracija suteikia mažesnį modifikuotos ir nemodifikuotos medžiagų ėsdinimo greitį. Į standartinį ėsdiklį įdėjus organinio tirpiklio priemaišą, ėsdiklis stipriau drėkina ėsdinamą paviršių. Dalies vandens ėsdiklyje pakeitimas izopropanoliu dėl cheminių reakcijų sumažina nemodifikuotos medžiagos ėsdinimo greitį. Kartu tai padidina modifikuotos medžiagos ėsdinimo greitį dėl didelio įrašytų nanogardelių paviršiaus ploto. Pasiektas apie 3000 selektyvumas naudojant 2 mol/l KOH tirpalą, kuriame 10% vandens buvo pakeista izopropanoliu.

3. UVFS SLE naudojamo ėsdiklio koncentracija keičia suformuotų paviršių šiurkštumą. Testuotais atvejais didesnė KOH koncentracija suteikia mažesnį paviršiaus šiurkštumą. Didžiausias paviršiaus šiurkštumas, 340 nm RMS, buvo gaunamas naudojant 1 mol/l KOH tirpalą, o mažiausias, 180 nm RMS, buvo gaunamas naudojant 8 mol/l KOH tirpalą.

4. Palyginus skirtingus safyro SLE algoritmus, pasirinkti tinkamiausi parametrai safyro SLE procesui. Safyro struktūros formavimui tinkami parametrai yra: 1030 nm bangos ilgis, 200 fs impulsų trukmė, 610 kHz impulsų kartojimo dažnis ir 300 – 500 nJ impulsų energija. Tik vienas iš testuotų ėsdiklių buvo tinkamas struktūros formavimui – tai 270°C temperatūros sieros ir fosforo rūgščių mišinys. Pasirinkto protokolo selektyvumas yra apie 66. Minėtas rūgščių mišinys vienintelis iš testuotų ėsdiklių, kuris gali ėsdinti įrašytas nanogardeles.

5. Naudojant SLE technologiją, buvo pagamintos kelios mikromechanikos ir mikrofluidikos struktūros, kaip kad: spyruoklė, Ženevos mechanizmas, lanksto tipo struktūra ir mikrofluidinis lustas. Iš pademonstruotų darinių matyti, kad SLE technika yra tinkama funkcinių įtaisų gamybai. Pagamintų mikromechaninių kompnentų judėjimo funkcijos buvo ištestuotos. Laboratorijos ant lusto sistema testuota kepenų ląstelių biomedicininiams tyrimams.

Curriculum vitae

Name:	Agne
Surname:	Butkute
Date of birth:	1994-09-07
Place of birth:	Kupiškis, Lithuania
E-mail:	agne.but.agne@gmail.com; agne.butkute@ff.vu.lt

Education:

2009-2013	Vilnius Žirmūnai gymnasium.
2013-2017	Vilnius University, Faculty of Physics, *Bachelor's degree.*
2017-2019	Vilnius University, Faculty of Physics, *Master's degree.*
2019-2023	Vilnius University, Faculty of Physics, Laser Research Center, *Ph.D. studies.*

Work experience:

2017-2018	Technical support engineer at Teltonika Ltd.
2018-Current	Researcher at Femtika Ltd.
2020-Current	Researcher, Junior Researcher at Vilnius University, Laser research center.

Trumpos žinios apie autorių

Vardas:	Agnė
Pavardė:	Butkutė
Gimimo data:	1994-09-07
Gimimo vieta:	Lietuva
E-paštas:	agne.but.agne@gmail.com; agne.butkute@ff.vu.lt

Išsilavinimas:

2009-2013	Vilniaus Žirmūnų gimnazija.
2013-2017	Vilniaus universitetas, Fizikos fakultetas, *Bakalauro laipsnis.*
2017-2019	Vilniaus universitetas, Fizikos fakultetas, *Magistro laipsnis.*
2019-2023	Vilniaus universitetas, Fizikos fakultetas, Lazerinių tyrimų centras, *Doktorantūra.*

Profesinė veikla:

2017-2018	Techninio palaikymo inžinierė, UAB Teltonika.
2018-Dabar	Tyrėja, UAB "Femtika"
2020–Dabar	Tyrėja, Jaunesnioji mokslo darbuotoja, Vilniaus universitetas, Lazerinių tyrimų centras.

Bibliography

[1] S. K. Sundaram, E. Mazur, Inducing and probing non-thermal transitions in semiconductors using femtosecond laser pulses, Nat. Mater. **1**(4), 217–224 (2002).

[2] M. Gedvilas, J. Mikšys, J. Berzinš, V. Stankevič, G. Račiukaitis, Multi-photon absorption enhancement by dual-wavelength double-pulse laser irradiation for efficient dicing of sapphire wafers, Sci. Rep. **7**(1), 1–10 (2017).

[3] T. Kudrius, G. Šlekys, S. Juodkazis, Surface-texturing of sapphire by femtosecond laser pulses for photonic applications, Journal of Physics D: Applied Physics **43**(14), 145501 (2010).

[4] L. Qi, K. Nishii, M. Yasui, H. Aoki, Y. Namba, Femtosecond laser ablation of sapphire on different crystallographic facet planes by single and multiple laser pulses irradiation, Optics and Lasers in Engineering **48**(10), 1000–1007 (2010).

[5] Y. Li, H. Liu, M. Hong, High-quality sapphire microprocessing by dual-beam laser induced plasma assisted ablation, Opt. Express **28**(5), 6242–6250 (2020).

[6] J. Chen, X. Lu, Z. Li, Q. Wen, J. Lu, F. Jiang, Anisotropy of material removal during laser-induced plasma assisted ablation of sapphire, Ceramics International **48**(10), 13880–13889 (2022).

[7] X. Ding, T. Sato, Y. Kawaguchi, , H. Niino, Laser-induced backside wet etching of sapphire, Jpn. J. Appl. Phys. **42**(Part 2, No. 2B), L176–L178 (2003).

[8] M. Y. Tsvetkov, N. V. Minaev, A. A. Akovantseva, P. S. Timashev, A. E. Muslimov, V. M. Kanevskii, Thermoplasmonic laser-induced backside wet etching of sapphire, Quantum Electronics **49**(2), 133–140 (2019).

[9] O. Zhigalina, D. N., Khmelenin, A. V. Atanova, N. V. Minaev, A. P. Sviridov, M. Y. Tsvetkov, A nanoscale modification of materials at thermoplasmonic laser-induced backside wet etching of sapphire, Plasmonics **15**, 599–608 (2020).

[10] X. Liu, Y. Zhang, Q. Li, J. Zheng, Y. Lu, S. Juodkazis, Q. Chen, H. Sun, Biomimetic sapphire windows enabled by inside-out femtosecond laser deep-scribing, PhotoniX **3**(1), 2662–1991 (2022).

[11] X. Cao, Y. Lu, H. Fan, H.Xia, L. Zhang, Y. Zhang, Wet-etching-assisted femtosecond laser holographic processing of a sapphire concave microlens array, Appl. Opt. **57**(32), 9604–9608 (2018).

[12] Y.-M. Lu, X.-Q. Liu, L. Zhu, Q.-D. Chen, S. Juodkazis, H.-B. Sun, Vector scanning subtractive manufacturing technology for laser rapid fabrication, Opt. Lett. **46**(8), 1963–1966 (2021).

[13] Q. Li, Q. Chen, L. Niu, Y. Yu, L. Wang, Y. Sun, H. Sun, Sapphire-based dammann gratings for uv beam splitting, IEEE Photon. J. **8**(6), 2500208 (2016).

[14] Q. Li, Y. Yu, L. Wang, X. Cao, X. Liu, Y. Sun, Q. Chena, J. Duan, H. Sun, Sapphire-based fresnel zone plate fabricated by femtosecond laser direct writing and wet etching, IEEE Photon. Technol. Lett. **28**(12), 1290–1293 (2016).

[15] N. R. Gottumukkala, M. C. Gupta, Laser processing of sapphire and fabrication of diffractive optical elements, Appl. Opt. **61**(9), 2391–2397 (2022).

[16] C. Hnatovsky, R. S. Taylor, E. Simova, V. R. Bhardwaj, D. M. Rayner, P. B. Corkum, Polarization-selective etching in femtosecond laser-assisted microfluidic channel fabrication in fused silica, Opt. Lett. **30**(14), 1867 – 1869 (2005).

[17] C. A. Ross, D. G. MacLachlan, D. Choudhury, R. R. Thomson, Optimisation of ultrafast laser assisted etching in fused silica, Opt. Express **26**(19), 24343–24356 (2018).

[18] J. Gottmann, M. Hermans, N. Repiev, J. Ortmann, Selective laser-induced etching of 3D precision quartz glass components for microfluidic applications-up-scaling of complexity and speed, Micromachines **8**(4), 110 (2017).

[19] M. Hermans, J. Gottmann, F. Riedel, Selective, laser-induced etching of fused silica at high scan-speeds using KOH, J. Laser. Micro. Nanoeng. **9**(2), 126 – 131 (2014).

[20] V. Stankevič, G. Račiukaitis, P. Gečys, Chemical etching of fused silica after modification with two-pulse bursts of femtosecond laser, Opt. Express **29**(20), 31393–31407 (2021).

[21] C. Hnatovsky, R. S. Taylor, E. Simova, P. P. Rajeev, D. M. Rayner, V. Bhardwaj, P. B. Corkum, Fabrication of microchannels in glass using focused femtosecond laser radiationand selectivechemical etching, Appl. Phys. A **84**, 47–61 (2006).

[22] S. Matsuo, H. Sumi, S. Kiyama, T. Tomita, S. Hashimoto, Femtosecond laser-assisted etching of pyrex glass with aqueous solution of KOH, Applied Surface Science **255**(24), 9758–9760, proceedings of the Sixth International Conference onPhoto-Excited Processes and Applications(6-ICPEPA) (2009).

[23] S. Matsuo, Y. Tabuchi, T. Okada, S. Juodkazis, H. Misawa, Femtosecond laser assisted etching of quartz: microstructuring from inside, Appl. Phys. A **84**(1-2), 99–102 (2006).

[24] S. Matsuo, K. Tokumi, T. Tomita, S. Hashimoto, Three-dimensional residue-free volume removal inside sapphire by high-temperature etching after irradiation of femtosecond laser pulses, Laser Chem. **2008**, 892721–1–892721–4 (2008).

[25] A. Rodenas, M. Gu, G. Corrielli, P. Paie, S. John, A. K. Kar, R. Osellame, Three-dimensional femtosecond laser nanolithography of crystals, Nature Photon. **13**, 105–109 (2019).

[26] J. Gottmann, D. Wortmann, M. Hörstmann-Jungemann, Fabrication of sub-wavelength surface ripples and in-volume nanostructures by fs-laser induced selective etching, Appl. Surf. Sci. **255**(10), 5641–5646 (2009).

[27] Y. Bellouard, Shape memory alloys for microsystems: A review from a material research perspective, Mater. Sci. Eng. A 582 – 589 (2008).

[28] P. Paiè, F. Bragheri, D. Di Carlo, R. Osellame, Particle focusing by 3d inertial microfluidics, Microsystems & nanoengineering **3**(1), 1–8 (2017).

[29] S. Kim, J. Kim, Y.-H. Joung, S. Ahn, J. Choi, C. Koo, Optimization of selective laser-induced etching (sle) for fabrication of 3d glass microfluidic device with multi-layer micro channels, Micro and Nano Systems Letters **7**(1), 1–7 (2019).

[30] S. LoTurco, R. Osellame, R. Ramponi, K. C. Vishnubhatla, Hybrid chemical etching of femtosecond laser irradiated structures for engineered microfluidic devices, J. Micromech. Microeng. **23**, 1–8 (2013).

[31] J. Kim, S. Kim, Y. Joung, J. Choi, C. Koo, Two-step hybrid process of movable part inside glass substrate using ultrafast laser, Micro Nano Syst. Lett. **9**(16), 2213–9621 (2021).

[32] Y. Bellouard, A. A. Said, P. Bado, Integrating optics and micromechanics in a single substrate: a step toward monolithic integration in fused silica, Opt. express **13**(17), 6635 – 6644 (2005).

[33] T. Tičkūnas, M. Perrenoud, S. Butkus, R. Gadonas, S. Rekštytė, M. Malinauskas, D. Paipulas, Y. Bellouard, V. Sirutkaitis, Combination of additive and subtractive laser 3d microprocessing in hybrid glass/polymer microsystems for chemical sensing applications, Opt. Express **25**(21), 26280–26288 (2017).

[34] V. Tomkus, V. Girdauskas, J. Dudutis, P. Gečys, V. Stankevič, G. Račiukaitis, Impact of the wall roughness on the quality of micrometric nozzles manufactured from fused silica by different laser processing techniques, Applied Surface Science **483**, 205–211 (2019).

[35] T. Brabec, F. Krausz, Intense few-cycle laser fields: Frontiers of nonlinear optics, Rev. Mod. Phys **72**(2), 545–585 (2000).

[36] R. Boyd, *Nonlinear Optics* (Academic Press, 2008).

[37] L. V. Keldysh, Ionization in the field of a strong electromagnetic wave, J. Exp. Theor. Phys. **20**(5), 1307–1314 (1965).

[38] Y. Bellouard, A. Said, M. Dugan, P. Bado, Fabrication of high-aspect ratio, micro-fluidic channels and tunnels using femtosecond laser pulses and chemical etching, Opt. express **12**(10), 2120–2129 (2004).

[39] A. B. Zhimalov, V. F. Solinov, V. S. Kondratenko, T. V. Kaplina, Laser cutting of float glass during production, Glass Ceram. **63**(9-10), 319–321 (2006).

[40] C. Zhao, H. Zhang, Y. Wang, Semiconductor laser asymmetry cutting glass with laser induced thermal-crack propagation, Opt. Lasers Eng. **63**, 43–52 (2014).

[41] Y. Kanemitsu, Y. Tanaka, Mechanism of crack formation in glass after high-power laser pulse irradiation, J. Appl. Phys. **62**(4), 1208–1211 (1987).

[42] I. Mirza, N. M. Bulgakova, J. Tomaštik, V. Michalek, O. Haderka, L. Fekete, T. Mocek, Ultrashort pulse laser ablation of dielectrics: Thresholds, mechanisms, role of breakdown, Sci. Rep. **6**(39133), 1–11 (2016).

[43] P. Dyer, R. J. Farley, R. Giedl, D. Karnakis, Excimer laser ablation of polymers and glasses for grating fabrication, Appl. Surf. Sci. **96-98**, 537 – 549 (1996).

[44] C. Buerhop, B. Blumenthal, R. Weissmann, Glass surface treatment with excimer and CO_2 lasers, Appl. Surf. Sci. **46**, 430 – 434 (1990).

[45] L. Jonušauskas, S. Juodkazis, M. Malinauskas, Optical 3D printing: bridging the gaps in the mesoscale, J. Opt. **20**(5), 053001 (2018).

[46] A. Jesacher, , M. J. Booth, Parallel direct laser writing in three dimensions with spatially dependent aberration correction, Opt. Express **18**(20), 21090 – 21099 (2010).

[47] D. Krol, Femtosecond laser modification of glass, J. Non-Cryst. Solids **354**, 416–424 (2008).

[48] A. A. Khalil, J.-P. Bérubé, S. Danto, T. Cardinal, Y. Petit, L. Canioni, R. Vallée, Comparative study between the standard type i and the type a femtosecond laser induced refractive index change in silver containing glasses, Opt. Mater. Express **9**(6), 2640–2651 (2019).

[49] Single femtosecond laser beam induced nanogratings in transparent media - mechanisms and applications, Journal of Materiomics **5**(1), 1–14 (2019).

[50] M. Beresna, M. Gecevičius, P. G. Kazansky, Ultrafast laser direct writing and nanostructuring in transparent materials, Advances in Optics and Photonics **6**(3), 293–339 (2014).

[51] Y. Liao, J. Ni, L. Qiao, M. Huang, Y. Bellouard, K. Sugioka, Y. Cheng, High-fidelity visualization of formation of volume nanogratings in porous glass by femtosecond laser irradiation, Optica **2**(4), 329–334 (2015).

[52] S. Richter, M. Heinrich, S. Döring, A. Tünnermann, S. Nolte, U. Peschel, Nanogratings in fused silica: Formation, control, and applications, Journal of Laser Applications **24**(4), 042008 (2012).

[53] M. Beresna, M. Gecevičius, P. G. Kazansky, T. Taylor, A. V. Kavokin, Exciton mediated self-organization in glass driven by ultrashort light pulses, Applied Physics Letters **101**(5), 053120 (2012).

[54] V. R. Bhardwaj, E. Simova, P. P. Rajeev, C. Hnatovsky, R. S. Taylor, D. M. Rayner, P. B. Corkum, Optically produced arrays of planar nanostructures inside fused silica, Phys. Rev. Lett. **96**, 057404 (2006).

[55] C. Hnatovsky, R. Taylor, P. Rajeev, E. Simova, V. Bhardwaj, D. Rayner, P. Corkum, Pulse duration dependence of femtosecond-laser-fabricated nanogratings in fused silica, Applied Physics Letters **87**(1), 014104 (2005).

[56] J. Qi, Z. Wang, J. Xu, Z. Lin, X. Li, W. Chu, Y. Cheng, Femtosecond laser induced selective etching in fused silica: optimization of the inscription conditions with a high-repetition-rate laser source, Opt. Express **26**(23), 29669 – 29678 (2018).

[57] S. Richter, M. Heinrich, S. Döring, A. Tünnermann, S. Nolte, Formation of femtosecond laser-induced nanogratings at high repetition rates, Applied Physics A **104**, 503–507 (2011).

[58] K. Itoh, W. Watanabe, S. Nolte, , C. B. Schaffer, Ultrafast processes for bulk modification of transparent materials, MRS Bull. **31**(08), 620–625 (2006).

[59] K. Sugioka, Y. Cheng, Ultrafast lasers-reliable tools for advanced materials processing, Light: Sci. Appl. **4**(e149), 2014 (3).

[60] K. Miura, J. Qiu, H. Inouye, T. Mitsuyu, K. Hirao, Photowritten optical waveguides in various glasses with ultrashort pulse laser, Appl. Phys. Lett **71**(23), 3329 – 3331 (1997).

[61] M. Rafayelyan, T. Gertus, E. Brasselet, Laguerre-gaussian quasi-modal q-plates from nanostructured glasses, Applied Physics Letters **110**(26), 261108 (2017).

[62] D. Gailevicius, V. Koliadenko, V. Purlys, M. Peckus, V. Taranenko, K. Staliunas, Photonic crystal microchip laser, Scientific reports **6**(1), 34173 (2016).

[63] X. Q. Liu, B. F. Bai, Q. D. Chen, H. B. Sun, Etching-assisted femtosecond laser modification of hard materials, Opto-Electron. Adv. **2**(9), 190021–1 – 190021–14 (2019).

[64] S. Butkus, D. Paipulas, D. Kaškelytė, E. Gaižauskas, V. Sirutkaitis, Improvement of cut quality in rapid-cutting of glass method via femtosecond laser filamentation, J. Laser Micro. Nanoeng. **10**(1), 59 – 63 (2015).

[65] T. Tamaki, W. Watanabe, J. Nishii, K. Itoh, Welding of transparent materials using femtosecond laser pulses, Japanese Journal of Applied Physics **44**(5L), L687 (2005).

[66] S. Richter, S. Nolte, A. Tünnermann, Ultrashort pulse laser welding - a new approach for high- stability bonding of different glasses, Physics Procedia **39**, 556–562, laser Assisted Net shape Engineering 7 (LANE 2012) (2012).

[67] S. Richter, F. Zimmermann, R. Eberhardt, A. Tunnermann, S. Nolte, Toward laser welding of glasses without optical contacting, Appl. Phys. A **121**, 1–9 (2015).

[68] A. Marcinkevičius, S. Juodkazis, M. Watanabe, M. Miwa, S. Matsuo, H. Misawa, J. Nishii, Femtosecond laser-assisted three-dimensional microfabrication in silica, Opt. Lett. **26**(5), 277–279 (2001).

[69] F. Chen, Z. Deng, Q. Yang, H. Bian, G. Du, J. Si, X. Hou, Rapid fabrication of a large-area close-packed quasi-periodic microlens array on BK7 glass, Opt. Lett. **39**(3), 606 – 609 (2014).

[70] S. Juodkazis, K. Yamasaki, V. Mizeikis, S. Matsuo, H. Misawa, Formation of embedded patterns in glasses using femtosecond irradiation, Appl. Phys. A **79**(4-6), 1549–1553 (2004).

[71] X. Li, J. Xu, Z. Lin, J. Qi, P. Wang, W. Chu, Z. Fang, Z. Wang, Z. Chai, Y. Cheng, Polarization-insensitive space-selective etching in fused silica induced by picosecond laser irradiation, Appl. Surf. Sci. **485**(15), 188 – 193 (2019).

[72] K. Sugioka, M. Masuda, T. Hongo, Y. Cheng, K.Shihoyama, K. Midorikawa, Three-dimensional microfluidic structure embedded in photostructurable glass by femtosecond laser for lab-on-chipapplications, Appl.Phys. A **79**, 815 – 817 (2004).

[73] S. Butkus, M. Rickus, R. Sirutkaitis, D. Paipulas, V. Sirutkaitis, Fabrication of high aspect ratio channels in fused silica using femtosecond pulses and chemical etching at different conditions, J. Laser Micro. Nanoen. **14**(1), 19 – 24 (2019).

[74] S. Kiyama, S. Matsuo, S. Hashimoto, Y. Morihira, Examination of etching agent and etching mechanism on femotosecond laser microfabrication of channels inside vitreous silica substrates, J. Phys. Chem. C **113**(27), 11560–11566 (2009).

[75] E. Casamenti, S. Pollonghini, Y. Bellouard, Few pulses femtosecond laser exposure for high efficiency 3d glass micromachining, Optics Express **29**(22), 35054–35066 (2021).

[76] M. Ochoa, P. Roldán-Varona, J. F. Algorri, J. M. López-Higuera, L. Rodríguez-Cobo, Polarisation-independent ultrafast laser selective etching processing in fused silica, Lab on a Chip (2023).

[77] M. Bu, T. Melvin, G. J. Ensell, J. S. Wilkinson, A. G. Evans, A new masking technology for deep glass etching and its microfluidic application, Sens. Actuators. A **115**(2-3), 476–482 (2004).

[78] F. Venturini, W. Navarrini, G. Resnati, P. Metrangolo, R. M. Vazquez, R. Osellame, G. Cerullo, Selective iterative etching of fused silica with gaseous hydro[U+FB02]uoric acid, J. Phys. Chem. C **114**(43), 18712–18716 (2010).

[79] S. LoTurco, Hybrid chemical etching of femtosecond irradiated 3D structures in fused silica glass, MATEC Web of Conferences **8** (2013).

[80] D. Choudhury, A. Ródenas, L. Paterson, D. Jaque, A. K. Kar, 3d microfabrication in yag crystals by direct laser writing and chemical etching, in *Conference on Lasers and Electro-Optics/Pacific Rim* (Optical Society of America, 2013), WPE_14.

[81] A. B. Randles, M. Esashi, S. Tanaka, Etch rate dependence on crystal orientation of lithium niobate, IEEE Transactions on Ultrasonics, Ferroelectrics and Frequency Control **57**(11), 2372–2380 (2010).

[82] D. Wortmann, J. Gottmann, N. Brandt, H. Horn-Solle, Micro- and nanostructures inside sapphire by fs-laser irradiation and selective etching, Opt. Express **16**(3), 1517 – 1522 (2008).

[83] M. Horstmann-Jungemann, J. Gottmann, D. Wortmann, Nano- and microstructuring of SiO_2 and sapphire with fs-laser induced selective etching, J. Laser. Micro. Nanoeng. **4**(2), 135–140 (2009).

[84] S. Juodkazis, K. Nishimura, H. Misawa, T. Ebisui, R. Waki, S. Matsuo, T. Okada, Control over the crystalline state of sapphire, Advanced Materials **18**(11), 1361–1364 (2006).

[85] M. Hörstmann-Jungemann, J. Gottmann, M. Keggenhoff, 3D-microstructuring of sapphire using fs-laser irradiation and selective etching, J. Laser. Micro. Nanoeng. **5**(2), 145 – 149 (2010).

[86] L. Capuano, R. Pohl, R. M. Tiggelaar, J. W. Berenschot, J. E. Gardeniers, G. R. B. E. Romer, Morphology of single picosecond pulse subsurface laser-induced modifications of sapphire and subsequent selective etching, Opt. Express **26**(22), 29283–29295 (2018).

[87] L. Capuano, R. Tiggelaar, J. Berenschot, J. Gardeniers, G. Römer, Fabrication of millimeter-long structures in sapphire using femtosecond infrared laser pulses and selective etching, Opt. Laser Eng. **133**, 106114 (2020).

[88] S. Juodkazis, Y. Nishi, H. Misawa, Femtosecond laser-assisted formation of channels in sapphire using KOH solution, Phys. Status Solidi RRL **2**(6), 275–277 (2008).

[89] L. Capuano, J. Berenschot, R. Tiggelaar, M. Feinaeugle, N. Tas, J. Gardeniers, G. Römer, Fabrication of microstructures in the bulk and on the surface of sapphire by anisotropic selective wet etching of laser-affected volumes, Journal of micromechanics and microengineering **32**(12), 125003 (2022).

[90] Y. Hu, S. Rao, S. Wu, P. Wei, W. Qiu, D. Wu, B. Xu, J. Ni, L. Yang, J. Li, J. Chu, K. Sugioka, All-glass 3D optofluidic microchip with built-in tunable microlens fabricated by femtosecond laser-assisted etching, Adv. Opt. Mater. **6**(9), 1701299 (2018).

[91] P. Paiè, F. Bragheri, D. D. Carlo, R. Osellame, Particle focusing by 3D inertial microfluidics, Microsyst. Nanoeng. **3**(1) (2017).

[92] K. Sugioka, Y. Cheng, K. Midorikawa, Three-dimensional micromachining of glass using femtosecond laser for lab-on-a-chip device manufacture, Appl.Phys. A **81**, 1 – 10 (2005).

[93] Y. Bellouard, T. Lehnert, J.-E. Bidaux, T. Sidler, R. Clavel, R. Gotthardt, Local annealing of complex mechanical devices: a new approach for developing monolithic micro-devices, Mater. Sci. Eng. 795–798 (1999).

[94] J. Gottmann, M. Hermans, J. ortmann, Microcutting and hollow 3D microstructures in glasses by in-volume selective laser-induced etching (ISLE), J. Laser. Micro. Nanoeng. **8**(1), 15 – 18 (2013).

[95] R. S. Taylor, C. Hnatovsky, E. Simova, P. P. Rajeev, D. M. Rayner, P. B. Corkum, Femtosecond laser erasing and rewriting of self-organized planar nanocracks in fused silica glass, Opt. Lett. **32**(19), 2888–2890 (2007).

[96] Y. Xia, G. M. Whitesides, Soft lithography, Annual Review of Materials Science **28**(1), 153–184 (1998).

[97] J. G. Vial, *Soluble silicates* (Reinhold, New York, 1952).

[98] N. Greenwood, A. Earnshaw, *Chemistry of the Elements* (Pergamon, 1986), 398.

[99] T. Monteiro, P. Kastytis, L. Gonçalves, G. Minas, S. Cardoso, Dynamic wet etching of silicon through isopropanol alcohol evaporation, Micromachines **6**(10), 1534–1545 (2015).

[100] I. Zubel, M. Kramkowska, Etch rates and morphology of silicon (h k l) surfaces etched in KOH and KOH saturated with isopropanol solutions, Sens. Actuators A Phys. **115**(2-3), 549–556 (2004).

[101] K. P. Rola, I. Zubel, Impact of alcohol additives concentration on etch rate and surface morphology of (100) and (110) si substrates etched in KOH solutions, Microsyst. Technol. **19**(4), 635–643 (2012).

[102] A. Butkutė, T. Baravykas, J. Stančikas, T. Tičkūnas, R. Vargalis, D. Paipulas, V. Sirutkaitis, L. Jonušauskas, Femtosecond laser assisted 3d etching using inorganic-organic etchant, Materials **15**(8), 2817 (2022).

[103] K. Saeedabadi, G. Tosello, M. Calaon, Optimization of injection molded polymer lab-on-a-chip for acoustic blood plasma separation using virtual design of experiment, Procedia CIRP **107**, 40–45, leading manufacturing systems transformation – Proceedings of the 55th CIRP Conference on Manufacturing Systems 2022 (2022).

[104] L. Ma, M. Petersen, X. Lu, Identification and antimicrobial susceptibility testing of campylobacter using a microfluidic lab-on-a-chip device, Applied and Environmental Microbiology **86**(9), e00096–20 (2020).

[105] Y. Sun, T. L. Quyen, T. Q. Hung, W. H. Chin, A. Wolff, D. D. Bang, A lab-on-a-chip system with integrated sample preparation and loop-mediated isothermal amplification for rapid and quantitative detection of salmonella spp. in food samples, Lab Chip **15**, 1898–1904 (2015).

[106] C. Tymm, J. Zhou, A. Tadimety, A. Burklund, J. X. Zhang, Scalable covid-19 detection enabled by lab-on-chip biosensors, Cellular and Molecular Bioengineering **13**, 313–329 (2020).

[107] J. Zhuang, J. Yin, S. Lv, B. Wang, Y. Mu, Advanced “lab-on-a-chip” to detect viruses – current challenges and future perspectives, Biosensors and Bioelectronics **163**, 112291 (2020).

[108] S. Srikanth, U. Jayapiriya, S. K. Dubey, A. Javed, S. Goel, A lab-on-chip platform for simultaneous culture and electrochemical detection of bacteria, Iscience **25**(11), 105388 (2022).

[109] X. Li, S. M. George, L. Vernetti, A. H. Gough, D. L. Taylor, A glass-based, continuously zonated and vascularized human liver acinus microphysiological system (vlamps) designed for experimental modeling of diseases and adme/tox, Lab on a Chip **18**(17), 2614–2631 (2018).

[110] S. Cho, S. Lee, S. I. Ahn, Design and engineering of organ-on-a-chip, Biomedical Engineering Letters 1–13 (2023).

[111] A. Shinde, K. Illath, U. Kasiviswanathan, S. Nagabooshanam, P. Gupta, K. Dey, P. Chakrabarty, M. Nagai, S. Rao, S. Kar, et al., Recent advances of biosensor-integrated organ-on-a-chip technologies for diagnostics and therapeutics, Analytical Chemistry (2023).

[112] J. R. Puryear III, J.-K. Yoon, Y. Kim, Advanced fabrication techniques of micro engineered physiological systems, Micromachines **11**(8), 730 (2020).

COPIES OF INCLUDED PUBLICATIONS

I

3D MANUFACTURING OF GLASS MICROSTRUCTURES USING FEMTOSECOND LASER

A. Butkutė and L. Jonušauskas
Micromachines 12(5), 499–526 (2021).

Review

3D Manufacturing of Glass Microstructures Using Femtosecond Laser

Agnė Butkutė [1,2,*] and Linas Jonušauskas [1,2,*]

[1] Femtika Ltd., Saulėtekio Ave. 15, LT-10224 Vilnius, Lithuania
[2] Laser Research Center, Vilnius University, Saulėtekio Ave. 10, LT-10223 Vilnius, Lithuania
* Correspondence: agne@femtika.lt (A.B.); linas@femtika.lt (L.J.)

Abstract: The rapid expansion of femtosecond (fs) laser technology brought previously unavailable capabilities to laser material processing. One of the areas which benefited the most due to these advances was the 3D processing of transparent dielectrics, namely glasses and crystals. This review is dedicated to overviewing the significant advances in the field. First, the underlying physical mechanism of material interaction with ultrashort pulses is discussed, highlighting how it can be exploited for volumetric, high-precision 3D processing. Next, three distinct transparent material modification types are introduced, fundamental differences between them are explained, possible applications are highlighted. It is shown that, due to the flexibility of fs pulse fabrication, an array of structures can be produced, starting with nanophotonic elements like integrated waveguides and photonic crystals, ending with a cm-scale microfluidic system with micro-precision integrated elements. Possible limitations to each processing regime as well as how these could be overcome are discussed. Further directions for the field development are highlighted, taking into account how it could synergize with other fs-laser-based manufacturing techniques.

Keywords: femtosecond laser; glass micromachining; 3D structuring

Citation: Butkutė, A.; Jonušauskas, L. 3D Manufacturing of Glass Microstructures Using Femtosecond Laser. *Micromachines* **2021**, *12*, 499. https://doi.org/10.3390/mi12050499

Academic Editors: Rebeca Martínez Vázquez, Francesca Bragheri and Petra Paiè

Received: 28 February 2021
Accepted: 12 April 2021
Published: 28 April 2021

Publisher's Note: MDPI stays neutral with regard to jurisdictional claims in published maps and institutional affiliations.

Copyright: © 2021 by the authors. Licensee MDPI, Basel, Switzerland. This article is an open access article distributed under the terms and conditions of the Creative Commons Attribution (CC BY) license (https://creativecommons.org/licenses/by/4.0/).

1. Introduction

Glass and related transparent dielectrics play an important role in huge variety of applications. Through the millennia it found its way into all aspects of life, starting from construction engineering and building expanding to nanotechnology and space exploration. Glass owns its applicability to a combination of superb properties, such as being mechanically robust, transparent to the visible part of the electromagnetic spectrum, chemically inert in organic solvents and biocompatible. While glasses are not as diverse as metals [1,2] or polymers [3,4], they also can be modified in various ways [5–8] expanding their applicability. Nevertheless, ways to process glass are surprisingly limited, mostly relying on various kinds of casting [9,10] or mechanical cutting [11,12]. Due to the rapid development of science and technology, the need for more advanced and, most importantly, precise and flexible ways to produce glass structures arose. To accommodate the needs for nanotechnology various chemical deposition [13,14] or wet etching [15,16] techniques were employed. At the same time, direct [17,18] and indirect [19,20] additive 3D manufacturing of glass was demonstrated. However, in all of the highlighted processes, severe drawbacks and compromises are limiting their applicability. A more diverse and flexible approach is highly sought after.

One of the premier candidates for the best possible blend between free-form fabrication capability, flexibility, and throughput is the usage of femtosecond (fs) laser [21]. Indeed, it was already employed in a huge variety of fields [22]. The primary advantage of using ultrashort pulses is the possibility to control the thermal aspects of the light-matter interaction [23–25]. Furthermore, interaction can be nonlinear, meaning that materials transparent to the incident wavelength can be processed [26]. Combined, these two aspects make fs pulses extremely attractive for glass processing. Thus, this review is dedicated to

highlighting how fs pulses can be employed for free-form 3D microstructuring of glass. Dielectric crystals will also be mentioned where relevant, as a lot of glass-related processing techniques can be applied for them as well. First, the physical phenomena of ultrafast light-matter interaction will be discussed, explaining how it can be tuned and localized. Then, various processing techniques based on these interactions will be explained. These include waveguide and other photonic element inscribing, zone plates, selective glass etching (SLE), and ablation. Primary attention will be given to real-life applications of shown techniques as well as connections with other manufacturing methodologies. Combined, this will provide a comprehensive outlook to the current progress of fs glass fabrication and highlight the directions where the field is headed.

2. Ultrafast Radiation and Material Interaction

2.1. The Nature of Nonlinear Radiation and Material Interaction

To give a proper background to the technologies that will be discussed further in the review, we will begin by explaining the nature of ultrafast light and material interaction. When the material is processed by using fs pulses radiation the material is affected by very high peak intensity I (more than GW/cm^2). As I is the ratio between the laser power P and focused spot size with a radius of ω_0, the two main ways to raise it are an increase in P or focus a laser beam to smaller spot size. The first requirement is fulfilled by high peak power (P_P) of fs pulses (∼GW), while small spot sizes are achieved by sharp focusing—high numerical aperture (NA > 0.2) objectives or lenses. Material response to high I is nonlinear and conceptually is different from the material response to low-intensity radiation which is generated by non-coherent light sources. When radiation travels through dielectric material it polarizes material. When radiation intensity is not high enough material polarization linearly depends on radiation electric field E (1). Keeping in mind that $I \sim |E^2|$, when radiation creates an electric field which is stronger than 10^7 V/m, material polarization dependency on the electric field becomes nonlinear (2).

$$P(t) = \epsilon_0 \chi^{(1)} E(t), \tag{1}$$

$$P(t) = \varepsilon_0 \chi^{(1)} E(t) + \varepsilon_0 \chi^{(2)} E^{(2)}(t) + \varepsilon_0 \chi^{(3)} E^{(3)}(t) + ..., \tag{2}$$

here ε_0 is vacuum dielectric permeability, $\chi^{(1)}$ is linear optical sensitivity, $\chi^{(2)}$—second order nonlinear optical sensitivity, $\chi^{(3)}$—third order nonlinear optical sensitivity.

Different member in nonlinear polarization equation decides different phenomenon observed in material. It also might exclude some materials from certain interaction regimes. For instance, effects that are decided by square nonlinear sensitivity, like sum and difference frequency generation, are observed only in non-central symmetrical crystals. Meanwhile, cubic nonlinear sensitivity affected phenomena are observed in all-dielectric materials. These effects are multi-photon absorption, tunneling ionization and other radiation self-interaction, such as light thread formation. It is important to note that various nonlinear light-interaction regimes can be induced simultaneously, leading to a quite complex picture of the process. Thus, when processing non-central symmetric materials a second-order interaction have to be taken into account, or how the Kerr effect might change propagation conditions when high I is present [27].

2.2. Nonlinear Effects

As it was mentioned before when the material is affected by high-intensity radiation various nonlinear light and material interaction effect appears which are governed by different order nonlinear sensitivity. One of these effects is multiphoton absorption. Multiphoton absorption is simultaneous two or more photons absorption through virtual levels from the ground to an excited state. Two-photon absorption is decided by second-order nonlinear optical sensitivity. Meanwhile, three-photon absorption is decided by third-order nonlinear optical sensitivity. Hence, higher-order multiphoton absorption is decided by higher-order nonlinear optical sensitivity respectively. Most of the time in nonlinear optics multiphoton

optics is a negative effect that distorts radiation. However multiphoton absorption can be used for positive practical applications such as multiphoton spectroscopy, microscopy, and transparent material laser processing.

In simplified terms, to induce a change in the dielectric material the electrons have to be excited from the valance band to the conductive band. Numerous processes might induce it. The most important and the most prevailing nonlinear effects when a material is illuminated with high I fs radiation are multiphoton ionization, tunneling ionization, and avalanche ionization. Multiphoton ionization is a process when an electron absorbs several photons simultaneously and is excited *via* virtual levels. The principal scheme of this process is shown in Figure 1b. Another nonlinear effect is tunneling ionization. Intense laser radiation can distort the potential barrier which holds electrons to material atoms. Because of the potential barrier decrease possibility of electron tunneling increases and in this way more and more electrons are excited to the conduction band. This process is depicted in Figure 1c.

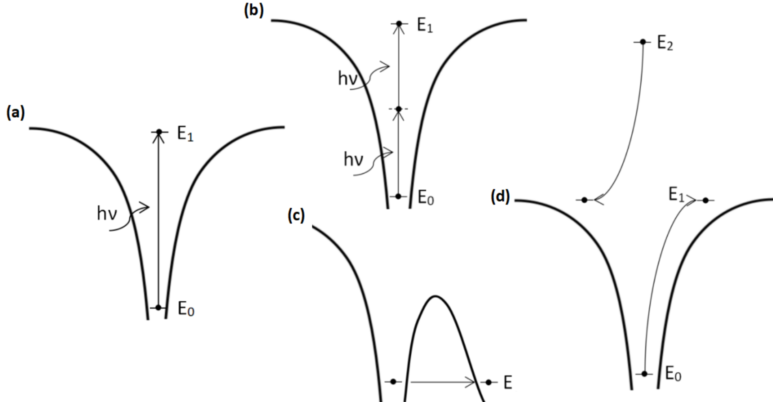

Figure 1. Principle schemes of main nonlinear processes: (**a**) linear ionization, (**b**) nonlinear (multi-photon) ionization, (**c**) tunneling ionization and (**d**) avalanche ionization.

Which process (multi-photon ionization or tunneling ionization) is going to dominate depends on laser ω and I. This dependency is described by Keldish parameter [28] which can be expressed as [29]:

$$\gamma = \frac{\omega}{e}\sqrt{\frac{m_e \Delta E \varepsilon_0}{I}}, \tag{3}$$

here e—electron charge, m—electron mass, c—speed of light, n—linear refraction index, I—laser intensity, ϵ_0—vacuum dielectric penetration, ΔE—reserve strip spacing.

When γ is more than 1.5, multi-photon ionization will dominate, when γ is less than 1.5, tunneling ionization will dominate. Meanwhile, when the Keldish parameter is close to 1.5, transitional regime ionization occurs. In this case, multi-photon and tunneling ionization have approximately the same influence on material ionization. To sum up, tunneling ionization prevails in high I and low ω regimes. In contrast, multi-photon ionization dominates in high I and high ω cases. In laser metrical processing to reach the desired effect, it is necessary to control which effect will dominate. Fortunately, modern amplified fs-laser systems can be easily tuned to cover all the processing regimes.

Another important process that appears because of nonlinear radiation and material interaction is avalanche ionization. The principal scheme of this process is shown in Figure 1d. When radiation interacts with material electrons are released from material atoms. Continuously, irradiating material by intense electric field-free electrons is accelerated and their energy can be enough to release other electrons from neighboring atoms. In this way more and more

electrons are released. Finally, the critical density of electrons in a material is reached and the material can be modified [27]. For this process to appear sufficient amount of seed electrons is required. At the same time, to achieve sufficiently high electron densities using avalanche the time for the process to appear have to be sufficiently long (>100 fs). Therefore, this process is more common when longer amplified pulses are used. Also, care should be taken, because if the process is too strong it can become uncontrollable, worsening structuring quality. Thus, care should be taken if this process is present during DLW.

2.3. Thermal Effects

When a material is processed with relatively long laser pulses (>10 ps) thermal effects can be observed in the material. It is the result of heat dissipation from the laser affected area which occurs while a long laser pulse is still interacting with the material in the focal point. This process takes its place around 1 ns after radiation absorption [30] and usually reduces material processing quality. When quantifying thermal effect the term Laser Affected Zone (LAZ) is introduced. It encompasses all the volume affected by the heat generated by a laser, even if it is outside of the focal point [31].

Usage of an ultrafast laser can allow control and if needed greatly reduce thermal effects caused by the light-matter interaction. Looking from the temporal perspective, interactions needed for processing occur rather fast. For instance, material ionization occurs after $\sim$1 ps, followed by ablation and removal after $\sim$100 ps [30]. Therefore, if no additional energy is introduced while subsequent thermal effects take place it can be greatly reduced. As a result in the fs pulses, the case material does not suffer from substantial thermal effects. In this way, LAZ is minimized. That is why femtosecond material laser processing sometimes is called cold material processing. Nevertheless, it is important to note that alongside pulse duration pulse repetition rate also plays important role in the thermal aspect of processing. If several pulses reach the affected zone before initial heat dissipation takes place, even fs pulses can induce material melting and noticeable LAZ. Another important factor for thermal accumulation process is the deposited energy. By maintaining the same pulse duration and pulse repetition rate and at the same time by increasing energy of each pulse the sample is affected by greater radiation dose. If the energy does not have enough time to be relaxed out of sample by increasing pulse energy we obtain higher thermal effects. Higher pulse energy shows greater affected volume around the laser focus [31] that means stronger thermal effects. While in some cases this might be detrimental, it can also be useful in some applications like laser welding. This distinction will be made through the article where it applies.

These thermal effects are especially important for glass processing. Glass is a quite fragile material that can be easily broken by treating it with stresses [32] or temperature caused volume tensions [33]. By processing glass with longer pulses or even CW laser it is very hard to avoid cracking of glass [34]. However, short pulses lasers development allows minimizing thermal effects by using shorter pulse duration [35] and process material locally without affecting surrounding volume.

3. Peculiarities of Glass Processing Using Fs Radiation

Light-based glass processing is not a straightforward process. Most glasses (with some exceptions like chalcogenide glasses) are transparent materials for near-UV, visible and near-IR radiation, meaning that linear interaction with such photons is negligible. As a result, one way to induce a modification in glasses is by choosing a wavelength that can be absorbed by a particular glass. Some works use such interaction for glass surface structuring based on linear glass absorption [36,37]. Such direct removal of the material by laser beam This is called laser ablation. Nevertheless, 3D processing in such cases is greatly limited due to direct absorption being a surface-bound process limiting its use for 3D structuring.

Alternatively, intense and focused radiation can be used. Then interaction becomes nonlinear, resulting in melting and removal of the focal volume. For this reason, most

laser-based glass 3D processing techniques are based on such processes. As we already have discussed, when radiation I is high enough (GW/cm^2–PW/cm^2) multiple photons (in most cases two) can be absorbed simultaneously during multi-photon ionisation [27]. Because high enough I for this interaction can only be reached by focused laser light, this creates inherent localization of the process. The scheme of this idea is shown in Figure 2. Keeping in mind, that in most cases NA in the range from 0.01 to 1.4 is used, the volume in which the modification is induced can range from a hundred nm to hundreds on µm in a transverse direction and from a few µm to several mm in a longitudinal direction. The elongated modification is an inherent feature of Gaussian beam normally used for such processing [38] while other types of voxel shapes being possible with beam structuring. Due to the nonlinear nature of these interactions sub-diffraction limited features are also possible, both directly and indirectly. Regardless, localization and selectivity of the process in the volume of glass is a critical component why fs laser is the primary tool for high precision 3D fabrication. Keeping in mind that laser can be used in a multitude of ways and not only for glass processing any laser-based fabrication process can be called direct laser writing DLW [39].

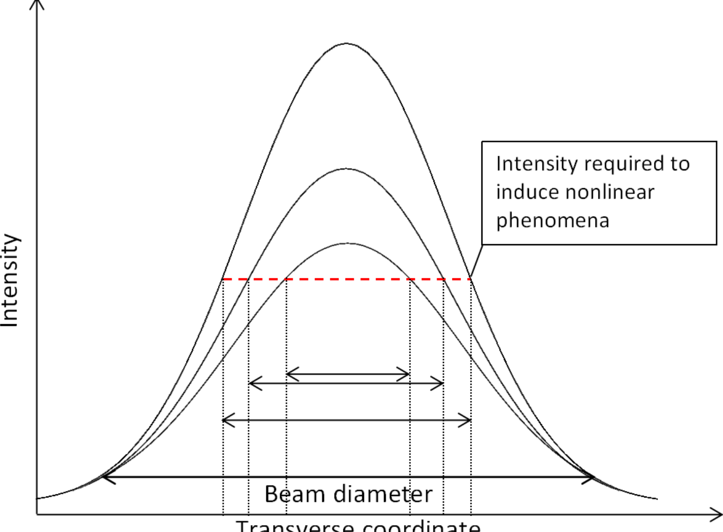

Figure 2. Focused laser beam spot diameter required to induce nonlinear effects dependency on radiation intensity.

Light-glass interactions used in DLW can induce different types of modifications. These depend on laser parameters such as radiation intensity, repetition rate, pulse duration, or wavelength to name a few [40]. Of course, induced modifications depend on the material itself [40,41]. Formally, in literature, it is possible to find 3 primary stable modification types that can be induced in the glass. Nevertheless, some exceptions apply at specific cases. For instance, silver clusters can be formed in silver containing glasses, resulting in type Argentum (or type A) modification [42]. However, in this review we will concentrate at the 3 primary modification types referring to any exceptions when it applies.

Type I modification is smooth material refraction index change. The change depends on various laser parameters and on the material itself. In a standard case, it is considered that such variation is mainly decided by pulse energy. An example photo of this modification can be seen in Figure 3b,c [40]. In the standard glass, the amplitude of change is in the order of 10^{-3}.

Type II of modification is periodical nanogratings in the glass. From optical standpoint, alongside changing just refractive index of the material, it also introduced birefringance. An example of nanogratings is shown in Figure 4. One of the key properties of this interaction is the tendency of nanogratings to be strongly influenced by the polarization of the incident beam. Nanograting ripple direction is perpendicular to polarization [41,43]. Moreover, the exact shape and properties of nanograting depend on other parameters as well. For instance, pulse repetition rate plays quite an important role, as it denotes the thermal aspect of the interaction [44]. The size of the ripples themselves is sub-diffraction, that is, in the range of tens of nm.

Type III modification denotes the formation of nano/micro-voids. When radiation intensity exceeds a particular value higher than needed for type II modification, micro-explosion in the volume of glass occurs and forms micro-cavities. This phenomenon is demonstrated in various works [45,46]. It is the most violent form of processing with an fs laser, leading to a relatively large modification area with several phase-change along the modified area. Particular radiation intensities to induce these types of modifications depend on the materials themselves.

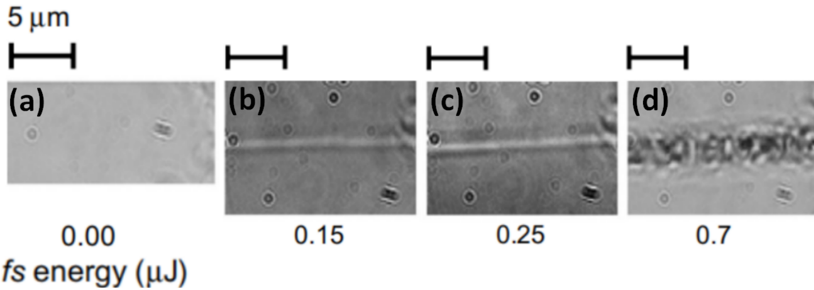

Figure 3. Glass modification examples. (**a**) unmodified material, (**b**,**c**) type I of glass modification or refractive index changes. (**d**)—type III modification or nano/micro-voids [40].

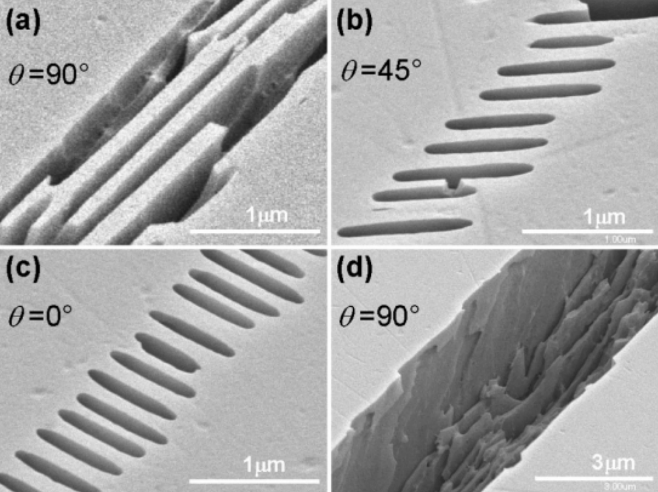

Figure 4. Examples of type II glass modification and visualization of nanogratings direction dependency to light polarization. (**a**) Nanogratings induced with light polarization perpendicular to scanning direction- the angle between polarization and scanning direction 90°, (**b**) 45° and (**c**) 0°. (**d**) Nanogratings modification after etching [41].

4. Fabrication of Functional 3d Structures

There are many laser glass processing techniques based on nonlinear light-matter interactions, and by inducing different types of modification it is possible to change the method by which we perform the processing of glass. Type I modification can be used for for smooth laser refractive index modification [40] and waveguides formation in glass [47,48], type II can be used for Q-plate manufacturing, while post-processing etching step of modification is necessary for selective laser etching (SLE) [49]. Meanwhile, type III modification is used for laser ablation [35] and welding [50]. These techniques have different natures and provide various possibilities of glass modification. We will describe various laser material modification techniques in more detail later.

4.1. Photonic Element Manufacturing

In a broad sense, the term photonics is used to encompass all advanced light-based science areas. In the light of this section, we will use it to describe very precise structures which exploit nm-level features and/or change in refractive index to control and/or confine light in accordance to application dictated requirements [51]. In general, manipulation of thin layers of materials with different kinds of refractive index is a very widely used phenomenon. One of the primary examples of it is dielectric mirrors [52]. The Bragg law for 2D system showing where the constructive interference is the strongest reads as:

$$2d \sin\theta = n_i\lambda, \tag{4}$$

where d is the distance between layers, θ—angle of incidence, λ—wavelength and n_i—positive integer. The most important parameter which can be controlled is the size of the features (d). Due to the already mention nonlinear nature of fs interaction with the transparent medium, it can be brought down to sub-diffraction level. Thus, one of the simplest examples of fs laser usage for photonic structure fabrication is the inscription of custom Bragg gratings into fibers [53]. In the simplest case, such structures are not strictly 3D. However, due to the flexibility of the technology fs laser allow forming fiber Bragg gratings (FBG) in arbitrary types of fiber, including non-photosensitized ones [54] or fibers made out of crystals [55]. At the same time, 3D capabilities are reflected by the capability to inscribe modifications in arbitrary place of the fiber, that is, not only in the core [56], or choose a specific core in multi-core fibers [57]. One of the main challenges here is focusing into the designated position within the fiber. Because the fiber shape normally is round, it defocuses the laser beam. Therefore, immersion oil [57], or flat ferules [58] might be used. This brings a lot of possibilities to the field, as it enables simple, on-demand fabrication of specialty FBGs which might be applied in various uses [53].

While FBG is a great example of a relatively simple photonic structure, 3D interactions could give substantially more diverse capabilities [51]. Therefore, the realization of 3D photonic crystals is quite an active field. Additive manufacturing was shown to be quite an attractive candidate [59]. However, in that case, the refractive index gradient between air and the polymer is around $\sim$0.5 which can be too sharp for some usages. At the same time, additively made 3D structures present objects on top of flat substrates, making them fragile and incompatible with anti-reflective coatings. In contrast, photonic elements embedded inside the volume of glass are robust, have a refractive index gradient of 10^{-2}–10^{-3} and could be potentially coated with the anti-reflective layer. Thus, glass-based 3D photonic devices occupy a very important niche in the field.

The first application is refractive index change in the glass is embedded 3D photonic crystals. It was shown that such photonic crystals can be used for spatial light filtering [60]. Indeed, the required spatial resolution and periodicity for such devices is close to the wavelength (in most cases HeNe 633 nm for simple testing) itself, making focused ultra-fast radiation a go-to tool. Simple woodpile-like geometries were used first. These were produced using both laser-assisted wet etching [61] and direct refractive index modification [62]. Nevertheless, these only allow filtering along X and Y axes of the photonic crystal, limiting applicability. A solution would be to use stacked ring geometry, which then would

grant this effect along all 360° in a perpendicular direction to the propagation [63]. Here possibility to integrate such a device into glass volume becomes an enabling factor. If such a device would be tried using additive manufacturing additional supports would be needed to support each ring. Furthermore, standard single-period photonic crystals only allow limiting angular filtering. As a solution to expand it asymmetrically and chirped [62] geometry was proposed and tested, again attesting to the design flexibility enabled of 3D fs fabrication. The device was then successfully tested with microchip laser filtering in transverse modes (Figure 5), enabling it to increase its brightness by 2.8–3.1 times and single transverse mode from 88 mW to 335 mW [64]. If a one-directional filter is acceptable photonic crystal writing process can be extremely sped-up by applying Bessel beams [65]. In other spatial filtering techniques, the embedded photonic crystal is one of the most compact and simple solutions available, showing clear potential wide-spread applications.

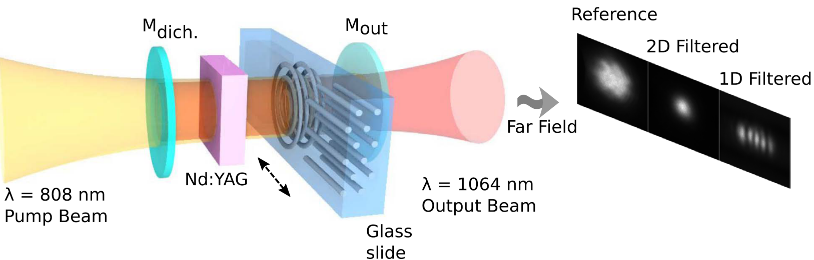

Figure 5. Principle of transverse mode filtering in microchip laser by application of laser-made photonic crystal embedded in a glass chip. The solution is compact and allows to achieve a high degree of control over the spatial characteristics of a laser, depending on the geometry of inserted element. Adopted from [64].

Laser-induced n modification can be exploited to not only shape light but also to confine and direct it. Indeed, embedded glass waveguides can be produced by using fs lasers [66]. Then, the structure has to meet the modification cross-section and Δn requirements. Interestingly, waveguides can be produced by both increasing and decreasing the n of the material. Regarding the direction, two primary modes are exploited. At first, focusing optics move up or down in relation to the surface of the sample. This is also called longitudinal writing geometry [67,68]. The advantage is a nearly perfectly round cross-section of the modification, as well as a very uniform gradient of n modification to all directions. Problems, on the other hand, lies in the fact that if the sample is thick, the working distance of sharply focusing optic might be insufficient. Thus, it is more suitable for lower NA optics. Also, if non-straight modifications are needed, the uniformity and high quality of the waveguide are compromised. Alternatively, the scanning might be performed alongside the horizontal plane, that is, in a transverse manner [69,70]. Then the length and shape of the waveguide can be arbitrary. On the other hand, due to Gaussian focusing properties, the modification is elongated in the Z direction, the Δn becomes highly non-uniform, especially in the Z direction. To remedy this additional elements, such as spatial light modulators (SLMs), might be needed in the optical system, complicating the setup and the process [71,72]. Alternatively, a multi-scan approach [73,74] or special light-matter interactions [75] might be exploited to make the cross-section of modification round. All of this can be combined with possibility to inscribe Bragg gratings into integrated waveguides, allowing creation of true functional 3D optical systems. It has to be stressed that it can be done in basically any kind of glass, including but not limited to borosilicate glass [76] or fused silica [77]. Thus, the needs of application dictate which of these two modes should be used. The waveguides themselves can be fabricated alone, or integrated into functional devices where they could act as a part of a sensor [78,79] or as an integrated interconnector between different types of devices [80]. This is especially attractive, as waveguide can

potentially be integrated during the same technological step as the rest of the structure [78], owning to huge flexibility of fs-based processing of transparent mediums.

The elements discussed so far relied on type I modification. As a result, the designs and applicability of the produced devices were to some extent limited. To gain even greater tunability type II modification can be applied for free-form embedded optical element manufacturing. This type of fs modification allows inducing volume-embedded nanogratings which, due to orientation of sub-diffraction limited features, have distinct birefringence [81]. What is more, the directionality of the optical phenomena induced depends on the light polarization [82,83], giving huge controllability to the process. While the selection of materials in which this process is pronounced is not extremely broad [84–87], it is still sufficient to acquire a broad selection of possible optical devices. As a result it was employed to produce various optical structures, for instance diffraction gratings [88], Fresnel zone plates [89], computer-generated holograms [90,91], S-wave plates [92,93] or metamaterials [94]. Remarkable selection of possible optical elements is the result of both possibility to induce refractive index change and birefringence as well as the possibility to precisely control these modifications in 3D by using focused fs laser light. Additionally, these modifications exhibit immense thermal stability (up to 1000 °C) [95] allowing them to be considered for usage in some extreme environments. On top of that, as these elements are embedded into glass volume, their laser-induced damage threshold is also quite high (∼J/cm^2) [96], that is, at the level of the host glass.

One extremely promising application of fs-laser-based embedded photonic structure fabrication is embedded optical memory. The idea to use light for encoding and reading memory dates back to the 1980s when the laser was employed to produce and read optical discs. Over the years due to progress in optical engineering, the wavelength used for the process could be reduced, in turn increasing the data density in the disk. This is due to the fundamental need to use diffraction-limited processes for both data recording and reading. This fundamentally limits achievable data density up to ∼0.25 Gb/cm^2 for standard systems using visible and near-UV systems [97]. However, as we discussed, fs-laser allows creating modifications not only on the surface of the material but also inside it paving the way for the volume memory [97,98]. Furthermore, single features created with fs laser can be extremely small (down to hundreds, or even tens of nm) allowing the extreme density of information [99]. Birefringence gives an additional degree of freedom as well, paving the way for true 5D memory (Figure 6) [100]. The modifications themselves have virtually unlimited lifetime [101], making them a valid candidate for extremely long-term big-data storage. Nevertheless, the modifications themselves can also be removed relatively simply if desired, granting the possibility to use the same medium to rewrite the information inside the same material volume. This can be achieved by subsequent laser exposure to the same volume [102]. Usage of crystals also allows to achieve it with relatively low temperatures (bellow 200 °C) [103] or exposure by loosely focused visible wavelength laser beam [104]. Admittedly, at the moment widespread adoption of this technology is limited due to the necessity to use expensive fs lasers and positioning. However, with the need to store up to massive amounts of information by numerous industries [105], this might become a more and more attractive solution for professional specialized extreme long-term data storage.

While the application of focused fs radiation has huge capabilities, there are some distinct limitations and hindrances native to light itself. First, if sharp focusing (NA > 0.4) is used, the polarization in the focal point has to be looked into more precisely than standard ray optics would suggest. Indeed, it is possible to show that sharply focusing fs light inside transparent medium changes E distribution in 3D [106,107]. Keeping in mind that the direction of type II modification heavily depends on the light polarization, this effect might have a severe influence on the result of fs processing and has to be accounted for. Furthermore, when working in the volume of a transparent medium, the laser beam is distorted due to aberrations [108]. This results in defusing effect, which changes the voxel's size and shape (aspect ratio) in different depths of the sample [109]. The functionality of photonic crystals and waveguides heavily depends on the shape of the modification as well as the precise modification of n. As a result, aberrations are substantial consideration in

those applications. Luckily, this issue can be solved in several ways. First, focusing optics might have some tunability, allowing to account for different depths of fabrication [110,111]. The next step is the usage of SLM [109,112]. It was shown to be a powerful tool to account for focusing deficiencies and control the aspect ratio of the feature. For instance, 1:1 to 1:1.5 aspect ratio lines can be inscribed in any depth of 1 mm sample using 0.9 NA objective [109]. Alternatively, when SLM is not used, the aspect ratio can be more than 1:25. Additionally, due to defocusing, features could not be effectively written in depths below ∼0.4 mm without significantly reoptimizing the process (i.e., increasing average laser power to compensate for defocusing. Even then, the feature aspect ratio would only increase with the depth. SLM also allows spatially shape incident beam (and, in turn, modification's shape in 3D) for advanced structure fabrication [72,113,114]. The process is flexible enough to account even for very high n, like diamond's 2.4 [115–117] or even anisotropic materials [118,119]. Unfortunately, SLM requires a very specialized setup, high precision in setup alignment, and advanced calculation algorithms alongside sufficient computing power [120]. On top of that standard SLMs are operating at relatively low frequencies of ∼tens of kHz limiting the possibilities for dynamic possibilities of processing, with faster systems being investigated at the moment [121]. Finally, the LIDT of SLMs is relatively low, with high-end experimental devices capable of operating at P∼100 W level using ultrafast lasers [122]. While solid-state SLMs might alleviate this issue [123], it remains a limiting factor. Thus, while SLMs offer a lot of interesting capabilities, their application remains limited.

Figure 6. An image depicting encoding of information using type II modification induced birefringence. While both of the images seem to be written in the same volume (image on the **left**) images of Maxwell (**center**) and Newton (**right**) can be separated by exploiting imaging along both optical axes. Taken from [100].

4.2. Selective Laser Etching (SLE)

Fundamentally, type II modification of glass leads to both, nanograting formation [43] and structural changes of material [124]. The photonic applications discussed so far mainly exploited the optical phenomena of inscribed modifications. Nevertheless, appreciation of chemical and mechanical changes can lead to a very interesting prospect for further applicability. Glass, or, more precisely, Si_2O compounds can be etched using hydrofluoric acid (HF) or Potassium Hydroxide (KOH). These etchants react with materials differently. The reaction equation of KOH and HF with one of the most popular glasses fused silica is shown in Equations (5) and (6). These reaction equations that concentrated KOH solution is beneficial over HF etchant due to least saturation behavior in elongating channel structures [125].

$$SiO_2 + 2KOH \rightarrow K_2SiO_3 + H_2O, \tag{5}$$

$$SiO_2 + 4HF \rightarrow SiF_4 + 2H_2O. \tag{6}$$

Normally, the etch rate of Fused silica is a few µm/h, of course, it depends on etchant [126]. Nevertheless, laser-induced type II modification can greatly expedite this process. Laser radiation induces material structural variations when binding angles of the lattice change. Oxygen atoms become more reactive and more effectively interacts with the etchant [124]. Also, formed nanogratings greatly increase the effective surface area at which etchant can interact with the material. Usually, for a description of this phenomenon definition of selectivity is used. Selectivity is the ratio of etching rates of modified and unmodified material. The utilization of this process allows obtaining selectivity up to 1000 [126]. Combined with the capability to inscribe such modifications in 3D it leads to the capability to selective glass etching (SLE) [124]. The most common material used in SLE is fused silica which is almost pure amorphous SiO_2. Fused silica SLE processing is a mostly studied process comparing to other materials. While other materials, such as borosilicate glass (BK7, Pyrex, Borofloat) [41,127,128], Foturan [129] can be used in SLE, these are rare occurrences. This is a result of lower selectivity [41] or requirement of post-processing [129,130], greatly favoring fused silica for widespread applications.

From the etchant side, HF and KOH are the most popular ones. KOH etching properties are strongly affected by KOH concentration and its temperature [131]. Usually, in the literature, we can find that 8–10 mol/L concentration KOH solution is used at 85–90 °C temperature [126,131,132]. Generally, a higher KOH concentration yield a higher etching rate. Nevertheless, a higher concentration of etchant does not guarantee better selectivity, potentially leading to contrary result [131]. This can be tied to the higher etching rate of both laser processed and unaffected areas. A similar trend can be observed with KOH temperature. When we are talking about the etching rate. It was shown, that the best selectivity is achieved at 80 °C [131]. Regarding the HF, if fast etching is desired, high (tens of %) HF concentrations should be used [133]. However, as one of the primary goals of SLE is achieving 3D structures, lower concentrations (5% or even lower) at ambient conditions are used to avoid overetching laser unexposed parts [126]. Curiously, experimentation on various conditions which might be used for SLE using HF (like temperature manipulation) is limited. Probably one of the main reasons, why more experiments are not performed which HF acid is a hazardous nature of this chemical. Subsequently, this is one of the reasons why more researcher groups prefer KOH over HF. Nevertheless, both etchants can find their applications. To get higher etching rates (up to a few hundred of µm/h) HF can be used [134]. Meanwhile, KOH should be used when high selectivity (up to 1000) is required [126], for instance producing high aspect ratio features. Of course, it is possible to combine both etchings one after another for one structure and use both etchant's advantages. This technique is called hybrid chemical etching [132,135].

One interesting prospect of SLE is the possibility to etch crystals like sapphire (Al_2O_3), Yttrium Aluminum Garnet ($Y_3Al_5O_{12}$ or YAG), lithium niobate ($LiNbO_3$) or crystalline quartz [136–139]. It is shown that nanogratings induced in a sapphire crystal are similar to ones inscribed to fused silica [140–142]. However, the etching mechanism of the crystals is slightly different from amorphous materials. When focused laser beam modifies crystalline sapphire modified region becomes amorphous [143]. Then, amorphous and porous regions are etched out in aggressive etchants like concentrated (40–50%) HF at room temperature [140–142,144–146] or around 35% KOH solution heated to 85–100 °C temperature [147]. Even more exotic etchant choices were demonstrated—sapphire was etched in phosphoric and sulfuric acid mixture at 300 °C temperature [148,149]. It showed that sapphire etched in 40% HF solution has selectivity which is in order of a few thousand (up to 5000) [140,141] and this value exceeds all the results showed on fused silica. YAG crystal shows even better selectivity which is estimated to be around 10^5 in HF acid. However, the SLE of crystals faces other problems: it is very hard to avoid cracks. Cracks are caused by modified crystalline material becoming amorphous and creating great volume tensions which lead to the crack of material [150]. Moreover, high selectivity comes from very low etching rates of unmodified material. Even modified material etching rate is very

low, as little as up to 100 μm/h [137,140], for practical usage when a quite large structure is required such a low etching rate can be unacceptable.

Various laser parameters strongly affect the SLE process. A different aspect of selectivity, etched structure quality, such as surface roughness, can be decided by multiple laser parameters. Selectivity itself strongly depends on pulse energy. While sufficient pulse energy is needed to induce type II modification, the formation of LAZ can also be induced if too powerful pulses are used. LAZ affects etching properties [31]. Higher laser pulse energy with wider LAZ zones results in the wider etched zone. This effect could be for scanning up large volumes and, on contrary, this phenomena could be disadvantageous in high aspect ratio structure fabrication. Moreover, pulse duration and laser repetition rate affect LAZ and changes etching properties as well [44,151,152]. Longer pulse duration leads to stronger thermal effects. Higher pulse repetition rates prevent energy from being relaxed from the lattice. On the other hand, pulse energy not only change LAZ but also changes the size of modification and nanograting configuration itself, which leads to different selectivity induced by various pulse energies [41,43,151]. However, almost all this research leads to optimal particular parameter value which varies by changing other parameters. We can see that not individual parameters, but rather the whole parameters set is important for the SLE process. Basically, by changing pulse energy, pulse repetition rate the deposited dose is changed. Hence, a particular radiation dose is hiding under these parameter sets. Overall, it can be seen that for SLE process need to be ensured specific conditions—specific radiation dose [151] and these conditions can be altered by different thermal regime [31].

Alongside radiation parameters, scanning strategies also play an immense role in SLE effectiveness. Overall, translation velocity and pulse overlap while hatching/slicing denote the pulse overlap, which, in turn, governs accumulated radiation dose[151]. Therefore, one can consider that scanning velocity gives quite a similar effect as pulse repetition rate. As a result, selectivity dependency on scanning velocity was investigated in many works [131,151,153]. Acquired results varied, painting a more complicated picture of interaction as different sets of laser and scanning parameters were shown to work quite effectively [131,151]. Interestingly, in some works, almost no significant selectivity dependency on scanning speed was noticed [153]. The translation velocity question, in general, is very important, as it is one of the main parameters determining structuring rate, that is, what volume will be processed in a given amount of time thus better understanding of these contradicting results is a topic for further research in the field. Nevertheless, the scanning strategy also plays an important role. During the inscribing process, the specific separation between scanning lines should be chosen. Unsurprisingly, it also influences etching rate and selectivity [126,131]. One of the non-trivial observations made was that optimal Z separation value varies when different etchant is chosen [126]. Separation along a horizontal axis (i.e., slicing step) should also not exceed the voxel height [131]. Overall, due to the complex nature of the process and a huge amount of independent parameters, the exact interplay is still an object to an active investigation, with the goals of different groups distributed between trying to achieve the best selectivity, highest etching rate, lowest surface roughness or some combination of all.

It is important to not overlook the importance of polarization during the SLE process. Polarization is responsible for the direction of the nanogratings as depicted in Figure 4. Numerous works investigated selectivity dependency to laser beam polarization. When radiation polarization is perpendicular to scanning direction we get the highest etching rate [41,43]. The same applies and to selectivity because the unmodified material etching rate in all the cases remains the same [126]. Meanwhile polarization parallel to scanning direction gives the lowest etching rate [41,43]. Interestingly, circular polarization gives a good etching rate as in perpendicular polarization case [41]. This is extremely important because then the polarization might be considered invariable for any scanning strategy, heavily simplifying an already complicated process, becoming favorable for application-oriented fabrication. Nevertheless, care should be taken when considering the interplay between pulse duration and polarization. Discussed trend always appears when femtosecond laser

pulses are used to write modification. Nevertheless, when ps pulses are used for SLE selectivity does not depend on radiation polarization [152]. This property comes from the nature of this process. By using femtosecond pulses it is possible to induce nanogratings modification, meanwhile, ps pulses yield modifications more reminiscent of nanocracks. These can be considered a different type of modification that is still suitable for SLE.

SLE stands in a relatively interesting place when considering piratical implementation. The process itself needs a lot of considerations in terms of laser parameters and writing strategies. On the other hand, it can be considered one of the most straightforward ways to produce 3D glass microstructures. It, as a result, possible applications were shown in microfluidics, micromechanics, optics, and photonics. In photonics, It is shown that SLE can be used for very precise photonic components fabrication. By using tightly focused laser beams it is possible to form very small (down to ∼100 nm) repeatable structures which after etching can be used as photonic components [137,148,149]. Micro optic element fabrication was also shown with SLE [130]. However, due to relatively high surface roughness after the SLE process (∼hundred nm RMS) direct fabrication of optical components is impossible. Thus, after etching some annealing or other smoothing procedure is needed.

SLE excels in the field of microfluidics for the fabrication of lab-on-chip (LOC) devices. Glass is a preferred material for a lot of set applications, as it is chemically inert in organic solvents, transparent, and mechanically robust. SLE provides a relatively easy and highly controllable method for producing both surface and embedded channels. Here, SLE allows to form even complicated, curved, embedded 3D structures in glass [132,137,154,155]. It is demonstrated such channels ability to focused particles in the loops of the channels [137]. Other mentioned systems have a potential to be used in liquids filtering such as on-chip flow cytometry [137]. In the case of LOC microfluidic channel and some sort of integrated device inside it is formed [153,156]. Moreover, complicated microfluidic chains including filter and free movable integrated micro-switcher can be fabricated [132]. The mentioned device can perform fluid filtering. In the bigger channels narrower channels volume are inserted, only the smallest particles can go through the most narrow channels. Moreover, fluid flow direction can be controlled by fabricating channels with a free movable valve. Other 3D microfluidic devices which would be extremely challenging for any other technique can be fabricated [154]. To highlight some examples, Figure 7a–c show nozzle for biological applications. Figure 7d demonstrates connector for capillary electrophoresis. Figure 8 shows a microfluidic chip for cell sorting.

SLE also demonstrated huge promise in the field of micromechanics. For instance, a glass mechanical gripper can be produced and coated with metal to thermally induce movement [157,158]. A similar optical sensor can also be made [48]. The SLE-made mechanical device is coated by a metallic coat layer, which then moves when the potential changes. Information is red through the already integrated waveguide and the signal strength depends on the displacement of the structure. The beauty of this device is that it can be fabricated out of one piece of fused silica and at once it is possible to integrate waveguide and fabricate structure combining both type I and type II modifications in one fabrication step just by changing the laser parameters. Also, the device can be of arbitrary size, downscaled, and used as a component in more complex systems. Free movable micromechanical structures are also doable with SLE, such as gear systems [159]. Devices mentioned in the paragraph before conceptually are completely different from this micro-mechanical structure. In the first case, we get movement by fabricating structure with very high aspect ratio detail, so very thin details of glass become flexible. In the second case, a movable glass structure is fabricated because a slight gap is etched out between rotating and not rotating parts. Thus, by using the SLE technique, various types of movable structures can be obtained.

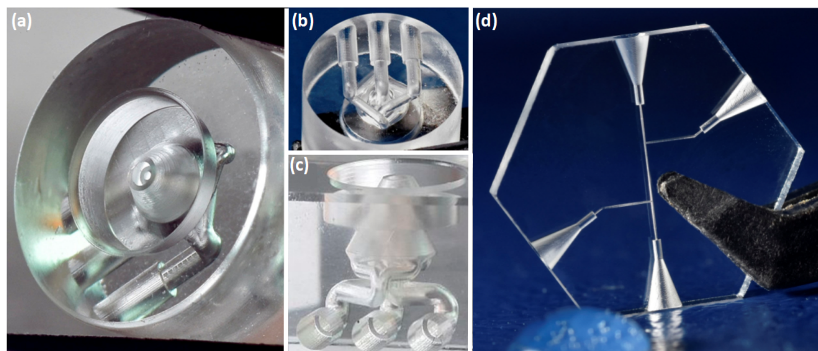

Figure 7. Example of microfluidic devices. (**a**–**c**) nozzle for biological applications, (**d**) glass connector for capillary electrophoresis, diameter 15 mm, thickness 2 mm [154].

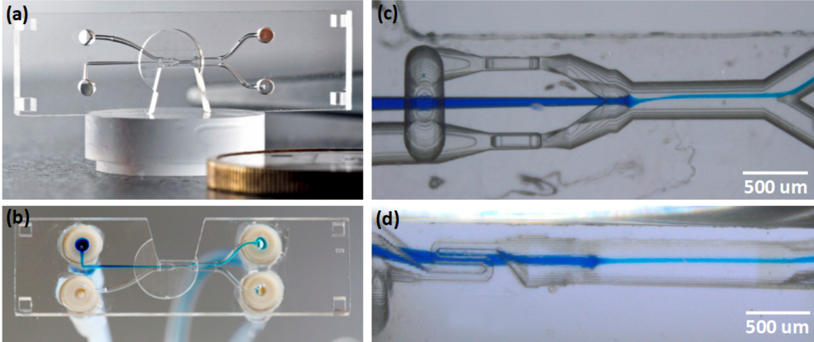

Figure 8. Example of microfluidic devices. (**a**,**b**) microfluidic chip created for cell sorting, (**c**,**d**) most important nodes of a chip are shown more detailed [154].

Finally, one must not forget that SLE is not an isolated tool and it can be combined with other DLW techniques, including multiphoton polymerization. Such fabrication is called hybrid fs laser manufacturing. For example, chemical liquid sensing application can be realized by combining SLE and multi-photon polymerization techniques [160]. Then, the channel and integrated cantilever are made out of glass in a single fabrication step. After the SLE process, a polymeric rod is produced by using multi-photon polymerization. When the whole structure is submerged into an organic solvent glass remains inert, while the rod expands or swells, a property well documented with laser-made 3D microstructures. Thus, such a device can act as a passive actuator or a mechanical sensor. This device is shown in Figure 9. Alternatively, it demonstrates that some hybrid devices can be used for cells sorting and detecting [161,162]. In closed SLE, the channels made are integrated with polymeric lend, which allows the detection of when the cell is moving through it as well as disturbing the signal.

Overall, SLE stands in quite a peculiar place in regards to its realization and applicability. The complexity of the process means realizing it is a rather complicated task, resulting in a steep learning curve for groups that attempt to do it. For this reason, a lot of researchers tend to use the substantially simpler type III modification base ablation, which will be discussed in the next subsection. Then, to achieve the same complex structures more fabrication steps of the simpler process might be needed. It also allows avoiding potentially hazardous HF-based chemical procedures. Alternatively, advanced high precision additive manufacturing-based solutions can be employed [163–165], forgoing the single step SLE process in favor of several simpler fabrication procedures. However, when SLE is employed

right and all the technical nuances are taken care of, it provides unmatched design freedom and flexibility in producing arbitrary shaped 3D glass structures with resolution down to µm with overall size in the cm range.

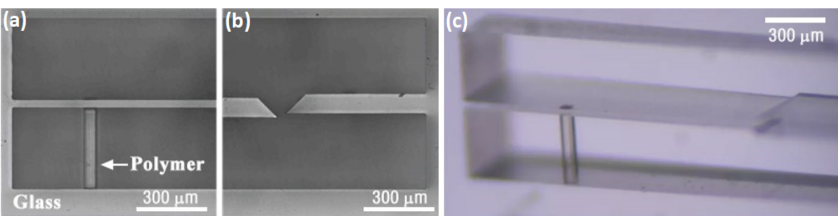

Figure 9. (**a**–**c**) Example of a hybrid microfluidic device [160].

4.3. Free-Form Cutting of Glasses

Fundamentally, direct laser ablation is the simplest of all DLW kinds. As the material is removed from the sample without any additional technological/post-processing steps it was quickly adopted in the industry using CW or long-pulsed (ns and longer) lasers [166]. Solid-state fs lasers are gaining popularity there, as well. The draw of ultrafast lasers in laser cutting is the possibility to control the thermal aspect of the process, subsequently allowing a smaller laser affected zone and cleaner cuts [23–25]. This capability is further expanded by the application of burst lasers, which allow both high structuring precision as well as very high throughput. There are also virtually no limitations for the application materials, which can be organic [167,168] (including living tissue [169]) dielectric [170–172] or metal [173,174]. However, when considering true 3D fabrication ablation have some severe drawbacks. In comparison to 3D printing [38], complex 3D architectures, arches, and integration of structures inside structures are either difficult or, for some geometries, impossible with direct ablation. Advanced techniques allow to achieve quasi-3D structures by either filliping [174] or turning samples [175] during processing, but it requires additional fabrication steps or a more complex setup, minimizing the main advantage of ablation—simplicity. Thus, in the following discussion, we will use the term 3D rather loosely, in many cases referring to structures that can otherwise be classified as 2.5D.

Among many applications where fs ablation of glasses can be exploited, microfluidics is one of the most common. Two types of channels can be produced in that case: on the glass surface [176–178], and embedded inside the volume [179,180]. Surface channels are substantially simpler to produce. Also, they allow integration of additional elements using other fabrication techniques, for instance, multiphoton polymerization (MPP) [181]. However, in that case, an additional channel sealing step is needed. It can be realized in numerous ways, including direct laser welding. It will be discussed in more detail further in the article. Nevertheless, it is an additional technological step that, if possible, should be avoided. Alternatively, channels inside the bulk of the material can be produced. Indeed, fs lasers allow surprisingly very fine control of type III modifications in glass volume [182]. Despite this, if ablation is used there is no direct way for debris to leave the embedded channel if this method is used. Luckily, if the process is carried out in the water, the debris removal is expedited, resulting in the possibility to produce clean and complex channel systems [179,180], or high aspect ratio holes (for instance 4 µm wide and more than 200 µm deep [183]). By applying Bessel beam ablation it is shown even higher aspect ratio narrow channels which is around 200 nm in diameter and 20 µm in depth [184]. Alternatively, water can assist in the structuring of the volume of porous/photosensitive glass [185–188]. Then, after laser exposure, glass is heated up and solidified, embedding produced 3D system inside a material. Additional etching and annealing steps can also follow. However, then the process becomes somewhat similar in complexity (if not more difficult to perform) to SLE yielding substantially worse shape control and surface finish of the channel walls.

At the same time, non-SLE methods allow using potentially simpler glasses. Regardless, apart from several demonstrations, this methodology is used sparingly.

Microoptics can also be produced using direct laser ablation. While extremely complex designs achievable using additive manufacturing are out of the question [189–191], ablation exceeds those methods by allowing to use of glass and achieve overall size from tens of µm to mm. Optical elements, like various type lenses [192–194] or axicons [195], can be produced this way. In virtually all the cases additional post-processing steps are mandatory due to the necessity to smooth the surface of the structure down to optical quality (less than $\lambda/10$). Annealing is the most popular option. It gently melts the surface of the optical element, allowing surface tension to increase surface smoothness without compromising the overall shape (Figure 10). This can be induced by heating the structure to a sufficient temperature (close to the melting of the material) [196], or by employing another laser such as CO_2 [192–195]. An alternative way to achieve lenses using type III laser modification is based on the idea, of inducing very fine modifications on the surface of the material. Then the sample is submerged to the etchant, which starts to etch out the material. The modification acts as a seed, which expands over time. Due to the nature of the process, expanded areas form lens-like profiles and, after some time reach each other [197,198]. Thus, a plano concave lens array is formed with an optical grade surface finish. Overall, while ablation allows achieving free-form optics, etching provides superior shape control and a possibility to produce more complex geometries, making both approaches somewhat comparable.

Surface roughness after type III processing is rather poor (∼several µm RMS). A laser can be employed to smooth it out. Normally, CO_2 [199] or high power solid-state lasers [200] are employed for this task. The process is based on inducing desired thermal interactions at the surface of the sample. It can be used to polish glass parts produced using SLE [201] or ablation [202]. However, the fs laser itself can be used for this task. The primary advantage of using ultrashort pulses is the possibility to extremely precisely control thermal accumulation on the surface of the sample [203]. This can be exploited to polish some exotic materials, like Germanium [204] or yttria-stabilized zirconia [205]. Additionally, due to the controlled manner of the process fs lasers allow avoiding some of the effects associated with polishing using different laser sources or mechanical polishing. Nevertheless, the application of fs lasers in polishing remains sparse. At the same time, the advent of burst-mode capable systems brings a new level of control of thermal aspects of the interaction, potentially reducing surface roughness during processing in the first place, bringing new capabilities to the field [25].

All the processes showcased so far mostly rely on Gaussian beam focusing using standard optics. However, as discussed previously, light is a flexible tool that can be spatiotemporally manipulated. To change the spatial distribution of the laser beam, passive elements can be inserted into the path of the laser beam. In more advanced cases, it can be done using SLM, which allows the changing of a projected mask dynamically on-demand [206]. However, due to the relatively low LIDT of such elements, their usage in direct ablation might be limited. Regarding the exact applications various examples exist. For instance, the Bessel beam can allow taper-less fabrication [184]. In other words, the channel walls are nearly vertical, which is hard to achieve with sharply focused Gaussian beams. It also can be used to achieve high aspect ratio (up to 1:100) features easily [207]. Also, in the case of top-hat laser beam distribution, the cut quality can be improved [208]. Beam shaping also can be exploited to create entire patterns to be ablated [206]. Regarding the temporal properties of fs radiation, it can also be tuned to achieve desirable ablation properties [209]. Manipulation of environmental aspects should also not be overlooked. By changing the pressure during the ablation process the debris formation tendencies can be influenced, which helps with the overall quality of the sample [210]. Alternatively, additional gasses are shown to help increase ablation depth [211]. Water, which was shown to be a rather popular additive in fs glass machining, can also be used to induce spontaneous spatiotemporal light filamentation. It can be used to cut arbitrary materials,

including glass, at relatively large thicknesses (1 mm and more) [212]. Thus, overall, while base fs laser ablation of glasses might be considered somewhat limited as far as 3D fabrication is concerned, some capabilities exist to enhance the result of processing. At the same time, then it somewhat complicated the processing, making it less attractive.

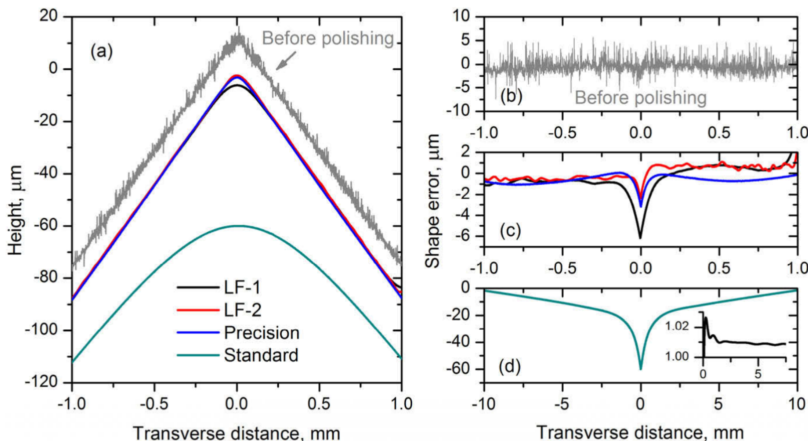

Figure 10. The precision of profile of the ultrafast laser-made axicon with subsequent CO_2 polishing and comparison to commercial high-precision and standard counterparts. The un-polished and polished laser-made profiles are offset to better reveal the difference between them. Reproduced from [195].

4.4. Laser Welding

Discussing 3D structure fabrication it is important to understand that in most cases a 3D structure is, in fact, multiple stacked 2D layers. Only a few processing techniques, for instance, selective laser etching, allow true 3D fabrication, yet it also relies hard on layering as it allows to minimize effects like shadowing. Sometimes the stacking is part of the process itself, like in 3D printing, while sometimes additional bonding step is required. Except for integrated free-form SLE structures, stacking glass onto glass to form 3D structures is also common, especially when parts are produced using ablation. There exist different bonding techniques such as direct, adhesive bonding, or others. Adhesive bonding is performed by using additional intermediate chemical materials [213], but it has limitations to strength as well as adds additional chemical constitutes which might be detrimental to some application. Direct bonding is performed by increasing the temperature of the samples, it starts to melt and connects with each other [214]. Thus, direct bonding by ultrafast laser welding becomes an attractive way to bond glass layers with each other forgoing most of the listed problems. Laser welding relies on type III modifications [215,216]. It can be considered one of the most advanced available bonding techniques, because of high spatial selectivity, localized material modification, and capability of completely sealing functional devices. Moreover, laser welding allows to achieve up to 95% breaking resistance of primary material [217,218]. What is more, laser welding does not require additional materials or other post-processing to be included. It is shown that laser welding can be used as a supplementary technology to strengthen other bonding techniques [219].

To weld two samples laser beam needs to be focused on the contact of those samples. Because of high radiation intensity, tunneling or multi-photon ionization occurs. Radiation is absorbed only in the focal spot where free-electron appears which mount increase because of avalanche ionization—plasma forms. Meanwhile, surrounding materials heats which enhance nonlinear which then, in turn, expedites the heating. The volume of melted material encompasses both samples which need to be bonded. Afterward, the material

cools and forms a firm connection between samples [220]. By melting material some of its chemical connections are broken. In the affected material some oxygen connection remains open forming a new chemical connection between samples [221]. After measuring welded samples cross-section Raman spectra was found that welded different material samples mix in the contact [222]. Thus, this explains high welded material breaking resistance.

For a process like this optical contact is required. Optical contact appears because of inter-molecular Van der Vals bonds. If the right conditions are created for two materials surfaces to be close enough to each other, those samples start to attract each other because of mentioned forces (forces decrease proportionally to the square of the distance). Thus, in this way, we get stable optical contact [223], which does not require to be additionally supported. Even more, additional external forces applied to the samples leads to cracks in the welded seam [224]. Therefore, clean and high-quality surfaces practically became a requirement for the laser welding process. Spacing between two samples should not be larger than a few hundreds of nm, otherwise, it is hard to avoid cracks in the seam or even ablation of one of the surfaces [225]. Optical contact is one of the greatest challenges for laser welding, because often it is hard to achieve it due to surfaces imperfection of the samples, due to high surface area, or imperfections/undulations in the sample caused by other processing techniques, like ablation.

Advances in laser engineering positively influence the ease with which welding can be realized. It was shown how to avoid the requirement of optical contact. Optical contact is still preferred, allowing us to reach a higher breaking resistance of a welded seam than welding without optical contact can [50]. However, for simpler, less challenging applications even simplified welding is sufficient. At this moment, it ihas been shown that laser welding of samples with gaps between each other up to 3 μm [220]. There a few factor with allows to walk around this requirement. First of all, the gaps which could be efficiently filled depends on the amount of material that is brought to the gap. This amount of material can be evaluated as the size of a welding seam. Seam size directly depends on laser radiation and scanning parameters (pulse energy, pulse repetition rate or scanning velocity, focus position in the Z direction in respect of the contact of samples) used for the welding process or even it could depend on material thermal conductivity. Thus, it possible to lower the high-quality contact requirement by increasing the size of the seam. Welded seam size can be increased in a few ways. The usage of high repetition rate (hundreds of kHz) radiation leads to a greater size of a seam [225]. The same applies to higher pulse energies [50,218,221]. This dependency is schematically shown in Figure 11b. By bringing more materials to the contact of the sample, it not only provides the possibility to weld samples with larger gaps but also affects the breaking resistance of welded samples. A larger welding seam will lead to higher breaking resistance [217]. Care should be taken, however, because of the possibilities of breaking material due to high internal tension instead of material welding [226,227].

It is important to understand how scanning properties affect the size of the seam. Lower scanning velocity will lead to higher pulse overlapping resulting in more energy being delivered to each point. As a consequence larger welding seam and higher breaking resistance are obtained [221,228]. What is more, the gap between separate seams, or hatching step, affects samples breaking resistance significantly [50,218]. It is quite intuitive that a larger amount of seams in the same sample allow the obtaining of a greater breaking resistance. On the other hand, welding sample by separate seams brings its own benefits to this process. Distinguished seams give a possibility to contact materials with different thermal expanding coefficients. Because the connection is very local, the spacing between seam compensates for the fact that the two materials expand differently. Unsurprisingly, the focal spot position in the Z direction in respect of gap position is also a critical parameter in laser welding. The way this parameter influences the process is shown in Figure 11a. It can be observed that, in laser welding, for the most effective process the focus of the radiation should be a little bit (∼100 μm) below the contact of the samples [220]. In this way, melted material comes up to the contact and fills it in the most efficient way. This

tactic allows us to melt more material and fill the gap between samples with the greatest amount of material.

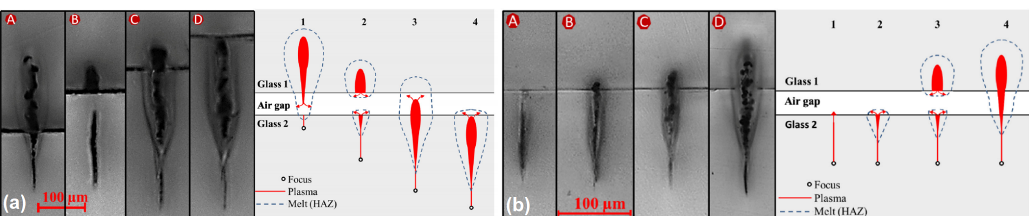

Figure 11. Cross-section of the welding process (**a**) welding dependency on focal position. The focal position is changed in this order from image A to D: −24.1 µm, −40.0 µm, −86.5 µm and −107.3 µm, Corresponding schemes of these process are shown from picture 1 to 4, (**b**) welding dependency on pulse energy, the pulse energy is increasing in this order from image A to D: 10.1, 11.23, 12.9 and 18.8 µJ, schemes of the corresponding process are shown in pictures 1 to 4 [220].

The advent of burst lasers have also been experimented with in welding. It allows improvement of the welding process in many aspects. Burst-welds have higher breaking resistance than that achieved by only welding in a high repetition rate regime [229]. Moreover, usage of burst enables us to weld materials with greater spacing in the contact between samples [50]. Another interesting approach is laser welding with Bessel beams [222]. One of the unique Bessel beams property is long focal length. Its relay length can up to a few hundred µm. Thus, in this way we do not need to have accurate information about the position of the contact of materials.

Laser welding can be applied in many functional device fabrication. It can be applied in such areas as electronics [230], microfluidics [213]. This technology could be extremely useful in electronics when the whole chip cannot be processed in other bonding techniques and local laser welding means that important parts of the chip can be left unaffected. Ultrafast welding is also advantageous, as it allows to easily bond glasses with other materials like metals or polymers. However, due to high technical requirements for both laser systems and surfaces of bonded samples, the advance of this technique is so far slow, with most demonstrations being done only in academia with proof-of-concept work.

5. Conclusions

The field fs laser-based processing of glasses and transparent dielectrics is wast. In this review, we have shown that:

1. Due to the nonlinear nature of fs pulses-based light-matter interaction, transparent to the used wavelength dielectrics can be processed, including glasses and crystals. This opens doors for true 3D processing, including inside the volume of the material. Due to interaction peculiarities, three distant types of modifications can be formed. Type I results in a localized smooth refractive index change in the range of $\Delta n = 10^{-3}$. This can be used to create embedded waveguides, Bragg gratings,and other integrated photonic structures.
2. Type II modification is created with higher pulse energy, which manifests as embedded, sub-diffraction-limited nanograting. Characteristics of such ripples depend on pulse energy and polarization. They also have pronounced birefringence. These can be used to produce various optical and photonic elements. If put into an etching solution, such as HF or KOH, these also etch out from tens to thousands of times faster, enabling selective 3D glass etching.
3. Due to the nature of type III modification, that is, ablation can be used for applications demanding less precision but higher precision, such as microfluidics. Application in optics is also possible, but additional post-processing is needed. Overall, this processing type partially sacrifices true 3D processing capability in exchange for being a lot simpler and faster.

4. As fs lasers allow us to precisely control thermal effects during processing, they can be employed for polishing and welding. In the latter case, it allows the joining of glasses of the same and different types, as well as glasses with plastics or metals, making it one of the most versatile tools available for such applications.

Overall, the key advantage of the fs laser is flexibility. Such processing can allow achievement of the same 3D structure using very different methodologies, allowing us to choose a process on a case-by-case basis. With this flexibility, one can expect the field of fs pulse-based glass processing to continue to grow rapidly in the near future, with both wider applications of existing methodologies and the creation of new ones.

Author Contributions: A.B. prepared sections of radiation and material interaction, selective laser etching and laser welding. L.J. prepared sections about photonic elements manufacturing and laser cutting. All authors have read and agreed to the published version of the manuscript.

Funding: This research was funded by EC Horizon 2020 program, ATOPLOT project, grant number 950785.

Acknowledgments: In this section you can acknowledge any support given which is not covered by the author contribution or funding sections. This may include administrative and technical support, or donations in kind (e.g., materials used for experiments).

Conflicts of Interest: The authors declare no conflict of interest.

References

1. Ivey, D.G.; Northwood, D.O. Storing energy in metal hydrides: A review of the physical metallurgy. *J. Mater. Sci.* **1983**, *18*, 321–347. [CrossRef]
2. Dewidar, M.M.; Yoon, H.C.; Lim, J.K. Mechanical properties of metals for biomedical applications using powder metallurgy process: A review. *Met. Mater. Int.* **2006**, *12*, 193–206. [CrossRef]
3. Thames, S.F.; Panjnani, K.G. Organosilane polymer chemistry: A review. *J. Inorg. Organomet. Polym.* **1996**, *6*, 59–94. [CrossRef]
4. Merkininkaitė, G.; Gailevičius, D.; Šakirzanovas, S.; Jonušauskas, L. Polymers for Regenerative Medicine Structures Made via Multiphoton 3D Lithography. *Int. J. Polym. Sci.* **2019**, *2019*, 1–23. [CrossRef]
5. Feng, X.; Qi, C.; Lin, F.; Hu, H. Tungsten–tellurite glass: A new candidate medium for Yb3-doping. *J. Non-Cryst. Solids* **1999**, *256–257*, 372–377. [CrossRef]
6. Colomban, P.; Schreiber, H.D. Raman signature modification induced by copper nanoparticles in silicate glass. *J. Raman Spectrosc.* **2005**, *36*, 884–890. [CrossRef]
7. Goh, Y.F.; Alshemary, A.Z.; Akram, M.; Kadir, M.R.A.; Hussain, R. Bioactive Glass: AnIn-VitroComparative Study of Doping with Nanoscale Copper and Silver Particles. *Int. J. Appl. Glass Sci.* **2014**, *5*, 255–266. [CrossRef]
8. Ahmadi, F.; Ebrahimpour, Z.; Asgari, A.; El-Mallawany, R. Role of silver/titania nanoparticles on optical features of Sm3+ doped sulfophosphate glass. *Opt. Mater.* **2020**, *105*, 109922. [CrossRef]
9. Inoue, A.; Shinohara, Y.; Yokoyama, Y.; Masumoto, T. Solidification Analyses of Bulky Zr60Al10Ni10Cu15Pd5 Glass Produced by Casting into Wedge-Shape Copper MoldSolidification Analyses of Bulky Zr60Al10Ni10Cu15Pd5 Glass Produced by Casting into Wedge-Shape Copper Mold. *Mater. Trans. JIM* **1995**, *36*, 1276–1281. [CrossRef]
10. Laws, K.J.; Gun, B.; Ferry, M. Influence of Casting Parameters on the Critical Casting Size of Bulk Metallic Glass. *Metall. Mater. Trans. A* **2009**, *40*, 2377–2387. [CrossRef]
11. Fujita, K.; Morishita, Y.; Nishiyama, N.; Kimura, H.; Inoue, A. Cutting Characteristics of Bulk Metallic Glass. *Mater. Trans.* **2005**, *46*, 2856–2863. [CrossRef]
12. Foy, K.; Wei, Z.; Matsumura, T.; Huang, Y. Effect of tilt angle on cutting regime transition in glass micromilling. *Int. J. Mach. Tools Manuf.* **2009**, *49*, 315–324. [CrossRef]
13. Huang, C.C.; Hewak, D.W.; Badding, J.V. Deposition and characterization of germanium sulphide glass planar waveguides. *Opt. Express* **2004**, *12*, 2501–2506. [CrossRef] [PubMed]
14. Ostomel, T.A.; Shi, Q.; Tsung, C.K.; Liang, H.; Stucky, G.D. Spherical Bioactive Glass with Enhanced Rates of Hydroxyapatite Deposition and Hemostatic Activity. *Small* **2006**, *2*, 1261–1265. [CrossRef]
15. Tay, F.E.H.; Iliescu, C.; Jing, J.; Miao, J. Defect-free wet etching through pyrex glass using Cr/Au mask. *Microsyst. Technol.* **2006**, *12*, 935–939. [CrossRef]
16. Iliescu, C.; Chen, B.; Miao, J. On the wet etching of Pyrex glass. *Sens. Actuators A-Phys.* **2008**, *143*, 154–161. [CrossRef]
17. Von Witzendorff, P.; Pohl, L.; Suttmann, O.; Heinrich, P.; Heinrich, A.; Zander, J.; Bragard, H.; Kaierle, S. Additive manufacturing of glass: CO_2-Laser glass deposition printing. *Proc. CIRP* **2018**, *74*, 272–275. [CrossRef]
18. Zaki, R.M.; Strutynski, C.; Kaser, S.; Bernard, D.; Hauss, G.; Faessel, M.; Sabatier, J.; Canioni, L.; Messaddeq, Y.; Danto, S.; et al. Direct 3D-printing of phosphate glass by fused deposition modeling. *Mater. Des.* **2020**, *194*, 108957. [CrossRef]

19. Kotz, F.; Arnold, K.; Bauer, W.; Schild, D.; Keller, N.; Sachsenheimer, K.; Nargang, T.M.; Richter, C.; Helmer, D.; Rapp, B.E. Three-dimensional printing of transparent fused silica glass. *Nature* **2017**, *544*, 337–339. [CrossRef]
20. Kotz, F.; Quick, A.S.; Risch, P.; Martin, T.; Hoose, T.; Thiel, M.; Helmer, D.; Rapp, B.E. Two-Photon Polymerization of Nanocomposites for the Fabrication of Transparent Fused Silica Glass Microstructures. *Adv. Mater.* **2021**, *33*, 2006341. [CrossRef]
21. Sibbett, W.; Lagatsky, A.A.; Brown, C.T.A. The development and application of femtosecond laser systems. *Opt. Express* **2012**, *20*, 6989–7001. [CrossRef]
22. Jonušauskas, L.; Mackevičiūtė, D.; Kontenis, G.; Purlys, V. Femtosecond lasers: The ultimate tool for high-precision 3D manufacturing. *Adv. Opt. Technol.* **2019**, *8*, 241–251. [CrossRef]
23. Chichkov, B.N.; Momma, C.; Nolte, S.; Alvensleben, F.; Tünnermann, A. Femtosecond, picosecond and nanosecond laser ablation of solids. *Appl. Phys. A* **1996**, *63*, 109–115. [CrossRef]
24. Leitz, K.H.; Redlingshöfer, B.; Reg, Y.; Otto, A.; Schmidt, M. Metal Ablation with Short and Ultrashort Laser Pulses. *Phys. Procedia* **2011**, *12*, 230–238. [CrossRef]
25. Kerse, C.; Kalaycıoğlu, H.; Elahi, P.; Çetin, B.; Kesim, D.K.; Akçaalan, Ö.; Yavaş, S.; Aşık, M.D.; Öktem, B.; Hoogland, H.; et al. Ablation-cooled material removal with ultrafast bursts of pulses. *Nature* **2016**, *537*, 84–88. [CrossRef]
26. Gattass, R.R.; Mazur, E. Femtosecond laser micromachining in transparent materials. *Nature Photon.* **2008**, *2*, 219–225. [CrossRef]
27. Brabec, T.; Krausz, F. Intense few-cycle laser fields: Frontiers of nonlinear optics. *Rev. Mod. Phys.* **2000**, *72*, 545–585. [CrossRef]
28. Keldysh, L.V. Ionization in the field of a strong electromagnetic wave. *J. Exp. Theor. Phys.* **1965**, *20*, 1307–1314.
29. Schaffer, C.B.; Brodeur, A.; Mazur, E. Laser-induced breakdown and damage in bulk transparent materials induced by tightly focused femtosecond laser pulses. *Meas. Sci. Technol.* **2001**, *12*, 1784–1794. [CrossRef]
30. Sundaram, S.K.; Mazur, E. Inducing and probing non-thermal transitions in semiconductors using femtosecond laser pulses. *Nat. Mater.* **2002**, *1*, 217–224. [CrossRef]
31. Bellouard, Y.; Said, A.; Dugan, M.; Bado, P. Fabrication of high-aspect ratio, micro-fluidic channels and tunnels using femtosecond laser pulses and chemical etching. *Opt. Express* **2004**, *12*, 2120–2129. [CrossRef] [PubMed]
32. Zhimalov, A.B.; Solinov, V.F.; Kondratenko, V.S.; Kaplina, T.V. Laser cutting of float glass during production. *Glass Ceram.* **2006**, *63*, 319–321. [CrossRef]
33. Zhao, C.; Zhang, H.; Wang, Y. Semiconductor laser asymmetry cutting glass with laser induced thermal-crack propagation. *Opt. Lasers Eng.* **2014**, *63*, 43–52. [CrossRef]
34. Kanemitsu, Y.; Tanaka, Y. Mechanism of crack formation in glass after high-power laser pulse irradiation. *J. Appl. Phys.* **1987**, *62*, 1208–1211. [CrossRef]
35. Mirza, I.; Bulgakova, N.M.; Tomaštik, J.; Michalek, V.; Haderka, O.; Fekete, L.; Mocek, T. Ultrashort pulse laser ablation of dielectrics: Thresholds, mechanisms, role of breakdown. *Sci. Rep.* **2016**, *6*, 1–11. [CrossRef]
36. Dyer, P.; Farley, R.J.; Giedl, R.; Karnakis, D. Excimer laser ablation of polymers and glasses for grating fabrication. *Appl. Surf. Sci.* **1996**, *96–98*, 537–549. [CrossRef]
37. Buerhop, C.; Blumenthal, B.; Weissmann, R. Glass surface treatment with excimer and CO_2 lasers. *Appl. Surf. Sci.* **1990**, *46*, 430–434. [CrossRef]
38. Jonušauskas, L.; Juodkazis, S.; Malinauskas, M. Optical 3D printing: Bridging the gaps in the mesoscale. *J. Opt.* **2018**, *20*, 053001. [CrossRef]
39. Jesacher, A.; Booth, M.J. Parallel direct laser writing in three dimensions with spatially dependent aberration correction. *Opt. Express* **2010**, *18*, 21090–21099. [CrossRef]
40. Krol, D. Femtosecond laser modification of glass. *J. Non-Cryst. Solids* **2008**, *354*, 416–424. [CrossRef]
41. Hnatovsky, C.; Taylor, R.S.; Simova, E.; Rajeev, P.P.; Rayner, D.M.; Bhardwaj, V.; Corkum, P.B. Fabrication of microchannels in glass using focused femtosecond laser radiationand selectivechemical etching. *Appl. Phys. A* **2006**, *84*, 47–61. [CrossRef]
42. Khalil, A.A.; Bérubé, J.P.; Danto, S.; Cardinal, T.; Petit, Y.; Canioni, L.; Vallée, R. Comparative study between the standard type I and the type A femtosecond laser induced refractive index change in silver containing glasses. *Opt. Mater. Express* **2019**, *9*, 2640–2651. [CrossRef]
43. Hnatovsky, C.; Taylor, R.S.; Simova, E.; Bhardwaj, V.R.; Rayner, D.M.; Corkum, P.B. Polarization-selective etching in femtosecond laser-assisted microfluidic channel fabrication in fused silica. *Opt. Lett.* **2005**, *30*, 1867–1869. [CrossRef]
44. QI, J.; Wang, Z.; Xu, J.; Lin, Z.; Li, X.; Chu, W.; Cheng, Y. Femtosecond laser induced selective etching in fused silica: Optimization of the inscription conditions with a high-repetition-rate laser source. *Opt. Express* **2018**, *26*, 29669–29678. [CrossRef] [PubMed]
45. Itoh, K.; Watanabe, W.; Nolte, S.; Schaffer, C.B. Ultrafast processes for bulk modification of transparent materials. *MRS Bull.* **2006**, *31*, 620–625. [CrossRef]
46. Sugioka, K.; Cheng, Y. Ultrafast lasers-reliable tools for advanced materials processing. *Light Sci. Appl.* **2014**, *3*, 4. [CrossRef]
47. Miura, K.; Qiu, J.; Inouye, H.; Mitsuyu, T.; Hirao, K. Photowritten optical waveguides in various glasses with ultrashort pulse laser. *Appl. Phys. Lett.* **1997**, *71*, 3329–3331. [CrossRef]
48. Bellouard, Y.; Said, A.A.; Bado, P. Integrating optics and micro-mechanics in a single substrate: A step toward monolithic integration in fused silica. *Opt. Express* **2005**, *13*, 6635–6644. [CrossRef]
49. Liu, X.Q.; Bai, B.F.; Chen, Q.D.; Sun, H.B. Etching-assisted femtosecond laser modification of hard materials. *Opto-Electron. Adv.* **2019**, *2*, 190021. [CrossRef]

50. Richter, S.; Zimmermann, F.; Eberhardt, R.; Tunnermann, A.; Nolte, S. Toward laser welding of glasses without optical contacting. *Appl. Phys. A* **2015**, *121*, 1–9. [CrossRef]
51. Li, W.; Meng, F.; Chen, Y.; Li, Y.; Huang, X. Topology Optimization of Photonic and Phononic Crystals and Metamaterials: A Review. *Adv. Theory Simul.* **2019**, *2*, 1900017. [CrossRef]
52. Apfel, J.H. Phase retardance of periodic multilayer mirrors. *Appl. Opt.* **1982**, *21*, 733. [CrossRef]
53. Pallarés-Aldeiturriaga, D.; Roldán-Varona, P.; Rodríguez-Cobo, L.; López-Higuera, J.M. Optical Fiber Sensors by Direct Laser Processing: A Review. *Sensors* **2020**, *20*, 6971. [CrossRef]
54. Wikszak, E.; Thomas, J.; Burghoff, J.; Ortaç, B.; Limpert, J.; Nolte, S.; Fuchs, U.; Tunnermann, A. Erbium fiber laser based on intracore femtosecond-written fiber Bragg grating. *Opt. Lett.* **2006**, *31*, 2390–2392. [CrossRef]
55. Grobnic, D.; Mihailov, S.; Smelser, C.; Ding, H. Sapphire Fiber Bragg Grating Sensor Made Using Femtosecond Laser Radiation for Ultrahigh Temperature Applications. *IEEE Photon. Technol. Lett.* **2004**, *16*, 2505–2507. [CrossRef]
56. Lai, Y.; Zhou, K.; Sugden, K.; Bennion, I. Point-by-point inscription of first-order fiber Bragg grating for C-band applications. *Opt. Express* **2007**, *15*, 18318–18325. [CrossRef] [PubMed]
57. Wolf, A.; Dostovalov, A.; Bronnikov, K.; Babin, S. Arrays of fiber Bragg gratings selectively inscribed in different cores of 7-core spun optical fiber by IR femtosecond laser pulses. *Opt. Express* **2019**, *27*, 13978–13990. [CrossRef] [PubMed]
58. Dostovalov, A.V.; Wolf, A.A.; Parygin, A.V.; Zyubin, V.E.; Babin, S.A. Femtosecond point-by-point inscription of Bragg gratings by drawing a coated fiber through ferrule. *Opt. Express* **2016**, *24*, 16232–16237. [CrossRef] [PubMed]
59. Maigyte, L.; Purlys, V.; Trull, J.; Peckus, M.; Cojocaru, C.; Gailevičius, D.; Malinauskas, M.; Staliunas, K. Flat lensing in the visible frequency range by woodpile photonic crystals. *Opt. Lett.* **2013**, *38*, 2376–2378. [CrossRef]
60. Maigyte, L.; Gertus, T.; Peckus, M.; Trull, J.; Cojocaru, C.; Sirutkaitis, V.; Staliunas, K. Signatures of light-beam spatial filtering in a three-dimensional photonic crystal. *Phys. Rev. A* **2010**, *82*, 043819. [CrossRef]
61. Wong, S.; Deubel, M.; Pérez-Willard, F.; John, S.; Ozin, G.; Wegener, M.; von Freymann, G. Direct Laser Writing of Three-Dimensional Photonic Crystals with a Complete Photonic Bandgap in Chalcogenide Glasses. *Adv. Mater.* **2006**, *18*, 265–269. [CrossRef]
62. Gailevičius, D.; Purlys, V.; Maigytė, L.; Peckus, M.; Staliūnas, K. Chirped axisymmetric photonic microstructures for spatial filtering. *J. Nanophotonics* **2014**, *8*, 084094. [CrossRef]
63. Purlys, V.; Maigyte, L.; Gailevičius, D.; Peckus, M.; Malinauskas, M.; Gadonas, R.; Staliunas, K. Spatial filtering by axisymmetric photonic microstructures. *Opt. Lett.* **2014**, *39*, 929–932. [CrossRef]
64. Gailevičius, D.; Koliadenko, V.; Purlys, V.; Peckus, M.; Taranenko, V.; Staliunas, K. Photonic crystal microchip laser. *Sci. Rep.* **2016**, *6*, 34173. [CrossRef]
65. Gailevičius, D.; Purlys, V.; Staliunas, K. Photonic crystal spatial filters fabricated by femtosecond pulsed Bessel beam. *Opt. Lett.* **2019**, *44*, 4969–4972. [CrossRef] [PubMed]
66. Davis, K.M.; Miura, K.; Sugimoto, N.; Hirao, K. Writing waveguides in glass with a femtosecond laser. *Opt. Lett.* **1996**, *21*, 1729–1731. [CrossRef] [PubMed]
67. Caulier, O.; Coq, D.; Bychkov, E.; Masselin, P. Direct laser writing of buried waveguide in As_2S_3 glass using a helical sample translation. *Opt. Lett.* **2013**, *38*, 4212. [CrossRef]
68. Long, X.; Bai, J.; Zhao, W.; Stoian, R.; Hui, R.; Cheng, G. Stressed waveguides with tubular depressed-cladding inscribed in phosphate glasses by femtosecond hollow laser beams. *Opt. Lett.* **2012**, *37*, 3138–3140. [CrossRef]
69. Shah, L.; Arai, A.Y.; Eaton, S.M.; Herman, P.R. Waveguide writing in fused silica with a femtosecond fiber laser at 522 nm and 1 MHz repetition rate. *Opt. Express* **2005**, *13*, 1999–2006. [CrossRef] [PubMed]
70. Yang, W.; Corbari, C.; Kazansky, P.G.; Sakaguchi, K.; Carvalho, I.C. Low loss photonic components in high index bismuth borate glass by femtosecond laser direct writing. *Opt. Express* **2008**, *16*, 16215–16226. [CrossRef]
71. Osellame, R.; Taccheo, S.; Marangoni, M.; Ramponi, R.; Laporta, P.; Polli, D.; Silvestri, S.; Cerullo, G. Femtosecond writing of active optical waveguides with astigmatically shaped beams. *J. Opt. Soc. Am. B* **2003**, *20*, 1559–1567. [CrossRef]
72. Liao, Y.; Qi, J.; Wang, P.; Chu, W.; Wang, Z.; Qiao, L.; Cheng, Y. Transverse writing of three-dimensional tubular optical waveguides in glass with a slit-shaped femtosecond laser beam. *Sci. Rep.* **2016**, *6*, 28790. [CrossRef]
73. Nasu, Y.; Kohtoku, M.; Hibino, Y. Low-loss waveguides written with a femtosecond laser for flexible interconnection in a planar light-wave circuit. *Opt. Lett.* **2005**, *30*, 723–725. [CrossRef]
74. Zhang, B.; Xiong, B.; Li, Z.; Li, L.; Lv, J.; Lu, Q.; Wang, L.; Chen, F. Mode tailoring of laser written waveguides in LiNbO3 crystals by multi-scan of femtosecond laser pulses. *Opt. Mater.* **2018**, *86*, 571–575. [CrossRef]
75. Eaton, S.M.; Zhang, H.; Herman, P.R.; Yoshino, F.; Shah, L.; Bovatsek, J.; Arai, A.Y. Heat accumulation effects in femtosecond laser-written waveguides with variable repetition rate. *Opt. Express* **2005**, *13*, 4708–4716. [CrossRef] [PubMed]
76. Zhang, H.; Eaton, S.M.; Li, J.; Herman, P.R. Femtosecond laser direct writing of multiwavelength Bragg grating waveguides in glass. *Opt. Lett.* **2006**, *31*, 3495–3497. [CrossRef] [PubMed]
77. Marshall, G.D.; Ams, M.; Withford, M.J. Direct laser written waveguide-Bragg gratings in bulk fused silica. *Opt. Lett.* **2006**, *31*, 2690–2691. [CrossRef] [PubMed]
78. Osellame, R.; Maselli, V.; Vazquez, R.M.; Ramponi, R.; Cerullo, G. Integration of optical waveguides and microfluidic channels both fabricated by femtosecond laser irradiation. *Appl. Phys. Lett.* **2007**, *90*, 231118. [CrossRef]

79. Vazquez, R.M.; Osellame, R.; Nolli, D.; Dongre, C.; Vlekkert, H.; Ramponi, R.; Pollnau, M.; Cerullo, G. Integration of femtosecond laser written optical waveguides in a lab-on-chip. *Lab Chip* **2009**, *9*, 91–96. [CrossRef] [PubMed]
80. Djogo, G.; Li, J.; Ho, S.; Haque, M.; Ertorer, E.; Liu, J.; Song, X.; Suo, J.; Herman, P.R. Femtosecond laser additive and subtractive micro-processing: Enabling a high-channel-density silica interposer for multicore fibre to silicon-photonic packaging. *Int. J. Extreme Manuf.* **2019**, *1*, 045002. [CrossRef]
81. Bricchi, E.; Klappauf, B.G.; Kazansky, P.G. Form birefringence and negative index change created by femtosecond direct writing in transparent materials. *Opt. Lett.* **2004**, *29*, 119–121. [CrossRef] [PubMed]
82. Sudrie, L.; Franco, M.; Prade, B.; Mysyrowicz, A. Writing of permanent birefringent microlayers in bulk fused silica with femtosecond laser pulses. *Opt. Commun.* **1999**, *171*, 279–284. [CrossRef]
83. Sakakura, M.; Lei, Y.; Wang, L.; Yu, Y.H.; Kazansky, P.G. Ultralow-loss geometric phase and polarization shaping by ultrafast laser writing in silica glass. *Light Sci. Appl.* **2020**, *9*, 15. [CrossRef] [PubMed]
84. Shimotsuma, Y.; Hirao, K.; Qiu, J.; Kazansky, P.G. Nano-modificationinside transparent materials by femtosecond laser single beam. *Mod. Phys. Lett. B* **2005**, *19*, 225–238. [CrossRef]
85. Shimotsuma, Y.; Hirao, K.; Qiu, J.; Miura, K. Nanofabrication in transparent materials with a femtosecond pulse laser. *J. Non-Cryst. Solids* **2006**, *352*, 646–656. [CrossRef]
86. Richter, S.; Miese, C.; Doring, S.; Zimmermann, F.; Withford, M.J.; Tunnermann, A.; Nolte, S. Laser induced nanogratings beyond fused silica—Periodic nanostructures in borosilicate glasses and ULE™. *Opt. Mater. Express* **2013**, *3*, 1161–1166. [CrossRef]
87. Liao, Y.; Ni, J.; Qiao, L.; Huang, M.; Bellouard, Y.; Sugioka, K.; Cheng, Y. High-fidelity visualization of formation of volume nanogratings in porous glass by femtosecond laser irradiation. *Optica* **2015**, *2*, 329–334. [CrossRef]
88. Beresna, M.; Kazansky, P.G. Polarization diffraction grating produced by femtosecond laser nanostructuring in glass. *Opt. Lett.* **2010**, *35*, 1662–1664. [CrossRef]
89. Bricchi, E.; Mills, J.D.; Kazansky, P.G.; Klappauf, B.G.; Baumberg, J.J. Birefringent Fresnel zone plates in silica fabricated by femtosecond laser machining. *Opt. Lett.* **2002**, *27*, 2200–2202. [CrossRef]
90. Papazoglou, D.G.; Loulakis, M.J. Embedded birefringent computer-generated holograms fabricated by femtosecond laser pulses. *Opt. Lett.* **2006**, *31*, 1441–1443. [CrossRef]
91. Cai, W.; Libertun, A.R.; Piestun, R. Polarization selective computer-generated holograms realized in glass by femtosecond laser induced nanogratings. *Opt. Express* **2006**, *14*, 3785–3791. [CrossRef] [PubMed]
92. Beresna, M.; Gecevičius, M.; Kazansky, P.G. Polarization sensitive elements fabricated by femtosecond laser nanostructuring of glass [Invited]. *Opt. Mater. Express* **2011**, *1*, 783–795. [CrossRef]
93. Beresna, M.; Gecevičius, M.; Kazansky, P.G.; Gertus, T. Radially polarized optical vortex converter created by femtosecond laser nanostructuring of glass. *Appl. Phys. Lett.* **2011**, *98*, 201101. [CrossRef]
94. Tsai, Y.J.; Larouche, S.; Tyler, T.; Llopis, A.; Royal, M.; Jokerst, N.M.; Smith, D.R. Arbitrary birefringent metamaterials for holographic optics at λ = 155 µm. *Opt. Express* **2013**, *21*, 26620–26630. [CrossRef] [PubMed]
95. Bricchi, E.; Kazansky, P.G. Extraordinary stability of anisotropic femtosecond direct-written structures embedded in silica glass. *Appl. Phys. Lett.* **2006**, *88*, 111119. [CrossRef]
96. Gallais, L.; Commandré, M. Laser-induced damage thresholds of bulk and coating optical materials at 1030 nm, 500 fs. *Appl. Opt.* **2013**, *53*, A186–A196. [CrossRef] [PubMed]
97. Gu, M.; Li, X. The Road to Multi-Dimensional Bit-by-Bit Optical Data Storage. *Opt. Photonics News* **2010**, *21*, 28–33. [CrossRef]
98. Shimotsuma, Y.; Sakakura, M.; Miura, K.; Qiu, J.; Kazansky, P.G.; Fujita, K.; Hirao, A. Application of Femtosecond-Laser Induced Nanostructures in Optical Memory. *J. Nanosci. Nanotechnol.* **2007**, *7*, 94–104. [CrossRef]
99. Gu, M.; Li, X.; Cao, Y. Optical storage arrays: A perspective for future big data storage. *Light Sci. Appl.* **2014**, *3*, e177. [CrossRef]
100. Beresna, M.; Gecevičius, M.; Kazansky, P.G.; Taylor, T.; Kavokin, A.V. Exciton mediated self-organization in glass driven by ultrashort light pulses. *Appl. Phys. Lett.* **2012**, *101*, 053120. [CrossRef]
101. Zhang, J.; Gecevičius, M.; Beresna, M.; Kazansky, P.G. Seemingly Unlimited Lifetime Data Storage in Nanostructured Glass. *Phys. Rev. Lett.* **2014**, *112*, 033901. [CrossRef]
102. Taylor, R.S.; Hnatovsky, C.; Simova, E.; Rajeev, P.P.; Rayner, D.M.; Corkum, P.B. Femtosecond laser erasing and rewriting of self-organized planar nanocracks in fused silica glass. *Opt. Lett.* **2007**, *32*, 2888–2890. [CrossRef] [PubMed]
103. Chen, F.S.; LaMacchia, J.T.; Fraser, D.B. Holographic storage in lithium niobate. In *Landmark Papers on Photorefractive Nonlinear Optics*; World Scientific: Singapore, 1995; pp. 33–35. [CrossRef]
104. Mizeikis, V.; Purlys, V.; Paipulas, D.; R, B.; Juodkazis, S. Direct Laser Writing: Versatile Tool for Microfabrication of Lithium Niobate. *J. Laser Micro. Nanoeng.* **2012**, *7*, 345–350. [CrossRef]
105. Rusitschka, S.; Curry, E. Big Data in the Energy and Transport Sectors. In *New Horizons for a Data-Driven Economy*; Springer International Publishing: Cham, Switzerland, 2016; pp. 225–244. [CrossRef]
106. Chon, J.W.M.; Gan, X.; Gu, M. Splitting of the focal spot of a high numerical-aperture objective in free space. *Appl. Phys. Lett.* **2002**, *81*, 1576–1578. [CrossRef]
107. Bomzon, Z.; Gu, M.; Shamir, J. Angular momentum and geometrical phases in tight-focused circularly polarized plane waves. *Appl. Phys. Lett.* **2006**, *89*, 241104. [CrossRef]
108. Wyant, J.C.; Creath, K. Basic wavefront aberration theory for optical metrology. *Appl. Opt. Opt. Eng.* **1992**, *11*, 2.

109. Kontenis, G.; Gailevičius, D.; Jonušauskas, L.; Purlys, V. Dynamic aberration correction via spatial light modulator (SLM) for femtosecond direct laser writing: Towards spherical voxels. *Opt. Express* **2020**, *28*, 27850–27864. [CrossRef]
110. Bonora, S.; Jian, Y.; Zhang, P.; Zam, A.; Pugh, E.N.; Zawadzki, R.J.; Sarunic, M.V. Wavefront correction and high-resolution in vivo OCT imaging with an objective integrated multi-actuator adaptive lens. *Opt. Express* **2015**, *23*, 21931–21941. [CrossRef]
111. Li, L.; Wang, D.; Liu, C.; Wang, Q.H. Zoom microscope objective using electrowetting lenses. *Opt. Express* **2016**, *24*, 2931–2940. [CrossRef]
112. Salter, P.S.; Baum, M.; Alexeev, I.; Schmidt, M.; Booth, M.J. Exploring the depth range for three-dimensional laser machining with aberration correction. *Opt. Express* **2014**, *22*, 17644. [CrossRef]
113. de la Cruz, A.R.; Ferrer, A.; Gawelda, W.; Puerto, D.; Sosa, M.G.; Siegel, J.; Solis, J. Independent control of beam astigmatism and ellipticity using a SLM for fs-laser waveguide writing. *Opt. Express* **2009**, *17*, 20853–20859. [CrossRef]
114. Sakakura, M.; Sawano, T.; Shimotsuma, Y.; Miura, K.; Hirao, K. Fabrication of three-dimensional 1 × 4 splitter waveguides inside a glass substrate with spatially phase modulated laser beam. *Opt. Express* **2010**, *18*, 12136–12143. [CrossRef] [PubMed]
115. Simmonds, R.D.; Salter, P.S.; Jesacher, A.; Booth, M.J. Three dimensional laser microfabrication in diamond using a dual adaptive optics system. *Opt. Express* **2011**, *19*, 24122–24128. [CrossRef]
116. Courvoisier, A.; Booth, M.J.; Salter, P.S. Inscription of 3D waveguides in diamond using an ultrafast laser. *Appl. Phys. Lett.* **2016**, *109*, 031109. [CrossRef]
117. Bharadwaj, V.; Courvoisier, A.; Fernandez, T.T.; Ramponi, R.; Galzerano, G.; Nunn, J.; Booth, M.J.; Osellame, R.; Eaton, S.M.; Salter, P.S. Femtosecond laser inscription of Bragg grating waveguides in bulk diamond. *Opt. Lett.* **2017**, *42*, 3451–3453. [CrossRef]
118. Wang, P.; Qi, J.; Liu, Z.; Liao, Y.; Chu, W.; Cheng, Y. Fabrication of polarization-independent waveguides deeply buried in lithium niobate crystal using aberration-corrected femtosecond laser direct writing. *Sci. Rep.* **2017**, *7*, 41211. [CrossRef] [PubMed]
119. Huang, L.; Salter, P.; Karpiński, M.; Smith, B.; Payne, F.; Booth, M. Waveguide fabrication in KDP crystals with femtosecond laser pulses. *Appl. Phys. A* **2014**, *118*, 831–836. [CrossRef]
120. Vizsnyiczai, G.; Kelemen, L.; Ormos, P. Holographic multi-focus 3D two-photon polymerization with real-time calculated holograms. *Opt. Express* **2014**, *22*, 24217–24223. [CrossRef] [PubMed]
121. Horie, Y.; Arbabi, A.; Arbabi, E.; Kamali, S.M.; Faraon, A. High-speed, phase-dominant spatial light modulation with silicon-based active resonant antennas. *ACS Photonics* **2017**, *5*, 1711–1717. [CrossRef]
122. Zhu, G.; Whitehead, D.; Perrie, W.; Allegre, O.J.; Olle, V.; Li, Q.; Tang, Y.; Dawson, K.; Jin, Y.; Edwardson, S.P.; et al. Investigation of the thermal and optical performance of a spatial light modulator with high average power picosecond laser exposure for materials processing applications. *J. Phys. D Appl. Phys.* **2018**, *51*, 095603. [CrossRef]
123. Park, J.; Jeong, B.G.; Kim, S.I.; Lee, D.; Kim, J.; Shin, C.; Lee, C.B.; Otsuka, T.; Kyoung, J.; Kim, S.; et al. All-solid-state spatial light modulator with independent phase and amplitude control for three-dimensional LiDAR applications. *Nature Nanotechnol.* **2020**, *16*, 69–76. [CrossRef] [PubMed]
124. Marcinkevičius, A.; Juodkazis, S.; Watanabe, M.; Miwa, M.; Matsuo, S.; Misawa, H.; Nishii, J. Femtosecond laser-assisted three-dimensional microfabrication in silica. *Opt. Lett.* **2001**, *26*, 277–279. [CrossRef] [PubMed]
125. Kiyama, S.; Matsuo, S.; Hashimoto, S.; Morihira, Y. Examination of Etching Agent and Etching Mechanism on Femotosecond Laser Microfabrication of Channels Inside Vitreous Silica Substrates. *J. Phys. Chem. C* **2009**, *113*, 11560–11566. [CrossRef]
126. Ross, C.A.; Maclachan, D.G.; Choudrury, D.; Thomson, R.R. Optimisation of ultrafast laser assisted etching in fused silica. *Opt. Express* **2018**, *26*, 24343–24356. [CrossRef] [PubMed]
127. Chen, F.; Deng, Z.; Yang, Q.; Bian, H.; Du, G.; Si, J.; Hou, X. Rapid fabrication of a large-area close-packed quasi-periodic microlens array on BK7 glass. *Opt. Lett.* **2014**, *39*, 606–609. [CrossRef]
128. Matsuo, S.; Sumi, H.; Kiyama, S.; Tomita, T.; Hashimoto, S. Femtosecond laser-assisted etching of Pyrex glass with aqueous solution of KOH. *Appl. Surf. Sci.* **2009**, *225*, 9758–9760. [CrossRef]
129. Juodkazis, S.; Yamasaki, K.; Mizeikis, V.; Matsuo, S.; Misawa, H. Formation of embedded patterns in glasses using femtosecond irradiation. *Appl. Phys. A* **2004**, *79*, 1549–1553. [CrossRef]
130. Hu, Y.; Rao, S.; Wu, S.; Wei, P.; Qiu, W.; Wu, D.; Xu, B.; Ni, J.; Yang, L.; Li, J.; et al. All-Glass 3D Optofluidic Microchip with Built-in Tunable Microlens Fabricated by Femtosecond Laser-Assisted Etching. *Adv. Opt. Mater.* **2018**, *6*, 1701299. [CrossRef]
131. Butkus, S.; Rickus, M.; Sirutkaitis, R.; Paipulas, D.; Sirutkaitis, V. Fabrication of High Aspect Ratio Channels in Fused Silica Using Femtosecond Pulses and Chemical Etching at Different Conditions. *J. Laser Micro. Nanoen.* **2019**, *14*, 19–24.
132. LoTurco, S.; Osellame, R.; Ramponi, R.; Vishnubhatla, K.C. Hybrid chemical etching of femtosecond laser irradiated structures for engineered microfluidic devices. *J. Micromech. Microeng.* **2013**, *23*, 1–8. [CrossRef]
133. Bu, M.; Melvin, T.; Ensell, G.J.; Wilkinson, J.S.; Evans, A.G. A new masking technology for deep glass etching and its microfluidic application. *Sens. Actuators A* **2004**, *115*, 476–482. [CrossRef]
134. Venturini, F.; Navarrini, W.; Resnati, G.; Metrangolo, P.; Vazquez, R.M.; Osellame, R.; Cerullo, G. Selective Iterative Etching of Fused Silica with Gaseous Hydrofluoric Acid. *J. Phys. Chem. C* **2010**, *114*, 18712–18716. [CrossRef]
135. LoTurco, S. Hybrid chemical etching of femtosecond irradiated 3D structures in fused silica glass. *MATEC Web Conf.* **2013**, *8*, 05009. [CrossRef]
136. Choudhury, D.; Ródenas, A.; Paterson, L.; Jaque, D.; Kar, A.K. 3D Microfabrication in YAG Crystals by Direct Laser Writing and Chemical Etching. In Proceedings of the Lasers and Electro-Optics Pacific Rim Conference (Optical Society of America, 2013), Kyoto, Japan, 30 June–4 July 2013; pp. 14.

137. Paiè, P.; Bragheri, F.; Carlo, D.D.; Osellame, R. Particle focusing by 3D inertial microfluidics. *Microsyst. Nanoeng.* **2017**, *3*. [CrossRef] [PubMed]
138. Randles, A.B.; Esashi, M.; Tanaka, S. Etch rate dependence on crystal orientation of lithium niobate. *IEEE Trans. Ultrason. Ferroelectr. Freq. Control.* **2010**, *57*, 2372–2380. [CrossRef] [PubMed]
139. Matsuo, S.; Tabuchi, Y.; Okada, T.; Juodkazis, S.; Misawa, H. Femtosecond laser assisted etching of quartz: Microstructuring from inside. *Appl. Phys. A* **2006**, *84*, 99–102. [CrossRef]
140. Wortmann, D.; Gottmann, J.; Brandt, N.; Horn-Solle, H. Micro- and nanostructures inside sapphire by fs-laser irradiation and selective etching. *Opt. Express* **2008**, *16*, 1517–1522. [CrossRef]
141. Gottmann, J.; Wortmann, D.; Horstmann-Jungemann, M. Fabrication of sub-wavelength surface ripples and in-volume nanostructures by fs-laser induced selective etching. *Appl. Surf. Sci.* **2009**, *255*, 5641–5646. [CrossRef]
142. Horstmann-Jungemann, M.; Gottmann, J.; Wortmann, D. Nano- and Microstructuring of SiO_2 and Sapphire with Fs-laser Induced Selective Etching. *J. Laser. Micro. Nanoeng.* **2009**, *4*, 135–140. [CrossRef]
143. Juodkazis, S.; Nishimura, K.; Tanaka, S.; Misawa, H.; Gamaly, E.G.; Luther-Davies, B.; Hallo, L.; Nicolai, P.; Tikhonchuk, V.T. Laser-Induced Microexplosion Confined in the Bulk of a Sapphire Crystal: Evidence of Multimegabar Pressures. *Phys. Rev. Lett.* **2006**, *96*, 166101. [CrossRef]
144. Hörstmann-Jungemann, M.; Gottmann, J.; Keggenhoff, M. 3D-Microstructuring of Sapphire using fs-Laser Irradiation and Selective Etching. *J. Laser. Micro. Nanoeng.* **2010**, *5*, 145–149. [CrossRef]
145. Capuano, L.; Pohl, R.; Tiggelaar, R.M.; Berenschot, J.W.; Gardeniers, J.E.; RÖMer, G.R.B.E. Morphology of single picosecond pulse subsurface laser-induced modifications of sapphire and subsequent selective etching. *Opt. Express* **2018**, *26*, 29283–29295. [CrossRef] [PubMed]
146. Capuanoa, L.; Tiggelaar, R.; Berenschot, J.; Gardeniers, J.; Römer, G. Fabrication of millimeter-long structures in sapphire using femtosecond infrared laser pulses and selective etching. *Opt. Laser Eng.* **2020**, *133*, 106114. [CrossRef]
147. Juodkazis, S.; Nishi, Y.; Misawa, H. Femtosecond laser-assisted formation of channels in sapphire using KOH solution. *Phys. Status Solidi RRL* **2008**, *2*, 275–277. [CrossRef]
148. Li, Q.; Chen, Q.; Niu, L.; Yu, Y.; Wang, L.; Sun, Y.; Sun, H. Sapphire-Based Dammann Gratings for UV Beam Splitting. *IEEE Photon. J.* **2016**, *8*, 2500208. [CrossRef]
149. Li, Q.; Yu, Y.; Wang, L.; Cao, X.; Liu, X.; Sun, Y.; Chena, Q.; Duan, J.; Sun, H. Sapphire-Based Fresnel Zone Plate Fabricated by Femtosecond Laser Direct Writing and Wet Etching. *IEEE Photon. Technol. Lett.* **2016**, *28*, 1290–1293. [CrossRef]
150. Matsuo, S.; Tokumi, K.; Tomita, T.; Hashimoto, S. Three-Dimensional Residue-Free Volume Removal inside Sapphire by High-Temperature Etching after Irradiation of Femtosecond Laser Pulses. *Laser Chem.* **2008**, *2008*, 892721. [CrossRef]
151. Hermans, M.; Gottmann, J.; Riedel, F. Selective, Laser-Induced Etching of Fused Silica at High Scan-Speeds Using KOH. *J. Laser. Micro. Nanoeng.* **2014**, *9*, 126–131. [CrossRef]
152. Li, X.; Xu, J.; Lin, Z.; Qi, J.; Wang, P.; Chu, W.; Fang, Z.; Wang, Z.; Chai, Z.; Cheng, Y. Polarization-insensitive space-selective etching in fused silica induced by picosecond laser irradiation. *Appl. Surf. Sci.* **2019**, *485*, 188–193. [CrossRef]
153. Sugioka, K.; Masuda, M.; Hongo, T.; Cheng, Y.; Shihoyama, K.; Midorikawa, K. Three-dimensional microfluidic structure embedded in photostructurable glass by femtosecond laser for lab-on-chipapplications. *Appl. Phys. A* **2004**, *79*, 815–817. [CrossRef]
154. Gottmann, J.; Hermans, M.; Repiev, N.; Ortmann, J. Selective Laser-Induced Etching of 3D Precision Quartz Glass Components for Microfluidic Applications-Up-Scaling of Complexity and Speed. *Micromachines* **2017**, *8*, 110. [CrossRef]
155. Kim, S.; Kim, J.; Joung, Y.H.; Ahn, S.; Choi, J.; Koo, C. Optimization of selective laser-induced etching (SLE) for fabrication of 3D glass microfluidic device with multi-layer micro channels. *Micro Nano Sys. Lett.* **2019**, *7*, 15. [CrossRef]
156. Sugioka, K.; Cheng, Y.; Midorikawa, K. Three-dimensional micromachining of glass using femtosecond laser for lab-on-a-chip device manufacture. *Appl. Phys. A* **2005**, *81*, 1–10. [CrossRef]
157. Bellouard, Y.; Lehnert, T.; Bidaux, J.E.; Sidler, T.; Clavel, R.; Gotthardt, R. Local annealing of complex mechanical devices: A new approach for developing monolithic micro-devices. *Mater. Sci. Eng.* **1999**, *273*, 795–798. [CrossRef]
158. Bellouard, Y. Shape memory alloys for microsystems: A review from a material research perspective. *Mater. Sci. Eng. A* **2008**, *481*, 582–589. [CrossRef]
159. Gottmann, J.; Hermans, M.; ortmann, J. Microcutting and Hollow 3D Microstructures in Glasses by In-volume Selective Laser-induced Etching (ISLE). *J. Laser. Micro. Nanoeng.* **2013**, *8*, 15–18. [CrossRef]
160. Tičkūnas, T.; Perrenoud, M.; Butkus, S.; Gadonas, R.; Rekštytė, S.; Malinauskas, M.; Paipulas, D.; Bellouard, Y.; Sirutkaitis, V. Combination of additive and subtractive laser 3D microprocessing in hybrid glass/polymer microsystems for chemical sensing applications. *Opt. Express* **2017**, *25*, 26280–26288. [CrossRef]
161. Wu, D.; Xu, J.; Niu, L.G.; Wu, S.Z.; Midorikawa, K.; Sugioka, K. In-channel integration of designable microoptical devices using flat scaffold-supported femtosecond-laser microfabrication for coupling-free optofluidic cell counting. *Light Sci. Appl.* **2015**, *4*, e228. [CrossRef]
162. Wu, D.; Niu, L.G.; Wu, S.Z.; Xu, J.; Midorikawa, K.; Sugioka, K. Ship-in-a-bottle femtosecond laser integration of optofluidic microlens arrays with center-pass units enabling coupling-free parallel cell counting with a 100% success rate. *Lab Chip* **2015**, *15*, 1515–1523. [CrossRef]

163. Bückmann, T.; Stenger, N.; Kadic, M.; Kaschke, J.; Frölich, A.; Kennerknecht, T.; Eberl, C.; Thiel, M.; Wegener, M. Tailored 3D mechanical metamaterials made by dip-in direct-laser-writing optical lithography. *Adv. Mater.* **2012**, *24*, 2710–2714. [CrossRef]
164. Jonušauskas, L.; Baravykas, T.; Andrijec, D.; Gadišauskas, T.; Purlys, V. Stitchless support-free 3D printing of free-form micromechanical structures with feature size on-demand. *Sci. Rep.* **2019**, *9*, 17533. [CrossRef]
165. Yang, D.; Liu, L.; Gong, Q.; Li, Y. Rapid Two-Photon Polymerization of an Arbitrary 3D Microstructure with 3D Focal Field Engineering. *Macromol. Rapid Commun.* **2019**, *40*, 1900041. [CrossRef]
166. Dubey, A.K.; Yadava, V. Laser beam machining—A review. *Int. J. Mach. Tools Manuf.* **2008**, *48*, 609–628. [CrossRef]
167. Garškaitė, E.; Alinauskas, L.; Drienovsky, M.; Krajcovic, J.; Cicka, R.; Palcut, M.; Jonušauskas, L.; Malinauskas, M.; Stankeviciute, Z.; Kareiva, A. Fabrication of a composite of nanocrystalline carbonated hydroxyapatite (cHAP) with polylactic acid (PLA) and its surface topographical structuring with direct laser writing (DLW). *RSC Adv.* **2016**, *6*, 72733–72743. [CrossRef]
168. Ye, G.; Wang, W.; Fan, D.; He, P. Effects of femtosecond laser micromachining on the surface and substrate properties of poly-lactic acid (PLA). *Appl. Surf. Sci.* **2020**, *538*, 148117. [CrossRef]
169. Binder, P.S. Flap dimensions created with the IntraLase FS laser. *J. Cataract. Refract. Surg.* **2004**, *30*, 26–32. [CrossRef]
170. Kruger, J.; Kautek, W.; Lenzner, M.; Sartania, S.; Spielmann, C.; Krausz, F. Laser micromachining of barium aluminium borosilicate glass with pulse durations between 20 fs and 3 ps. *Appl. Surf. Sci.* **1998**, *127–129*, 892–898. [CrossRef]
171. Ben-Yakar, A.; Byer, R.L. Femtosecond laser ablation properties of borosilicate glass. *J. Appl. Phys.* **2004**, *96*, 5316–5323. [CrossRef]
172. Xu, S.; Qiu, J.; Jia, T.; Li, C.; Sun, H.; Xu, Z. Femtosecond laser ablation of crystals SiO_2 and YAG. *Opt. Commun.* **2007**, *274*, 163–166. [CrossRef]
173. Furusawa, K.; Takahashi, K.; Kumagai, H.; Midorikawa, K.; Obara, M. Ablation characteristics of Au, Ag, and Cu metals using a femtosecond Ti:sapphire laser. *Appl. Phys. A* **1999**, *69*, S359–S366. [CrossRef]
174. Žemaitis, A.; Gaidys, M.; Gečys, P.; Račiukaitis, G.; Gedvilas, M. Rapid high-quality 3D micro-machining by optimised efficient ultrashort laser ablation. *Opt. Lasers Eng.* **2018**, *114*, 83–89. [CrossRef]
175. Gafner, M.; Kramer, T.; Remund, S.M.; Holtz, R.; Neuenschwander, B. Ultrafast pulsed laser high precision micromachining of rotational symmetric parts. *J. Laser Appl.* **2021**, *33*, 012053. [CrossRef]
176. Giridhar, M.S.; Seong, K.; Schülzgen, A.; Khulbe, P.; Peyghambarian, N.; Mansuripur, M. Femtosecond pulsed laser micromachining of glass substrates with application to microfluidic devices. *Appl. Opt.* **2004**, *43*, 4584–4589. [CrossRef]
177. Nikumb, S.; Chen, Q.; Li, C.; Reshef, H.; Zheng, H.; Qiu, H.; Low, D. Precision glass machining, drilling and profile cutting by short pulse lasers. *Thin Solid Films* **2005**, *477*, 216–221. [CrossRef]
178. Queste, S.; Salut, R.; Clatot, S.; Rauch, J.Y.; Malek, C.G.K. Manufacture of microfluidic glass chips by deep plasma etching, femtosecond laser ablation, and anodic bonding. *Microsyst. Technol.* **2010**, *16*, 1485–1493. [CrossRef]
179. Ke, K.; Hasselbrink, E.F.; Hunt, A.J. Rapidly Prototyped Three-Dimensional Nanofluidic Channel Networks in Glass Substrates. *Anal. Chem.* **2005**, *77*, 5083–5088. [CrossRef] [PubMed]
180. Li, Y.; Qu, S.; Guo, Z. Fabrication of microfluidic devices in silica glass by water-assisted ablation with femtosecond laser pulses. *J. Micromech. Microeng.* **2011**, *21*, 075008. [CrossRef]
181. Jonušauskas, L.; Rekštytė, S.; Buividas, R.; Butkus, S.; Gadonas, R.; Juodkazis, S.; Malinauskas, M. Hybrid Subtractive-Additive-Welding Microfabrication for Lab-on-Chip (LOC) Applications via Single Amplified Femtosecond Laser Source. *Opt. Eng.* **2017**, *56*, 094108. [CrossRef]
182. Bellouard, Y.; Hongler, M.O. Femtosecond-laser generation of self-organized bubble patterns in fused silica. *Opt. Express* **2011**, *19*, 6807–6821. [CrossRef]
183. Li, Y.; Itoh, K.; Watanabe, W.; Yamada, K.; Kuroda, D.; Nishii, J.; Jiang, Y. Three-dimensional hole drilling of silica glass from the rear surface with femtosecond laser pulses. *Opt. Lett.* **2001**, *26*, 1912. [CrossRef]
184. Bhuyan, M.K.; Courvoisier, F.; Lacourt, P.A.; Jacquot, M.; Furfaro, L.; Withford, M.J.; Dudley, J.M. High aspect ratio taper-free microchannel fabrication using femtosecond Bessel beams. *Opt. Express* **2010**, *18*, 566–574. [CrossRef]
185. Liao, Y.; Ju, Y.; Zhang, L.; He, F.; Zhang, Q.; Shen, Y.; Chen, D.; Cheng, Y.; Xu, Z.; Sugioka, K.; et al Three-dimensional microfluidic channel with arbitrary length and configuration fabricated inside glass by femtosecond laser direct writing. *Opt. Lett.* **2010**, *35*, 3225. [CrossRef]
186. Sugioka, K.; Hanada, Y.; Midorikawa, K. Three-dimensional femtosecond laser micromachining of photosensitive glass for biomicrochips. *Laser Photonics Rev.* **2010**, *4*, 386–400. [CrossRef]
187. Ju, Y.; Liao, Y.; Zhang, L.; Sheng, Y.; Zhang, Q.; Chen, D.; Cheng, Y.; Xu, Z.; Sugioka, K.; Midorikawa, K. Fabrication of large-volume microfluidic chamber embedded in glass using three-dimensional femtosecond laser micromachining. *Microfluid. Nanofluid.* **2011**, *11*, 111–117. [CrossRef]
188. Liao, Y.; Song, J.; L., E.; Luo, Y.; Shen, Y.; Chen, D.; Cheng, Y.; Xu, Z.; Sugioka, K.; Midorikawa, K. Rapid prototyping of three-dimensional microfluidic mixers in glass by femtosecond laser direct writing. *Lab Chip* **2012**, *12*, 746–749. [CrossRef] [PubMed]
189. Gissibl, T.; Thiele, S.; Herkommer, A.; Giessen, H. Two-photon direct laser writing of ultracompact multi-lens objectives. *Nature Photon.* **2016**, *10*, 554–560. [CrossRef]
190. Dietrich, P.I.; Blaicher, M.; Reuter, I.; Billah, M.; Hoose, T.; Hofmann, A.; Caer, C.; Dangel, R.; Offrein, B.; Troppenz, U.; et al. In situ 3D nanoprinting of free-form coupling elements for hybrid photonic integration. *Nature Photon.* **2018**, *12*, 241–247. [CrossRef]

191. Hahn, V.; Kalt, S.; Sridharan, G.M.; Wegener, M.; Bhattacharya, S. Polarizing beam splitter integrated onto an optical fiber facet. *Opt. Express* **2018**, *26*, 33148–33157. [CrossRef] [PubMed]
192. Choi, H.K.; Ryu, J.; Kim, C.; Noh, Y.C.; Sohn, I.B.; Kim, J.T. Formation of Micro-lens Array using Femtosecond and CO_2 lasers. *J. Laser Micro. Nanoeng.* **2016**, *11*, 341–345.
193. Schwarz, S.; Hellmann, R. Fabrication of Cylindrical Lenses by CombiningUltrashort Pulsed Laser and CO_2 Laser. *J. Laser Micro. Nanoeng.* **2017**, *12*, 76–79. [CrossRef]
194. Schwarz, S.; Gotzendorfer, B.; Rung, S.; Esen, C.; Hellmann, R. Compact Beam Homogenizer Module with Laser-Fabricated Lens-Arrays. *Appl. Sci.* **2021**, *11*, 1018. [CrossRef]
195. Dudutis, J.; Pipiras, J.; Schwarz, S.; Rung, S.; Hellmann, R.; Račiukaitis, G.; Gečys, P. Laser-fabricated axicons challenging the conventional optics in glass processing applications. *Opt. Express* **2020**, *28*, 5715–5730. [CrossRef]
196. Lin, C.H.; Jiang, L.; Chai, Y.H.; Xiao, H.; Chen, S.J.; Tsai, H.L. Fabrication of microlens arrays in photosensitive glass by femtosecond laser direct writing. *Appl. Phys. A* **2009**, *97*, 751–757. [CrossRef]
197. Pan, A.; Gao, B.; Chen, T.; Si, J.; Li, C.; Chen, F.; Hou, X. Fabrication of concave spherical microlenses on silicon by femtosecond laser irradiation and mixed acid etching. *Opt. Express* **2014**, *22*, 15245–15250. [CrossRef] [PubMed]
198. Zhang, F.; Wang, C.; Yin, K.; Dong, X.R.; Song, Y.X.; Tian, Y.X.; Duan, J.A. Quasi-periodic concave microlens array for liquid refractive index sensing fabricated by femtosecond laser assisted with chemical etching. *Sci. Rep.* **2018**, *8*, 2419. [CrossRef] [PubMed]
199. Weingarten, C.; Schmickler, A.; Willenborg, E.; Wissenbach, K.; Poprawe, R. Laser polishing and laser shape correction of optical glass. *J. Laser Appl.* **2017**, *29*, 011702. [CrossRef]
200. Martinez, S.; Lamikiz, A.; Ukar, E.; Calleja, A.; Arrizubieta, J.A.; de Lacalle, L.N.L. Analysis of the regimes in the scanner-based laser hardening process. *Opt. Lasers Eng.* **2017**, *90*, 72–80. [CrossRef]
201. Weingarten, C.; Steenhusen, S.; Hermans, M.; Willenborg, E.; Schleifenbaum, J.H. Laser polishing and 2PP structuring of inside microfluidic channels in fused silica. *Microfluid. Nanofluid* **2017**, *21*. [CrossRef]
202. Serhatlioglu, M.; Ortaç, B.; Elbuken, C.; Biyikli, N.; Solmaz, M.E. CO_2 laser polishing of microfluidic channels fabricated by femtosecond laser assisted carving. *J. Micromech. Microeng.* **2016**, *26*, 115011. [CrossRef]
203. Xu, G.; Dai, Y.; Cui, J.; Xiao, X.; Mei, H.; Li, H. Simulation and experiment of femtosecond laser polishing quartz material. *Integr. Ferroelectr.* **2017**, *181*, 60–69. [CrossRef]
204. Taylor, L.L.; Xu, J.; Pomerantz, M.; Smith, T.R.; Lambropoulos, J.C.; Qiao, J. Femtosecond laser polishing of germanium. *Opt. Mater. Express* **2019**, *9*, 4165–4177. [CrossRef]
205. Fan, Z.; Sun, X.; Zhuo, X.; Mei, X.; Cui, J.; Duan, W.; Wang, W.; Zhang, X.; Yang, L. Femtosecond laser polishing yttria-stabilized zirconia coatings for improving molten salts corrosion resistance. *Corros. Sci.* **2021**, *184*, 109367. [CrossRef]
206. Mills, B.; Heath, D.J.; Feinaeugle, M.; Grant-Jacob, J.A.; Eason, R.W. Laser ablation via programmable image projection for submicron dimension machining in diamond. *J. Laser Appl.* **2014**, *26*, 041501. [CrossRef]
207. Courvoisier, F.; Zhang, J.; Bhuyan, M.K.; Jacquot, M.; Dudley, J.M. Applications of femtosecond Bessel beams to laser ablation. *Appl.Phys. A* **2012**, *112*, 29–34. [CrossRef]
208. Kim, H.Y.; Yoon, J.W.; Choi, W.S.; Kim, K.R.; Cho, S.H. Ablation depth control with 40 nm resolution on ITO thin films using a square, flat top beam shaped femtosecond NIR laser. *Opt. Lasers Eng.* **2016**, *84*, 44–50. [CrossRef]
209. Hernandez-Rueda, J.; Götte, N.; Siegel, J.; Soccio, M.; Zielinski, B.; Sarpe, C.; Wollenhaupt, M.; Ezquerra, T.A.; Baumert, T.; Solis, J. Nanofabrication of Tailored Surface Structures in Dielectrics Using Temporally Shaped Femtosecond-Laser Pulses. *ACS Appl. Mater. Interfaces* **2015**, *7*, 6613–6619. [CrossRef] [PubMed]
210. Singh, S.; Argument, M.; Tsui, Y.Y.; Fedosejevs, R. Effect of ambient air pressure on debris redeposition during laser ablation of glass. *J. Appl. Phys.* **2005**, *98*, 113520. [CrossRef]
211. Gerhard, C.; Roux, S.; Brückner, S.; Wieneke, S.; Viöl, W. Low-temperature atmospheric pressure argon plasma treatment and hybrid laser-plasma ablation of barite crown and heavy flint glass. *Appl. Opt.* **2012**, *51*, 3847–3852. [CrossRef]
212. Butkus, S.; Gaižauskas, E.; Paipulas, D.; Viburys, Ž.; Kaškelyė, D.; Barkauskas, M.; Alesenkov, A.; Sirutkaitis, V. Rapid microfabrication of transparent materials using filamented femtosecond laser pulses. *Appl. Phys. A* **2013**, *114*, 81–90. [CrossRef]
213. Pan, Y.J.; Yang, R.J. A glass microfluidic chip adhesive bonding method at room temperature. *J. Micrromech. Microeng.* **2006**, *16*, 2666–2672. [CrossRef]
214. Haisma, J.; Hattu, N.; Pulles, J.T.; Steding, E.; Vervest, J.C. Direct bonding and beyond. *Appl. Opt.* **2007**, *46*, 6793–6803. [CrossRef]
215. Tamaki, T.; Watanabe, W.; Nishii, J.; Itoh, K. Welding of transparent materials using femtosecond laser pulses. *Jpn. J. Appl. Phys. Part 2* **2005**, *44*, L687–L689. [CrossRef]
216. Tamaki, T.; Watanabe, W.; Itoh, K. Laser micro-welding of transparent materials by a localized heat accumulation effect using a femtosecond fiber laser at 1558 nm. *Opt. Express* **2006**, *14*, 10460–10468. [CrossRef] [PubMed]
217. Richter, S.; Nolte, S.; Tunnermann, A. Ultrashort pulse laser welding—A new approach for high-stability bonding of different glass. *Phys. Procedia* **2012**, *39*, 556–562. [CrossRef]
218. Richter, S.; Zimmermann, F.; Shutter, D.; Budnicki, A.; Tunnermann, A.; Nolte, S. Ultrashort pulse induced laser wlding of glasses without optical contacting. In Proceedings of the SPIE LASE, San Francisco, CA, USA, 28 January–2 February 2017; Volume 10094, p. 1009411.

219. Helie, D.; Begina, M.; Lacroix, F.; Vallee, R. Reinforced direct bonding of optical materials by femtosecond laser welding. *Appl. Opt.* **2012**, *51*, 2098–2106. [CrossRef] [PubMed]
220. Chen, J.; Carter, R.M.; Thomson, R.R.; Hand, D.P. Avoiding the requirement for pre-existing optical contact during picosecond laser glass-to-glass welding. *Opt. Express* **2015**, *23*, 18645–18657. [CrossRef] [PubMed]
221. Watanabe, W.; Onda, S.; Tamaki, T.; Itoh, K.; Nishii, J. Space-selective laser joining of dissimilar transparent materials using femtosecond laser pulses. *Appl. Phys. Lett.* **2006**, *89*, 021106. [CrossRef]
222. Zhang, G.; Stoian, R.; Zhao, W.; Cheng, G. Femtosecond laser Bessel beam welding of transparent to non-transparent materials with large focal-position tolerant zone. *Opt. Express* **2018**, *26*, 917–926. [CrossRef]
223. Greco, V.; Marchesini, F.; Molesini, G. Optical contact and Van der Waals interactions: The role of the surface topography in determining the bonding strength of thick glass plates. *J. Opt. A Pure Appl. Opt.* **2001**, *3*, 85–88. [CrossRef]
224. Cvecek, K.; Odato, R.; Dehmel, S.; Miyamoto, I.; Schmidt, M. Gap bridging in joining of glass using ultrashort laser pulses. *Opt. Exp.* **2015**, *23*, 5681–5693. [CrossRef] [PubMed]
225. Miyamoto, I.; Cvecek, K.; Schmidt, M. Crack-free conditions in welding of glass by ultrashort laser pulse. *Opt. Express* **2013**, *21*, 14291–14302. [CrossRef] [PubMed]
226. Miyamoto, I.; Cvecek, K.; Okamoto, Y.; Schmidt, M. Novel fusion welding technology of glass sing ultrashort pulse lasers. *Phys. Procedia* **2010**, *5*, 482–493. [CrossRef]
227. Shimizu, M.; Sakakura, M.; Ohnishi, M.; Shimotsuma, Y.; Nakaya, T.; Miura, K.; Hirao, K. Mechanism of heat-modification inside a glass after irradiation with high-repetition rate femtosecond laser pulses. *J. Appl. Phys.* **2010**, *108*, 073533. [CrossRef]
228. Huang, H.; Yang, L.M.; Liu, J. Ultrashort pulsed fiber laser welding and sealing of transparent materials. *Appl. Opt.* **2012**, *51*, 2979–2986. [CrossRef]
229. Zimmermann, F.; Richter, S.; Döring, S.; Tünnermann, A.; Nolte, S. Ultrastable bonding of glass with femtosecond laser bursts. *Appl. Opt.* **2013**, *52*, 1149–1154. [CrossRef] [PubMed]
230. Carter, R.M.; Troughton, M.; Chen, J.; Elder, I.; Thomson, R.R.; Esser, M.J.D.; Lamb, R.A.; Hand, D.P. Towards industrial ultrafast laser microwelding: SiO_2 and BK7 to aluminum alloy. *Appl. Opt.* **2017**, *56*, 4873–4881. [CrossRef] [PubMed]

II

OPTIMIZATION OF SELECTIVE LASER ETCHING (SLE) FOR GLASS MICROMECHANICAL STRUCTURE FABRICATION

A. Butkutė, T. Baravykas, J. Stančikas, T. Tičkūnas, R. Vargalis, D. Paipulas, V. Sirutkaitis and L. Jonušauskas

Opt. Express. 29(15), 23487– 23499 (2021).

Research Article | Vol. 29, No. 15 / 19 July 2021 / *Optics Express* 23487

Optics EXPRESS

Optimization of selective laser etching (SLE) for glass micromechanical structure fabrication

AGNĖ BUTKUTĖ,[1,*] TOMAS BARAVYKAS,[2] JOKŪBAS STANČIKAS,[1,2] TITAS TIČKŪNAS,[2] ROKAS VARGALIS,[2] DOMAS PAIPULAS,[1] VALDAS SIRUTKAITIS,[1] AND LINAS JONUŠAUSKAS[1,2]

[1] *Laser Research Center, Vilnius University, Saulėtekio Ave. 10, Vilnius LT- 10223, Lithuania*
[2] *Femtika Ltd., Saulėtekio Ave. 15, Vilnius LT- 10224, Lithuania*
[*] *agne.butkute@ff.vu.lt*

Abstract: In this work, we show how femtosecond (fs) laser-based selective glass etching (SLE) can be used to expand capabilities in fabricating 3D structures out of a single piece of glass. First, an investigation of the etching process is performed, taking into account various laser parameters and scanning strategies. These results provide critical insights into the optimization of the process allowing to increase manufacturing throughput. Afterward, various complex 3D glass structures such as microfluidic elements embedded inside the volume of glass or channel systems with integrated functional elements are produced. A single helix spring of 1 mm diameter is also made, showing the possibility to compress it by 50%. Finally, 3D structuring capabilities are used to produce an assembly-free movable ball-joint-based chain and magnet-actuated Geneva mechanism. Due to minimized friction caused by low (down to 200 nm RMS) surface roughness of SLE-produced structures, the Geneva mechanism was shown to be capable of rotating up to 2000 RPM.

© 2021 Optical Society of America under the terms of the OSA Open Access Publishing Agreement

1. Introduction

Over the years glass was proven to be material of choice in a multitude of rapidly developing science: microfluidics [1–3], micromechanics [4,5] and microoptics [6]. The reason for such popularity lies in the superb mechanical properties of the material, alongside it being completely transparent in the visible and near-infrared (IR) and chemically inert in organic solvents. As a result, there is a substantial drive to produce various functional microdevices out of this material. True 3D mesoscale structures are especially interesting. In essence, mesoscale objects combine overall size in practically usable mm-cm range with functionality enabled by the nano-/microfeatures. Various glass processing techniques exist. However, most of them are complicated and/or unable to produce 3D structures in mesoscale. Direct laser ablation [7] is a simple solution or , but it lacks the 3D aspect. Direct 3D printing has been shown as a tool to make 3D objects, yet the resolution is then limited to tens-hundreds of μm [8,9]. Stereolithography and subsequent heat treatment is another option, but then the resolution is still in the range of μm [10]. Due to the rapid development of light structural polymers [11], a similar operation can be performed employing two-photon polymerization (2PP/TPP) based 3D laser lithography (3DLL) [12]. However, the necessity for highly specialized monomer resins and complex post-processing remains. Therefore, all these methods have some severe drawbacks if straightforward glass 3D meso-fabrication is in question.

The most promising technology to produce 3D mesoscale glass structures is SLE [13,14]. The technology is based on selectively modifying transparent medium *via* femtosecond (fs) laser radiation which is becoming a more and more widespread tool for material processing [15]. During ultrashort pulses exposure, modifications of type II (i.e. nanogratings) are formed in the volume of the material [16]. Subsequently, the exposed sample is submerged in the etchant (such

#430623 https://doi.org/10.1364/OE.430623
Journal © 2021 Received 3 May 2021; revised 20 Jun 2021; accepted 25 Jun 2021; published 9 Jul 2021

as potassium hydroxide (KOH) or hydrofluoric acid (HF)). Then, modified regions dissolve up to ~ thousand times faster than surrounding medium [17]. The ratio between the etching rate of unmodified and modified regions is called selectivity. SLE allows true 3D glass manufacturing [2,18]. Potentially, many types of glasses and crystals such as fused silica [13], borosilicate [19,20], crystalline sapphire [21–23] or Yttrium aluminum garnet (YAG) [24] can be processed in this manner. However, so far this process is not exploited widely. The problem lies in the complex nature of light-matter interaction and difficulties in optimizing the technique for true 3D fabrication, sparking various works aimed at improving this aspect of the technique [25,26].

Due to the 3D capability of SLE, one of the main parameters to consider is selectivity. It is influenced by both SLE process steps. On one hand, selectivity depends on a created material modification which is governed by scanning peculiarities and laser parameters. Selectivity is also highly affected by etchant [17] and etching properties [27]. In practice, various etchants such as HF [19,28] and KOH [1,29,30] can be used. However, it has been already demonstrated that KOH allows obtaining higher selectivity than etching with HF [17]. The process dependency on various laser and scanning parameters such as pulse energy [19,29], pulse duration [29,30], polarization [16], pulse repetition rate [31] or even scanning velocity [3,29] and scanning spacing [17] were already reported to some extent. However, most of these studies were done for single-line (1D) channels and are lacking a 3D aspect. To fully understand these nuances, the selectivity of different 2D planes out of which complex arbitrary 3D structures can be constructed have to be understood. Furthermore, selectivity dictates that to acquire complex shapes the geometry of the structure should be altered to account for the dissolving of unmodified regions. Thus, overall, while the premise of SLE is simple, so far realization was proven to be rather complicated.

This work aims to optimize SLE 3D structure fabrication. We will concentrate on optimizing laser exposure and scanning parameters as these can be easily tuned using standard laser systems. We will begin by exploring the optimal laser and scanning parameters for 2D plane formation alongside streamlining the whole exposure algorithm. All of this is shown to simplify and accelerate the processing. Proposed methods are then employed to manufacture complex assembly-free microfluidic and micromechanical structures. These include embedded microfluidic channels with integrated micro mechanical elements, ball joint-like structure, high compression spring, and Geneva mechanism. All of these structures are evaluated qualitatively and quantitatively showing that improved fabrication techniques do not compromise the quality or functionality of the structures. The acquired results are shown in the broader perspective, relating it to previous SLE works, additive manufacturing, and potential application areas.

2. Materials and methods

In this work, we used almost pure amorphous SiO_2 which is normally referred to as fused silica (UVFS). "Laser Nanofactory" setup (Femtika Ltd.) was used in this work [32]. "Pharos" laser (Light Conversion Ltd.) is used as a radiation source. Radiation parameters: 1030 nm wavelength, pulse duration ~ 700 fs, pulse repetition rate - 610 kHz. The laser beam is focused on the sample with a 20x 0.45 NA objective with automated aberrations correction. That means, aberration compensation depends on the writing depth in the glass. Thus, aberrations are compensated for all modifications written in described experiments. For all modifications written in XY plane focusing depth was 500 μm. Spot size: 1.5 μm diameter focused beam spot in XY direction and ~15 μm in the Z direction. For sample positioning, Aerotech positioning stages and Galvano scanners are used. After the sample is exposed to fs laser, the modified volume is etched out in 10 mol/l concentration KOH solution at 90°C. Samples were characterized using various optical microscopes and scanning electron microscopes (SEM). The surface roughness was measured using an atomic force microscope (AFM).

3. Results

3.1. Optimization of manufacturing process

Through the years SLE processing peculiarities were investigated in numerous articles. However, to fully comprehend the process of 3D object manufacturing, the link between translation velocity, polarization, and structuring direction in relation to the etching direction has to be understood. This study was started by performing a set of experiments related to this topic. First, a 1D experiment was performed, the general schematics of this test are given in Fig. 1(a). By translating the sample in XY direction single lines were written inside the volume of the glass with particular sets of parameters such as different pulse energies, scanning velocities, and polarisation. Afterward, the selectivity tests of the planes (i.e. 2D case) were performed. A set of lines with particular spacing in XY or Z direction were written inside the glass according to the schemes shown in Fig. 2. Despite the varying spacing between lines, the width of the line blocks for hatching tests and the depth of the line blocks for the slicing test were kept the same (40 μm). Next, the substrates of the glass were cut in the middle according to the markings on the scheme. Sample cutting was needed only in those cases when modifications were completely inside the volume of glass and have no exit to any surface. Samples were subsequently immersed into the etchant for 1 hour, then rinsed into distilled water and dried in ambient air. Finally, the length of the etched channels was measured by using an optical microscope. This way 1D experiment showed selectivity dependence on the pulse energy, writing velocity, and light polarization. Meanwhile, 2D experiments showed plane selectivity dependence on the overlapping of scanned lines, pulse energy, light polarization, and etching direction.

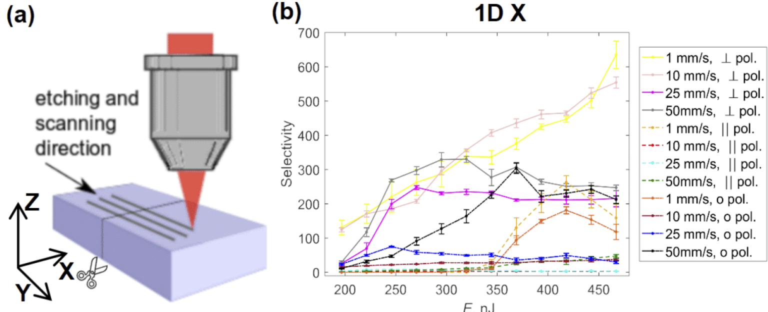

Fig. 1. (a) Schematics of 1D selectivity experiment. (b) Single line selectivity test results. Single lines are written in XY plane with various parameters such as different pulse energies, scanning velocities, and light polarization.

The results of 1D experiments are shown in Fig. 1. After writing single lines in the XY plane the highest obtained selectivity value is around ~650. It was observed with the polarization perpendicular to the scanning direction, the lowest tested scanning velocity (1 mm/s), and the highest tested pulse energy (492 nJ). Particular scanning velocity and pulse repetition rate combination control overlapping between pulses which define thermal relaxation of the energy. Overall, the femtosecond pulse duration is too short to transfer the energy to the lattice of the material, thus processing can be called "cold" [33]. However, if pulse spatial and temporal overlapping is high, volume heats. On the other hand, overlapping of the pulses change and the total dose absorbed by volume unit. Thus, with lower scanning velocity we transfer more energy to the material and observe stronger thermal effects which leads to greater volume modification, changes modification morphology [19] and gives higher selectivity. Also, it can be

Optics EXPRESS

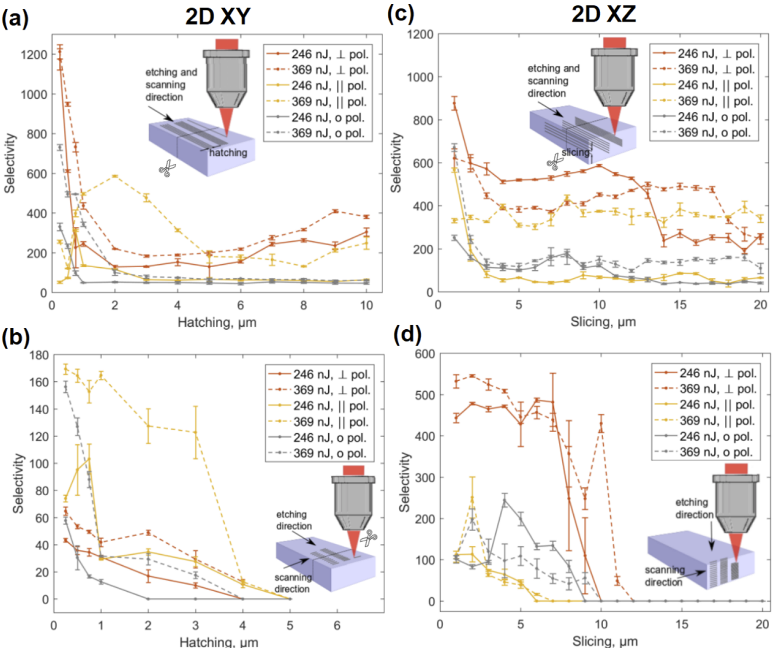

Fig. 2. 2D (plane) selectivity test results. (a) XY plane etched parallel to the scanning direction selectivity dependency to hatching, (b) XY planes etched perpendicularly to the scanning direction selectivity dependency to hatching, (c) XZ planes etched parallel to the scanning direction selectivity dependency to slicing, (d) XZ planes etched perpendicular to the scanning direction selectivity dependency to slicing.

seen that polarization perpendicular to the scanning direction gives the highest selectivity value. Meanwhile, polarization parallel to the scanning direction shows the lowest selectivity. Thus, these etching process dependency on polarization have been already reported in previous works [16] and in this work obtained results correlates with previously reported results. Furthermore, the selectivity has a tendency to saturate for the most tested parameters. Interestingly, the selectivity even starts to drop when the pulse energy is increased. This was also demonstrated in previous works [19,29]. However, the absolute value of pulse energy depends on the whole parameter set. Thus, optimal pulse energy values need to be chosen for the most effective SLE process.

As the goal of this work was to optimize processing for high-throughput 3D glass manufacturing, several important conclusions were drawn from acquired results. The highest tested translation velocity (50 mm/s) was chosen for further experiments in order to get the highest throughput. Also, we choose 2 pulse energies - the lowest possible pulse energy which gives selectivity value close to the maximum in case of polarization perpendicular to the scanning direction (246 nJ), and pulses energy value which gives the highest value with circular polarization (369 nJ). Higher pulse energy is not a practical choice for complex 3D structure fabrication due to high volume tensions which lead to cracks in the structure. Usually, the lowest possible pulse energy

Optics EXPRESS

is beneficial because lower pulse energy leads to lower tensile stress in the volume minimizing the possibility of cracks formation.

While 1D experiments give interesting insights into the process, it does not paint the full picture. 2D experiments are a lot closer to the real experimental conditions of 3D fabrication and, thus, are investigated next. The motivation underlying such experiments lies in a rather limited understanding of the etching process outside single-line fabrication (i.e. 1D case). It is known that light polarization effects nanogratings orientation direction [16]. In the case of polarization perpendicular to the scanning direction, pores parallel to the scanned lines are obtained. When considering it in the context of SLE, this configuration of the nanogratings allows for the etchant to penetrate deep inside the modification. In this way of light polarization parallel to the scanning direction, pores perpendicular to the scanning direction are obtained. With this nanogratings configuration etchant easily penetrates only to the first pore, resulting in a thin wall between pores that need to be etched. These thin walls between the pores slow down the etching. However, these insights are viable when considering single lines. The process becomes more complex when we form the planes of multiple lines. Different polarization-induced modifications might be induced in the same volume of the material, potentially overlapping each other [34]. Additionally, in the case of planes, the initial opening formed during etching is bigger, allowing easier diffusion of etched glass, further expediting the process. It has been already reported some planes such as XZ plane etching properties, however, due to the voxel shape, this does not represent the full picture of the process for 3D structure formation. Thus, here we present a broader picture of 2D plane research which leads to a better understanding of arbitrary shape structure formation.

The primary goal of 2D experiments was to test etching rate peculiarities depending on the direction of the inscribed plane and etching direction. The ultra-fast laser can be used to fabricate free-form 3D shapes without the usage of slicing and hatching, for instance, microlenses can be made as continuous spirals [35]. However, such cases are rare and the most common, practical, and simplest way to 3D fabricate structures is simply slicing and hatching. Thus, for this discussion, we will only consider orthogonal planes tied to axes of the positioning system: XY, XZ, and YZ. From a laser structuring perspective, XZ and YZ planes can be considered to be equivalent, as in Gaussian focusing case voxel is symmetrical in XY plane, leaving only two types of planes: horizontal and vertical. From the etching experiment side, one additional variable is etching direction, i.e. from which side inscribed modifications will be exposed to the etchant. Therefore, 4 distinct cases need to be tested to get the full picture of the process [Fig. 2].

2D horizontal (XY) plane test results when etching directions are parallel and perpendicular to the scanning directions are shown in Figs. 2(a) and 2(b) respectively. When the etching direction is parallel to the line writing direction, the highest selectivity of around 1200 is obtained by inscribing lines with the lowest tested hatching step (0.25 μm) and also by adopting polarization perpendicular to the scanning direction. In our experiment, by increasing hatching values to more than 2 μm the overlapping between adjacent lines is lost (spot diameter of used 0.45 NA objective - $2\omega_0$ = 1.5 μm) and selectivity drops to the values below 500. It is remarkably similar to the single-line selectivity achieved in 1D experiments. As expected, when the etching direction is perpendicular to the scanning direction maximum the obtained selectivity is around 6 times lower than in the previous case test (up to $\sim$17). However, this test determines the maximum possible hatching step, which in this case is 4 μm. From the practical perspective, during structuring, both cases are combined (if XZ and YZ planes are fabricated without tuning polarization), leading to undesired results, as if selectivity is close to 0 for at least one direction it will be impossible to etch the entire 3D structure. As an outcome, fast polarization control is needed if light polarization is to be tied to the translation direction. As a realization of such an approach is hard to achieve, a lot simpler solution is to use circular polarization. Then, translation direction is no more a variable during structuring. Additionally, as shown in this work, the etching rate does not drop

dramatically when circular polarization is used. Thus, due to practical considerations, circular polarization was used to fabricate all the 3D structures shown in this work.

Later, vertical 2D (XZ/YZ) plane tests were performed. The results of these tests are shown in Figs. 2(c) and 2(d). The highest selectivity is achieved with the lowest tested slicing between scanning lines (1 μm). When slicing is increased selectivity drops drastically. However, when polarization is parallel to the scanning direction, a further increment in slicing starts to slightly increase the etching rate. This indicates that interference between modifications creates suitable volume nanopatterns which affect the etching properties. The test with the etching direction perpendicular to the scanning direction determines the maximum possible slicing parameter which is around 10 μm and higher slicing values will be an obstacle for surface etching. Overall, the higher maximal slicing step can be explained by the already mentioned inherent elongation of the voxel in the Z direction due to Gaussian focusing properties. Here we find out that with our tested setup maximum hatching could be 4 μm and slicing 10 μm. Nonetheless, for the practical 3D structure formation lower values are desired to have higher selectivity.

Finally, it was decided to measure the surface roughness of the etched surfaces. Here we measured both XY and XZ/YZ surfaces roughness. These results are depicted in Figs. 3(a) and 3(b). In both plane cases, the lowest surface roughness of around 200 nm RMS is obtained with the lowest tested slicing/hatching (0.5 μm). By increasing the spacing between lines, the roughness value rises together and reaches around 800 nm RMS. Looking back to the same surface selectivity, it can be concluded that higher surface selectivity gives lower surface roughness. Selectivity correlation with surface roughness has been already reported in other works [27]. However, polarization influence on fabricated structure surface roughness was not studied before. As shown before polarization strongly affects selectivity. Nonetheless, obtained surface roughness dependency on polarization is not very significant and the lowest value in both cases is obtained independent of polarization. In conclusion spacing between scanning lines affects formed surfaces more significantly than pulse energy or light polarization. Also, in addition to minimal surface roughness, SLE allows achieving minimal taper on vertical surfaces [Fig. 3(c)]. This is very attractive for usage in precise microfluidics or as an extremely rigid molding master for soft lithography [36].

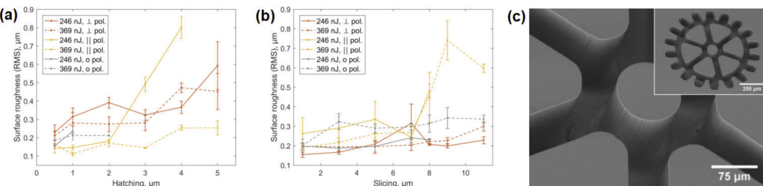

Fig. 3. Surface roughness (calculated as RMS) acquired using SLE of horizontal (a) and vertical (b) surfaces. All values are below 1 μm. (c) - Zoomed in SEM image of surfaces of an example structure (with the whole element being in the inset), showing good surface quality and minimal taper achievable in practice.

In the case of 3D structure formation scanning strategies is also a factor that should not be overlooked. Intuitively, when producing a 3D structure, it would seem that the most convenient and simplest way to fabricate the required shape would be to modify and then etch out all the unnecessary volume. That means all volume should be scanned out line by line with fixed slicing and hatching between each line and by maintaining voxel overlapping. This strategy is illustrated in Fig. 4(a). However, it is an extremely slow approach. Additionally, it might result in cracks, which appear due to excessive internal stress caused by volume overexposure. Both of these difficulties can be tackled by employing the strategy of segment scanning. Then,

Optics EXPRESS

only the contours of the structure are exposed to the laser light, while the rest of the material is divided into smaller pieces. This scanning strategy is shown in Fig. 4(b). In this way, all inscribed structures are combined out of contours and surfaces which should be scanned out by maintaining the same voxel overlapping. This strategy allows saving lots of fabrication time. For instance, dividing the standard structure into cubes with dimensions of 50 μm x 50 μm x 50 μm allows reducing fabrication time by the factor of 7. If 100 μm x 100 μm x 100 μm cubes are used manufacturing is around 14 times faster and by dividing into 200 μm x 200 μm x 200 μm cubes - around 28 faster. There is another option to scan out only the contours of the structure. This option is demonstrated in Fig. 4(c). This approach is useful for 2D structure fabrication and would allow saving even more fabrication time than dividing material into the cube.

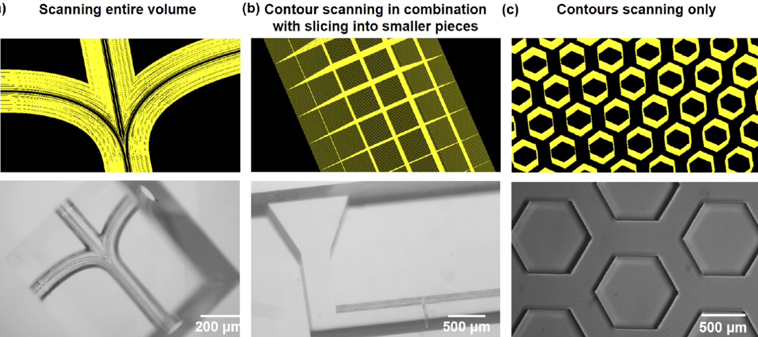

Fig. 4. Demonstration of how different scanning strategies can be applied in various structures formation. (a) Scanning entire volume used for closed channel fabrication, (b) contour scanning in combination with slicing into smaller pieces applied in open channel chip fabrication, (c) contours scanning only applied in the production of hexagon-shaped hole manufacturing.

Another advantage is that by minimizing the number of scanned lines we reduce volume tensions. The downside of this approach is the necessity to make such features at the top of the sample, as otherwise non-etched segments could not fall out. This limits the usage of such an approach in embedded structure fabrication. Additionally, segmenting prolongs etching time. It is a result of etchant needing to reach underneath produced segments. In consequence, a taper of modifications might increase, as unaffected material is also being continuously etched. For complex shape and long channel systems most of the time it is useful to scan all the volume needed to be etched. These two strategies can also be mixed together, with rougher parts of the system being segments, and more fine details being exposed in full. Thus, the scanning strategy needs to be chosen carefully for each structure individually in order to get the best compromise between the highest throughput and quality.

3.2. Fabricated 3D glass structures

There are multiple fields that could benefit from high-precision 3D mesoscale glass structure fabrication. One of the most promising applications for SLE is microfluidics. As shown in this work, SLE-made channels can have a relatively low surface roughness (~200 nm RMS). At the same time, the throughput of the technology, if the whole volume needs to be exposed, is relatively low. In contrast, laser-ablated glass channels usually will have worse surface roughness and are produced faster [37], without the need for an etching technological step. Nevertheless, SLE greatly exceeds ablation in terms of flexibility and allows to produce 3D free-form structures,

such as channels with integrated functional elements, or 3D channel systems embedded inside the volume of glass, as shown in Figs. 5(a) and 5(b), bringing new capabilities and flexibility to the field. These properties give a possibility to avoid other supplementary processes such as sealing of ablated channels or the necessity to use other manufacturing techniques for integration of some more trivial structures. To demonstrate what can be integrated, we created a microfluidic system with integrated deformable cantilever Figs. 5(c) and 5(d). Thin glass cantilevers are extremely simple yet potent structures that have a lot of usages [38]. In the case of cantilevers integrated into microfuildical channels, such a device was demonstrated to possibly perform a task of a very precise flow meter [39]. The main difference and improvement from the example given in the literature that SLE allows to fabricate such cantilever structure in relatively simpler manner. While normally glass is perceived as a hard material, in size range bellow ~100 μm glass can be deformed without breaking [40]. Therefore, produced 250 μm x 200 μm x 25 μm dimension cantilever could be bent using probe up to ~30 μm without breaking it.

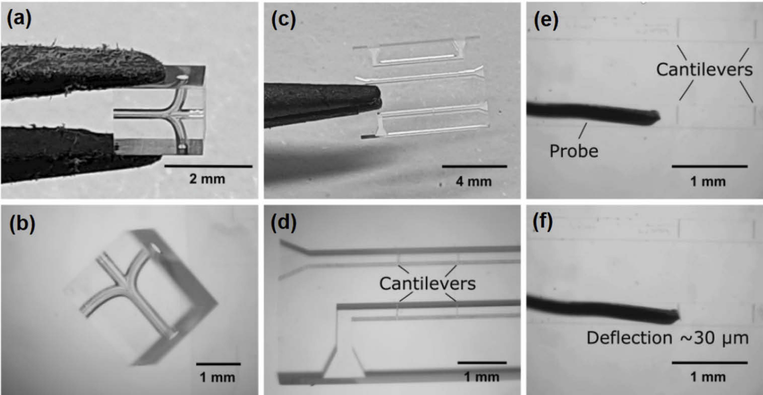

Fig. 5. Examples of various 3D microfluidic structures produced applying SLE. (a) and (b) - embedded channel sections. As such systems are in the volume of glass no sealing step is required. Furthermore, due to very low (down to ~200 nm surface roughness such systems are basically transparent. (c) and (d) - a channel system housing integrated 250 μm x 200 μm x 25 μm cantilevers. Channel cross-section - 300 μm x 300 μm. (e) and (f) shows bending of the cantilever using a hard probe. Possible deflection - up to ~30 μm.

Continuing on the topic of deformable glass structures, a single helix 4 turn spring was produced out of glass [Fig. 6(a)]. The diameter of the structure is 1 mm, with the width of the helix itself being 50 μm. The combined length of the whole helix was around 12 mm. As a result, this allowed to repeatedly compress the spring up to 50% (from 600 μm to 300 μm) without damaging it. The fabrication of such structure employed both segmenting (in the middle of the structure) and full volume exposure (for fine springs). Due to it, such a structure can be produced in ~4 min. Such springs, as they can be mass-produced on-demand in mass-customized series, could prove to be attractive in such fields as the watch industry. While not trivial at the first sight, but such structures can be made to be mechanically resistant to compressive forces and at the same time robust against shock, due to the possibility of using some advanced architectures like gyroids in the support part of the spring (which in our case is a simple bulk plate). Combined with a very small weight, such structures could be proven to be extremely mechanically resilient

to shock and vibrations, at the same time surpassing polymer-made micromcehanics [32] of the same type in terms of chemical and thermal resilience.

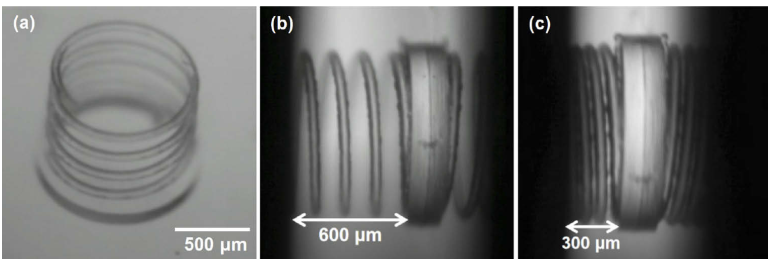

Fig. 6. Images of fused silica single helix 4 turn spring. (a) - overall view. (b) and (c) shows compression of the spring. Due to the small thickness (diameter - 50 μm) and relatively long length of the helix (12 mm) it can be compressed repeatedly from 600 to 300 μm (50% of overall helix height) without any damage to the structure.

Alternatively from deformable micromechanics, one might consider structures made out of different independently moving components. Normally, such systems are made part by part and then assembled. However, SLE allows true 3D modification of glass volume. As a result, openings needed for structure motion can be embedded before etching and then revealed by it. Therefore, assembly-free movable multi-part 3D glass structures can be produced, relatively easily, expanding current capabilities of the field of micro-mechanics. To demonstrate it, we first produced a chain with free movable ball joints. This structure employing the idea of etching out the narrow gaps between the separate parts of the structure. In this way, we create a joint-like structure that is able to move. The exact model and optical microscope photos of the manufactured structure are shown in Fig. 7. The bending amplitude of the produced structure (which is 30°) coincides well with the value predicted from the mechanical CAD model. As the structure is very complex, and the opening of the outer ball is 450 μm in diameter, the whole inside of the outer ball was exposed to the laser radiation. For this reason, the fabrication of such a structure heavily relies on the understanding of etching rates. If chosen processing parameters would be insufficient, the fine opening would either not etch out, or etch out too much, resulting in disassembly of the ball joint. Therefore, when manufacturing such fine structures substantial attention should be paid to both process and model optimization, in order to achieve the best possible result.

Finally, we fabricated a complex micromechanical structure called the Geneva mechanism [Fig. 8]. This structure contains two intermeshing elements. By rotating one gear every 360° rotation it moves and another gear by fixed 90° increments. SLE technology allows fabricating such mechanisms out of a single piece of glass without the need for an assembly step. As this structure is assembly-free, it can be produced at a very small scale (down to hundreds of μm) without the need for extremely complex micromanipulation. Moreover, by attaching a small magnet to this mechanism and placing it over a rotating magnet we show the smooth movement of this structure. It is possible due to very fine gaps between different moving parts of the structure (less than 10 μm) and very good surface roughness (~200 nm RMS) possible due to optimisation presented previously in this article, which allows minimizing excessive friction. Pictures of Geneva mechanism movement are shown in Fig. 8(g). In the testing, it was shown that it can rotate up to 2000 RPM and that it can run for more than 100 hours continuously without any damage or other adverse impacts to the functionality. It is important to note that the measurement of Geneva mechanism rotation was carried out using simple rotating magnet underneath the

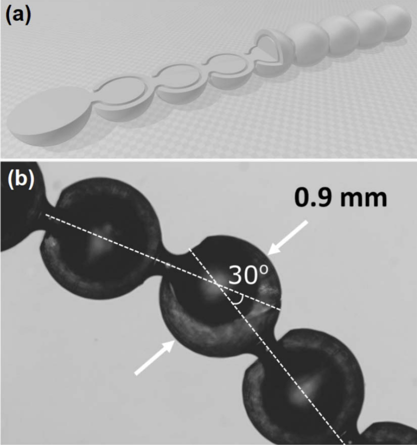

Fig. 7. Flexible chain with ball joints. (a) - 3D model of a structure, with 1/4 of the structure cut away to show hollow openings separating outer and inner balls in the joint. (b) optical microscope image of part of the structure. Bending at modeled 30° is achieved. Also, inner and outer balls in the joint are clearly visible.

structure itself. As it was proof of concept experiment, our goal was to see if the mechanism would rotate without any trouble. Thus, the upper limit of the experiment was determined not by the structure, but by the measurement equipment. We estimate that at particularly high rotation speeds fragile mechanism axis would not be able to hold the rotation of the whole mechanism and break. However, we did not manage to reach such RPM in this work, leaving this investigation for future research.

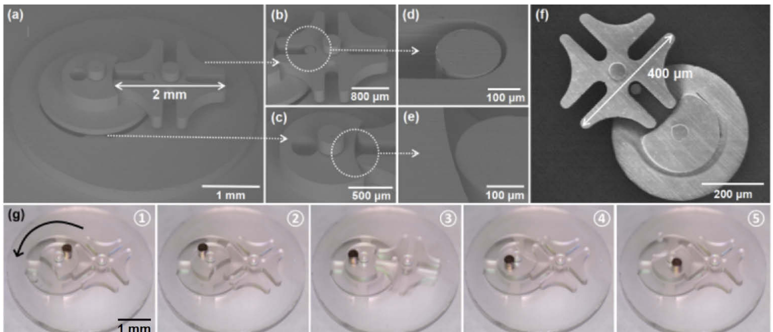

Fig. 8. Pictures of produced Geneva mechanism: (a) scanning electron microscope (SEM) image of the whole mechanism, (b)-(e) SEM pictures of the most important features and surfaces of the mechanism, and (f) SEM image of 5 times smaller Geneva mechanism than in part (a). (g) - Chronological pictures of Geneva mechanism movement, black arrow indicates the rotation direction. Magnet is attached to the structure the whole mechanism is inserted into a changing magnetic field for the movement automation.

The scalability of SLE should also be commended. As such structures will most likely find it's way to being used in high-precision complex devices, the possibility to easily tune the size and shape of structures towards mass customization is one of the top priorities. To demonstrate that SLE complies with such requirement we made a Geneva mechanism which is 5 times smaller than the original one [Fig. 8(f)]. Of course, some peculiarities exist in such a scale. The most important role in this process is played by the phenomena of selectivity. As a result, reducing the size of a structure is relatively easier than making it bigger. To avoid over-etching of unexposed parts of the structure, the etching rate should be sufficient if bigger structures are needed. An increase in selectivity has a fundamental limit, bounding complex SLE 3D fabrication to structures that are below several cm. Nevertheless, this is not a hard limit, if some compromises can be made to the structure accuracy, as the main hindrance of long etching times is an excessive dissolving of laser unaffected glass volume. If some taper can be tolerated, even cm-sized structures can be produced using SLE.

4. Discussion

The field of micro-robotics and micromechanics is extremely active [41,42]. Multitude of deformable [43,44], intertwined [32,45] or assembled [46] structures were presented over the years. However, most of them are produced either from polymers, metals, or some composite containing both. Glass, on the other hand, is highly underutilized in this field. In this work, we showed that glass can be exploited in the field of micromechanics a lot more, opening the door for was array of novel structures which were never tried before at this scale, like Geneva mechanism or related multi-component structures. Indeed, the mechanical properties of glass are very well known, repeatable, and not dependent on the SLE process itself. This is in sharp contrast to polymers, which, when microstructured with fs-laser in 3D present a multitude of degrees of freedom in terms of mechanical and optical properties. These depend on cross-linking [47] degree and even on surrounding medium [48]. Additionally, even the most resilient polymers can withstand only temperatures up to several hundred degrees [49], while the melting point of fused silica is around 1500°C. Therefore, glass offers a substantially better alternative to many currently popular materials in micro-robotics if the application in question requires the constant presence of organic solvents, high temperatures, or is otherwise hazardous and can cause polymers to degrade.

At the same time, SLE should not be entirely considered as a possible alternative for additive manufacturing *via* 3DLL. These two methodologies can supplement each other as well. It was already showed that using chemically inert SLE etched cantilever and integrated polymer rod a passive actuator, which moves in accordance to the organic solvent present in the system, might be created [38]. Some micromechanical elements were fabricated in our work are smaller than what has been shown in the literature so far, allowing us to think about even more exotic applications. For instance, glass and polymer might be used in tandem to create polymer-glass structures, resembling already shown bi-polymer elements [50]. Alternatively, SLE, which is very efficient in fabricating microchannels, can be used for lab-on-chip system manufacturing, while 3DLL can provide integrated elements, like a filter, with a lot smaller features than SLE allows [51]. Such mix and matching of technologies are made even more attractive by the possibility to realize it using just a single amplified fs laser source integrated into a highly customizable fabrication setup [15]. Therefore, the work presented here gives a comprehensive look at what structures can be produced using SLE and what are the process peculiarities and ways to optimize it for the best possible result.

5. Author contributions

A. Butkutė planned and performed all the experiments, analyzed results. T. Baravykas prepared all the 3D structures designs, CAD models, and fabrication algorithms. A. Butkutė, J. Stančikas,

and T. Tičkūnas fabricated and characterized 3D structures. R. Vargalis, L. Jonušauskas and T. Tičkūnas made SEM images. A. Butkutė and L. Jonušauskas have written the manuscript. V. Sirutkaitis, D. Paipulas, L. Jonušauskas and T. Tičkūnas provided general consulting about the topic and manuscript preparation. All authors reviewed the manuscript and gave improvement advises.

Funding. European Regional Development Fund (project 01.2.2-LMT-K-718-03-0029) with the Research Council of Lithuania.

Disclosures. The authors declare no conflicts of interest.

Data availability. Data underlying the results presented in this paper are not publicly available at this time but may be obtained from the authors upon reasonable request.

References

1. S. LoTurco, R. Osellame, R. Ramponi, and K. C. Vishnubhatla, "Hybrid chemical etching of femtosecond laser irradiated structures for engineered microfluidic devices," J. Micromech. Microeng. **23**(8), 085002 (2013).
2. J. Gottmann, M. Hermans, N. Repiev, and J. Ortmann, "Selective laser-induced etching of 3D precision quartz glass components for microfluidic applications-up-scaling of complexity and speed," Micromachines **8**(4), 110 (2017).
3. S. Kim, J. Kim, Y.-H. Joung, S. Ahn, J. Choi, and C. Koo, "Optimization of selective laser-induced etching (SLE) for fabrication of 3D glass microfluidic device with multi-layer micro channels," Micro Nano Sys. Lett. **7**(1), 15 (2019).
4. Y. Bellouard, "Shape memory alloys for microsystems: A review from a material research perspective," Mater. Sci. Eng., A **481-482**, 582–589 (2008).
5. J. Gottmann, M. Hermans, and J. ortmann, "Microcutting and hollow 3D microstructures in glasses by in-volume selective laser-induced etching (ISLE)," J. Laser Micro/Nanoeng. **8**(1), 15–18 (2013).
6. Y. Hu, S. Rao, S. Wu, P. Wei, W. Qiu, D. Wu, B. Xu, J. Ni, L. Yang, J. Li, J. Chu, and K. Sugioka, "All-glass 3D optofluidic microchip with built-in tunable microlens fabricated by femtosecond laser-assisted etching," Adv. Opt. Mater. **6**(9), 1701299 (2018).
7. S. Butkus, D. Paipulas, D. Kaškelyte, E. Gaižauskas, and V. Sirutkaitis, "Improvement of cut quality in rapid-cutting of glass method via femtosecond laser filamentation," J. Laser Micro/Nanoeng. **10**(1), 59–63 (2015).
8. P. von Witzendorff, L. Pohl, O. Suttmann, P. Heinrich, A. Heinrich, J. Zander, H. Bragard, and S. Kaierle, "Additive manufacturing of glass: CO2-laser glass deposition printing," Proc. CIRP **74**, 272–275 (2018).
9. R. M. Zaki, C. Strutynski, S. Kaser, D. Bernard, G. Hauss, M. Faessel, J. Sabatier, L. Canioni, Y. Messaddeq, S. Danto, and T. Cardinal, "Direct 3D-printing of phosphate glass by fused deposition modeling," Mater. Des. **194**, 108957 (2020).
10. F. Kotz, K. Arnold, W. Bauer, D. Schild, N. Keller, K. Sachsenheimer, T. M. Nargang, C. Richter, D. Helmer, and B. E. Rapp, "Three-dimensional printing of transparent fused silica glass," Nature **544**(7650), 337–339 (2017).
11. G. Merkininkaitė, D. Gailevičius, S. Šakirzanovas, and L. Jonušauskas, "Polymers for regenerative medicine structures made via multiphoton 3D lithography," Int. J. Polym. Sci. **2019**, 1–23 (2019).
12. F. Kotz, A. S. Quick, P. Risch, T. Martin, T. Hoose, M. Thiel, D. Helmer, and B. E. Rapp, "Two-photon polymerization of nanocomposites for the fabrication of transparent fused silica glass microstructures," Adv. Mater. **33**(9), 2006341 (2021).
13. A. Marcinkevičius, S. Juodkazis, M. Watanabe, M. Miwa, S. Matsuo, H. Misawa, and J. Nishii, "Femtosecond laser-assisted three-dimensional microfabrication in silica," Opt. Lett. **26**(5), 277–279 (2001).
14. A. Butkutė and L. Jonušauskas, "3D manufacturing of glass microstructures using femtosecond laser," Micromachines **12**(5), 499 (2021).
15. L. Jonušauskas, D. Mackevičiūtė, G. Kontenis, and V. Purlys, "Femtosecond lasers: the ultimate tool for high-precision 3D manufacturing," Adv. Opt. Technol. **8**(3-4), 241–251 (2019).
16. C. Hnatovsky, R. S. Taylor, E. Simova, V. R. Bhardwaj, D. M. Rayner, and P. B. Corkum, "Polarization-selective etching in femtosecond laser-assisted microfluidic channel fabrication in fused silica," Opt. Lett. **30**(14), 1867–1869 (2005).
17. C. A. Ross, D. G. Maclachan, D. Choudrury, and R. R. Thomson, "Optimisation of ultrafast laser assisted etching in fused silica," Opt. Express **26**(19), 24343–24356 (2018).
18. P. Paiè, F. Bragheri, D. D. Carlo, and R. Osellame, "Particle focusing by 3D inertial microfluidics," Microsyst. Nanoeng. **3**(1), 17027 (2017).
19. C. Hnatovsky, R. S. Taylor, E. Simova, P. P. Rajeev, D. M. Rayner, V. Bhardwaj, and P. B. Corkum, "Fabrication of microchannels in glass using focused femtosecond laser radiationand selectivechemical etching," Appl. Phys. A **84**(1-2), 47–61 (2006).
20. S. Matsuo, H. Sumi, S. Kiyama, T. Tomita, and S. Hashimoto, "Femtosecond laser-assisted etching of pyrex glass with aqueous solution of KOH," Appl. Surf. Sci. **255**(24), 9758–9760 (2009).
21. S. Juodkazis, Y. Nishi, and H. Misawa, "Femtosecond laser-assisted formation of channels in sapphire using KOH solution," Phys. Status Solidi RRL **2**(6), 275–277 (2008).
22. M. Hörstmann-Jungemann, J. Gottmann, and M. Keggenhoff, "3D-microstructuring of sapphire using fs-laser irradiation and selective etching," J. Laser Micro/Nanoeng. **5**(2), 145–149 (2010).

23. L. Capuanoa, R. Tiggelaar, J. Berenschot, J. Gardeniers, and G. Römer, "Fabrication of millimeter-long structures in sapphire using femtosecond infrared laser pulses and selective etching," Opt. Laser Eng. **133**, 106114 (2020).
24. A. Rodenas, M. Gu, G. Corrielli, P. Paie, S. John, A. K. Kar, and R. Osellame, "Three-dimensional femtosecond laser nanolithography of crystals," Nat. Photonics **13**(2), 105–109 (2019).
25. J. Hua, H. Ren, A. Jia, Z. Tian, L. Wang, S. Juodkazis, Q. Chen, and H. Sun, "Convex silica microlens arrays via femtosecond laser writing," Opt. Lett. **45**(3), 636–639 (2020).
26. Y. Lu, X. Liu, L. Zhu, Q. Chen, S. Juodkazis, and H. Sun, "Vector scanning subtractive manufacturing technology for laser rapid fabrication," Opt. Lett. **46**(8), 1963–1966 (2021).
27. S. Butkus, M. Rickus, R. Sirutkaitis, D. Paipulas, and V. Sirutkaitis, "Fabrication of high aspect ratio channels in fused silica using femtosecond pulses and chemical etching at different conditions," J. Laser Micro/Nanoeng. **14**(1), 19–24 (2019).
28. S. Juodkazis, K. Yamasaki, V. Mizeikis, S. Matsuo, and H. Misawa, "Formation of embedded patterns in glasses using femtosecond irradiation," Appl. Phys. A **79**(4-6), 1549–1553 (2004).
29. M. Hermans, J. Gottmann, and F. Riedel, "Selective, laser-induced etching of fused silica at high scan-speeds using koh," J. Laser Micro/Nanoeng. **9**(2), 126–131 (2014).
30. X. Li, J. Xu, Z. Lin, J. Qi, P. Wang, W. Chu, Z. Fang, Z. Wang, Z. Chai, and Y. Cheng, "Polarization-insensitive space-selective etching in fused silica induced by picosecond laser irradiation," Appl. Surf. Sci. **485**, 188–193 (2019).
31. J. Qi, Z. Wang, J. Xu, Z. Lin, X. Li, W. Chu, and Y. Cheng, "Femtosecond laser induced selective etching in fused silica: optimization of the inscription conditions with a high-repetition-rate laser source," Opt. Express **26**(23), 29669–29678 (2018).
32. L. Jonušauskas, T. Baravykas, D. Andrijec, T. Gadišauskas, and V. Purlys, "Stitchless support-free 3D printing of free-form micromechanical structures with feature size on-demand," Sci. Rep. **9**(1), 17533 (2019).
33. S. K. Sundaram and E. Mazur, "Inducing and probing non-thermal transitions in semiconductors using femtosecond laser pulses," Nat. Mater. **1**(4), 217–224 (2002).
34. R. S. Taylor, C. Hnatovsky, E. Simova, P. P. Rajeev, D. M. Rayner, and P. B. Corkum, "Femtosecond laser erasing and rewriting of self-organized planar nanocracks in fused silica glass," Opt. Lett. **32**(19), 2888–2890 (2007).
35. L. Jonušauskas, D. Gailevičius, S. Rekštytė, T. Baldacchini, S. Juodkazis, and M. Malinauskas, "Mesoscale laser 3D printing," Opt. Express **27**(11), 15205–15221 (2019).
36. Y. Xia and G. M. Whitesides, "Soft lithography," Annu. Rev. Mater. Sci. **28**(1), 153–184 (1998).
37. L. Jonušauskas, S. Rekštytė, R. Buividas, S. Butkus, R. Gadonas, S. Juodkazis, and M. Malinauskas, "Hybrid subtractive-additive-welding microfabrication for lab-on-chip (LOC) applications via single amplified femtosecond laser source," Opt. Eng. **56**(9), 094108 (2017).
38. T. Tičkūnas, M. Perrenoud, S. Butkus, R. Gadonas, S. Rekštytė, M. Malinauskas, D. Paipulas, Y. Bellouard, and V. Sirutkaitis, "Combination of additive and subtractive laser 3D microprocessing in hybrid glass/polymer microsystems for chemical sensing applications," Opt. Express **25**(21), 26280–26288 (2017).
39. N. Noeth, S. S. Keller, and A. Boisen, "Integrated cantilever-based flow sensors with tunable sensitivity for in-line monitoring of flow fluctuations in microfluidic systems," Sensors **14**(1), 229–244 (2013).
40. Y. Bellouard, R. Clavel, J.-E. Bidaux, R. Gotthardt, and T. Sidler, "A concept for monolithic shape memory alloys micro-devices," J. Phys. IV **07**(C5), C5-603–C5-608 (1997).
41. S. Koo, "Advanced micro-actuator/robot fabrication using ultrafast laser direct writing and its remote control," Appl. Sci. **10**(23), 8563 (2020).
42. A.-I. Bunea, D. Martella, S. Nocentini, C. Parmeggiani, R. Taboryski, and D. S. Wiersma, "Light-powered microrobots: Challenges and opportunities for hard and soft responsive microswimmers," Adv. Intell. Syst. **3**(4), 2000256 (2021).
43. R. Suriano, T. Zandrini, C. de Marco, R. Osellame, S. Turri, and F. Bragheri, "Nanomechanical probing of soft matter through hydrophobic AFM tips fabricated by two-photon polymerization," Nanotechnology **27**(15), 155702 (2016).
44. I. Spanos, Z. Vangelatos, C. Grigoropoulos, and M. Farsari, "Design and characterization of microscale auxetic and anisotropic structures fabricated by multiphoton lithography," Nanomaterials **11**(2), 446 (2021).
45. M. Power, A. J. Thompson, S. Anastasova, and G.-Z. Yang, "A monolithic force-sensitive 3D microgripper fabricated on the tip of an optical fiber using 2-photon polymerization," Small **14**(16), 1703964 (2018).
46. J. Kohler, S. I. Ksouri, C. Esen, and A. Ostendorf, "Optical screw-wrench for microassembly," Microsyst. Nanoeng. **3**(1), 16083 (2017).
47. L. Pertoldi, V. Zega, C. Comi, and R. Osellame, "Dynamic mechanical characterization of two-photon-polymerized SZ2080 photoresist," J. Appl. Phys. **128**(17), 175102 (2020).
48. S. Rekštytė, D. Paipulas, M. Malinauskas, and V. Mizeikis, "Microactuation and sensing using reversible deformations of laser-written polymeric structures," Nanotechnology **28**(12), 124001 (2017).
49. L. Jonušauskas, D. Gailevičius, L. Mikoliūnaitė, D. Sakalauskas, S. Šakirzanovas, S. Juodkazis, and M. Malinauskas, "Optically clear and resilient free-form μ-optics 3D-printed via ultrafast laser lithography," Materials **10**(1), 12 (2017).
50. J. Qu, M. Kadic, A. Naber, and M. Wegener, "Micro-structured two-component 3D metamaterials with negative thermal-expansion coefficient from positive constituents," Sci. Rep. **7**(1), 40643 (2017).
51. D. Wu, S.-Z. Wu, J. Xu, L.-G. Niu, K. Midorikawa, and K. Sugioka, "Hybrid femtosecond laser microfabrication to achieve true 3D glass/polymer composite biochips with multiscale features and high performance: the concept of ship-in-a-bottle biochip," Laser Photonics Rev. **8**(3), 458–467 (2014).

III

FEMTOSECOND LASER ASSISTED 3D ETCHING USING INORGANIC-ORGANIC ETCHANT

A. Butkutė, G. Merkininkaitė, T. Jurkšas, J. Stančikas, T. Baravykas, R. Vargalis, T. Tičkūnas, J. Bachmann, S. Šakirzanovas, V. Sirutkaitis and L. Jonušauskas
Metarials 15(8), 2817–2826 (2022).

Article

Femtosecond Laser Assisted 3D Etching Using Inorganic-Organic Etchant

Agnė Butkutė [1,2,*], Greta Merkininkaitė [1,3], Tomas Jurkšas [1], Jokūbas Stančikas [2], Tomas Baravykas [1], Rokas Vargalis [1], Titas Tičkūnas [1], Julien Bachmann [4], Simas Šakirzanovas [3], Valdas Sirutkaitis [2] and Linas Jonušauskas [2]

1 Femtika Ltd., Saulėtekio Ave. 15, LT-10224 Vilnius, Lithuania; greta.merkininkaite@femtika.com (G.M.); tomas.jurksas@femtika.com (T.J.); tomas.baravykas@femtika.com (T.B.); rokas.vargalis@femtika.com (R.V.); titas.tickunas@femtika.com (T.T.)
2 Laser Research Center, Vilnius University, Saulėtekio Ave. 10, LT-10223 Vilnius, Lithuania; jokubas.stancikas@ff.stud.vu.lt (J.S.); valdas.sirutkaitis@ff.vu.lt (V.S.); linas.jonusauskas@ff.vu.lt (L.J.)
3 Faculty of Chemistry and Geoscience, Vilnius University, Naugarduko Str. 24, LT-03225 Vilnius, Lithuania; simas.sakirzanovas@chf.vu.lt
4 Chemistry of Thin Film Materials, Department of Chemistry and Pharmacy, IZNF, Friedrich-Alexander University of Erlangen-Nürnberg, Cauerstr. 3, 91058 Erlangen, Germany; julien.bachmann@fau.de
* Correspondence: agne.butkute@femtika.com

Abstract: Selective laser etching (SLE) is a technique that allows the fabrication of arbitrarily shaped glass micro-objects. In this work, we show how the capabilities of this technology can be improved in terms of selectivity and etch rate by applying an etchant solution based on a Potassium Hydroxide, water, and isopropanol mixture. By varying the concentrations of these constituents, the wetting properties, as well as the chemical reaction of fused silica etching, can be changed, allowing us to achieve etching rates in modified fused silica up to 820 µm/h and selectivity up to ∼3000. This is used to produce a high aspect ratio (up to 1:1000), straight and spiral microfluidic channels which are embedded inside a volume of glass. Complex 3D glass micro-structures are also demonstrated.

Keywords: selective laser etching; 3D laser microfabrication; glass microprocessing

Citation: Butkutė, A.; Merkininkaitė, G.; Jurkšas, T.; Stančikas, J.; Baravykas, T.; Vargalis, R.; Tičkūnas, T.; Bachmann, J.; Šakirzanovas, S.; Sirutkaitis, V.; et al. Femtosecond Laser Assisted 3D Etching Using Inorganic-Organic Etchant. *Materials* **2022**, *15*, 2817. https://doi.org/10.3390/ma15082817

Received: 11 March 2022
Accepted: 7 April 2022
Published: 12 April 2022

Publisher's Note: MDPI stays neutral with regard to jurisdictional claims in published maps and institutional affiliations.

Copyright: © 2022 by the authors. Licensee MDPI, Basel, Switzerland. This article is an open access article distributed under the terms and conditions of the Creative Commons Attribution (CC BY) license (https://creativecommons.org/licenses/by/4.0/).

1. Introduction

Glass micro-processing using femtosecond (fs) lasers is a vast field with capabilities of producing different structures with arbitrary geometries [1]. This can be achieved using various light-matter interaction regimes. II type modification-based selective laser etching (SLE) stands out among all of them due to the possibility of producing arbitrary shaped 3D glass structures which can be on the surface of the glass samples or embedded inside the volume of the sample. This technology was also shown to be suitable for processing crystals [2–4], making it even more appealing.

The underlying idea behind SLE is that the etchant etches laser-induced modified volume of dielectric substantially faster than unmodified material. To characterize it, two primary parameters can be used: etching rate, which is the speed at which modified material dissolves in the etchant, as well as selectivity, which denotes the ratio between etching rates of modified and unmodified glass. Due to different requirements dictated by various applications where SLE is used, different etching rates and selectivities might be desired. As a result, an extensive variety of works have been dedicated to understanding the underlying physical and chemical mechanisms, which might lead to different etching rates and selectivities [5]. Most of them concentrate on changing laser exposure parameters [3,5,6]. In the absolute majority of works, aqueous Hydrofluoric acid (HF) or Potassium Hydroxide (KOH) solutions are being discussed [5]. Nevertheless, varying only these parameters, it is hard to achieve selectivity which would be higher than ∼1400 [6]. This limits SLE usage as a true 3D manufacturing technique which could rival additive 3D printing [7].

This work is dedicated to expanding SLE selectivity further by employing etchant with additional organic solvents mixed in it. This technique is already used in standard lithography, which also deals with wet etching [8]. It results in different wetting and chemical peculiarities of the process, subsequently enhancing etching rate and selectivity. These capabilities are explored in this work, showing what maximum etching rate and selectivity can be achieved using this solution. Additionally, the phenomenon is explained from the chemical interaction side, allowing us to understand it towards a better exploitation in producing a high aspect ratio and/or complex embedded 3D structures.

2. Materials and Methods

The work was performed using a "Laser Nanofactory" (Femtika, Ltd., Vilnius, Lithuania) setup. The system is based on amplified Yb:KGW fs laser "Pharos" (Light Conversion, Ltd., Vilnius, Lithuania)). In this work, the laser parameters were set to 1030 nm wavelength, 610 kHz repetition rate, and ∼700 fs pulse duration. Positioning is performed using Aerotech linear stages and galvo-scanners, which operate in a synchronized manner to avoid any stitching-related defects. Translation velocity and average laser power used for modification inscription were −10 mm/s and 300 mW, respectively. The system also has a built-in polarization control, which allows it to be dynamically tuned during fabrication. To obtain the highest possible selectivity, linear polarization perpendicular to the scanning direction was used for selectivity testing experiments. More precise details on the setup can be found elsewhere [9]. Fused silica glass (amorphous SiO_2) was used for the fabrication. The main idea of the experiment is to inscribe single scanning lines in the XY plane volume of the glass. This method was already presented elsewhere [10]. The process is also shown in Figure 1. Five identical lines are written in one sample to check the repeatability of the process. After the inscription process, the sample is cut in the middle perpendicularly to the written lines. The cut edge of the sample is polished and then the sample is etched in the chosen etchants. Etching was performed in an aqueous KOH solution with varying isopropanol and KOH concentrations at 85 °C. Exact concentrations will be listed where applicable. After a specified amount of time, etched channel lengths are measured by using an optical microscope. Optical microscope images were taken using Olympus IX73. By dividing channel length by etching time, the etching rate is calculated. To calculate selectivity, we needed to measure the unmodified material etching rate for each case. This was done by measuring the thickness of the bulk of glass and etching the glass bulk for 24 h. After the etching process, glass thickness was measured again and the unmodified material etching rate was calculated by dividing etched glass thickness by etching time. After all, by dividing the modified material etching rate by the unmodified material etching rate, the selectivity is calculated.

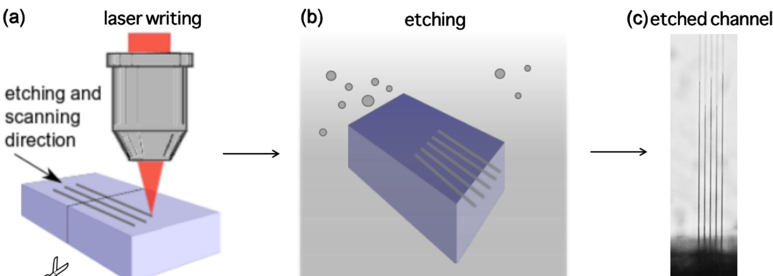

Figure 1. The sequence of the performed experiment. (**a**) First of all, laser modifications are inscribed inside the volume of glass in the XY plane. The sample is cut in the middle perpendicularly to the inscribed lines, the cut edge is polished. (**b**) Then, etching is performed in various enchants. (**c**) Finally, etched single line channel lengths are measured under the optical microscope.

The contact angle characterization was performed by using the optical contact angle measuring and contour analysis system (KSV Instruments LTD CAM 200, The Imaging Source Europe GmbH DMK 21F04) equipped with a CCD camera (ImagingSource DMK 21F04 fps). The camera, the etchant droplet, and the illumination source equipped with a light-emitting diode were aligned into one line. Therefore, the droplet shadow was projected and captured by the digital camera. Average values of contact angle and measurement errors were obtained by software (The Imaging Source Europe GmbH DMK 21F04).

3. Results

We began this work by testing isopropanol's influence on the etching rates of unmodified fused silica by changing KOH and isopropanol concentrations. The chosen range was 1–10 mol/L for KOH and 0%–50% for isopropanol. The unmodified material etching rate measurement was performed by measuring the thickness of the fused silica sample before etching and then etching it for 24 h. After etching, the thickness was measured again and the etching rate of unmodified material was calculated. Since the etchant does not need to penetrate inside the volume of glass and the diffusion of the etchant is not confined, the etching rate of unmodified material should remain practically the same over the experiment time scale. Results are shown in Figure 2a. As expected, for unmodified material, the etching rate was far more influenced by the KOH concentration than the amount of isopropanol in the mixture. The peak value of ∼1.5 µm/h was achieved at the highest KOH concentration and a low 5% concentration of isopropanol.

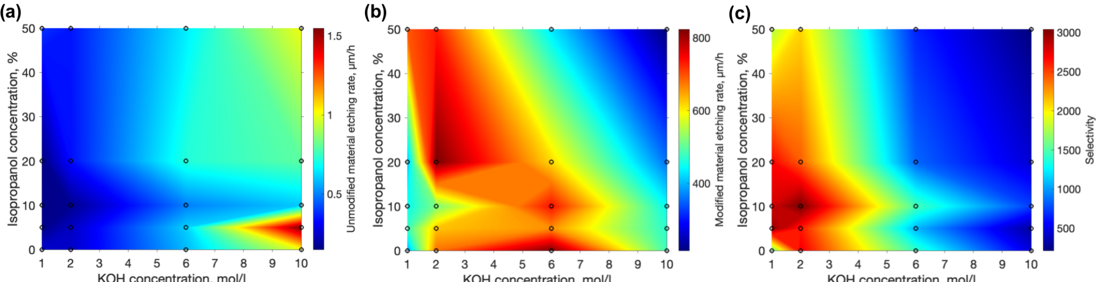

Figure 2. Etching rates of unmodified (**a**) and laser modified (**b**) fused silica acquired with different KOH and isopropanol concentrations. The highest achieved values are ∼1.50 µm/h and ∼820 µm/h respectively. (**c**) selectivity is derived by dividing results of part (**b**) by part (**a**). The highest value is ∼3000 at 2 mol/L KOH and 10% isopropanol, showing a clear tendency that lower KOH concentrations and a moderate amount of isopropanol positively impact the selectivity.

Next, the etching rate of the modified material was measured. The experiment protocol followed the idea of inscribing horizontal lines into the material one after another. The etching rate was determined by measuring the length of a 1 h etched channel that was formed during the described process. Measured values are plotted in Figure 2. In contrast to unmodified results, the highest etching rate (∼820 µm/h) here was achieved at a moderate KOH concentration of 6 mol/L and with no isopropanol. However, another peak of the higher etching rate of ∼820 µm/h was observed at the 2 mol/L KOH concentration and with 20% of isopropanol, showing that organic solvent, under special conditions, can have a positive impact on the etching rate of laser modified material.

SLE was shown to be able to produce complex 3D glass structures, rivaling those produced using additive manufacturing out of polymers [1]. However, the complexity and size of SLE-produced structures are always limited by the selectivity, i.e., even if laser exposed regions etch much faster, unaffected material is removed as well. This results in limitations to the shape complexity, which might be detrimental to many applications, such as precise microfluidics or micromechanics. Therefore, the most important parameter of the SLE is selectivity. The selectivity calculated in this work is given in Figure 2c. The

highest achieved value is ∼3000, which is more than two times higher than the highest value reported in the literature to the best of our knowledge [6]. In addition, it was achieved in a mixture containing small amounts of both KOH (2 mol/L) and isopropanol (10%). This is also far from both peak etching rates of unmodified and modified materials. If no isopropanol was used, 2 mol/L of KOH would yield a selectivity of ∼2700, which is ∼13% lower compared with the maximum value. Therefore, a positive impact on selectivity by using small amounts of isopropanol is evident. Interestingly, it is a far higher value in comparison to the selectivity of ∼500 at 10 mol/L KOH—a standard value used by multiple groups. Thus, another conclusion that can be drawn from this work is that even a reduction in KOH can help increase selectivity. However, care should be taken when applying this methodology, since a decrease in KOH concentration would result in longer etching times.

The primary idea behind introducing isopropanol to the aqueous KOH mixture is to improve the wetting properties of the liquid and, hence, allowing easier diffusion of dissolved silicate ions from the fused silica-etchant interface. Thus, to obtain further insights into acquired etching results contact angles of different ratios of KOH and isopropanol on fused silica were measured. Results are given in Figure 3. Generally, with the increase of isopropanol concentration, the contact angle becomes smaller, generally proving the idea that this organic solvent should help with wetting. However, the area with the lowest contact angle, which is between and 2 mol/L KOH and above 20% of isopropanol coincides neither with the highest etching rates nor with the highest selectivity. On the contrary, the highest etching rates are at experimental conditions with relatively high contact angles −34.5° for the highest etching rate for unmodified material and 32.1° for laser affected volume. Nevertheless, the highest selectivity value coincides pretty well with the area where the contact angle starts to drop significantly (17°) at the highest selectivity conditions. At the same time, it is not at the lowest achieved contact angle −5.2°. Therefore, some other interactions should be considered.

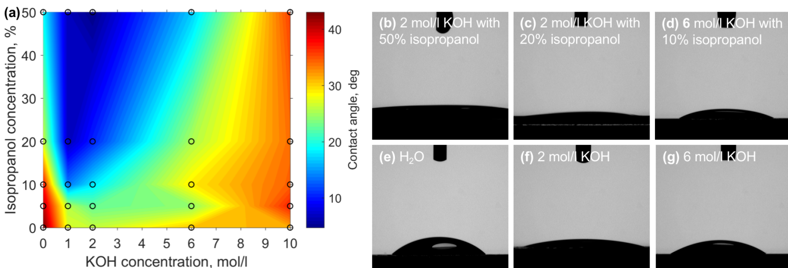

Figure 3. (**a**) Contact angle at different mixtures of KOH and isopropanol. While at the point of highest selectivity contact angle is relatively reduced, it is not the lowest measured value. (**b**–**g**) different etching solutions contact angle measurement pictures.

To understand the full picture of the process, the chemical aspect has to be considered. Indeed, when etching is performed, the resulting chemical reaction is the same in both cases with and without isopropanol. When fused quartz is exposed to a solution of KOH, potassium silicate and water are formed (see Figure 1). However, in addition to the increased wetting effect of fused quartz described above, the introduction of isopropanol into the system also has a negative influence on selectivity. The requirement for the reaction is the formation and dissolution of K_4SiO_4 in the reaction mixture. Potassium silicate is soluble in water (it is possible to dissolve salt with boiling water) and slightly or completely insoluble in alcohols [11]. Potassium silicate dissolves more readily under pressure at a temperature of 80 °C [12,13]. Even though the etching was carried out at a temperature of 85 °C, in a closed system, the temperature of etchants had to be lower because of the boiling point of isopropanol, which is 82.5 °C. Consequently, the higher isopropanol concentration

determines the lower temperature of the mixture and the lower amount of a more suitable solvent, resulting in a slower etching process at extremely high isopropanol concentrations.

$$SiO_{2(s)} + 4K^{+}OH^{-}_{(aq)} \rightarrow K^{+}_{4}[SiO_4]^{4-}_{(aq)} + 2H_2O_{(l)}. \quad (1)$$

The solubility of potassium hydroxide is ∼11 g /10 mL (28 °C) and 121 g/100 mL (25 °C) in isopropanol and water, respectively. It can be suggested that isopropanol acts as a surfactant, accumulates at the solid/liquid interface, and thereby prevents access of KOH to the surface of the silica sample. We considered a model of the behavior of isopropanol molecules at the surface during etching. The described model takes into consideration that, for a saturated concentration, a layer of isopropanol molecules is formed at the surface of the solution, rather than being diluted. The abundance of isopropanol affects the formation of a monolayer of alcohol molecules at the surface of the sample [14–16]. The highest selectivity value was obtained for 2 mol/L (10.89 g/100 mL, here KOH molar mass 56.1056 g/mol, isopropanol density at 28 °C is 0.7783 g/mL) KOH concentration, which corresponds to the maximum alkali solubility in isopropanol. Further increasing the alkali concentration in the mixture results in a decrease in selectivity. This evidence confirms the described model of isopropyl-alcohol monolayer formation on the surface because the etching reaction takes place only at the surface and the etchant contact. However, to prove this hypothesis, further studies need to be performed.

Thus, overall, while a lower contact angle helps with easier etchant and product diffusion between the solution and the fused silica interface, behaviors of isopropanol, such as lower boiling point and limited dissolution of KOH, result in a slowed down reaction, forming an ideal balance at experimental conditions of 2 mol/L KOH and 10% isopropanol.

Despite an impressive etching rate together with selectivities which were demonstrated, etching rates tend to diminish. We have measured how the etching rate is changing over time. The results of the etching rate after 2, 4, 8 and 12 h are depicted in Figure 4a–d. Comparing etching rates after the mixture was just mixed after 2 additional hours' etching rates drop approximately twice (a). After 4 h, etching rates decrease twice again. Finally, after 8 and 12 h, the etching rate is between 100 and 200 µm. The explanation for such a decrease in etching rate is simple—the deeper the etchant needs to penetrate into the channels, the more it dilutes and struggles to etch the channel at the deepest point. Nonetheless, here we can notice the special property of the etchant with isopropanol. Isopropanol allows the maintenance of a higher etching rate. Possibly, isopropanol induces more effective penetration into the channel. Thus, another positive side of isopropanol is the possibility to not only achieve but also maintain a higher etching rate for longer. In general, according to these graphs, we can conclude that if high selectivity and a high etching rate are desired, the etching time should be short enough (shorter than 2–3 h). Otherwise, it is impossible to maintain selectivity and an aspect ratio higher than 1000, because of the loss of etching rate during longer etching times. This might be problematic if relatively big or long structures are needed.

After we performed some experiments we have noticed one more interesting property which is affected by the etchant. We have observed that structures etched with lower KOH concentration etchants tend to have worse surface quality than structures etched with high concentration etchants. To test this property we inscribed the surface in the XY plane and etched it away with different concentrations of etchant. After all, surfaces were inspected with a Scanning Electron Microscope (SEM). SEM pictures of made surfaces are shown in Figure 5a–g. Although surfaces look different, surface roughness was measured for these surfaces by using an optical profilometer. The correlation between surface roughness and etchant concentrations is shown in Figure 5h. The higher the etchant concentration is, the lower the surface roughness that could be obtained. On the other hand, looking back to previous results, lower concentrations of etchant allow obtaining higher sensitivities. For comparison in Figure 5h, we added a surface etched with 5% HF solution with a surface roughness of around 200 nm root mean square (RMS). Usually, HF shows substantially lower selectivities than KOH [5]. Thus, here we conclude that the higher the selectivity,

the higher the surface roughness obtained. However, in most applications, it is a desire to maintain both. To get that result, combined etching techniques need to be used. For example, etch the structure with low concentration KOH etchant and smooth the surface with low concentration HF solution. The hybrid etching technique was already demonstrated elsewhere [17], on the other side, reasons are different, a combination of a few different types of etchant, such as HF and KOH, allow us to obtain the highest throughput because HF shows a higher etching rate for effective large volume removal, meanwhile KOH allows us to achieve high selectivity for precise feature etching.

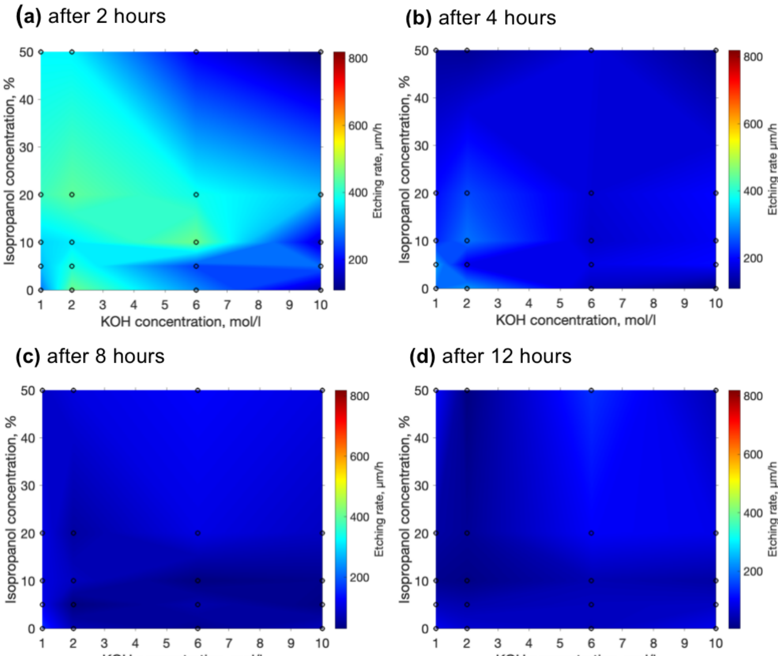

Figure 4. Etching rate evolution over time. (**a**) etching rate after 2 h of etching, (**b**) after 4 h, (**c**) after 8 h, and (**d**) after 12 h.

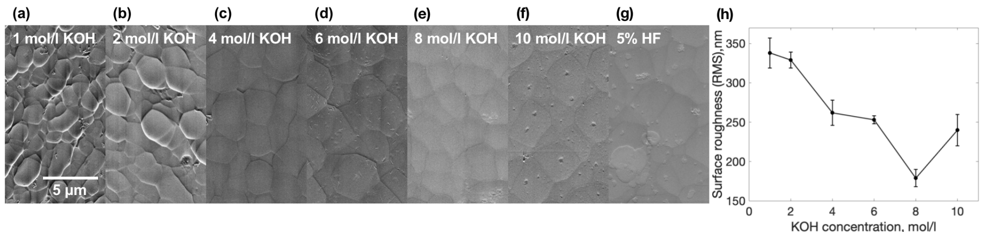

Figure 5. (**a**–**g**) SEM micrographs of surfaces etched in various concentrations etchants. (**h**) Surface roughness dependency on etchant concentration.

From a practical perspective, the best way to demonstrate the potency of the developed methodology was the formation of high aspect ratio embedded fluidic channels. Indeed, while SLE shows huge promise in microfluidic system fabrication, in many cases channels have to be produced open and then be sealed afterwards using other techniques, such as fs laser welding [18], or have limitations on their physical dimensions. Here we demonstrate high aspect ratio channels embedded in the glass and etched out using the highest, KOH

enabled selectivity. The thickness of the sample is 2 mm, while the channels are ∼10 µm in diameter. This places their aspect ratio at 1:1000. Channels were filled with liquid and optical images were taken from the side (Figure 6a,b). The presented optical microscope pictures allow us to estimate that the diameter is well maintained through the channel while the surface roughness is around hundreds of nanometers RMS. It is important to note that, due to the thickness of a sample, an objective with automated aberration correction might be required if this methodology is used with relatively thick samples (more than 1 mm). In the future, Spatial Light Modulators (SLM) can be used for the same purpose with more parameter control [19]. Non-diffracting Bessel beam-based fabrication might also be attractive to fabricate such long and straight channels with a very high aspect ratio [20].

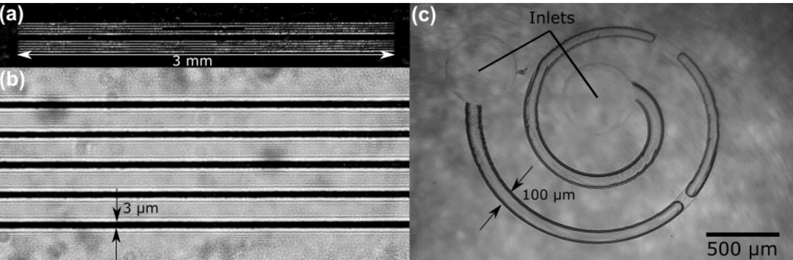

Figure 6. (**a**,**b**) Enhanced contrast pictures of straight-through high aspect ratio (1:1000) channels embedded inside fused silica. (**c**) microfluidic system within the volume of glass, consisting of two outlets and a spiral channel. All of the structures are etched using the best KOH and isopropanol ratio solution (2 mol/L and 10% appropriately).

The primary attraction of SLE is the possibility to produce complex embedded glass structures, such as microfluidic channels. While the straight channels shown so far might be used for some application, the possibility to have bent channels opens a lot of new possibilities for applications. One of them is passive particle separation. Indeed, spiral channels allow for separating particles due to their size without using any additional elements [21], such as filters [18]. The spiral-based separator provides a very high throughput, as none of the channel cross-section is blocked by the filter. To demonstrate that such a channel is possible, a prototype of an embedded spiral channel system was made. The combined length of the channel is 7 mm, with a channel width of 100 µm, resulting in an effective aspect ratio of 1:70. Testing with water showed nonrestrictive flow, which means that the channel is well etched and has no leftovers (Figure 6b). Due to the nature of the SLE, the inlet and outlets of such a system can be produced during the same fabrication step, simplifying production.

Another exemplary structure demonstrated in this work is the 3D fullerene model. An SEM picture of this structure is demonstrated in Figure 7 This structure is also a high aspect ratio and porosity complex 3D structure example. By using a combined etching technique, we achieve both high surface roughness and high selectivity which creates a possibility for complex architecture high aspect ratio structure production. For the first step of etching, 2 mol/L KOH solution with 10% of isopropanol is used to maintain the highest selectivity. Subsequently, the structure is etched additionally in 5% HF solution to smooth the surface. A fullerene structure demonstration proves that SLE is a suitable technology for a high aspect ratio porous complex structures fabrication which could lead to glass metamaterials fabrication.

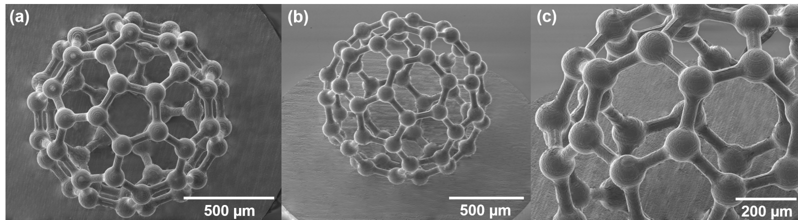

Figure 7. Model of fullerene molecule made out of glass. (**a**) top view of the fullerene structure, (**b**) isometric view to the whole structure, and (**c**) closed look to the same structure. This structure represents the possibility of a high aspect ratio, high surface quality, and high porosity structure which is similar to metamaterials.

4. Discussion

Three dimensional (3D) manufacturing, especially at scales down to the µm range, is becoming increasingly explored by academia, with industry following closely behind. So far it has been considered that 3D additive manufacturing is the preferred option due to its flexibility and wide array of possibilities to realize it [7,22]. However, while there are many technologies for it [23], on this scale, fabrication out of inorganic compounds is difficult. If direct fs fabrication is considered, special hybrid materials and/or nanocomposites need to be used [24–27], with potentially limited fabrication windows and multiple post-processing steps needed to realize it. SLE would seem to be an attractive candidate to potentially substitute complicated additive methodologies if 3D glass microstructures are needed. Nevertheless, the main problem with SLE was always selectivity, limiting how complex 3D structures can be [1]. Results shown in this work show the potential of SLE to have good enough selectivity to be directly compared to additive manufacturing. The SLE process also involves fewer technological steps than, let us say, glass manufacturing using optical 3D printing [28,29]. At the same time, SLE requires the usage of potentially hazardous chemicals (HF and KOH) which can also limit its proliferation. Therefore, while SLE is approaching additive manufacturing in terms of possibilities to produce 3D microstructures, there are some distinct advantages and disadvantages involved with this technique.

Another important takeaway from this work is the dynamics of surface roughness depending on the etching parameters. Indeed, there are many technologies tested for the production of micro-optical elements [30]. For this discussion, we will again compare SLE with additive fs-based printing, where it is inherently easy to achieve surface roughness suitable for optics manufacturing (bellow 10 nm RMS) [24]. As a result, there is a multitude of works using additive fs-based manufacturing for complex micro-optics production [31–33]. However, additive manufacturing forces the usage of organic materials for fabrication, which inherently have a relatively low laser-induced damage threshold [34]. Attempts to manufacture inorganic micro-optics using additive manufacturing exist, but these involve all the previously listed challenges, plus require the performance of all the manufacturing steps with extreme attention to deformations that occur during such processing [35]. Direct micro-optic manufacturing using subtractive processing is limited, as ablation and SLE do not have good enough surface roughness for optics. This leads to the necessity to use annealing [36] or polishing [37] after laser exposure, making shape control quite hard. However, in this work, we show that by manipulating the etchant, both a complex 3D shape and relatively good surface roughness can be achieved. While it is still not of optical quality, it points to the possibility of using etchant manipulations for single-step surface smoothing during etching itself. This is an area of research worth exploring in the future.

5. Conclusions

Overall, this work demonstrated the general dynamics of etching rates as well as selectivity when the concentrations of KOH and isopropanol are varied in the etchant. The highest etch rate of unmodified material is ∼1.5 µm/h, which is achieved with the

highest tested concentration of KOH (10 mol/L) and a minor amount of isopropanol (5%). This is in sharp contrast to the highest etch rate of laser effected volume (∼820 µm/h), which is acquired at 6% KOH and no isopropanol. Finally, the highest achieved selectivity is ∼3000, which is around two times higher than the highest selectivity reported in the literature to the best of our knowledge. It is achieved at a minor concentration of KOH and a small amount of isopropanol. This result can be explained by a minimized etching rate of unmodified material and a high etch rate of modified glass. Both of these effects are a result of changes in the wetting properties of the etchant alongside the modified diffusion properties of the formed chemical constitutes of the reaction. On the other hand, over time, the etching rate drops down significantly to 100–200 µm for all etchants. Thus, to maintain a high etching rate, the etching process needs to be quite short—up to 4 h. In this work, we have also shown that even the surface roughness of the etched sample depends on the etchant type and its concentration. Low concentration etchants make rough surfaces, meanwhile, high concentration KOH or HF etchants make smoother surfaces. Hence, to maintain both high selectivity and surface quality, combined etching techniques need to be used. To show how all of these improvements can be exploited for various 3D structures, such as the model of fullerene molecule, embedded curves and straight channel systems in the glass were fabricated. The demonstrated straight channels aspect ratio is in the range of 1:1000 and spiral channel aspect ratio is in the 1:70 range with good repeatability of the fabrication. Fluidic testing showed no left-overs or debris from the channel point to well-etched channels. Complex 3D structures were also made, showing that with this improvement 3D SLE is getting ever closer to the capabilities of additive micro-and nanomanufacturing. Therefore, the results of this work allow SLE to become even more suitable for high-precision 3D glass structure fabrication.

Author Contributions: A.B. planned and led the research, fabricated demonstration structures, conducted part of the measurements, prepared the publication and the figures. G.M. consulted on the chemistry part and made contact angle measurements. T.J. performed most of selectivity and etching rate measurements. J.S. started experiments with different concentration solutions. T.B. prepared models for demonstration structures. R.V. characterised structures with the scanning electron microscope. T.T., J.B., S.Š. and V.S. consulted. L.J. consulted and contributed to publication preparation. All authors have read and agreed to the published version of the manuscript.

Funding: This research was funded by EC Horizon 2020 program, ATOPLOT project, grant number 950785 and by The Research Council of Lithuania (No. S-MIP-19-60).

Conflicts of Interest: The authors declare no conflict of interest.

References

1. Butkutė, A.; Jonušauskas, L. 3D Manufacturing of Glass Microstructures Using Femtosecond Laser. *Micromachines* **2021**, *12*, 499. [CrossRef] [PubMed]
2. Matsuo, S.; Tabuchi, Y.; Okada, T.; Juodkazis, S.; Misawa, H. Femtosecond laser assisted etching of quartz: Microstructuring from inside. *Appl. Phys. A* **2006**, *84*, 99–102. [CrossRef]
3. Hasse, K.; Huber, G.; Kränkel, C. Selective etching of fs-laser inscribed high aspect ratio microstructures in YAG. *Opt. Mater. Express* **2019**, *9*, 3627–3637. [CrossRef]
4. Wortmann, D.; Gottmann, J.; Brandt, N.; Horn-Solle, H. Micro- and nanostructures inside sapphire by fs-laser irradiation and selective etching. *Opt. Express* **2008**, *16*, 1517–1522. [CrossRef] [PubMed]
5. Ross, C.A.; MacLachlan, D.G.; Choudhury, D.; Thomson, R.R. Optimisation of ultrafast laser assisted etching in fused silica. *Opt. Express* **2018**, *26*, 24343–24356. [CrossRef] [PubMed]
6. Gottmann, J.; Hermans, M.; Repiev, N.; Ortmann, J. Selective Laser-Induced Etching of 3D Precision Quartz Glass Components for Microfluidic Applications-Up-Scaling of Complexity and Speed. *Micromachines* **2017**, *8*, 110. [CrossRef]
7. Jonušauskas, L.; Juodkazis, S.; Malinauskas, M. Optical 3D printing: Bridging the gaps in the mesoscale. *J. Opt.* **2018**, *20*, 053001. [CrossRef]
8. Zubel, I.; Rola, K.; Kramkowska, M. The effect of isopropyl alcohol concentration on the etching process of Si-substrates in KOH solutions. *Sens. Actuator A Phys.* **2011**, *171*, 436–445. [CrossRef]
9. Jonušauskas, L.; Baravykas, T.; Andrijec, D.; Gadišauskas, T.; Purlys, V. Stitchless support-free 3D printing of free-form micromechanical structures with feature size on-demand. *Sci. Rep.* **2019**, *9*, 17533. [CrossRef]

10. Butkutė, A.; Baravykas, T.; Stančikas, J.; Tičkūnas, T.; Vargalis, R.; Paipulas, D.; Sirutkaitis, V.; Jonušauskas, L. Optimization of selective laser etching (SLE) for glass micromechanical structure fabrication. *Opt. Express* **2021**, *29*, 23487–23499. [CrossRef]
11. Rabinovich, V.A.; Havin, Z.Y. *Brief Chemical Handbook*; Khimia: Leningrad, Russia, 1977; p. 69.
12. Vial, J.G. *Soluble Silicates*; Reinhold: New York, NY, USA, 1952.
13. Greenwood, N.; Earnshaw, A. *Chemistry of the Elements*; Elsevier: Pergamon, Turkey, 1986; p. 398.
14. Monteiro, T.; Kastytis, P.; Gonçalves, L.; Minas, G.; Cardoso, S. Dynamic Wet Etching of Silicon through Isopropanol Alcohol Evaporation. *Micromachines* **2015**, *6*, 1534–1545. [CrossRef]
15. Zubel, I.; Kramkowska, M. Etch rates and morphology of silicon (h k l) surfaces etched in KOH and KOH saturated with isopropanol solutions. *Sens. Actuators A Phys.* **2004**, *115*, 549–556. [CrossRef]
16. Rola, K.P.; Zubel, I. Impact of alcohol additives concentration on etch rate and surface morphology of (100) and (110) Si substrates etched in KOH solutions. *Microsyst. Technol.* **2012**, *19*, 635–643. [CrossRef]
17. LoTurco, S.; Osellame, R.; Ramponi, R.; Vishnubhatla, K.C. Hybrid chemical etching of femtosecond laser irradiated structures for engineered microfluidic devices. *J. Micromech. Microeng.* **2013**, *23*, 085002. [CrossRef]
18. Jonušauskas, L.; Rekštytė, S.; Buividas, R.; Butkus, S.; Gadonas, R.; Juodkazis, S.; Malinauskas, M. Hybrid Subtractive-Additive-Welding Microfabrication for Lab-on-Chip (LOC) Applications via Single Amplified Femtosecond Laser Source. *Opt. Eng.* **2017**, *56*, 094108. [CrossRef]
19. Kontenis, G.; Gailevičius, D.; Jonušauskas, L.; Purlys, V. Dynamic aberration correction via spatial light modulator (SLM) for femtosecond direct laser writing: Towards spherical voxels. *Opt. Express* **2020**, *28*, 27850–27864. [CrossRef]
20. Wang, Z.; Jiang, L.; Li, X.; Wang, A.; Yao, Z.; Zhang, K.; Lu, Y. High-throughput microchannel fabrication in fused silica by temporally shaped femtosecond laser Bessel-beam-assisted chemical etching. *Opt. Lett.* **2018**, *43*, 98–101. [CrossRef]
21. Bhagat, A.A.S.; Kuntaegowdanahalli, S.S.; Papautsky, I. Continuous particle separation in spiral microchannels using dean flows and differential migration. *Lab Chip* **2008**, *8*, 1906–1914. [CrossRef]
22. Vaezi, M.; Seitz, H.; Yang, S. A review on 3D micro-additive manufacturing technologies. *Int. J. Adv. Manuf. Technol.* **2013**, *67*, 1721–1754. [CrossRef]
23. Hassanin, H.; Essa, K.; Elshaer, A.; Imbaby, M.; El-Mongy, H.H.; El-Sayed, T.A. Micro-fabrication of ceramics: Additive manufacturing and conventional technologies. *J. Adv. Ceram.* **2021**, *10*, 1–27. [CrossRef]
24. Jonušauskas, L.; Gailevičius, D.; Mikoliūnaitė, L.; Sakalauskas, D.; Šakirzanovas, S.; Juodkazis, S.; Malinauskas, M. Optically Clear and Resilient Free-Form μ-Optics 3D-Printed via Ultrafast Laser Lithography. *Materials* **2017**, *10*, 12. [CrossRef] [PubMed]
25. Sänger, J.C.; Pauw, B.R.; Sturm, H.; Günster, J. First time additively manufactured advanced ceramics by using two-photon polymerization for powder processing. *Open Ceram.* **2020**, *4*, 100040. [CrossRef]
26. Vyatskikh, A.; Ng, R.C.; Edwards, B.; Briggs, R.M.; Greer, J.R. Additive Manufacturing of High-Refractive-Index, Nanoarchitected Titanium Dioxide for 3D Dielectric Photonic Crystals. *Nano Lett.* **2020**, *20*, 3513–3520. [CrossRef]
27. Merkininkaitė, G.; Aleksandravičius, E.; Malinauskas, M.; Gailevičius, D.; Šakirzanovas, S. Laser additive manufacturing of Si/ZrO2 tunable crystalline phase 3D nanostructures. *Opto-Electron. Adv.* **2022**, *0*, 210077–210077. [CrossRef]
28. Kotz, F.; Schneider, N.; Striegel, A.; Wolfschläger, A.; Keller, N.; Worgull, M.; Bauer, W.; Schild, D.; Milich, M.; Greiner, C.; et al. Glassomer-Processing Fused Silica Glass Like a Polymer. *Adv. Mater.* **2018**, *30*, 1707100. [CrossRef]
29. Kotz, F.; Quick, A.S.; Risch, P.; Martin, T.; Hoose, T.; Thiel, M.; Helmer, D.; Rapp, B.E. Two-Photon Polymerization of Nanocomposites for the Fabrication of Transparent Fused Silica Glass Microstructures. *Adv. Mater.* **2021**, *33*, 2006341. [CrossRef] [PubMed]
30. Zolfaghari, A.; Chen, T.; Yi, A.Y. Additive manufacturing of precision optics at micro and nanoscale. *Int. J. Extrem. Manuf.* **2019**, *1*, 012005. [CrossRef]
31. Gissibl, T.; Thiele, S.; Herkommer, A.; Giessen, H. Two-photon direct laser writing of ultracompact multi-lens objectives. *Nat. Photonics* **2016**, *10*, 554–560. [CrossRef]
32. Hahn, V.; Kalt, S.; Sridharan, G.M.; Wegener, M.; Bhattacharya, S. Polarizing beam splitter integrated onto an optical fiber facet. *Opt. Express* **2018**, *26*, 33148–33157. [CrossRef]
33. Dietrich, P.I.; Blaicher, M.; Reuter, I.; Billah, M.; Hoose, T.; Hofmann, A.; Caer, C.; Dangel, R.; Offrein, B.; Troppenz, U.; et al. In situ 3D nanoprinting of free-form coupling elements for hybrid photonic integration. *Nat. Photonics* **2018**, *12*, 241–247. [CrossRef]
34. Butkutė, A.; Čkanavičius, L.; Rimšelis, G.; Gailevičius, D.; Mizeikis, V.; Melninkaitis, A.; Baldacchini, T.; Jonušauskas, L.; Malinauskas, M. Optical damage thresholds of microstructures made by laser three-dimensional nanolithography. *Opt. Lett.* **2019**, *45*, 13–16. [CrossRef]
35. Gonzalez-Hernandez, D.; Varapnickas, S.; Merkininkaitė, G.; Čiburys, A.; Gailevičius, D.; Šakirzanovas, S.; Juodkazis, S.; Malinauskas, M. Laser 3D Printing of Inorganic Free-Form Micro-Optics. *Photonics* **2021**, *8*, 577. [CrossRef]
36. Sala, F.; Paié, P.; Vázquez, R.M.; Osellame, R.; Bragheri, F. Effects of Thermal Annealing on Femtosecond Laser Micromachined Glass Surfaces. *Micromachines* **2021**, *12*, 180. [CrossRef] [PubMed]
37. Dudutis, J.; Pipiras, J.; Schwarz, S.; Rung, S.; Hellmann, R.; Račiukaitis, G.; Gečys, P. Laser-fabricated axicons challenging the conventional optics in glass processing applications. *Opt. Express* **2020**, *28*, 5715–5730. [CrossRef] [PubMed]

VI

SAPPHIRE SELECTIVE LASER ETCHING DEPENDENCE ON RADIATION WAVELENGTH AND ETCHANT

A. Butkutė , R. Sirutkaitis, D. Gailevičius, D. Paipulas and V. Sirutkaitis

Micromachines 14(1), 7–16 (2023).

Article

Sapphire Selective Laser Etching Dependence on Radiation Wavelength and Etchant

Agnė Butkutė [1,*], Romualdas Sirutkaitis [2], Darius Gailevičius [1], Domas Paipulas [1] and Valdas Sirutkaitis [1,*]

[1] Laser Research Center, Vilnius University, Saulėtekio ave. 10, LT-10223 Vilnius, Lithuania
[2] Institute of Biochemistry, Vilnius University, Mokslininkų str. 12, LT-08622 Vilnius, Lithuania
* Correspondence: agne.butkute@ff.vu.lt (A.B.); valdas.sirutkaitis@ff.vu.lt (V.S.)

Abstract: Transparent and high-hardness materials have become the object of wide interest due to their optical and mechanical properties; most notably, concerning technical glasses and crystals. A notable example is sapphire—one of the most rigid materials having impressive mechanical stability, high melting point and a wide transparency window reaching into the UV range, together with impressive laser-induced damage thresholds. Nonetheless, using this material for 3D micro-fabrication is not straightforward due to its brittle nature. On the microscale, selective laser etching (SLE) technology is an appropriate approach for such media. Therefore, we present our research on C-cut crystalline sapphire microprocessing by using femtosecond radiation-induced SLE. Here, we demonstrate a comparison between different wavelength radiation (1030 nm, 515 nm, 343 nm) usage for material modification and various etchants (hydrofluoric acid, sodium hydroxide, potassium hydroxide and sulphuric and phosphoric acid mixture) comparison. Due to the inability to etch crystalline sapphire, regular SLE etchants, such as hydrofluoric acid or potassium hydroxide, have limited adoption in sapphire selective laser etching. Meanwhile, a 78% sulphuric and 22% phosphoric acid mixture at 270 °C temperature is a good alternative for this process. We present the changes in the material after the separate processing steps. After comparing different processing protocols, the perspective is demonstrated for sapphire structure formation.

Keywords: selective laser etching; 3D laser microfabrication; crystals microprocessing; sapphire 3D structures; femtosecond laser microprocessing

Citation: Butkutė, A.; Sirutkaitis, R.; Gailevičius, D.; Paipulas, D.; Sirutkaitis, V. Sapphire Selective Laser Etching Dependence on Radiation Wavelength and Etchant. *Micromachines* **2023**, *14*, 7. https://doi.org/10.3390/mi14010007

Academic Editor: Francesco Ruffino

Received: 19 November 2022
Revised: 9 December 2022
Accepted: 16 December 2022
Published: 20 December 2022

Copyright: © 2022 by the authors. Licensee MDPI, Basel, Switzerland. This article is an open access article distributed under the terms and conditions of the Creative Commons Attribution (CC BY) license (https://creativecommons.org/licenses/by/4.0/).

1. Introduction

Sapphire is an attractive material for many applications. It has outstanding mechanical, chemical and optical properties. High-end optical and mechanical components made from sapphire benefit from all of these properties. However, the microprocessing of sapphire is highly complicated. It tends to crack when affected by high-intensity radiation due to the high strain induced during processing. Various laser machining techniques have already been adapted for sapphire micromachining: to make 2D surface structures, dicing [1] or direct laser ablation could be used [2,3]. Direct laser processing can be applied to any material, such as metals [4–7]. Direct ablation is a relatively efficient and comparably simple process that enables surface functionalization. To improve the quality of laser-processed surfaces, ablation could be combined with additional processes such as laser-induced plasma-assisted ablation [8,9] or laser-induced backside wet etching [10–12]. By using ablation in combination with additional thermal processing [13] or direct laser writing in combination with chemical post-processing, optical components such as lenses [14,15] or diffractive optical elements [16–18] could be made. Nevertheless, these technologies are limited to the microprocessing and achievement of 2D geometries, and most cannot produce arbitrary-shaped 3D structures. Meanwhile, the selective laser etching (SLE) technique could be a good alternative for 3D structure formation out of sapphire.

SLE is a unique technology that allows the production of 3D structures out of solid-state transparent materials [19]. SLE implementation consists of several steps. First, laser-induced periodic modifications called nanogratings are formed in the bulk of the material by using ultrashort pulsed beams. In amorphous materials, nanaogratings appear as porous modifications, while in crystalline materials, nanaoratings are dominantly regions of amorphized material. Afterwards, laser-modified material is etched out using aggressive etchants such as hydrofluoric acid (HF) or potassium hydroxide (KOH). A similar etching process is applied in the semiconductor industry to make surface structures on silicon [20] or silicon carbide [21]. The capabilities of SLE have been widely investigated on amorphous silica glasses [22–25]. Critical parameters to describe SLE effectiveness are etching rate and selectivity. The etching rate defines how fast material can be etched, and the selectivity is the ratio between the etching rate of modified and unmodified material. Selectivity describes the highest aspect ratio, which is obtained using a specific SLE processing protocol. Selectivity values above 1000 could be obtained for fused silica by laser parameter optimization [22]. Meanwhile, selectivity values above 2000 can be achieved by introducing a particular burst regime [26] or adding organic solvents to the etchant [27]. SLE is a perfect technology for high aspect ratio structure fabrication. The SLE-made structures could be applied in many areas such as micromechanics [28,29] and microfluidics [30–32].

In some works, researchers have already applied SLE to various crystals, such as YAG [33–35] or crystalline quartz [36]. More than a decade ago, the first ideas about SLE processed sapphire were published [37]. This publication suggests writing nanogratings inside the sapphire volume and etching it with KOH. A similar procedure was demonstrated with HF acid [38,39]. Etching selectivity values up to 10,000 [40–42] have been shown since then. Compared with the value shown in fused silica, this is at least four to five times more. Fused silica features both high etching rates for modified and unmodified regions simultaneously, whereas sapphire features low etching rates for both regions. The significant selectivity in sapphire arises because its etching rate of the unmodified region is negligible, even hard to measure. Even though the selectivity in sapphire is high, only a few simple structures have been shown to come out of sapphire by SLE [39,42,43]. The lack of investigation impedes further development of SLE for transparent materials. In this work, we present research on a sapphire SLE comparison between different approaches such as various laser wavelength and etching protocols. We have chosen widely adopted potassium hydroxide, sodium hydroxide [44], hydrofluoric acid [42], and a mixture of sulphuric and phosphoric acids [43] etching protocols and compared them. Moreover, different radiation wavelengths were tested because the induced nanogratings periodicity is determined by wavelength [45], which later affects the etching properties. Finally, we identified the best protocol for sapphire SLE and made structures using this approach.

2. Materials and Methods

SLE experiments were performed with C-cut crystalline sapphire. In these tests, 0.5 mm thickness sapphire substrates were exploited. Many different laser parameters, as well as various etching protocols, were tested. In these experiments, different wavelengths—1st (1030 nm), 2nd (515 nm), and 3rd (343 nm) harmonics of Yb: KGV femtosecond laser (Pharos, Light Conversion Ltd., Lithuania)—were examined. Various focusing optics were chosen to maintain the same focusing conditions and radiation intensity for all tested wavelengths. To focus 1030 nm radiation, a 0.4 NA aspherical lens was used. To focus 515 nm radiation, a 0.2 NA aspherical lens was used, and to focus 343 nm radiatio, an 0.1 NA objective was used. All tested wavelengths were focused to an approximately 1.5 μm beam spot.

Within specific radiation exposition conditions, porous materials modifications called nanogratings can be written inside the volume of glass [46]. Radiation wavelength could change the size of pores and the thickness of the wall between pores. The smaller the wavelength used, the lower the period of the nanogratings [45]. This phenomenon

affects the etching properties of the laser-modified volume. In general, the etching mechanism of nanogratings consists of two main aspects. First, the surface area in a material is increased by creating porous structures, therefore increasing reactive surface area, which is one of the reasons it can be etched more efficiently. Another reason is localized amorphization, which makes modified material less resistant to chemical processing [42]. Here, for the disclosed experimental results, circular and linear polarized light was used. It has already been shown that, in fused silica, the light polarization determines the orientation of the nanogratings, which affects the etching rate significantly [46]. Perpendicularly to the scanning direction, polarized light creates nanogratings elongated towards the scanning direction. In this way, prolonged pores enable the penetration and etching of modified material more efficiently than by writing a modification with parallel polarization. A similar tendency of nanogratings' orientation depending on light polarization has been demonstrated in crystalline sapphire samples, as well [47]. Thus, in single-line experiments, linear polarization perpendicular to the scanning direction was used to maintain a high etching rate. Meanwhile, circularly polarized radiation was used in the experiment where scanning in all XY directions was needed. Sample positioning was performed by using XYZ linear positioning stages (Aerotech, Pittsburgh, PA, USA).

In this work, written nanogratings were etched with various chemicals such as a 35% potassium hydroxide (KOH) mixture with water, a 25% sodium hydroxide (NaOH) mixture with water, and a 48% hydrofluoric acid (HF) and 78% sulphuric, and 22% phosphoric acid mixture (H_2SO_4 and H_3PO_4). Utilization of all of these etchants differs: KOH and NaOH were used at 90 °C, HF was used at the ambient temperature (20 °C), and H_2SO_4 and H_3PO_4 were used at 270 °C. The performance of these etchants in the described condition has already been presented widely in other works [42–44]. However, etching substances have different properties, notably the boiling point. For water-based alkali mixtures such as KOH or NaOH [48], it is around 120 °C. For HF, it is 106 °C. Meanwhile, the sulphuric acid boiling point is above 300 °C, and the phosphoric acid boiling temperature is above 150 °C. Therefore, different temperatures are required to obtain optimal etching efficiency for these chemicals. Thus, four separate well-known etching protocols were examined and compared for sapphire etching.

First of all, principal experiments of single lines in the nXY plane were performed to test how pulse energy (100, 200, 300, 400 and 500 nJ), radiation wavelength (1030 nm, 515 nm, 343 nm), and the used etchants (NaOH, KOH, HF, H_2SO_4 and H_3PO_4) affect the etching rate. In this experiment, pulse duration (200 fs) and pulse repetition rate (610 kHz) remain constant. The light was linearly polarized perpendicularly to the scanning direction to obtain etching rates that were as high as possible. The experiment's main idea was to write single lines inside the bulk of the sapphire. Then, the plate was divided perpendicularly to the written lines in the middle. Finally, the side of the divided plate was polished (using a fine diamond powder on lapping machine), and modifications were etched. The etching rate was evaluated by measuring the length of the etched channel and dividing it by the etching time. This experiment gives us data about the etching rate of the modified material. The idea of this test is shown in Figure 1a. Additionally, during the same experiment, etching rates of unmodified material were evaluated by measuring substrate thickness before and after etching. The etching rate of unaffected material allows us to estimate selectivity in each case. Selectivity is defined as a ratio of modified and unmodified material etching rates. However, since the unmodified material etching rate is negligible in NaOH, KOH, and HF, it cannot be accurately evaluated. For these etching rates, the material was etched for 24 h and the etched material's thickness was around 1 µm, which is on a scale of fidelity of the used device. Thus, we only can think about possible boundaries of selectivity of each etching protocol.

Subsequently, etching experiments of 3D structures were executed. During this experiment, cylindrical 1 mm diameter 3D structures were written into a plate of sapphire. The scheme of this experiment is depicted in Figure 1b. This experiment tested etching

dependency on radiation wavelengths, pulse duration (200 fs-1 ps), and different etchants, to find a protocol for 3D structure fabrication. Finally, when optimal parameters for the etching were found, the morphology of the modified areas was investigated after and before the etching process. For that, 10 µm wide surface modifications were written and etched in the various previously mentioned etchants. The scheme of this experiment is shown in Figure 1c. These morphologies provide some insights into why some etchants are not suitable for sapphire 3D structures' fabrication. After all, a few 3D structures were fabricated out of sapphire using the same setup and employing the found fabrication protocol.

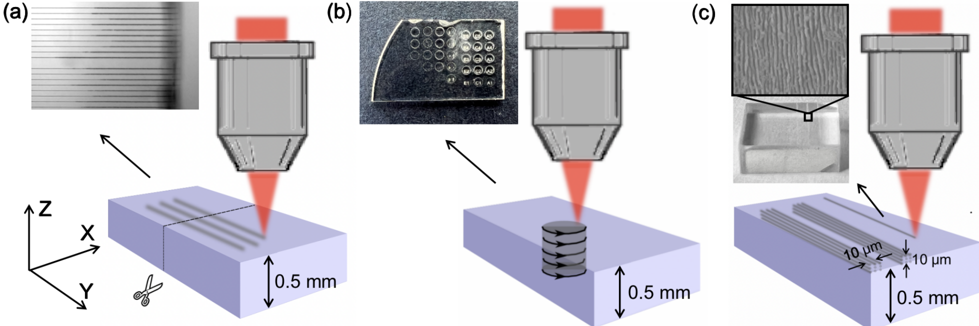

Figure 1. The schemes and the resulting pictures after the etching of performed experiments. (**a**) Single lines experiment when lines from a single scanning are written in the volume of material to test the etching rate of modified material. (**b**) Scheme of 3D experiments when cylindrical structures are written through the whole plate thickness. (**c**) Laser-induced surface changes for modification morphology observation after the etching procedure.

3. Results

The results of single line tests are discussed first. The results of this experiment are shown in Figure 2a. After a single lines investigation, we have found that the highest etching rate (200 µm/h) is obtained with an H_2SO_4 and H_3PO_4 mixture when the material is irradiated with 1st harmonic radiation and the highest tested pulse energy of 500 nJ, which corresponds to 28.2 J/cm^2 energy density. Meanwhile, lower etching rates up to 100 µm/h were obtained with NaOH and KOH enchant. The lowest etching rates of up to 50 µm/h were demonstrated by modifications etched with HF. In all the cases, the modification written with 1st harmonic radiation showed the highest etching rates, which was at least a few percent higher than those of the results achieved with the 2nd harmonic, and at least a few times higher than the etching rates obtained with the 3rd harmonic. This result could be explained by the higher periodicity of the nanogratings. The nanogratings' period is equal to $\lambda/2n$, where λ is the wavelength of used radiation and n- is the refractive index of the material [49]. Nanogratings are the result of the interaction between the plasma induced by laser radiation and consecutive pulses in the pulse train. Induced electron plasma waves inside the material interfere with incident radiation to produce interference patterns [45,50] that result in permanent periodic modifications. Subsequently, longer periods that result from higher wavelengths enable easier liquid penetration into the nanogratings due to the capillary forces and surface-wetting properties [27]. Etching rates that were only slightly lower than the maximum results were achieved by using 2nd harmonic 500 nJ pulse energy or 28.2 J/cm^2 energy density radiation. Meanwhile, modifications created by the 3rd harmonic radiation show only a few µm/h etching rates. To fabricate 3D structures, the etching rate of modified versus unmodified regions also matters. A high ratio between modified and unmodified material etching rates is required to obtain a high aspect ratio of fabricated structure features. The unmodified material etching rate was evaluated and, subsequently, the selectivity value could be calculated. For some tested

etchants, the unmodified material etching rate value was in the range of the accuracy of the used device. Therefore, only approximate selectivity values are provided. The results of the unmodified material etching rate and the evaluation of selectivity are shown in Figure 2b. Only the H_2SO_4 and H_3PO_4 mixture showed a significant unmodified material etching rate of around 3 µm/h. Meanwhile, unmodified material could be barely etched by using NaOH, KOH, or HF. When we try to evaluate selectivity with such a low unmodified material etching rate for NaOH, KOH, and HF, it leads to high selectivity values starting from 1000. The high etching rate of unmodified material with sulphuric and phosphoric acid leads to a low selectivity value of 66; despite that, this etchant shows the highest etching rate of modified material.

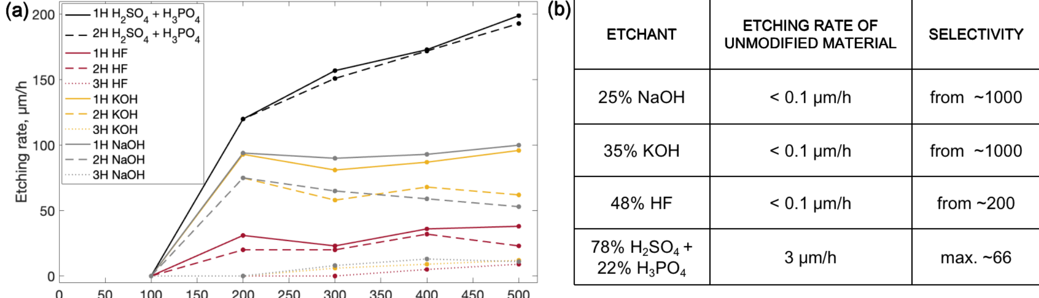

ETCHANT	ETCHING RATE OF UNMODIFIED MATERIAL	SELECTIVITY
25% NaOH	< 0.1 µm/h	from ~1000
35% KOH	< 0.1 µm/h	from ~1000
48% HF	< 0.1 µm/h	from ~200
78% H_2SO_4 + 22% H_3PO_4	3 µm/h	max. ~66

Figure 2. (**a**) Graphs of etchings rates of single lines written and etched by different processing protocols. 1H, 2H and 3H stand for 1st, 2nd and 3rd harmonics of 1030 nm wavelength laser, which is 1030 nm, 515 nm and 343 nm, respectively. (**b**) Table of the etching rate of unmodified material etched by different etchants and selectivity evaluation according to modified and unmodified material etching rate results.

In this work, our main goal is to demonstrate 3D structures that come out of sapphire. Thus, after single lines tests, 3D tests were performed to find out the protocol that could allow us to obtain 3D structures. Identical parameters set for the single lines test were investigated. Additionally, various pulse durations were tested. Cylindrical structures through the whole sample depth were written into a 500 µm thickness sapphire plate by changing parameters for each cylinder. The results of this experiment can be seen in Figure 3. The 3D experiment has shown that the best parameters, which allow the most efficient etching of the structures, are 1st harmonic radiation with 200 fs duration pulses and 300–500 nJ pulse energies that correspond to 16.9–28.2 J/cm^2 energy densities of one pulse. The only etchant which etched the structures out of the plate was a H_2SO_4 and H_3PO_4 mixture. By using other tested etchants KOH, NaOH and HF, cylindrical structures could not be etched out of the plate even after 48 h of etching. This result raised the question of what is the reason the other tested etchants cannot etch out 3D structures.

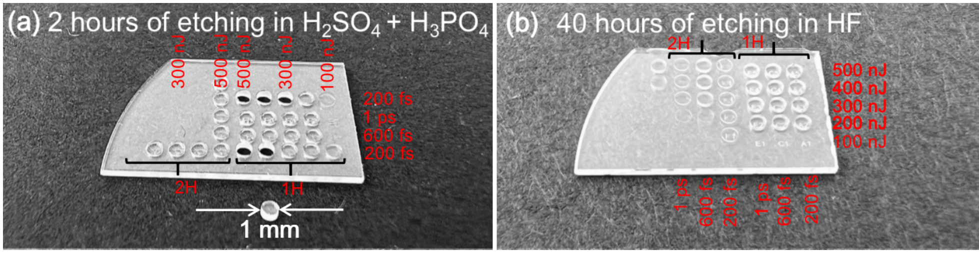

Figure 3. Cylindrical structures written with different wavelengths and pulse duration radiation. (**a**) Structure etched in H_2SO_4 and H_3PO_4 mixture, (**b**) structure etched in HF acid.

To test this phenomenon, it was decided to investigate etched and unetched surface modifications and indicate its behavior before and after the etching. Surface modifications were written within the parameter set determined as the most efficient in the previous experiment (1030 nm wavelength radiation, 600 kHz pulse repetition rate, 200 fs pulse duration, and 500 nJ pulse energy). Written 10 µm deep and 10 µm wide modifications on the surface of the sample were etched in different etchants. Scanning electron microscope (SEM) pictures of variously etched and unetched modifications are presented in Figure 4. Moreover, the depth of the etched modifications were measured in each case. In Figure 4a, an unetched modification can be seen right after the laser processing. Before the etching, material modifications are covered by residue remaining after the processing. The unetched modification already has a depth of approximately 0.5 µm. After 1 h of etching in 35% of KOH and 25% of NaOH at 90 °C and at 48% of HF, all the residue is etched and nanogratings are uncovered. Pictures of nanogratings after the etching are depicted in Figure 4b–d. Depths of modifications etched in KOH, NaOH and HF are 3 µm, 3 µm and 7 µm, respectively. In contrast, after the etching modification only for 20 min in the H_2SO_4 and H_3PO_4 mixture, not only is there residue of lasering, but the nanogratings themselves are etched, which can be seen in Figure 4e. The depth of the etched groove is 9 µm. All these etchants react to material differently. Visually, HF etches out impurities from the surface the most efficiently, meanwhile, after etching in NaOH, the highest amount of residue remains. In comparison with single lines results, HF tends to etch everything from the surface, NaOH and KOH tends to penetrate inside nanogratings. Nevertheless, none of these etchants does etch nanogratings, or in other words, walls between laser-created pores. Thus, KOH, NaOH, and HF etchants cannot etch out 3D structures because part of the laser affected material remains unetched. This insight provokes us to think that not all material in nanogratings becomes amorphous or the amorphized material partly recrystallizes after laser-material interaction stops. Due to the crystalline phase dominant in the nanogratings, HF, KOH and NaOH cannot be used effectively because it does not etch crystalline sapphire, as shown in Figure 2. On the other hand, H_2SO_4 and H_3PO_4 could etch both crystalline and amorphous materials.

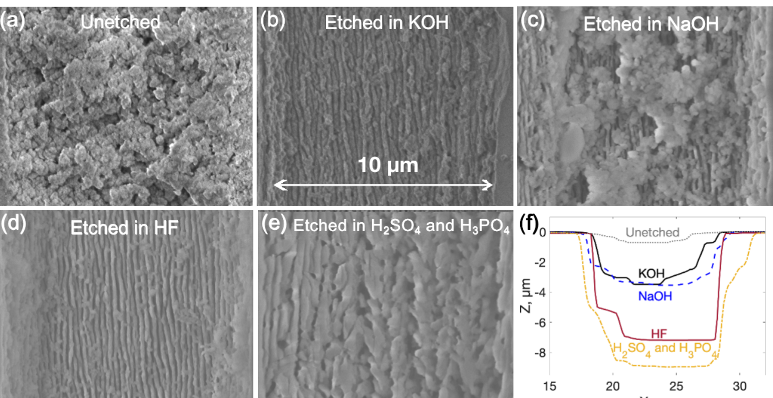

Figure 4. SEM pictures of laser-irradiated surface morphologies and measured profiles of the processed material. (**a**) Unetched surface modification, (**b**) surface modification etched in 35% KOH solution for 1 h, (**c**) surface modification etched in 25% NaOH solution for 1 h, (**d**) surface modification etched in 48% HF for 1 h, and (**e**) surface modification etched in H_2SO_4 and H_3PO_4 for 20 min. (**f**) Optical profilometer measured processed profiles of all presented modifications.

After all the previous insights were made, the most efficient tested protocol was used for structure fabrication out of crystalline sapphire. A few basic 3D structures were fabricated for demonstration. These structures were fabricated out of a 0.5 mm C-cut

sapphire plate using H_2SO_4 and H_3PO_4 mixtures as an enchant. The first demonstrational structure was a hole array. In one case, holes of 100 μm diameter through the complete height of the plate with a pitch of 1 mm were produced, see Figure 5a,b. Additionally, a narrow single Z scanning line channels fabrication with a pitch of 10 μm is demonstrated in Figure 5c,d. In Figure 5, it can be seen that, after the etching, the etched walls are not perfectly vertical. The edges of the structure have non-written planes cut and it forms after the etching due to the sapphire crystalline lattice. This is caused by the high etching rate of unmodified crystalline material. Subsequently, the honeycomb structure was produced out of sapphire. A structure with a 400 μm wall of hexagon and a 200 μm wall thickness between hexagons is shown in Figure 5e–g. The surface roughness of the mentioned structure was measured using an optical profilometer by placing the structure on its side giving a value of 300 nm RMS. This value is comparable with those shown in fused silica SLE-made surfaces [51]. The lowest demonstrated etched fused silica surface roughness is approximately 100 nm RMS. Surface roughness is mostly determined by the morphology of induced nanogratings and how effectively material between nanogratings could be etched. Since fused silica is a less chemically inert material than sapphire, the expected etched sapphire structure roughness should be higher than for the same surfaces made in fused silica. To show the versatility of this technology, similar honeycomb designs with 100 μm and 50 μm wall thicknesses were also made (Figure 5h,i). Walls thinner than 50 μm were fragile and did not survive the etching procedure. Since we were working with crystalline sapphire, it shows different etching rates of unmodified material in various crystalline orientations [43]. Thus, the tendency of a repeating sapphire crystalline structure can be seen in honeycomb structures. The edges of etched structures appear to have a chamfer and are inclined according to a sapphire crystalline lattice. Nonetheless, these structures show the possibility of producing 3D structures out of crystalline sapphire. Due to the high mechanical and chemical resistance of sapphire, such structures show potential as micromechanical components in complex miniaturized systems.

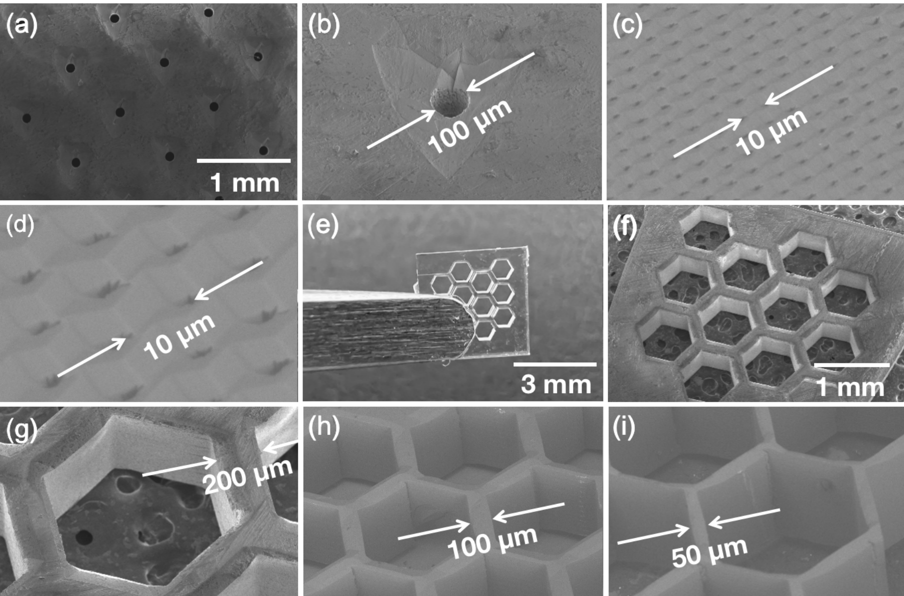

Figure 5. Structures fabricated out of crystalline C-cut sapphire. (**a**,**b**) 100 μm diameter hole matrix, (**c**,**d**) single line 10 μm pitch hole matrix, (**e**–**g**) honeycomb structure where the side of the hexagon is 400 μm, and the walls between hexagon are 200 μm, (**h**,**i**) similar hexagon structure with diminished walls between hexagon respectively 100 μm and 50 μm.

4. Discussion

In SLE, we always desire to have high selectivity and a high etching rate. High selectivity values are needed to maintain good accuracy and a high aspect ratio of etched features. On the other hand, a high etching rate is required for fast processes. The main problem is that, usually, these two are achieved with different etching protocols. This means that, at the same time, we cannot obtain both, but in one structure, it is possible to combine both etching protocols. For fused silica, this was already demonstrated [52] when structure parts that do not require precision are etched with HF and precise features are etched with KOH solutions which give the highest selectivity. The same could be done with the etching of sapphire by combining KOH, NaOH, or HF etching with a sulphuric and phosphoric acid mixture. In that way, etching time with H_2SO_4 and H_3PO_4 can be minimized and, as a result, higher accuracy could be obtained.

5. Conclusions

In this work, we have presented a comparison between different sapphire SLE processing algorithms. During previously shown tests, various laser parameters for creating laser-irradiated volume were tested. The best results were obtained with 1030 nm wavelength 200 fs pulse duration radiation, which could be explained by higher periodicity nanogratings and easier etchant penetration. Moreover, four different etchants—HF, NaOH, KOH, and H_2SO_4 with H_3PO_4—were tested. The only etchant which allows the total removal of laser-modified sapphire is a H_2SO_4 with H_3PO_4 mixture, while the other tested etchants only etch material in between laser-formed nanogratings. After a moderate protocol, a few structures were found: hole matrix and honeycomb structures were fabricated out of C-cut crystalline sapphire. We noticed that sapphire repeats its crystalline lattice during the etching due to different etching rates in separate crystalline orientations. This property leads to less accurate features of the fabricated object and self-organized patterns on the structure's surface. However, this effect could be diminished by combining two different etching steps for the same structure. Thus, in this work, we have demonstrated a protocol that allows 3D structure formation out of crystalline sapphire. However, additional improvements, such as etching protocol optimization or combined etching development, could be made to the protocol to refine the quality of the produced structures. These results will contribute to the rapid SLE fabrication of future devices.

Author Contributions: A.B. planned and led the research, fabricated demonstration structures, did part of the measurements, and prepared publication and figures. R.S. performed etching procedures. R.S., D.G., D.P. and V.S. consulted and contributed in publication preparation. All authors have read and agreed to the published version of the manuscript.

Funding: This research was funded by the European Regional Development Fund (project 01.2.2-LMT-K-718-03-0029) with the Research Council of Lithuania.

Institutional Review Board Statement: Not applicable.

Informed Consent Statement: Not applicable.

Data Availability Statement: Not applicable.

Conflicts of Interest: The authors declare no conflict of interest.

References

1. Gedvilas, M.; Mikšys, J.; Berzinš, J.; Stankevič, V.; Račiukaitis, G. Multi-photon absorption enhancement by dual-wavelength double-pulse laser irradiation for efficient dicing of sapphire wafers. *Sci. Rep.* **2017**, *7*, 1–10. [CrossRef] [PubMed]
2. Kudrius, T.; Šlekys, G.; Juodkazis, S. Surface-texturing of sapphire by femtosecond laser pulses for photonic applications. *J. Phys. D Appl. Phys.* **2010**, *43*, 145501. [CrossRef]
3. Qi, L.; Nishii, K.; Yasui, M.; Aoki, H.; Namba, Y. Femtosecond laser ablation of sapphire on different crystallographic facet planes by single and multiple laser pulses irradiation. *Opt. Lasers Eng.* **2010**, *48*, 1000–1007. [CrossRef]
4. Song, Y.; Wang, C.; Dong, X.; Yin, K.; Zhang, F.; Xie, Z.; Chu, D.; Duan, J. Controllable superhydrophobic aluminum surfaces with tunable adhesion fabricated by femtosecond laser. *Opt. Laser Technol.* **2018**, *102*, 25–31. [CrossRef]

5. Jia, X.; Chen, Y.; Liu, L.; Wang, C.; Duan, J. Combined pulse laser: Reliable tool for high-quality, high-efficiency material processing. *Opt. Laser Technol.* **2022**, *153*, 108209. [CrossRef]
6. Ding, K.; Wang, C.; Li, S.; Zhang, X.; Lin, N.; Duan, J. Large-area cactus-like micro-/nanostructures with anti-reflection and superhydrophobicity fabricated by femtosecond laser and thermal treatment. *Surf. Interfaces* **2022**, *33*, 102292. [CrossRef]
7. Ding, K.; Wang, C.; Li, S.; Zhang, X.; Lin, N.; Duan, J. Single-Step femtosecond laser structuring of multifunctional colorful metal surface and its origin. *Surf. Interfaces* **2022**, *34*, 102386. [CrossRef]
8. Li, Y.; Liu, H.; Hong, M. High-quality sapphire microprocessing by dual-beam laser induced plasma assisted ablation. *Opt. Express* **2020**, *28*, 6242–6250. [CrossRef]
9. Chen, J.; Lu, X.; Li, Z.; Wen, Q.; Lu, J.; Jiang, F. Anisotropy of material removal during laser-induced plasma assisted ablation of sapphire. *Ceram. Int.* **2022**, *48*, 13880–13889. [CrossRef]
10. Ding, X.; Sato, T.; Kawaguchi, Y.; Niino, H. Laser-Induced Backside Wet Etching of Sapphire. *Jpn. J. Appl. Phys.* **2003**, *42*, L176–L178. [CrossRef]
11. Tsvetkov, M.Y.; Minaev, N.V.; Akovantseva, A.A.; Timashev, P.S.; Muslimov, A.E.; Kanevskii, V.M. Thermoplasmonic laser-induced backside wet etching of sapphire. *Quantum Electron.* **2019**, *49*, 133–140. [CrossRef]
12. Zhigalina, O.; Khmelenin, D.N.; Atanova, A.V.; Minaev, N.V.; Sviridov, A.P.; Tsvetkov, M.Y. A Nanoscale Modification of Materials at Thermoplasmonic Laser-Induced Backside Wet Etching of Sapphire. *Plasmonics* **2020**, *15*, 599–608. [CrossRef]
13. Liu, X.; Zhang, Y.; Li, Q.; Zheng, J.; Lu, Y.; Juodkazis, S.; Chen, Q.; Sun, H. Biomimetic sapphire windows enabled by inside-out femtosecond laser deep-scribing. *PhotoniX* **2022**, *3*, 1. [CrossRef]
14. Cao, X.; Lu, Y.; Fan, H.; Xia, H.; Zhang, L.; Zhang, Y. Wet-etching-assisted femtosecond laser holographic processing of a sapphire concave microlens array. *Appl. Opt.* **2018**, *57*, 9604–9608. [CrossRef]
15. Lu, Y.M.; Liu, X.Q.; Zhu, L.; Chen, Q.D.; Juodkazis, S.; Sun, H.B. Vector scanning subtractive manufacturing technology for laser rapid fabrication. *Opt. Lett.* **2021**, *46*, 1. [CrossRef]
16. Li, Q.; Chen, Q.; Niu, L.; Yu, Y.; Wang, L.; Sun, Y.; Sun, H. Sapphire-Based Dammann Gratings for UV Beam Splitting. *IEEE Photon. J.* **2016**, *8*, 2500208. [CrossRef]
17. Li, Q.; Yu, Y.; Wang, L.; Cao, X.; Liu, X.; Sun, Y.; Chena, Q.; Duan, J.; Sun, H. Sapphire-Based Fresnel Zone Plate Fabricated by Femtosecond Laser Direct Writing and Wet Etching. *IEEE Photon. Technol. Lett.* **2016**, *28*, 1290–1293. [CrossRef]
18. Gottumukkala, N.R.; Gupta, M.C. Laser processing of sapphire and fabrication of diffractive optical elements. *Appl. Opt.* **2022**, *61*, 2391–2397. [CrossRef]
19. Marcinkevičius, A.; Juodkazis, S.; Watanabe, M.; Miwa, M.; Matsuo, S.; Misawa, H.; Nishii, J. Femtosecond laser-assisted three-dimensional microfabrication in silica. *Opt. Lett.* **2001**, *26*, 277–279. [CrossRef]
20. Chen, Y.; Chen, Y.; Long, J.; Shi, D.; Chen, X.; Hou, M.; Gao, J.; Liu, H.; He, Y.; Fan, B.; et al. Achieving a sub-10 nm nanopore array in silicon by metal-assisted chemical etching and machine learning. *Int. J. Extrem. Manuf.* **2021**, *3*, 035104. [CrossRef]
21. Shi, D.; Chen, Y.; Li, Z.; Dong, S.; Li, L.; Hou, M.; Liu, H.; Zhao, S.; Chen, X.; Wong, C.P.; et al. Anisotropic Charge Transport Enabling High-Throughput and High-Aspect-Ratio Wet Etching of Silicon Carbide. *Small Methods* **2022**, *6*, 2200329. [CrossRef] [PubMed]
22. Hermans, M.; Gottmann, J.; Riedel, F. Selective, Laser-Induced Etching of Fused Silica at High Scan-Speeds Using KOH. *J. Laser. Micro. Nanoeng.* **2014**, *9*, 126 – 131. [CrossRef]
23. Ross, C.A.; MacLachlan, D.G.; Choudhury, D.; Thomson, R.R. Optimisation of ultrafast laser assisted etching in fused silica. *Opt. Express* **2018**, *26*, 24343–24356. [CrossRef]
24. Qi, J.; Wang, Z.; Xu, J.; Lin, Z.; Li, X.; Chu, W.; Cheng, Y. Femtosecond laser induced selective etching in fused silica: Optimization of the inscription conditions with a high-repetition-rate laser source. *Opt. Express* **2018**, *26*, 29669–29678. [CrossRef]
25. Li, X.; Xu, J.; Lin, Z.; Qi, J.; Wang, P.; Chu, W.; Fang, Z.; Wang, Z.; Chai, Z.; Cheng, Y. Polarization-insensitive space-selective etching in fused silica induced by picosecond laser irradiation. *Appl. Surf. Sci.* **2019**, *485*, 188–193. [CrossRef]
26. Stankevič, V.; Račiukaitis, G.; Gečys, P. Chemical etching of fused silica after modification with two-pulse bursts of femtosecond laser. *Opt. Express* **2021**, *29*, 31393–31407. [CrossRef]
27. Butkutė, A.; Baravykas, T.; Stančikas, J.; Tičkūnas, T.; Vargalis, R.; Paipulas, D.; Sirutkaitis, V.; Jonušauskas, L. Femtosecond Laser Assisted 3D Etching Using Inorganic-Organic Etchant. *Materials* **2022**, *15*, 2817. [CrossRef]
28. Bellouard, Y. Shape memory alloys for microsystems: A review from a material research perspective. *Mater. Sci. Eng. A* **2008**, *481–482*, 582–589. [CrossRef]
29. Butkutė, A.; Baravykas, T.; Stančikas, J.; Tičkūnas, T.; Vargalis, R.; Paipulas, D.; Sirutkaitis, V.; Jonušauskas, L. Optimization of selective laser etching (SLE) for glass micromechanical structure fabrication. *Opt. Express* **2021**, *29*, 23487–23499. [CrossRef]
30. Sugioka, K.; Cheng, Y.; Midorikawa, K. Three-dimensional micromachining of glass using femtosecond laser for lab-on-a-chip device manufacture. *Appl. Phys. A* **2005**, *81*, 1 – 10. [CrossRef]
31. Gottmann, J.; Hermans, M.; Repiev, N.; Ortmann, J. Selective Laser-Induced Etching of 3D Precision Quartz Glass Components for Microfluidic Applications-Up-Scaling of Complexity and Speed. *Micromachines* **2017**, *8*, 110. [CrossRef]
32. Kim, J.; Kim, S.; Joung, Y.; Choi, J.; Koo, C. Two-step hybrid process of movable part inside glass substrate using ultrafast laser. *Micro Nano Syst. Lett.* **2021**, *9*, 2213–9621. [CrossRef]

33. Choudhury, D.; Ródenas, A.; Paterson, L.; Jaque, D.; Kar, A.K. 3D microfabrication in YAG crystals by direct laser writing and chemical etching. In *Conference on Lasers and Electro-Optics/Pacific Rim*; Optical Society of America: Washington, DC, USA, 2013; p. WPE_14.
34. Rodenas, A.; Gu, M.; Corrielli, G.; Paie, P.; John, S.; Kar, A.K.; Osellame, R. Three-dimensional femtosecond laser nanolithography of crystals. *Nat. Photon.* **2019**, *13*, 105–109. [CrossRef]
35. Hasse, K.; Huber, G.; Kränkel, C. Selective etching of fs-laser inscribed high aspect ratio microstructures in YAG. *Opt. Mater. Express* **2019**, *9*, 3627–3637. [CrossRef]
36. Matsuo, S.; Tabuchi, Y.; Okada, T.; Juodkazis, S.; Misawa, H. Femtosecond laser assisted etching of quartz: Microstructuring from inside. *Appl. Phys. A* **2006**, *84*, 99–102. [CrossRef]
37. Juodkazis, S.; Nishi, Y.; Misawa, H. Femtosecond laser-assisted formation of channels in sapphire using KOH solution. *Phys. Status Solidi RRL* **2008**, *2*, 275–277. [CrossRef]
38. Matsuo, S.; Tokumi, K.; Tomita, T.; Hashimoto, S. Three-Dimensional Residue-Free Volume Removal inside Sapphire by High-Temperature Etching after Irradiation of Femtosecond Laser Pulses. *Laser Chem.* **2008**, *2008*, 892721–1–892721–4. [CrossRef]
39. Moser, R.; Ojha, N.; Kunzer, M.; Schwarz, U.T. Sub-surface channels in sapphire made by ultraviolet picosecond laser irradiation and selective etching. *Opt. Express* **2011**, *19*, 24738–24745. [CrossRef]
40. Wortmann, D.; Gottmann, J.; Brandt, N.; Horn-Solle, H. Micro- and nanostructures inside sapphire by fs-laser irradiation and selective etching. *Opt. Express* **2008**, *16*, 1517 – 1522. [CrossRef]
41. Horstmann-Jungemann, M.; Gottmann, J.; Wortmann, D. Nano- and Microstructuring of SiO_2 and Sapphire with Fs-laser Induced Selective Etching. *J. Laser. Micro. Nanoeng.* **2009**, *4*, 135–140. [CrossRef]
42. Hörstmann-Jungemann, M.; Gottmann, J.; Keggenhoff, M. 3D-Microstructuring of Sapphire using fs-Laser Irradiation and Selective Etching. *J. Laser. Micro. Nanoeng.* **2010**, *5*, 145–149. [CrossRef]
43. Capuano, L.; Berenschot, J.; Tiggelaar, R.M.; Feinaeugle, M.; Tas, N.R.; Gardeniers, H.J.; Römer, G.W.R. Fabrication of Microstructures in the Bulk and on the Surface of Sapphire by Anisotropic Selective Wet Etching of Laser Affected Volumes. *J. Micromech. Microeng.* **2022**, *32*, 125003. [CrossRef]
44. Casamenti, E.; Pollonghini, S.; Bellouard, Y. Few pulses femtosecond laser exposure for high efficiency 3D glass micromachining. *Opt. Express* **2021**, *29*, 35054–35066. [CrossRef] [PubMed]
45. Gottmann, J.; Wortmann, D.; Hörstmann-Jungemann, M. Fabrication of sub-wavelength surface ripples and in-volume nanostructures by fs-laser induced selective etching. *Appl. Surf. Sci.* **2009**, *255*, 5641–5646. [CrossRef]
46. Hnatovsky, C.; Taylor, R.S.; Simova, E.; Rajeev, P.P.; Rayner, D.M.; Bhardwaj, V.; Corkum, P.B. Fabrication of microchannels in glass using focused femtosecond laser radiationand selectivechemical etching. *Appl. Phys. A* **2006**, *84*, 47–61. [CrossRef]
47. Capuanoa, L.; Tiggelaar, R.; Berenschot, J.; Gardeniers, J.; Römer, G. Fabrication of millimeter-long structures in sapphire using femtosecond infrared laser pulses and selective etching. *Opt. Laser Eng.* **2020**, *133*, 106114. [CrossRef]
48. Zhang, Y.; Li, Z.; Xu, H.; Zheng, S.; Qi, T.; Li, H. Sub-molten salt environmentally benign technology. In Proceedings of the 100th AICHE Annual Meeting, Philadelphia, PA, USA, 16–21 November 2008.
49. Bhardwaj, V.R.; Simova, E.; Rajeev, P.P.; Hnatovsky, C.; Taylor, R.S.; Rayner, D.M.; Corkum, P.B. Optically Produced Arrays of Planar Nanostructures inside Fused Silica. *Phys. Rev. Lett.* **2006**, *96*, 057404. [CrossRef]
50. Zhang, B.; Liu, X.; Qiu, J. Single femtosecond laser beam induced nanogratings in transparent media—Mechanisms and applications. *J. Mater.* **2019**, *5*, 1–14. [CrossRef]
51. Butkus, S.; Rickus, M.; Sirutkaitis, R.; Paipulas, D.; Sirutkaitis, V. Fabrication of High Aspect Ratio Channels in Fused Silica Using Femtosecond Pulses and Chemical Etching at Different Conditions. *J. Laser Micro. Nanoen.* **2019**, *14*, 19–24.
52. LoTurco, S.; Osellame, R.; Ramponi, R.; Vishnubhatla, K.C. Hybrid chemical etching of femtosecond laser irradiated structures for engineered microfluidic devices. *J. Micromech. Microeng.* **2013**, *23*, 1–8. [CrossRef]

Disclaimer/Publisher's Note: The statements, opinions and data contained in all publications are solely those of the individual author(s) and contributor(s) and not of MDPI and/or the editor(s). MDPI and/or the editor(s) disclaim responsibility for any injury to people or property resulting from any ideas, methods, instructions or products referred to in the content.

V

COMBINED FEMTOSECOND LASER GLASS MICROPROCESSING FOR LIVER-ON-CHIP DEVICE FABRICATION

A. Butkutė, T. Jurkšas, T. Baravykas, B. Leber,
G. Merkininkaitė, R. Žilėnaitė, D. Čereška, A. Gulla,
M. Kvietkauskas, K. Marcinkevičiūtė, P. Schemmer and K. Strupas
Materials 16(6), 2174–2183 (2023).

Article

Combined Femtosecond Laser Glass Microprocessing for Liver-on-Chip Device Fabrication

Agnė Butkutė [1,2,*], Tomas Jurkšas [1], Tomas Baravykas [1], Bettina Leber [3], Greta Merkininkaitė [1,4], Rugilė Žilėnaitė [1], Deividas Čereška [1], Aiste Gulla [5], Mindaugas Kvietkauskas [5], Kristina Marcinkevičiūtė [5], Peter Schemmer [3] and Kęstutis Strupas [5]

[1] Femtika Ltd., Keramikų Str. 2, LT-10233 Vilnius, Lithuania
[2] Laser Research Center, Vilnius University, Saulėtekio Ave. 10, LT-10223 Vilnius, Lithuania
[3] General, Visceral and Transplant Surgery, Department of Surgery, Medical University of Graz, Auenbruggerplatz 29, AT-8036 Graz, Austria
[4] Faculty of Chemistry and Geosciences, Vilnius University, Naugarduko Str. 24, LT-03225 Vilnius, Lithuania
[5] Institute of Clinical Medicine, Faculty of Medicine, Center of Visceral Medicine and Translational Research,Vilnius University, M. K. Čiurlionio g. 21, LT-03101 Vilnius, Lithuania
* Correspondence: agne.butkute@femtika.com

Abstract: Nowadays, lab-on-chip (LOC) devices are attracting more and more attention since they show vast prospects for various biomedical applications. Usually, an LOC is a small device that serves a single laboratory function. LOCs show massive potential for organ-on-chip (OOC) device manufacturing since they could allow for research on the avoidance of various diseases or the avoidance of drug testing on animals or humans. However, this technology is still under development. The dominant technique for the fabrication of such devices is molding, which is very attractive and efficient for mass production, but has many drawbacks for prototyping. This article suggests a femtosecond laser microprocessing technique for the prototyping of an OOC-type device—a liver-on-chip. We demonstrate the production of liver-on-chip devices out of glass by using femtosecond laser-based selective laser etching (SLE) and laser welding techniques. The fabricated device was tested with HepG2(GS) liver cancer cells. During the test, HepG2(GS) cells proliferated in the chip, thus showing the potential of the suggested technique for further OOC development.

Keywords: selective laser etching; 3D laser microfabrication; laser welding; glass microfluidics; femtosecond laser microprocessing

Citation: Butkutė, A.; Jurkšas, T.; Baravykas, T.; Leber, B.; Merkininkaitė, G.; Žilėnaitė, R.; Čereška, D.; Gulla, A.; Kvietkauskas, M.; Marcinkevičiūtė, K.; et al. Combined Femtosecond Laser Glass Microprocessing for Liver-on-Chip Device Fabrication. *Materials* **2023**, *16*, 2174. https://doi.org/10.3390/ma16062174

Academic Editors: Tsung-Yuan Kuo and Hong-Chuong Tran

Received: 15 February 2023
Revised: 3 March 2023
Accepted: 7 March 2023
Published: 8 March 2023

Copyright: © 2023 by the authors. Licensee MDPI, Basel, Switzerland. This article is an open access article distributed under the terms and conditions of the Creative Commons Attribution (CC BY) license (https://creativecommons.org/licenses/by/4.0/).

1. Introduction

Nowadays, a remarkable idea in medical treatment and diagnostics is that of lab-on-chip (LOC) devices, which allow the miniaturization of massive diagnostic tools and the reduction of testing on live organisms. The LOC technology has become more and more promising as an innovation in the research field because of such devices' functionality. Usually, a single chip is integrated with one or several laboratory functions, allowing laboratory processes to proceed quickly with high precision. In combination with the working principles of microfluidics, these devices show potential in health applications, medicine, and more. The designs and applications go in various directions—for example, injection-molded polymeric LOC for blood plasma separation [1], plastic LOC for herbicide residue monitoring in soil [2], and devices for the detection of various pathogens in food [3,4], for the detection of viruses [5,6], and for the detection of bacteria [7]. The applications of LOC devices do not end here; they could be used for research on various cells, such as research on the growth of fungal cultures [8] or on cancer and tumor cells [9–11]. LOC devices could also be used for tissue or organ research. These devices are usually called organ-on-chips [12] or organoids-on-chips (OOCs); as the name suggests, these are chips with an organ/organ tissue that is grown inside the chip and will later be used for various

tests, such as tests on drugs [13,14], toxins [15], and others [16]. One example is a liver-on-chip device [17]. OOC devices are becoming more popular because of their versatility and advantages in comparison with usual testing methods. LOC devices are rapidly merging directions. However, this is still an open area for innovations—from new materials to innovative design research.

The dominant technology in the production of such devices is molding [18,19]. On one hand, molding is a very effective and cheap technique for mass production [20]. Molded chips can cost a few euros per piece. On the other hand, the price can increase by many times (even hundreds of times) for prototyping when new master structures are needed for any changes in the chip design. We propose an alternative solution based on ultrafast laser material processing in this work. Even though laser micromachining is quite an expensive process, with which the price of a chip could be in the range of tens to hundreds of euros, it is a good tool for the prototyping of complex devices. Femtosecond-pulse lasers are a powerful tool and bring a few significant advantages for material processing, such as high precision and high quality. In addition, this tool leads to entirely new microprocessing techniques based on nonlinear material–light interactions, which are impossible with other tools. One example is the multi-photon polymerization [21,22] technique, which enables the fabrication of hundreds of 3D structures with nanometer precision and resolution out of polymers. Furthermore, a femtosecond laser is an excellent tool for glass microprocessing. Due to nonlinear light–material interactions, glass can be modified directly in the volume without damaging its surface [23]. A few different modifications can be created inside a volume of glass: changes in the refractive index [24], nanogratings [25], or microvoids [26]. The type of modification induced depends on the radiation intensity used [24]. However, each type of modification can be used for the microprocessing of different materials. For instance, by inscribing a refractive index or nanogratings, refractive optical elements can be formed [27]. A combination of the inscription of nanogratings with subsequent selective laser etching (SLE) could be implemented [28,29]. Meanwhile, microvoid modifications were formed during laser ablation [30] to remove a material directly or during the laser welding process [31] to bond two materials together in their contact. Therefore, many different tasks could be accomplished with a single femtosecond laser source.

This study demonstrates a combination of a few different femtosecond glass microprocessing techniques for liver-on-chip device manufacturing. Here, we combine the selective laser etching and welding techniques to produce a liver-on-chip device. At the end, we provide the results of tests on the manufactured devices.

2. Materials and Methods

The main idea was to create an OOC prototype that is suitable for liver-on-chip testing by using femtosecond laser microprocessing methods. First of all, the concept of the device design was chosen. The central principle was to create a microfluidic system with three individual channels that were separated in the center with filters. The center channel needed to be filled with liver cells. Meanwhile, the side channels could be filled with other materials, such as drugs or different types of cells. The reactions between liver cells and the drug could be observed in the mentioned chip area. A similar design concept with pillar filters has already been published elsewhere [32]. However, the design of the microfluidic channels was significantly changed. The critical requirements in microfluidics are keeping channels as short as possible and avoiding microwells, dead-ends, or sharp forms in the channels. The microfluidic chip design that was created is shown in Figure 1. These adjustments make microfluidic systems more user friendly because the channels can be filled without sophisticated microfluidic pumps. In the described experiments, simple lab pipettes were used to manipulate substrates and fill the designed chip.

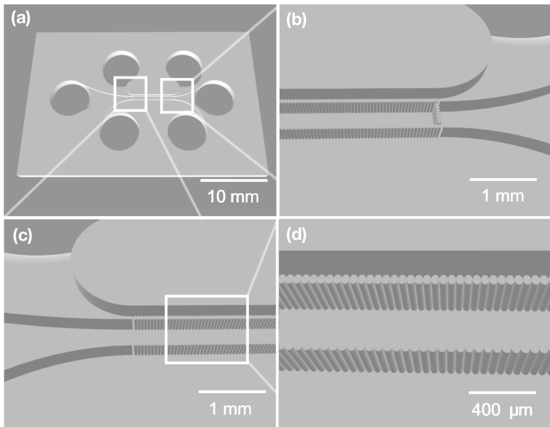

Figure 1. A picture of the liver-on-chip model that was created. (**a**) A full view of the chip model; three cylindrical holes serve as inlets for each channel, and three cylindrical holes are outlets for each of the three channels. All three channels meet in the center and are separated by a pillar-type filter. (**b**,**c**) An enlarged view of specific parts of the channel system. (**d**) Glass-type filters in the center of the chip.

For liver-on-chip fabrication, two different laser microprocessing methods were used. Plates with channel systems and integrated filters were fabricated with the SLE method. SLE is a technology that enables the production of 3D structures out of solid-state transparent materials [33,34]. The implementation of SLE consisted of several steps. First, laser-induced periodic modifications called nanogratings were formed in the volume of the material by using ultrashort pulses. Subsequently, a laser-modified material was etched out with aggressive etchants, such as hydrofluoric acid (HF) or potassium hydroxide (KOH) [35]. SLE was performed on amorphous UV-grade fused silica (UVFS) with a 1 mm thickness. The UVFS substrates were chosen for the fabrication of the channel system. Laser microfabrication was performed by using a Laser NanoFactory workstation (Femtika Ltd., Lithuania). The utilized workstation was equipped with a Yb:KGV femtosecond laser (Pharos, Light Conversion Ltd., Lithuania). For the SLE experiments, a fundamental wavelength of 1030 nm, a 700 fs pulse duration, and a frequency of 610 kHz laser radiation was used. The laser radiation was focused with 20 $\times$ 0.45 NA Nikon focusing objective equipped with automated aberration correction (add-on device from Femtika Ltd., Vilnius, Lithuania). Within specific radiation exposition conditions, modifications in porous materials called nanogratings could be inscribed inside the volume of the glass [25]. Subsequently, after inscribing particular material modifications, the sample was etched in a potassium hydroxide (KOH, Eurochemicals, Lithuania) solution at a 6 mol/L concentration with distilled water at a temperature of 90 °C. The etching protocols were optimized for the fastest etching procedure. This optimization has already been published elsewhere [36].

Since we needed an encapsulated microfluidic channel system, the channels formed on the plates had to be sealed. Another femtosecond-laser-radiation-based technique—laser welding [37,38]—was used for that. Only the contact between two plates could be affected without damaging the surface by using high-intensity radiation due to nonlinear light–material interactions. With high power, the material in the contact could be melted, and a firm connection was formed in the mentioned samples. The laser welding part was carried out with the same Laser NanoFactory workstation. The laser welding experiments are conducted with the same 1030 nm wavelength, a pulse duration of approximately 200 fs, and a 610 kHz pulse repetition rate. The laser radiation was focused with a 0.5 NA aspherical lens. After the etching and before the welding, the samples were washed in a piranha solution (4:1 *v*/*v* of sulfuric acid (95–98%, Sigma-Aldrich, Darmstadt, Germany) and

hydrogen peroxide (50%, Sigma-Aldrich, Darmstadt, Germany), respectively). Afterward, the samples were rinsed in distilled water and isopropanol. The basic scheme of the fabrication of the chips is shown in Figure 2.

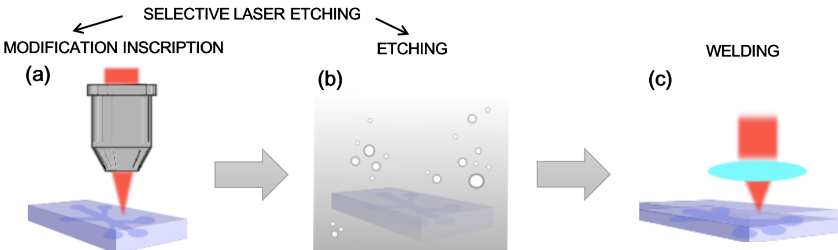

Figure 2. A basic scheme of the laser processing of the lab-on-chip devices. (**a**) Inscription of nanogratings on the glass plate by focusing light with a microscopic objective. (**b**) Subsequent etching of the laser-processed sample. (**a**,**b**) Presentation of the SLE technique. (**c**) The laser welding process used to seal the channel system with an additional glass plate.

The manufactured liver-on-chip prototypes were rinsed with sterilized aqua dest, submerged in 70% ethanol solvent for initial disinfection, and UV irradiated for 20 min for further sterilization. The chips were coated with poly-L-lysine polymers to promote cell adhesion. The coating was performed by filling the chamber with 10 µL of poly-L-lysine solution (Sigma Aldrich, Vienna, Austria) through a seeding channel, followed by an incubation period at 37 °C until they had completely dried. These prepared liver-on-chip systems were stored in standard sterile conditions until use.

The human liver HCC cell line HepG2(GS) (originating from ATCC, Rockville, MD, USA) was used for biocompatibility testing. These cells were cultivated under standard conditions (37 °C, 5% CO_2 in a humidified atmosphere) in MEM media (Gibco, Thermo Fisher Scientific, Vienna, Austria) supplemented with 10% fetal bovine serum (GE Healthcare Life Sciences, UT, USA) and 1% penicillin/streptomycin (Sigma Aldrich, Vienna, Austria). The media were renewed every other day, and cells were passaged once they grew to 80–90% confluence. The chambers of the liver-on-a-chip systems were filled with 10 µL of a cell suspension to reach 2×10^4 HepG2(GS) cells/cm² through the seeding channels. The chips were submerged in culture media in a Petri dish and placed in a cell incubator under standard conditions (37 °C, 5% CO_2 in the humidified atmosphere) overnight to avoid evaporation. Then, cell adherence and growth were determined through daily microscopic examination. The media were renewed every other day in a standard manner. Finally, the Trypan Blue exclusion test was conducted to further confirm cell viability. The total testing time frame for a single sample was nine days. This experiment was repeated three times in separate pieces. Every sample was used for a single experiment and then disposed of as waste due to the biological exhaustion of the sample.

3. Results and Discussion

3.1. Fabrication of the Microfluidic Chips

We began the research by producing microfluidic chips with integrated filters on a glass substrate. A picture of a fabricated chip and SEM pictures of its particular parts are shown in Figure 3. In general, the filter was a row of elliptical glass pillars. The dimensions of every pillar were a width of 36 µm and a length of 55 µm. The spacing between each pillar was 14 µm, corresponding to the filter's pores. The height of the fabricated pillars was 200 µm, which was identical to the depth of the microfluidic channel. The filters were integrated into a channel that was 5 mm long and 0.9 mm wide. In the mentioned area, two rows of pillars divided that zone into three distinguished channels; the side channels were 200 µm wide, and the central one was 400 µm wide.

Visually, smooth features and a high channel aspect ratio were obtained. However, not only modified but also unmodified material was etched during the etching process. Thus, this led to widened channels and features. The mentioned effect created a critical limitation of the aspect ratio, which is especially important in microfilter fabrication. Since the cells were micro-scale objects, the precision of the integrated filter was essential. In the model, the gap between pillars shown in Figure 3c,g was a single-line inscription, which was a minimal laser modification between pillars. However, after the etching, the gap between pillars tended to increase up to 14 µm, which limited the accuracy and minimal features of the filter. In LOC applications, the surface quality of the channel is also critical. This feature affects liquid flow. The higher roughness of the surface, the more friction it creates. Thus, the channels become difficult to fill due to the higher surface roughness. The surface quality of the processed channels was evaluated with an optical profilometer. The surface roughness of the etched channels was around 250 nm root mean square (RMS). The surface topology of the channel is shown in Figure 3b.

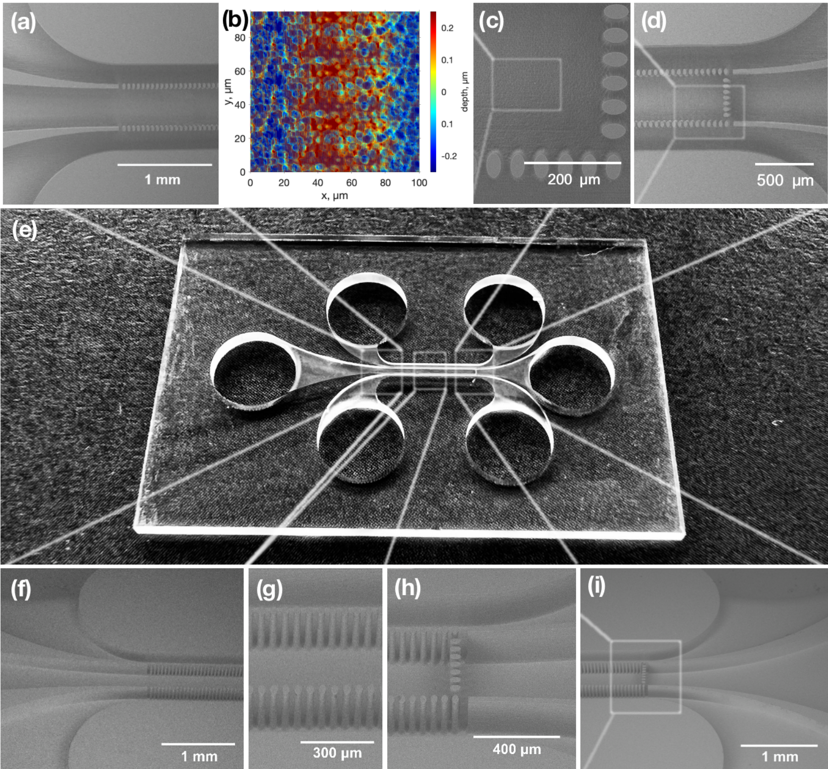

Figure 3. Pictures of the produced liver-on-chip device. (**e**) Optical picture of a full device. (**a**,**c**,**d**) SEM images of the tops of the specified chip parts. (**f**–**i**) SEM images of specified chip parts at 45°. (**b**) Surface topology of the channel surface.

3.2. Welding of the Microfluidic Chips

The chips were sealed through laser welding. Optical contact was required to create firm contact between plates. That meant that the gap between two surfaces should be a few times smaller than the wavelength used, which was 1030 nm. To achieve that, the high cleanness and surface quality of the samples was needed. Thus, the samples were washed in piranha solution to remove all organic remains from the chip. Before welding, the chip was rinsed in isopropanol and distilled water. Two glass plates were put on each other

when the chip was still wet. Isopropanol is a liquid that forms a low contact angle with glass [36], which means that it wets surfaces. Thus, due to the wet contact with isopropanol, the two plates tended to have a smaller gap between each other, which enhanced the welding quality. The two plates were welded in contact everywhere around the channel system without damaging or affecting the channels or the filers themselves. Welding seams were made within a spacing of 100 µm. An image of the welding seams around the microfluidic channels is provided in Figure 4b. An optical picture of the produced chip is shown in Figure 4a.

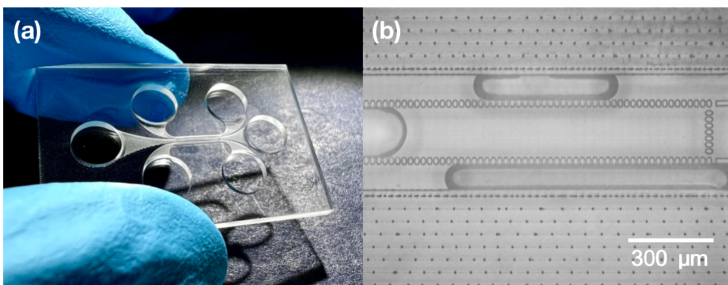

Figure 4. (**a**) Picture of a final liver-on-chip device. (**b**) Optical picture of the produced microfluidic chip part where a channel with a filter and welding seams can be observed.

It was already demonstrated that the welding strength could be close to the mechanical strength of the bulk material [38]. However, we performed an additional experiment to test the welding quality. The main idea was to affect the chip with a particular force and test what forces led to the breaking of the chip. This experiment is shown in Figure 5a,d. The force was gradually increased, and the chip broke when it was affected by a 9.3 N force. A broken chip after the test is presented in Figure 5b,e. After the sample was broken, the chip was destroyed. Nonetheless, in most places, the welding seam still held the two glass plates together. Pictures were taken of the welding seam from the side of the broken chip Figure 5c,f. The welding seam seemed to have small periodic cracks; however, the material in between seemed to be completely fused between the two plates. The provided material contributed to the statement that the strength of the welding seam was comparable to the strength of the bulk material. The welding seam was not the weakest part of the chip. The chip tended to break through the channels, which were the most fragile parts of the chip.

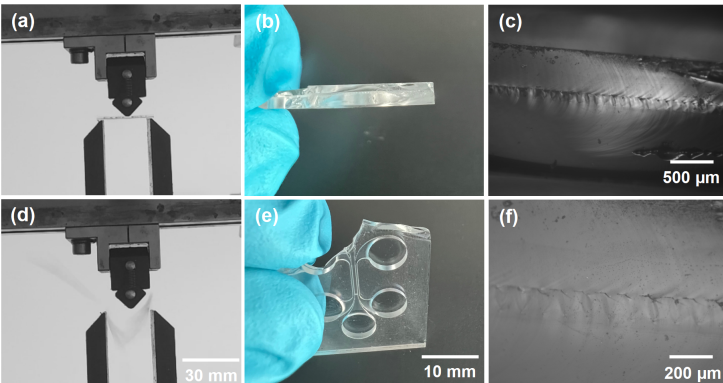

Figure 5. (**a**,**d**) Mechanical resistance test on the chip. (**b**,**e**) Photos of the broken chip after the mechanical resistance test. (**c**,**f**) Optical pictures of the broken structure's welding seam from the side of the sample.

3.3. Testing of the Liver-on-Chip's Functionality

The prototype device's functionality was tested with liver cells. A homogeneous film of poly-L-lysine was formed on the surface of the liver-on-chip systems. Uncoated chips were also tested; however, HepG2(GS) did not adhere due to the smooth chips' surface, while cells attached well on the coated surfaces. A total of 24 h after seeding, HepG2(GS) cells started to grow in a monolayer. The number of spheroids and size were consistent with the starting cell density. During the media change, the cell monolayers remained adherent to the surface and continuously grew. After 96 h of culture, the HepG2(GS) cells created large irregular spheroids. After 7 days of culture, the growth of spheroids led to the formation of large clusters of spheroids in the whole liver-on-ship system. A picture of the mentioned test is shown in Figure 6. From day 7, the cell viability decreased, as seen from the roundish shape of some of the cells. After 9 days, most of the cells had died according to the Trypan Blue test; this can be seen in Figure 6i,j. In general, the Trypan Blue exclusion test showed that the adhesive cells had good viability for 7 days of the experimental period.

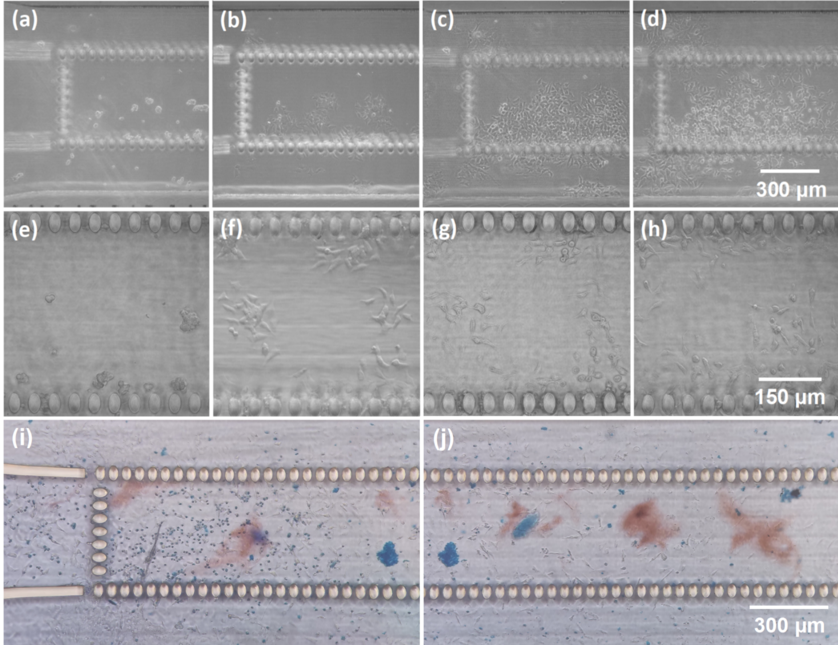

Figure 6. Optical pictures of the fabricated microfluidic channels seeded with HepG2(GS) liver cancer cells (**a**): (**e**) right after the seeding, (**b**,**f**) after 24 h, (**c**,**g**) after 96 h, (**d**,**h**) after 7 days, (**i**,**j**) after 9 days with Trypan Blue.

3.4. Future Prospects

The results show that femtosecond laser glass microfabrication is suitable for the development of liver-on-chip devices. However, there is still space for manufacturing improvements and more flexible design implementations. One of the observed challenges was the filter's accuracy and the minimum pore size. For example, the accuracy of SLE-made features depends on the etching rate between the modified and unmodified material. With the currently used chip design and etching protocol, the minimum spacing between pillars is 14 µm. Therefore, during the tests, it was noticed that a fraction of cells could pass through the filter and appear in other channels. Thus, the mentioned spacing between the pillars must be reduced to keep all of the cells inside the center channels. Therefore, the accuracy and sharpness of the structural etching rate of the modified material can

be increased. This can be achieved in a few ways, such as by optimizing the etching process, the etching solution [36], and the laser parameters [39], or by introducing a specific femtosecond burst regime [40]. Such improvements can create the possibility of tuning the filter size more accurately. Moreover, the surface quality of the fabricated chips can be increased by applying additional post-processing, such as heat treatment [41,42] or CO_2 laser annealing [43]. Such enhancements should decrease the friction between the surface of the channels and substances inserted in the chip, making it easier to fill the chip and test its functionality.

4. Conclusions

Here, we demonstrated a flexible method for microfluidic prototyping. A microprocessing tool with a single femtosecond laser source was used to produce microfluidic channel systems with integrated glass pillar filters. The channels were hermetically sealed by welding a glass plate on top of the channels with the same femtosecond processing tool. In this way, the whole liver-on-chip device was manufactured with a single workstation. Afterward, the produced chips were tested as liver-on-chip devices by filling the central channel with HepG2(GS) liver cancer cells. The cells tended not to adhere to uncoated glass surfaces. However, the cells aggregated on channels coated with a homogeneous film of poly-L-lysine, making it possible to test other cells' reactions to various stimuli introduced to the chip. These experiments show that femtosecond glass microprocessing is a potential and attractive technique for developing liver-on-chip devices. Here, we showed a potential platform for HepG2(GS) liver cancer cell testing; however, some improvements to these technologies still need to be made.

Author Contributions: Conceptualization, A.B., B.L., A.G., P.S. and K.S.; Methodology, A.B., T.B., B.L. and P.S.; Software, T.B.; Validation, B.L.; Formal analysis, B.L.; Investigation, A.B., T.J., T.B., B.L., G.M. and R.Ž.; Data curation, T.J., T.B. and B.L.; Writing—original draft, A.B., D.Č. and M.K.; Writing—review & editing, G.M., R.Ž., D.Č., A.G., M.K., K.M., P.S. and K.S.; Visualization, A.B., T.J., B.L. and M.K.; Supervision, A.B. and P.S.; Project administration, K.S.; Funding acquisition, K.S. All authors have read and agreed to the published version of the manuscript.

Funding: This research was funded by the European Commission's program "EUREKA", Nr.01.2.2-MITA-K-702-10-0006.

Institutional Review Board Statement: Not applicable.

Informed Consent Statement: Not applicable.

Data Availability Statement: Data is contained within the article.

Conflicts of Interest: The authors declare no conflict of interest.

References

1. Saeedabadi, K.; Tosello, G.; Calaon, M. Optimization of injection molded polymer lab-on-a-chip for acoustic blood plasma separation using virtual design of experiment. *Procedia CIRP* **2022**, *107*, 40–45. [CrossRef]
2. Thaisa-nga, R.; Chaumpluk, P. Aptamer based simple plastic lab-on-a-chip for rapid on-site monitoring of paraquat herbicide residue in soils. *Mater. Today Proc.* **2022**, *2023*, 124–131. [CrossRef]
3. Ma, L.; Petersen, M.; Lu, X. Identification and Antimicrobial Susceptibility Testing of Campylobacter Using a Microfluidic Lab-on-a-Chip Device. *Appl. Environ. Microbiol.* **2020**, *86*, e00096-20. [CrossRef] [PubMed]
4. Sun, Y.; Quyen, T.L.; Hung, T.Q.; Chin, W.H.; Wolff, A.; Bang, D.D. A lab-on-a-chip system with integrated sample preparation and loop-mediated isothermal amplification for rapid and quantitative detection of Salmonella spp. in food samples. *Lab Chip* **2015**, *15*, 1898–1904. [CrossRef]
5. Tymm, C.; Zhou, J.; Tadimety, A.; Burklund, A.; Zhang, J.X. Scalable COVID-19 detection enabled by lab-on-chip biosensors. *Cell. Mol. Bioeng.* **2020**, *13*, 313–329. [CrossRef]
6. Zhuang, J.; Yin, J.; Lv, S.; Wang, B.; Mu, Y. Advanced "lab-on-a-chip" to detect viruses—Current challenges and future perspectives. *Biosens. Bioelectron.* **2020**, *163*, 112291. [CrossRef]
7. Srikanth, S.; Jayapiriya, U.; Dubey, S.K.; Javed, A.; Goel, S. A lab-on-chip platform for simultaneous culture and electrochemical detection of bacteria. *Iscience* **2022**, *25*, 105388. [CrossRef]

8. Krakos (Podwin), A.; Śniadek, P.; Jurga, M.; Białas, M.; Kaczmarek-Pieńczewska, A.; Matkowski, K.; Walczak, R.; Dziuban, J. Lab-on-Chip Culturing System for Fungi—Towards Nanosatellite Missions. *Appl. Sci.* **2022**, *12*, 627. [CrossRef]
9. Rahmanian, M.; Sartipzadeh Hematabad, O.; Askari, E.; Shokati, F.; Bakhshi, A.; Moghadam, S.; Olfatbakhsh, A.; Al Sadat Hashemi, E.; Khorsand Ahmadi, M.; Morteza Naghib, S.; et al. A micropillar array-based microfluidic chip for label-free separation of circulating tumor cells: The best micropillar geometry? *J. Adv. Res.* **2022**. [CrossRef]
10. Aslan, M.; Yalcin, Y.D.; Ozgur, E.; Gunduz, U.; Eminoglu, S.; Kulah, H.; Akin, T. A High Throughput Lab-On-A-Chip System for Label Free Quantification of Breast Cancer Cells under Continuous Flow. *Procedia Technol.* **2017**, *27*, 59–61. [CrossRef]
11. Volpe, A.; Krishnan, U.; Chiriacò, M.S.; Primiceri, E.; Ancona, A.; Ferrara, F. A Smart Procedure for the Femtosecond Laser-Based Fabrication of a Polymeric Lab-on-a-Chip for Capturing Tumor Cell. *Engineering* **2021**, *7*, 1434–1440. [CrossRef]
12. Strelez, C.; Jiang, H.Y.; Mumenthaler, S.M. Organs-on-chips: A decade of innovation. *Trends Biotechnol.* **2023**, *41*, 278–280. [CrossRef]
13. Ahmed, T. Organ-on-a-chip microengineering for bio-mimicking disease models and revolutionizing drug discovery. *Biosens. Bioelectron. X* **2022**, *11*, 100194. [CrossRef]
14. Berlo, D.V.; Nguyen, V.V.; Gkouzioti, V.; Leineweber, K.; Verhaar, M.C.; Balkom, B.W.V. Stem cells, organoids, and organ-on-a-chip models for personalized in vitro drug testing. *Curr. Opin. Toxicol.* **2021**, *28*, 7–14. [CrossRef]
15. Kim, S.; Richardson, L.; Radnaa, E.; Chen, Z.; Rusyn, I.; Menon, R.; Han, A. Molecular mechanisms of environmental toxin cadmium at the feto-maternal interface investigated using an organ-on-chip (FMi-OOC) model. *J. Hazard. Mater.* **2022**, *422*, 126759. [CrossRef]
16. Van de Stolpe, A.; Den Toonder, J. Workshop meeting report Organs-on-Chips: Human disease models. *Lab Chip* **2013**, *13*, 3449–3470. [CrossRef]
17. Li, X.; George, S.M.; Vernetti, L.; Gough, A.H.; Taylor, D.L. A glass-based, continuously zonated and vascularized human liver acinus microphysiological system (vLAMPS) designed for experimental modeling of diseases and ADME/TOX. *Lab Chip* **2018**, *18*, 2614–2631. [CrossRef]
18. Cho, S.; Lee, S.; Ahn, S.I. Design and engineering of organ-on-a-chip. *Biomed. Eng. Lett.* **2023**, *2023*, 1–13. [CrossRef]
19. Shinde, A.; Illath, K.; Kasiviswanathan, U.; Nagabooshanam, S.; Gupta, P.; Dey, K.; Chakrabarty, P.; Nagai, M.; Rao, S.; Kar, S.; et al. Recent Advances of Biosensor-Integrated Organ-on-a-Chip Technologies for Diagnostics and Therapeutics. *Anal. Chem.* **2023**, *95*, 3121–3146. [CrossRef]
20. Puryear, J.R., III; Yoon, J.K.; Kim, Y. Advanced fabrication techniques of micro engineered physiological systems. *Micromachines* **2020**, *11*, 730. [CrossRef]
21. Faraji Rad, Z.; Prewett, P.D.; Davies, G.J. High-resolution two-photon polymerization: The most versatile technique for the fabrication of microneedle arrays. *Microsyst. Nanoeng.* **2021**, *7*, 71. [CrossRef] [PubMed]
22. Liao, C.; Wuethrich, A.; Trau, M. A material odyssey for 3D nano/microstructures: Two photon polymerization based nanolithography in bioapplications. *Appl. Mater. Today* **2020**, *19*, 100635. [CrossRef]
23. Butkutė, A.; Jonušauskas, L. 3D Manufacturing of Glass Microstructures Using Femtosecond Laser. *Micromachines* **2021**, *12*, 499. [CrossRef] [PubMed]
24. Krol, D. Femtosecond laser modification of glass. *J.-Non-Cryst. Solids* **2008**, *354*, 416–424. [CrossRef]
25. Hnatovsky, C.; Taylor, R.S.; Simova, E.; Bhardwaj, V.R.; Rayner, D.M.; Corkum, P.B. Polarization-selective etching in femtosecond laser-assisted microfluidic channel fabrication in fused silica. *Opt. Lett.* **2005**, *30*, 1867–1869. [CrossRef]
26. Bellouard, Y.; Hongler, M.O. Femtosecond-laser generation of self-organized bubble patterns in fused silica. *Opt. Express* **2011**, *19*, 6807–6821. [CrossRef]
27. Gailevičius, D.; Purlys, V.; Staliunas, K. Photonic crystal spatial filters fabricated by femtosecond pulsed Bessel beam. *Opt. Lett.* **2019**, *44*, 4969–4972. [CrossRef]
28. Gottmann, J.; Hermans, M.; Repiev, N.; Ortmann, J. Selective Laser-Induced Etching of 3D Precision Quartz Glass Components for Microfluidic Applications-Up-Scaling of Complexity and Speed. *Micromachines* **2017**, *8*, 110. [CrossRef]
29. Butkutė, A.; Baravykas, T.; Stančikas, J.; Tičkūnas, T.; Vargalis, R.; Paipulas, D.; Sirutkaitis, V.; Jonušauskas, L. Optimization of selective laser etching (SLE) for glass micromechanical structure fabrication. *Opt. Express* **2021**, *29*, 23487–23499. [CrossRef]
30. Butkus, S.; Gaižauskas, E.; Paipulas, D.; Viburys, Ž.; Kaškelyė, D.; Barkauskas, M.; Alesenkov, A.; Sirutkaitis, V. Rapid microfabrication of transparent materials using filamented femtosecond laser pulses. *Appl. Phys. A* **2014**, *114*, 81–90. [CrossRef]
31. Zhang, G.; Stoian, R.; Zhao, W.; Cheng, G. Femtosecond laser Bessel beam welding of transparent to non-transparent materials with large focal-position tolerant zone. *Opt. Express* **2018**, *26*, 917–926. [CrossRef]
32. Toh, Y.C.; Lim, T.C.; Tai, D.; Xiao, G.; van Noort, D.; Yu, H. A microfluidic 3D hepatocyte chip for drug toxicity testing. *Lab Chip* **2009**, *9*, 2026–2035. [CrossRef]
33. Marcinkevičius, A.; Juodkazis, S.; Watanabe, M.; Miwa, M.; Matsuo, S.; Misawa, H.; Nishii, J. Femtosecond laser-assisted three-dimensional microfabrication in silica. *Opt. Lett.* **2001**, *26*, 277–279. [CrossRef]
34. Kim, J.; Kim, S.; Joung, Y.; Choi, J.; Koo, C. Two-step hybrid process of movable part inside glass substrate using ultrafast laser. *Micro Nano Syst. Lett.* **2021**, *9*, 2213–9621. [CrossRef]
35. Ross, C.A.; MacLachlan, D.G.; Choudhury, D.; Thomson, R.R. Optimisation of ultrafast laser assisted etching in fused silica. *Opt. Express* **2018**, *26*, 24343–24356. [CrossRef]

36. Butkutė, A.; Baravykas, T.; Stančikas, J.; Tičkūnas, T.; Vargalis, R.; Paipulas, D.; Sirutkaitis, V.; Jonušauskas, L. Femtosecond Laser Assisted 3D Etching Using Inorganic-Organic Etchant. *Materials* **2022**, *15*, 2817. [CrossRef]
37. Tamaki, T.; Watanabe, W.; Nishii, J.; Itoh, K. Welding of Transparent Materials Using Femtosecond Laser Pulses. *Jpn. J. Appl. Phys.* **2005**, *44*, L687. [CrossRef]
38. Richter, S.; Nolte, S.; Tünnermann, A. Ultrashort Pulse Laser Welding—A New Approach for High- Stability Bonding of Different Glasses. *Phys. Procedia* **2012**, *39*, 556–562. [CrossRef]
39. Hermans, M.; Gottmann, J.; Riedel, F. Selective, Laser-Induced Etching of Fused Silica at High Scan-Speeds Using KOH. *J. Laser Micro/Nanoeng.* **2014**, *9*, 126–131. [CrossRef]
40. Stankevič, V.; Račiukaitis, G.; Gečys, P. Chemical etching of fused silica after modification with two-pulse bursts of femtosecond laser. *Opt. Express* **2021**, *29*, 31393–31407. [CrossRef]
41. Sala, F.; Paié, P.; Martínez Vázquez, R.; Osellame, R.; Bragheri, F. Effects of Thermal Annealing on Femtosecond Laser Micromachined Glass Surfaces. *Micromachines* **2021**, *12*, 180. [CrossRef]
42. Widmer, R.N.; Bischof, D.; Jurczyk, J.; Michler, M.; Schwiedrzik, J.; Michler, J. Smooth or not: Robust fused silica micro-components by femtosecond-laser-assisted etching. *Mater. Des.* **2021**, *204*, 109670. [CrossRef]
43. Zhao, L.; Cheng, J.; Chen, M.; Yuan, X.; Liao, W.; Liu, Q.; Yang, H.; Wang, H. Formation mechanism of a smooth, defect-free surface of fused silica optics using rapid CO_2 laser polishing. *Int. J. Extrem. Manuf.* **2019**, *1*, 035001. [CrossRef]

Disclaimer/Publisher's Note: The statements, opinions and data contained in all publications are solely those of the individual author(s) and contributor(s) and not of MDPI and/or the editor(s). MDPI and/or the editor(s) disclaim responsibility for any injury to people or property resulting from any ideas, methods, instructions or products referred to in the content.

NOTES

NOTES

NOTES

Vilniaus universiteto leidykla
Saulėtekio al. 9, III rūmai, LT-10222 Vilnius
El. p. info@leidykla.vu.lt, www.leidykla.vu.lt
bookshop.vu.lt, journals.vu.lt
Tiražas 20 egz.